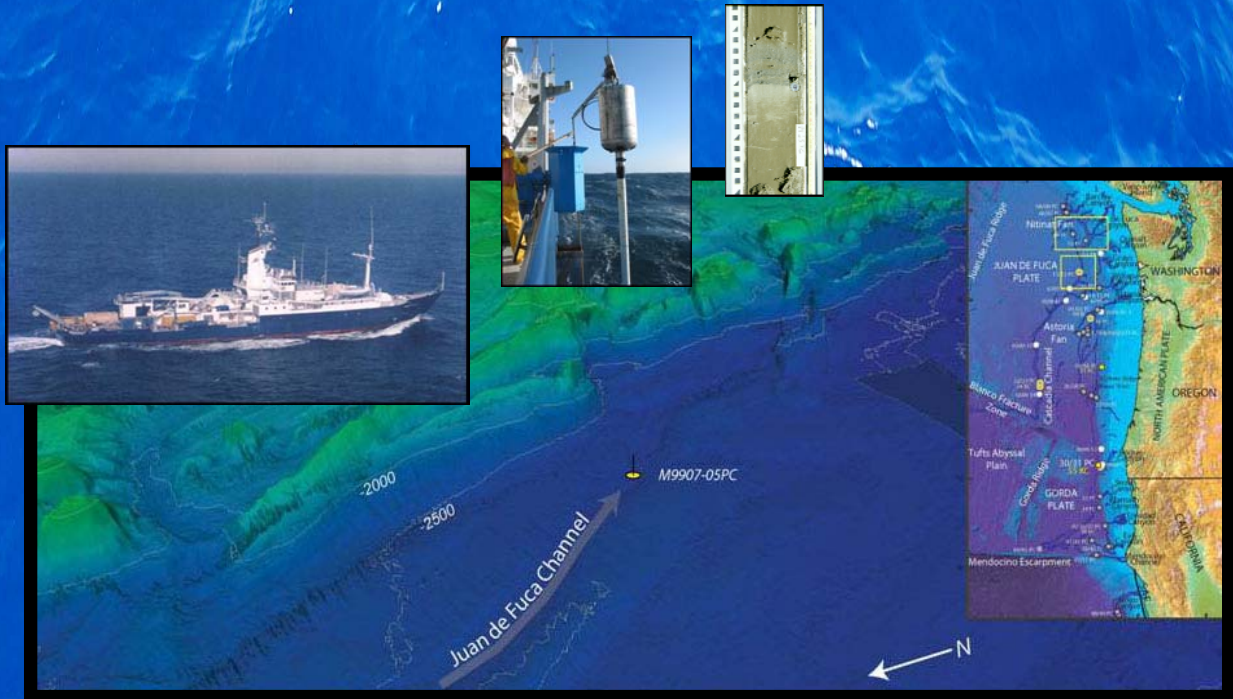




IACT (UGR-CSIC)

FREQUENCY AND SEDIMENTOLOGY OF HOLOCENE SEISMO-TURBIDITES ON THE CASCADIA SUBDUCTION ZONE AND NORTHERN SAN ANDREAS FAULT CONTINENTAL MARGINS OFF NORTH AMERICA

FRECUENCIA Y SEDIMENTOLOGÍA DE SEISMO-TURBIDITAS HOLOCENAS EN LOS MARGENES
CONTINENTALES DE SUBDUCCIÓN DE CASCADIA Y NORTE DE LA FALLA DE SAN ANDRÉS,
OESTE DE AMERICA DEL NORTE



Julia Gutiérrez Pastor

Ph.D. Thesis

2009

Tesis Doctoral



**INSTITUTO ANDALUZ DE CIENCIAS DE LA TIERRA
(CONSEJO SUPERIOR DE INVESTIGACIONES CIENTÍFICAS-
UNIVERSIDAD DE GRANADA)**

TESIS DOCTORAL

**FREQUENCY AND SEDIMENTOLOGY OF HOLOCENE
SEISMO-TURBIDITES ON THE CASCADIA SUBDUCTION ZONE
AND NORTHERN SAN ANDREAS FAULT CONTINENTAL
MARGINS OFF NORTH AMERICA**

FRECUENCIA Y SEDIMENTOLOGÍA DE SEISMO-TURBIDITAS
HOLOCENAS EN LOS MARGENES CONTINENTALES DE
SUBDUCCIÓN DE CASCADIA Y NORTE DE LA FALLA DE SAN
ANDRÉS, OESTE DE AMERICA DEL NORTE

JULIA GUTIÉRREZ PASTOR

Editor: Editorial de la Universidad de Granada
Autor: Julia Gutiérrez Pastor
D.L.: GR. 2611-2009
ISBN: 978-84-692-3874-5



INSTITUTO ANDALUZ DE CIENCIAS DE LA TIERRA
(CONSEJO SUPERIOR DE INVESTIGACIONES CIENTÍFICAS-
UNIVERSIDAD DE GRANADA)

TESIS DOCTORAL

**FREQUENCY AND SEDIMENTOLOGY OF HOLOCENE
SEISMO-TURBIDITES ON THE CASCADIA SUBDUCTION ZONE
AND NORTHERN SAN ANDREAS FAULT CONTINENTAL
MARGINS OFF NORTH AMERICA**

FRECUENCIA Y SEDIMENTOLOGÍA DE SEISMO-TURBIDITAS
HOLOCENAS EN LOS MARGENES CONTINENTALES DE
SUBDUCCIÓN DE CASCADIA Y NORTE DE LA FALLA DE SAN
ANDRÉS, OESTE DE AMERICA DEL NORTE

Granada, Junio de 2009

Memoria de Tesis que presenta **Julia Gutiérrez Pastor** para optar al grado de Doctor por la Universidad de Granada.

Vº Bº de los Directores

La Doctoranda

Carlota Escutia Dotti

C. Hans Nelson

Julia Gutiérrez Pastor

A Migue,
Julia y Carolina,
Por vosotros

"Cada uno da lo que recibe
luego recibe lo que da
nada es mas simple
no hay otra norma
nada se pierde, todo se transforma"

(Jorge Drexler)

AGRADECIMIENTOS

Esta tesis es el fruto de mucho trabajo que no se podría haber llevado a cabo si no es por el apoyo de todas las personas que me han rodeado durante estos preciosos años de aprendizaje. Mis comienzos en esta aventura científica se remontan a mi época de estudiante de Geología, cuando todavía cursaba cuarto de carrera. Ya por entonces tuve el privilegio de hacer mis primeros pinitos en Geología Marina.

Doy especial gracias a Hans, mi “padre científico”, el profesor de profesores, el investigador por excelencia, el hombre que confió en mí desde el primer momento que pisé un barco oceanográfico donde trabajábamos sin cesar día y noche (allá por el año 1999). Gracias por enseñarme todo lo que he aprendido y aun estoy aprendiendo, gracias también por tu apoyo incondicional como persona y amigo.

Especial gracias, también, a Carlota, “mi madre científica”, por enseñarme otros “mundos” en geología, por enriquecer mi conocimiento, por apostar y dar continuidad a mi trabajo, por tu calidad humana y científica, un ejemplo a seguir.

Gracias, Jesús Galindo, que me diste el pasaporte para embarcarme en esta “aventura Paleosísmica” al ofrecer a los estudiantes la posibilidad de participar como voluntarios a bordo del Melville y, gracias Pascual Rivas, por apoyarnos económicamente.

Gracias, Pepe Martín, que me apoyaste con tus recomendaciones, tu posición de tutor en mis dos primeros años de doctorado y que seguiste mi trayectoria hasta el día de hoy. Fuiste tu, Pepe, quien me convenció para desarrollar una tesis doctoral.

Mi más sinceros agradecimientos a Chris Goldfinger por apostar por mi trabajo en las dos campañas oceanográficas (que junto a Hans lideró), por acogerme en su grupo de Investigación (Active Tectonic Group) de la Oregon State University durante mis estancias en Estados Unidos y por hacerme partícipe de sus proyectos y contar conmigo, siempre, como investigadora. Agradezco también la ayuda que Ann me brindó, siempre dispuesta a todo.

Agradezco a toda la tripulación, tanto técnica como científica, de los buques de investigación Melville y Roger Revelle: Mike Winkler, Pete Kalk, Antonio Camarero, Clara Morri, Gita Dunhill, Luis Ramos, Alex Raab, Nick Piasias Jr., Mark Pourmanoutscheri, David Van Rooij, Lawrence Amy, Churn-Chi “Charles” Liu, Chris Moser, Devin Etheridge, Heidi Stenner, Chris Popham, Claire McKee, Duncan MacMillan, Chris Crosby, Susanne Schmid, Eulalia Gracia, Suzanne Lovelady, Chris Romsos, Jason Chaytor, Vincent Rinterknecht, Rondi Robison, David Casas, Francois Charlet, Britta Hinrichsen, Jeremiah Oxford, Miquel Marin, Marta Mas, Sergio Montes, Raquel Villalonga, Alexis Vizcaino, Santiago Jimenez, Mayte Pedrosa, Silvia Perez, Jorge Pérez,

Andreu Turra, David Lamas, Himar Falcon y Andres Barranco. Con ellos tuve el placer de trabajar en mis dos primeras campañas oceanográficas frente a las costas de Oregon y California. Gracias a todos por el inmenso compañerismo y colaboración que contribuyeron a mi crecimiento científico y personal.

También quiero expresar mi gratitud al personal científico de la Expedición 308 “Gulf of Mexico Hydrogeology” del International Ocean Drilling Program (IODP) (en el mar Caribe, desde Alabama hasta Panama), en donde tuve el placer de ser invitada a participar como sedimentóloga. En especial doy gracias a Carlos, por brindarme siempre su ayuda y a Peter, Cedric y Jan, por confiar en mi trabajo. Del mismo modo, mi más sincero agradecimiento a todo el personal de la sede de IODP en College Station, Texas, donde se me permitió dar continuidad a las investigaciones post-campaña en laboratorios especializados.

Por estar involucrada en el programa IODP, es de agradecer también a Menchu Comas su apoyo en todo momento, ofreciéndome incluso un hueco en la gestión de IODP en España.

Agradezco a los organismos que han financiado los proyectos de investigación sobre Paleosismicidad en los que he participado, tales como United States Geological Survey y National Science Foundation, permitiendo la creación de mis becas pre-doctorales, gestionadas a través de la Universidad de Granada. Gracias, por tanto, a la Universidad de Granada, sobre todo al Vicerrectorado de investigación, por gestionar estas becas con fondos internacionales y del mismo modo al Ministerio de Innovación y Ciencia que a través del CSIC ha dado continuidad a mi trabajo mediante becas pre-doctorales de investigación y acciones complementarias.

Mil gracias a todo el personal científico y administrativo del Instituto Andaluz de Ciencias de la Tierra y departamentos de Geología, que me han hecho la vida más fácil durante todos estos años.

Tampoco quiero olvidarme del director del departamento de Geodinámica, que en su día fue, Paco Lodeiro, por ubicarme, cediéndome un espacio en diferentes despachos del departamento y permitirme, por tanto, el desarrollo de este trabajo.

Como no mencionar con cariño a mis compañeros de fatigas, cafés, marchas, días del becario..., en definitiva, mis amigos, que desde los tiempos primigenios con Concha (la elegancia), Fermín (el más granaíno), David (el alternativo), constituimos el escuadrón de la muerte, y con Claudio (el Magníficus), Patricia (la mami), Ana (amiga de amigos), Vicente (el guasón), “Ozemia” (el zezeo), José Alberto (el candor), Maja (la eslovena), Alpiste (la ayuda), Pedrito (el músico), Francis (el compañero de promoción)...lo ampliamos a un ejército que se hizo aún más numeroso con la llegada de nuevos becarios e investigadores: Jhon Jairo, Antonio Acosta, Pedro “80”, Silvia, Paco Lobo, Carlos, Antonio Pedrera, Iñaki, José María “el chiquitillo”,”et al”(la lista es tan numerosa que casi podría llenar una tesis).

Personalmente, te doy gracias, Jhon, por prestarme tu habilidad en cuestiones técnicas en esta última etapa de trabajo, sin ti hubiese sido mucho más difícil.

Quiero aprovechar esta ocasión para acordarme de mis amigos de promoción, Jesús, que viviendo en Granada siempre se ha apuntado a un bombardeo, Elenilla, David “Pipo”, “La Pilar”, Juanillo... que después de tantos años pasados aún siguen estando ahí,..., y, de más amigos de otros ámbitos como Holly, Neel y Jesse, mis apoyos en Oregon y Paula, Ivan, Pierre, Massimo, amistad perenne forjada en Nottingham desde el 2001.

Y no me quiero dejar en el tintero a mi familia política, siempre dispuesta a echar una mano.

Pero termino estas líneas de agradecimiento homenajeando a las personas que desde pequeña, fueron responsables de mis inquietudes profesionales, mis padres y hermanos, gracias por estar ahí siempre, sin condiciones, en mis momentos de subidas y bajadas.

Y como colofón, gracias a Migue, con todo mi amor, mi compañero para todo y el motor que me impulsa a lanzarme a todos los retos sin miedos ni tapujos, siempre apoyando todas mis decisiones y padeciendo mis agobios. Gracias a mis hijas, Julia y Carolina, por existir, porque basta una sonrisa para darle sentido a tanto esfuerzo y porque en estos dos últimos años me han enseñado a valorar lo que es realmente importante en la vida. ¡Os quiero con locura!

TABLA DE CONTENIDOS

Resumen	1
Abstract	3
Estructura de Tesis	5
CAPÍTULO I: INTRODUCCIÓN	13
I.1 ANTECEDENTES	13
I.2 OBJETIVOS	15
I.3 MARCO GEOLÓGICO	16
I.4 MÉTODOS RESUMIDOS	18
I.5 CONCEPTOS BÁSICOS	21
CAPÍTULO II: FRECUENCIA DE SEISMO-TURBIDITAS	
<i>ARTICULO: EARTHQUAKE CONTROL OF HOLOCENE TURBIDITE FREQUENCY CONFIRMED BY HEMPELAGIC SEDIMENTATION CHRONOLOGY ON THE CASCADIA AND NORTHERN CALIFORNIA ACTIVE TECTONIC CONTINENTAL MARGINS.</i>	
Abstract	35
1. INTRODUCTION	36
2. GEOLOGICAL SETTING	38
2.1. <i>Tectonic setting</i>	38
2.2. <i>Turbidite Systems and the Turbidite Record</i>	39
2.2.1. <i>Juan de Fuca Channel (JDF)</i>	39
2.2.2 <i>Cascadia Deep-Sea Channel (CC)</i>	39
2.2.3. <i>Noyo Channel (NC)</i>	41
2.3. <i>Character of Turbidites</i>	41
3. METHODS	41

3.1. Core Recovery and Swath Bathymetry	41
3.2. General Sediment Analysis Methods	43
4. METHODOLOGY FOR HEMIPELAGIC SEDIMENT	45
4.1. Evaluation of Maximum Erosion by Turbidity Currents Based on Thickness of Total Holocene Hemipelagic Sediment	46
4.2. Best Hemipelagic Sediment Thickness (BT)	48
4.3. Hemipelagic Sedimentation Rates Using ¹⁴ C Calibrated years Before Present (cal. yr B.P.) Ages	48
4.4. Effects of Hemipelagic Sediment Erosion on ¹⁴ C and BT Data: Testing Reliability of Ages	48
4.5. Datum Ages	51
4.6. Recurrence Times Based on Hemipelagic Sediment	51
4.7. Recurrence Time based on ¹⁴ C Age	51
4.8. Ages of Turbidites Based on Best Hemipelagic Sediment Thickness (BT)	52
4.9. Analysis of Noyo Independent Hemipelagic Sediment Thickness for ¹⁴ C Oxcal Age Corrections	52
5. DISCUSSION	54
5.1. Contribution of Hemipelagic Sediment Thickness Analysis to Paleoseismic Studies	54
5.2. Turbidite Recurrence Times in the Cascadia Subduction Zone	55
5.3. Turbidite Recurrence Times on the Northern California Margin	56
5.4. Global Implications	57
6. CONCLUSIONS	57
ACKNOWLEDGEMENTS	58
REFERENCES	59

CAPÍTULO III: PALEOSISMICIDAD EN EL MARGEN DE CALIFORNIA

ARTICULO: RUPTURE LENGTHS AND TEMPORAL HISTORY OF SIGNIFICANT EARTHQUAKES ON THE OFFSHORE AND NORTH COAST SEGMENTS OF THE NORTHERN SAN ANDREAS FAULT BASED ON TURBIDITE STRATIGRAPHY

Abstract	65
1. INTRODUCTION	66
2. GEOLOGICAL SETTING AND BACKGROUND	68
2.1. <i>NSAF Seismotectonic Setting</i>	68
2.2. <i>Northern San Andreas Onshore Paleoseismicity</i>	68
3. TURBIDITE METHODOLOGY AND ANALYTICAL METHODS	69
3.1. <i>Turbidite Methodology and Application to Cascadia and the San Andreas</i>	69
3.1.1. <i>Identifying Earthquake-Triggered Turbidites</i>	69
3.1.2. <i>Tests of Synchronous Triggering and Correlative Deposition of Turbidites</i>	71
3.2. <i>Analytical Methods</i>	71
3.2.1. <i>Stratigraphic Correlation and Event “Fingerprinting”</i>	71
3.2.2. <i>Radiocarbon Analysis</i>	72
4. RESULTS: NORTHERN SAN ANDREAS TURBIDITE RECORD	74
4.1. <i>Confluences and Mineralogy</i>	74
4.2. <i>Stratigraphic Correlation</i>	79
4.3. <i>Radiocarbon Time Series and Comparison to Onshore Paleoseismic Sites</i>	80
5. DISCUSSION	82

6. CONCLUSIONS	84
ACKNOWLEDGEMENTS	84
REFERENCES	85

CAPÍTULO IV: CARACTERIZACIÓN SEDIMENTOLÓGICA DE SEISMO-TURBIDITAS

ARTICULO: SEDIMENTOLOGY OF SEISMO-TURBIDITES OFF THE CASCADIA AND NORTHERN CALIFORNIA ACTIVE TECTONIC CONTINENTAL MARGINS, NORTHEAST PACIFIC OCEAN

Abstract	93
1. INTRODUCTION	94
2. GEOLOGICAL SETTING AND TURBIDITE SYSTEMS	95
<i>2.1. Cascadia Continental Margin</i>	95
<i>2.2. Northern California Continental Margin</i>	95
3. SEDIMENT ANALYSIS METHODS	96
4. PALEOSEISMIC TURBIDITE RECORD: PREVIOUS RESULTS	98
5. RESULTS: SEDIMENTOLOGICAL CHARACTERIZATION OF TURBIDITES	101
<i>5.1. Cascadia Margin</i>	101
<i>5.1.1. Turbidite 3 in Juan De Fuca Channel</i>	101
<i>5.1.2. Turbidite 3 in Cascadia Channel</i>	102
<i>5.1.3. T3/T6 in Willapa Channel</i>	104
<i>5.2. Northern California Margin</i>	106
<i>5.2.1. Noyo Channel turbidites in 49 PC</i>	107
<i>5.2.2. Gualala Channel turbidites in 13PC</i>	107
<i>5.2.3. Gualala Channel turbidites in 12 PC</i>	110

5.2.4. <i>Noyo/Gualala/Viscaino confluence turbidites in 24GC</i>	111
5.2.5. <i>Gualala/Viscaino /Cordell confluence turbidites at 31PC</i>	114
6. DISCUSSION	115
6.1. <i>Features of turbidites in Cascadia Margin</i>	115
6.2. <i>Features of turbidites in the Northern California Margin</i>	116
6.3. <i>Comparison between features of turbidites at Cascadia and northern California margins and implications for other active and passive margins</i>	118
7. CONCLUSIONS	120
ACKNOWLEDGEMENTS	121
REFERENCES	121
CAPÍTULO V: CONCLUSIONES	133
CONCLUSIONS	135
CAPÍTULO VI: PERSPECTIVAS FUTURAS	139
ANEXO 1: INVESTIGACIÓN RELEVANTE ASOCIADA	141
1.1 LATE HOLOCENE RUPTURE OF THE NORTHERN SAN ANDREAS FAULT AND POSSIBLE STRESS LINKAGE TO THE CASCADIA SUBDUCTION ZONE	
1.2 EXTERNAL CONTROLS ON MODERN CLASTIC TURBIDITE SYSTEMS: THREE CASE STUDIES	
1.3 TURBIDITE EVENT HISTORY: METHODS AND IMPLICATIONS FOR HOLOCENE PALEOSEISMICITY OF THE CASCADIA SUBDUCTION ZONE	
ANEXO 2: OTRAS PUBLICACIONES	
2.1 HOLOCENE EARTHQUAKE RECORDS FROM THE CASCADIA SUBDUCTION ZONE AND NORTHERN SAN ANDREAS FAULT BASED ON PRECISE DATING OF OFFSHORE TURBIDITES	

2.2 DEEP-WATER TURBIDITES AS HOLOCENE EARTHQUAKE PROXIES: THE CASCADIA SUBDUCTION ZONE AND NORTHERN SAN ANDREAS FAULT SYSTEMS

2.3 OVERPRESSURE AND FLUID FLOW PROCESSES IN THE DEEPWATER GULF OF MEXICO: SLOPE STABILITY, SEEPS, AND SHALLOW-WATER FLOW

2.4 DATA REPORT: AR/AR CHRONOLOGY OF DISCRETE ASH LAYERS IN THE NORTHWESTERN PACIFIC: ODP SITES 1149 AND 1179.

2.5 PALEOENVIRONMENTAL IMPLICATIONS OF TEPHRA SEDIMENTATION IN THE NORTHWESTERN PACIFIC SINCE THE LATE MIOCENE.

RESUMEN

Mi tesis doctoral analiza la frecuencia y las características sedimentológicas de turbiditas Holocenas como parte de un estudio que utiliza las turbiditas como indicadores de grandes terremotos (≥ 8 Mw) en los márgenes tectónicamente activos de subducción de Cascadia y transformante del Norte de California. En ambos márgenes, los canales turbidíticos y cañones tributarios fueron barridos con multibeam sonar para definir los trazados, las confluencias entre canales y para localizar el registro turbidítico más completo. En los sistemas de cañón y canal se recuperaron testigos de sondeo de pistón, de gravedad, de caja y “kasten” (de grandes dimensiones). Sobre estos testigos se hizo un análisis minucioso del espesor del sedimento hemipelágico justo debajo de cada turbidita para datación por ^{14}C . Los diferentes niveles (pulsos en la versión en inglés) turbidíticos fueron muestreados para realizar estudios de granulometría y mineralogía, poniendo especial interés en las confluencias entre canales, ya que estos ofrecen la oportunidad de comprobar el mecanismo sincrónico desencadenante de corrientes de turbidez, los terremotos. Todos los testigos fueron escaneados para obtener un registro de alta resolución de las propiedades físicas del sedimento, como las ondas P, la densidad y la susceptibilidad magnética y en algunos testigos seleccionados se obtuvieron radiografías de rayos-X. Estudios previos usaron edades relativas de las turbiditas en las confluencias de los canales basándose en el datum de las cenizas volcánicas de la erupción Mazama, dataciones por ^{14}C , y en correlaciones estratigráficas de las propiedades físicas para determinar que las turbiditas depositadas en sistemas de cañones separados espacialmente son correlativos e implican que fueron generadas por un mismo evento sísmico.

Mi investigación compara la edad, la frecuencia, e intervalos de recurrencia entre turbiditas en múltiples testigos de sondeo de dos canales del margen de Cascadia (Canales Juan de Fuca y Cascadia), y uno de el norte de el margen de California, el canal de Noyo, mediante dos métodos: 1) datación absoluta (Método de ^{14}C) y 2) datación relativa usando espesor de sedimento hemipelágico y tasas de sedimentación (Método de H). En estos márgenes tectónicamente activos, cuando el nivel del mar es alto (durante el Holoceno) el mecanismo que controla de generación de turbiditas son terremotos, encontrándose que las seismo-turbiditas tienen periodos de recurrencia ~ 550 años, en el margen de Cascadia y de ~ 200 años, en el margen Norte de California. Esta diferencia de frecuencias entre estos dos márgenes: 1) verifica la diferente actividad de los terremotos a lo largo de cada uno, 2) elimina la posibilidad de que las corrientes de turbidez fueran desencadenadas por tormentas o tsunamis, ya que los terremotos sacuden todo el margen a la misma frecuencia, y 3) se correlaciona con las frecuencias obtenidas con otros indicadores paleosísmicos en áreas costeras. El hallazgo más interesante de cara a los riesgos sísmicos en estos márgenes es que la mínima frecuencia entre turbiditas es la calculada en base al espesor de sedimento hemipelágico (margen de Cascadia es ~ 300 años y en el norte de California es ~ 175 años) y que esto indica que ambos márgenes pueden estar entrando en una era con probabilidad de ocurrencia de terremotos de elevada magnitud ya que, por ejemplo, el último terremoto en Cascadia tuvo lugar hace 309 años.

El análisis sedimentológico de turbiditas Holocenas coetáneas de ambos márgenes ha ayudado a identificar algunas características fundamentales resultantes de su origen sísmico. En los canales proximales de Juan de Fuca y Willapa del margen de Cascadia, la ausencia de muchas cabeceras de cañones de tributarios y la morfología simple de los canales proximales sin confluencias, normalmente genera turbiditas de un solo pulso con secuencias grano-decrecientes. Sin embargo, la presencia algunas turbiditas atípicamente multi-pulsadas que correlacionan con otras turbiditas de características sedimentológicas y propiedades físicas similares a lo largo de la cuenca, sugieren que estas turbiditas multi-pulsadas en canales proximales exhiben la señal de un terremoto de elevada magnitud y/o sus réplicas. A lo largo

del norte de California, en los canales proximales sobre las confluencias entre canales, las turbiditas son generalmente uni-pulsadas y, ocasionalmente, multi-pulsadas probablemente porque en la base del talud, atravesada por los canales proximales, está alimentada por múltiples cañones/canal tributarios.

En ambos márgenes, bajo la confluencia entre canales las turbiditas son multi-pulsadas de arena/limo con secuencias de Bouma incompletas. Al no existir sedimento hemipelágico ente pulsos y tener cada pulso una mineralogía diferente atribuible a distintos cañones tributarios, interpretamos que estas turbiditas multi-pulsadas son causadas por múltiples corrientes de turbidez de diferentes cañones tributarios que se han generado sincrónicamente por un terremoto de elevada magnitud. Cuando estas corrientes de turbidez se depositan en el mismo lugar, los múltiples pulsos de arena/limo se apilan uno sobre otro, truncando las estructuras sedimentarias del anterior, hasta depositar la cola de la turbidita de grano fino. Por tanto, los terremotos como mecanismo sincrónico atribuible al depósito de turbiditas es una explicación más a los lechos amalgamados de turbiditas. En general en estos márgenes activos, la confluencia entre canales y cañones tributarios y la elevada magnitud de un terremoto deben de ser la explicación a las características de las turbiditas multi-pulsadas. El análisis detallado de las turbiditas registradas tanto en el margen de Cascadia como el del Norte de California revela que tienen características sedimentológicas únicas que ponen de manifiesto un mecanismo de generación sincrónico a través de terremotos de elevada magnitud y pueden ser, por tanto, usadas para distinguir seismo-turbiditas en otros márgenes activos del mundo.

ABSTRACT

My thesis research analyzes the frequency and sedimentological characteristics of Holocene turbidites as part of a study that uses turbidite history as proxies for great earthquakes (≥ 8 Mw) on the Cascadia and northern California active tectonic margins of western Northern America. In both margins turbidite channel system and tributary canyons on the abyssal sea floor were mapped with multibeam sonar to define pathways and channel confluences, and to find locations with the most complete turbidite records. Multiple piston, trigger, box and giant kasten cores were obtained from channels and tributary canyons. Careful analysis of hemipelagic sediment thickness was done and this sediment was sampled immediately below turbidites for ^{14}C ages. Individual turbidite pulses were sampled for grain size and mineralogy with particular attention paid to sites downstream from channel confluences, because these areas afford opportunities to test for synchronous triggering of turbidity currents by earthquakes. All cores were scanned for high-resolution physical properties of P-wave velocity, gamma-ray density, and magnetic susceptibility, and some cores were imaged with X-radiography. Previous studies used relative dating tests at channel confluences based on Mazama ash marker beds, ^{14}C ages, ages based on hemipelagic thickness and sedimentation rates, and stratigraphic correlation using physical properties to determine that turbidites deposited in separate channel systems are correlative and imply that they were triggered by a common earthquake event.

My research compared the age, frequency, and recurrence time intervals of turbidites in multiple cores from two channels of the Cascadia margin (Juan de Fuca and Cascadia channels) and Noyo Channel of the northern California margin using two methods: 1) radiometric dating, (^{14}C method) and 2) relative dating, using hemipelagic sediment thickness and sedimentation rates (H method). On these tectonically active continental margins, during the sea-level highstand of Holocene time, triggering of turbidity currents is dominantly controlled by earthquakes, and paleoseismic turbidites have an average recurrence time of ~ 550 yr in northern Cascadia Basin and ~ 200 yr along the northern California margin. The significant differences in frequencies between these two margins, 1) verifies different earthquake activity, 2) eliminates the possibility of storm or tsunami triggering of turbidites because they strike both margins with the same frequency, and 3) correlates with the frequencies of other independent paleoseismic indicators onshore. Critical importance to earthquake hazards studies, the most accurate minimum turbidite recurrence times are determined by hemipelagic thickness (~ 300 yr in northern Cascadia Basin and ~ 175 yr in California), and indicate that the Cascadia margin is entering the window for a possible new great earthquake because the last great earthquake was 309 years ago.

The sedimentologic analysis of synchronous Holocene turbidites from both continental margins has helped to identify some fundamental characteristics that result from their seismic triggering. In the proximal Juan de Fuca and Willapa channel sites of the Cascadia margin, the absence of many tributary canyon heads and the simple morphology of single channels, without confluences of tributary channels, usually generate uni-pulsed simple fining upward graded turbidites. However, the presence of some unusually thick turbidites with multiple coarse-grained pulses, that correlate with and have the same physical property signatures of similar thick turbidites throughout Cascadia basin, suggests that these proximal multi-pulsed turbidites exhibit the signature of the strongest great earthquakes and/or aftershocks. Along the northern California margin, in proximal channels upstream from channel confluences, turbidites occasionally are uni-pulsed, but most commonly are multi-pulsed, apparently because most base-of-slope proximal channels are fed by multiple tributary canyons.

In both the Cascadia and California margins, below multiple tributary canyon and channel confluences

the individual turbidites are multi-pulsed sandy/silt beds with incomplete truncated Bouma sequences. Because no hemipelagic sediment exists between pulses, and each pulse has a distinct mineralogy from a different tributary canyon, we interpret that these multi-pulsed turbidites are caused by multiple turbidity currents from tributary canyons with synchronous triggering by a great earthquake. When these closely-spaced turbidity currents deposit at the same site, the multiple coarse-grained pulses stack one above the other until the final turbidite tail deposits. Hence, synchronous earthquake triggering in multiple tributary canyons becomes an important explanation for amalgamated turbidite beds in active tectonic continental margins. Both downstream confluences of tributary canyons or channels and the strongest great earthquakes may contribute to the characteristic multiple pulses of seismo-turbidites. The detailed analyses of the turbidites recovered in the Cascadia and northern California margins reveals common sedimentological characteristics of turbidites triggered by great earthquakes that can be used to distinguish seismo-turbidites in other active tectonic margins around the world.

ESTRUCTURA DE TESIS

El volumen de esta tesis doctoral consta de la investigación realizada como queda reflejada en los artículos científicos publicados, en prensa y enviados a revistas y libros internacionales. Cabe mencionar que los manuscritos aquí presentados son fieles a su formato de publicación original en cuanto a nomenclatura de figuras, acrónimos y referencias.

- El **Capítulo I, INTRODUCCIÓN**, aborda, en primer lugar, las investigaciones antecedentes a este estudio. En segundo lugar se plantean los objetivos de este trabajo de tesis, que se sitúan en el marco de dos proyectos de investigación de Paleosismicidad en los márgenes continentales de subducción de Cascadia (Vancouver Island, Canada; Washington y Oregón) y transformante de California, ligado a la falla de San Andrés (norte de California). Los proyectos enmarcados en este trabajo son: “Holocene Seismicity of the Northern San Andreas Fault Based on Precise Dating of the Turbidite Event Record “ y “Holocene Seismicity of the Cascadia Subduction Zone Based on Precise Dating of the Turbidite Event Record”, y están financiados por el United States Geological Survey-National Earthquake Hazard Program y la National Science Foundation. Se ha podido trabajar en estos proyectos de investigación gracias a la colaboración entre Universidad de Granada y la Oregon State University.

Además, el Capítulo de Introducción incluye una sección de enmarque geológico del área de estudio y otra de metodología, que se presenta de manera general, refiriéndose a los artículos que conforman los sucesivos capítulos de la tesis y donde se explica detalladamente cada una de las metodologías utilizadas para cada objetivo particular. Por último se incluye una sección con los conceptos básicos en sedimentología de turbiditas y sus mecanismos de generación.

-El **Capítulo II, FRECUENCIA DE SEISMO-TURBIDITAS: Gutiérrez- Pastor, J.,** Nelson, C. H., Goldfinger, C., Johnson, J. E., Escutia, C., Eriksson, A., Morey, A. E., and the Shipboard Scientific Party “***EARTHQUAKE CONTROL OF HOLOCENE TURBIDITE FREQUENCY CONFIRMED BY HEMIPELAGIC SEDIMENTATION CHRONOLOGY ON THE CASCADIA AND NORTHERN CALIFORNIA ACTIVE TECTONIC CONTINENTAL MARGINS***“, recopila la investigación realizada en una publicación internacional en prensa (“in press”) como capítulo de libro en el volumen especial de la SEPM (“Society for Sedimentary Geology”) nº 92 (B. Kneller, W. McCaffrey and O.J. Martinsen Eds, *External Controls on Deepwater Depositional Systems*, ISBN 978-1-.56576-136-0, p. xxx-xxx).

Tema que aborda y contribución

Uno de los objetivos primordiales en los estudios de paleosismicidad es el obtener los intervalos de recurrencia, es decir, la frecuencia a la que ocurren los terremotos en zonas tectónicamente activas. En los estudios de paleosismicidad en los que se utilizan como indicadores los niveles de turbiditas generados por terremotos, las dataciones de ^{14}C son utilizadas para obtener dicha frecuencia. Sin embargo, ese método de datación es inexacto debido a que los márgenes de error causados por la instrumentación y grado de erosión generado por las corrientes de turbidez pueden ser de varios cientos de años, modificando la estimación real de los intervalos de recurrencia entre los terremotos. En el artículo de este capítulo se desarrolla una nueva metodología para la corrección de las edades de las turbiditas Holocenas datadas mediante ^{14}C ., que permite una mayor precisión a la hora de determinar las frecuencias de los eventos turbidíticos en los márgenes de Cascadia y del Norte de California. El objetivo es, por tanto, minimizar el cálculo de

los intervalos de recurrencia entre los terremotos que generan la turbiditas. Para ello se hace el estudio detallado del grosor de sedimento hemipelágico depositado entre turbiditas que nos da un valor de tiempo real entre el deposito de cada una de ellas, y por tanto, entre terremotos. Una vez realizadas las correcciones de edades de ^{14}C por el método de espesores de sedimento hemipelágico se comprueba la mayor precisión en la determinación de los intervalos de recurrencia en comparación con los obtenidos solamente mediante la datación absoluta por ^{14}C .

- El **Capítulo III, PALEOSISMICIDAD EN EL MARGEN DE CALIFORNIA**: Goldfinger, C., Morey, A., Nelson, C.H., **Gutiérrez-Pastor, J.**, Jhonson, J.E., Karabanov, E., Chaytor, J., and the Shipboard Scientific Party ***“RUPTURE LENGTHS AND TEMPORAL HISTORY OF SIGNIFICANT EARTHQUAKES ON THE OFFSHORE AND NORTH COAST SEGMENTS OF THE NORTHERN SAN ANDREAS FAULT BASED ON TURBIDITE STRATIGRAPHY”***, recopila la investigación realizada y publicada en la revista Earth and Planetary Science Letters del año 2007 , v. 257, p. 9-27, doi:10.1016/j.epsl.2006.11.017

Tema que aborda y contribución

Este capítulo aborda la correlación de turbiditas Holocenas generadas por terremotos y depositadas en diferentes canales turbidíticos a lo largo del segmento norte de la falla de San Andrés. La correlación se basa, principalmente, en las propiedades físicas del sedimento, y se complementa con dataciones absolutas de ^{14}C y relativas producto de la corrección de las anteriores mediante las mediciones precisas del sedimento hemipelágico entre turbiditas. En este artículo se interpretan las señales de las propiedades físicas del sedimento como indicadores de la granulometría y se contrasta con el estudio detallado del tamaño de grano en turbiditas seleccionadas para este objetivo. También se incluyen estudios mineralógicos de las partículas que componen las turbiditas depositadas por debajo de las confluencias entre canales con el objetivo de determinar su área fuente y por tanto, comprobar su sincronía de depósito a lo largo del margen. Como objetivo final, se han estimado los intervalos de recurrencia entre terremotos en el margen continental norte de California y las longitudes de ruptura de la falla que generan los seismos.

- El **Capítulo IV, CARACTERIZACIÓN SEDIMENTOLOGICA DE SEISMO-TURBIDITAS**: **Gutiérrez-Pastor J.**, Nelson, C. H., Escutia, C., Goldfinger, C. and Eriksson, A., ***“SEDIMENTOLOGY OF SEISMO-TURBIDITES OFF THE CASCADIA AND NORTHERN CALIFORNIA ACTIVE TECTONIC CONTINENTAL MARGINS, NORTHEAST PACIFIC OCEAN”***, recopila la investigación realizada como publicación que va a ser enviada a la revista internacional “Marine Geology “.

Tema que aborda y contribución

Este capítulo aborda un análisis sedimentológico detallado de las turbiditas Holocenas generadas por terremotos en los márgenes de Cascadia y del norte de California. Para ello se hace un análisis de la granulometría del sedimento y se integra con un análisis: 1) visual macroscópico de facies sedimentarias, 2) cualitativo de la composición del sedimento mediante su lavado y levigado, 3) de las texturas y estructuras sedimentarias mediante radiografías de rayos X, 4) de las propiedades físicas del sedimento, y 5) de la composición mineralógica del sedimento. La recopilación de estos análisis permite caracterizar las turbiditas generadas por terremotos en regímenes de subida de nivel del mar (en este caso Holoceno) y en márgenes tectónicamente activos. La búsqueda de patrones que caractericen estas seismo-turbiditas tiene especial

relevancia para su diferenciación con otras turbiditas generadas por otros mecanismos en margenes tanto activos como pasivos. Además, las características de las seismo-turbiditas nos dan una idea relativa de la magnitud de un terremoto y de cómo influye la morfología de los sistemas cañón/canal turbidítico en el depósito de las turbiditas.

- El **Capítulo V, CONCLUSIONES**, resume los hallazgos más relevantes asociados a la investigación que aquí se presenta como un compendio de los 3 capítulos anteriores así como de la investigación relevante asociada que se pone de manifiesto en los anexos 1 y 2.

- El **Capítulo VI, PERSPECTIVAS DE TRABAJO FUTURAS** esboza los principales objetivos de investigaciones post-doctorales consecuencia de este trabajo de tesis.

Además de los capítulos mencionados anteriormente se han recogido en dos anexos contribuciones adicionales de la doctoranda en otros artículos relacionados con los objetivos de la investigación de esta tesis doctoral.

El **ANEXO 1** muestra la contribución científica de la doctoranda que es relevante a los objetivos principales de esta tesis en relación a la caracterización sedimentológica y cálculo de intervalos de recurrencia de seismo-turbiditas Holocenas en los márgenes de Cascadia y norte de California. Para ello se presentan 3 publicaciones:

1.) la primera publicación Goldfinger, C., Grijalva, K., Bürgmann, R., Morey, A. E., Johnson, J. E., Nelson, C. H., **Gutiérrez-Pastor, J.**, Ericsson, A., Karabanov, E., Chaytor, J. D., Patton, J., and Gràcia, E., **LATE HOLOCENE RUPTURE OF THE NORTHERN SAN ANDREAS FAULT AND POSSIBLE STRESS LINKAGE TO THE CASCADIA SUBDUCTION ZONE** publicada en la revista "Bulletin Seimological Society of America" Vol. 98, No. 2, pp. 861–889, April 2008, doi: 10.1785/0120060411, donde los registros paleosísmicos de los últimos ~ 2800 años en el margen norte de California se comparan con los de la parte sur del margen de Cascadia. En ambas áreas se estiman intervalos de recurrencia entre turbiditas muy similares (~ 200 años). También se sugiere la propagación del efecto generado por los grandes terremotos de Cascadia en el norte del margen de California, estableciéndose un modelo de ruptura relacionando los mecanismos de esfuerzo-deformación de ambos márgenes. Todos los datos de sedimentología de turbiditas generados en el contexto de esta tesis, como son los espesores de sedimento hemipelágico y la granulometría del sedimento, se han incluido en este artículo.

2.) la segunda publicación (en prensa) Nelson, C. H., Escutia, C., Goldfinger, C. Karabanov, E., and **Gutiérrez-Pastor, J.**, **EXTERNAL CONTROLS ON MODERN CLASTIC TURBIDITE SYSTEMS: THREE CASE STUDIES**, SEPM Special Publication No. 92, Copyright © 2009, SEPM (Society for Sedimentary Geology), ISBN 978-1-56576-136-0, p. xxx–xxx., analiza los factores, tales como los tectónicos, sísmicos, cambios relativos del nivel del mar y erupciones volcánicas, que controlan el desarrollo de sistemas turbidíticos recientes en los márgenes continentales de Cascadia (noroeste de EEUU), del Lago Baikal (Rusia) y del Ebro (noroeste del Mar Mediterraneo). La contribución a este artículo pone de manifiesto el control tectónico ligado a grandes terremotos (8-9 Mw) en la sedimentación de turbiditas en el margen de Subducción de Cascadia mediante el estudio sedimentológico de las seismo-turbiditas y el sedimento hemipelágico así como sus correlaciones estratigráficas, recopilando los datos necesarios

mostrados en las publicaciones de los capítulos principales de esta tesis.

3.) la tercera publicación Goldfinger, C., Nelson, C. H., Johnson, J. E., Morey, A. E., **Gutiérrez-Pastor, J.**, Karabanov, E., Eriksson, A., Gràcia, E., Dunhill, G., Patton, J., Enkin, R., Dallimore, A., Valliers, T., and the Shipboard Scientific Party, ***TURBIDITE EVENT HISTORY: METHODS AND IMPLICATIONS FOR HOLOCENE PALEOSEISMICITY OF THE CASCADIA SUBDUCTION ZONE***, USGS Professional Paper, 100 p., es una monografía del “United States Geological Survey” y que, dada su larga extensión, en este volumen de tesis doctoral solo se presenta el resumen y la referencia bibliográfica. Esta monografía resume toda la investigación realizada en cuanto a metodologías aplicadas (e.g., recuperación de testigos, batimetría, análisis de sedimento, correlaciones entre turbiditas...etc), caracterización de sistemas turbidíticos (e.g., El canal Juan de Fuca y el canal de Cascadia) y aplicación de técnicas paleosísmicas en turbiditas del margen de subducción de Cascadia y su comparación con el registro turbidítico del segmento norte de la Falla de San Andrés. Esta publicación pone de manifiesto que las turbiditas Holocenas en los márgenes de Cascadia y norte de California son indicadores reales de terremotos y que las técnicas paleosísmicas utilizadas en estos márgenes pueden ser aplicadas a otros tectónicamente activos en regímenes transgresivos

El **ANEXO 2** hace referencia a otros 3 trabajos de investigación en los que se ha participado en un estadio más inicial asociado a la temática de esta tesis.

Dos de estas publicaciones contienen los resultados preliminares de las campañas oceanográficas en los márgenes continentales de Cascadia y norte de California en los años 1999 y 2002 a bordo de los buques Melville y Roger Revelle, respectivamente y son: **1)** Goldfinger, C., Nelson, C.H., Johnson, J., and the Shipboard Scientific Party, 2003a, ***HOLOCENE EARTHQUAKE RECORDS FROM THE CASCADIA SUBDUCTION ZONE AND NORTHERN SAN ANDREAS FAULT BASED ON PRECISE DATING OF OFFSHORE TURBIDITES***: Annual Reviews of Geophysics, v. 31, p. 555–577, y **2)** Goldfinger, C., Nelson, C.H., Johnson, J.E., and the Shipboard Scientific Party, 2003b, ***DEEP-WATER TURBIDITES AS HOLOCENE EARTHQUAKE PROXIES: THE CASCADIA SUBDUCTION ZONE AND NORTHERN SAN ANDREAS FAULT SYSTEMS***: Annali Geofisica, v. 46, p. 1169–1194.

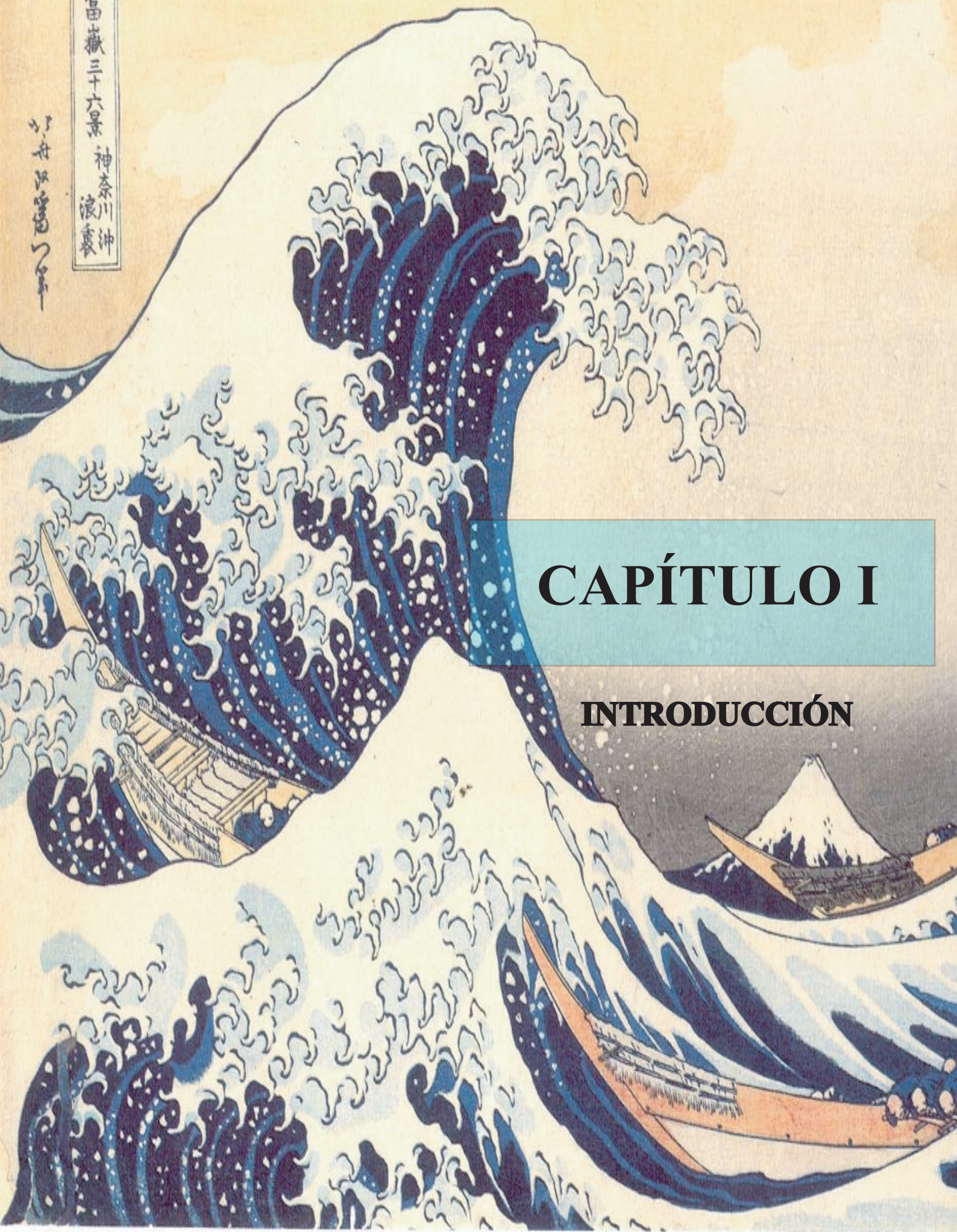
La tercera publicación **3)** Flemings, P.B., Behrmann, J.H., John, C.M., and the **Expedition 308 Scientists**, ***PROCEEDINGS OF THE INTEGRATED OCEAN DRILLING PROGRAM, VOLUME 308***, doi:10.2204/iodp.proc.308.101.2006, está relacionada con las perspectivas de trabajo futuras de la doctoranda como resultado de su participación en la Expedición 308 del Integrated Ocean Drilling Program (IODP), “Gulf of Mexico Hydrogeology” (2005). En esta publicación se presentan los resultados preliminares post-expedición y en concreto, mi contribución queda puesta de manifiesto en el estudio sedimentológico detallado de los testigos de sondeo que incluían, principalmente, niveles turbidíticos y depósitos de transportes en masa (con algunas intercalaciones de sedimento hemipelágico) en las Cuencas de Brazos Trinity y Ursa del margen pasivo del Golfo de México.

Se incluyen además otras dos publicaciones en las que se ha trabajado en otro ámbito de investigación: **1)** Escutia, C., Canon, M., and **Gutiérrez-Pastor**, ***⁴⁰AR/³⁹AR CHRONOLOGY OF DISCRETE ASH LAYERS IN THE NORTHWESTERN PACIFIC: SITES 1149 AND 1179***, 2006, <http://www-odp>.

tamu.edu/publications/185_SR/015/015.htm y 2) Escutia, C., **Gutierrez-Pastor, J.**, and Canon, M., 2008, ***PALEOENVIROMENTAL IMPLICATIONS OF TEPHRA SEIDMENTATION IN THE NORTHWESTERN PACIFIC SINCE THE LATE MIOCENE***, Geotemas (VII Congreso Geológico Español, 2008), v. 10, p. 194. La investigación abordó el estudio sedimentológico, cronológico e implicaciones paleo-ambientales y paleoclimáticas a partir del estudio de cenizas volcánicas en dos testigos de sondeo recuperados durante los Legs 185 y 191 de ODP (Ocean Drilling Program) en el noreste Pacífico y en concreto en las proximidades de la fosa Izu – Bonin y en la llanura abisal al este de Japón.

富嶽三十六景 神奈川沖
浪裏

舟は浪に揺る



CAPÍTULO I

INTRODUCCIÓN

I. INTRODUCCIÓN

ANTECEDENTES

Los depósitos turbidídicos, muy frecuentes en la base del talud y la llanura abisal de márgenes continentales, tanto activos como pasivos, han sido ampliamente investigados como indicadores de los cambios del nivel del mar, en relación con la inestabilidad del talud continental, como potenciales reservorios de hidrocarburos, y más recientemente, como indicadores de la actividad paleosísmica durante el Holoceno. Las turbiditas Holocenas depositadas en los márgenes continentales de subducción de Cascadia y norte de la falla de San Andrés, California, han sido objeto de un estudio detallado en los últimos 40 años (Figs. 1 y 2) (Nelson, 1968; 1976; Griggs, 1969; Carlson and Nelson, 1969; Griggs and Kulm, 1970; Duncan et al., 1970; Adams, 1990; Nelson et al., 2000; Goldfinger et al., 2003a; 2003b; 2007). Originalmente, la zona de subducción de Cascadia se consideró aseísmica por la falta de registros de terremotos históricos en esta área; sin embargo, evidencias claras asociables a terremotos en áreas costeras, tales como bosques rápidamente enterrados que dan lugar a zonas pantanosas, y evidencias de tsunamis, tales como niveles arenosos encontrados entre sedimentos costeros, demuestran justo lo contrario (Atwater, 1987; Nelson et al., 1995).

El estudio del origen de los terremotos ha sido estudiado y registrado en tierra por razones de prevención de daños sísmicos. Por ello, el objetivo primordial de estos estudios siempre ha radicado en estimar cada cuanto ocurren los terremotos, donde se originan y a que extensión afecta tanto en el espacio como en el tiempo. De este modo, la estimación de las mínimas frecuencias a las que ocurren los terremotos se convierte en el objetivo primordial de los estudios paleosísmicos siendo de gran repercusión social. Conociendo un registro paleosísmico bien documentado en áreas costeras, se plantea examinar la cuenca de Cascadia y el margen de California mediante nuevas técnicas paleosísmicas basadas en el análisis sedimentario, geofísico y de datación de turbiditas recuperadas a través de la extracción de testigos de sondeo del subsuelo oceánico. El estudio de las turbiditas como indicadores de terremotos en el Holoceno, nos permiten conocer la historia paleosísmica de una región tectónicamente activa para los últimos 10.000 años, en comparación al registro costero que ofrece una historia paleosísmica bastante más reciente a través de la datación radiométrica, dendrocronología y cronología del coral (Atwater y Hempl-Haley, 1997; Karlin et al., 2004). Las turbiditas se convierten, por tanto, en indicadores de terremotos y definen un mecanismo sincrónico de generación de corrientes de turbidez. Estas técnicas no recurren al afloramiento de las fallas que generan los terremotos, ya que estas están inaccesibles bajo el subsuelo oceánico pero nos permiten muestrear y correlacionar turbiditas que han sido depositadas bajo el mar sobre el suelo oceánico en diferentes sistemas turbidíticos abarcando grandes extensiones en el espacio y tiempo (cientos de kilómetros y miles de años) a lo largo del mismo margen.

Previos estudios paleosísmicos basados en el registro turbidítico han sido llevados a cabo en Cascadia (Adams, 1990; Nelson et al., 1996; 2000; Goldfinger and Nelson, 1999; Blais-Stevens and Clague, 2001; Goldfinger et al., 2003a). Del mismo modo, en lagos se han registrado turbiditas y depósitos de deslizamiento que han sido estudiados y correlacionados con terremotos históricos, como las del lago Biwa (Inouchi et al., 1996), el lago Lucerne (Schnellmann et al., 2002) y Puget Sound (Karlin and Abella, 1992; Karlin et al., 2004). En mares estrechos o confinados, como el Mediterráneo (Anastasakis and Piper, 1991; Kastens, 1984), el Mar Muerto (Niemi and Ben-Avraham, 1994), o en Taiwan (Huh et al., 2006) las turbiditas han sido interpretadas como registro de terremotos al ser originadas consecuencia de la ruptura de fallas que los generan, como el caso de la falla de Analtolia que generó corrientes de turbidez y deslizamientos en el mar de Marmara relativamente recientes (McHugh et al., 2006; Beck et al., 2007). También en el

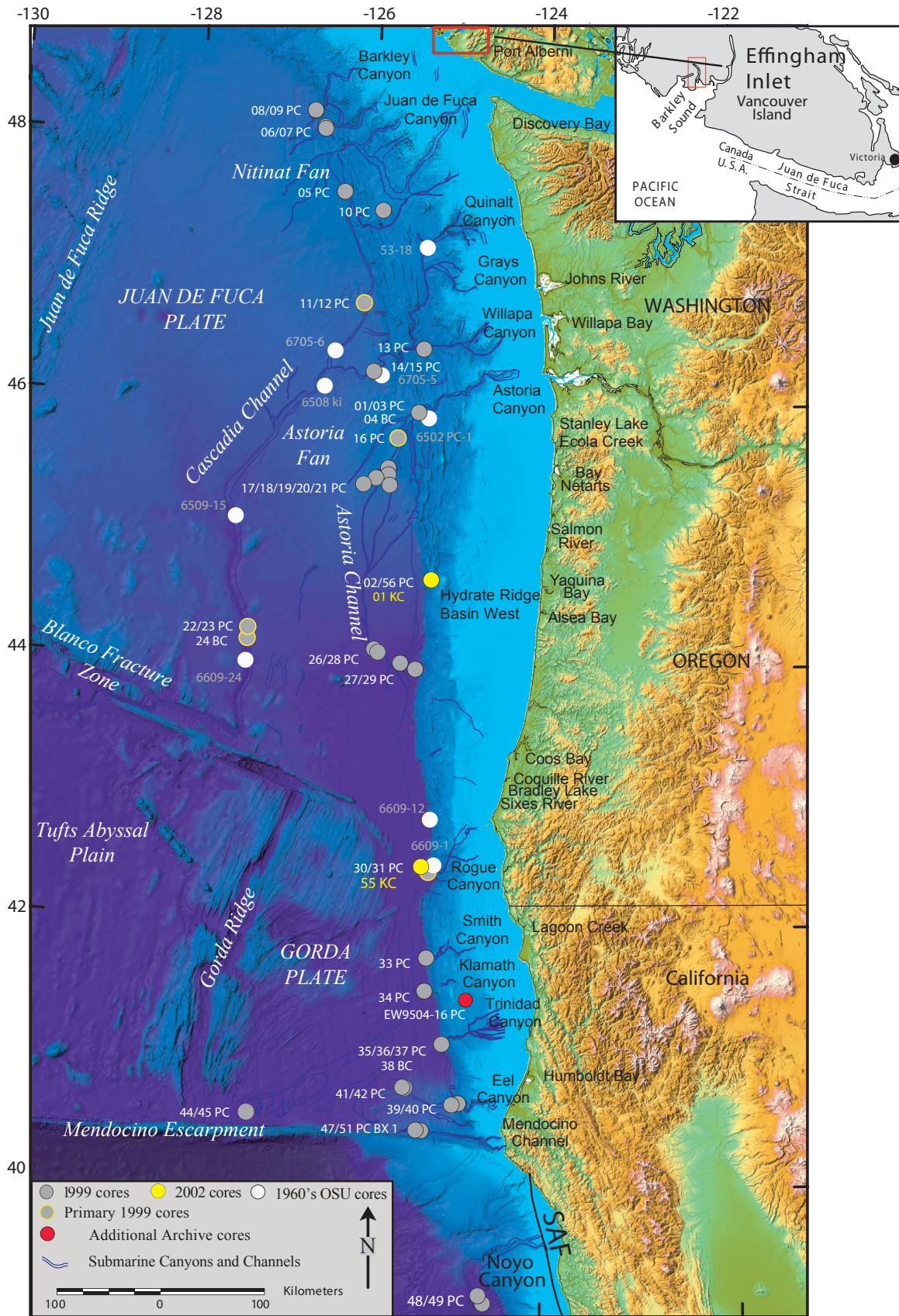


Figura 1. Margen Continental de Subducción de Cascadia: Sistemas turbidíticos y localización de testigos de sondeo (de Goldfinger et al., in press).

norte de California (Field et al., 1982; Field, 1984; Garfield et al., 1994; Goldfinger et al., 2007, 2008), el suroeste del margen Ibérico (Vizcaino et al., 2006; submitted) y en el margen de Sunda, Sumatra (Patton et al., 2007) se han registrado turbiditas correlacionadas con terremotos históricos bien conocidos. Incluso en el océano Artico (Grantz et al., 1996), se han hallado turbiditas que han sido interpretadas con un origen sísmico aunque nos se han correlacionado con una historia sísmica de la región. Los resultados de estas investigaciones sugieren que el estudio de turbiditas Holocenas es una herramienta poderosa en sismotectónica. Aunque estudios paleosísmicos han sido llevados a cabo con anterioridad, ninguno ofrece la ventaja de abarcar grandes extensiones en el espacio (cientos de kilómetros) y en el tiempo (más de 10.000 años) mediante la correlación de turbiditas desencadenadas por un mismo evento común (terremoto de elevada magnitud $\geq 8Mw$) en diferentes sistemas turbidíticos a lo largo de un margen tectónicamente activo.

En el margen de Cascadia, la correlación de las turbiditas depositadas en sistemas de cañón-canal separados entre si cientos de kilómetros a lo largo de margen y en régimen de subida de nivel del mar (siendo que clásicamente los depósitos turbidíticos son típicos en regimenes de bajo nivel del mar cuando la línea de costa está más cerca de la cabecera de los cañones submarinos), implica, por tanto, un mecanismo desencadenante que sea sincrónico, tal como un terremoto. Esta hipótesis fue inicialmente planteada por Adams (1990) al encontrar el mismo número de turbiditas (13 turbiditas) bien correlacionadas en la cuenca de Cascadia, tanto por encima como por debajo de las confluencias de canales turbidíticos y por encima de un nivel de cenizas volcánicas procedentes de un conocido evento bien datado, como es la erupción del volcán Mazama ($7627 \pm$ cal. yr B.P) que formó el actual Crater Lake, Oregón (Fig. 1 del capítulo 2) (Nelson et al., 1968; Nelson, et al., 1988; Zdanowicz et al., 1999). Para Adams (1990), este hecho demostró la sincronía de las turbiditas como consecuencia de terremotos y posteriores estudios lo corroboran (Nelson et al., 2000; Goldfinger et al., 2003a; 2003b).

OBJETIVOS

En el presente trabajo de tesis se hace una contribución, fundamentalmente sedimentológica tanto cualitativa como cuantitativa a los Proyectos de Investigación “Holocene Seismicity of the Northern San Andreas Fault Based on Precise Dating of the Turbidite Event Record” y “Holocene Seismicity of the Cascadia Subduction Zone Based on Precise Dating of the Turbidite Event Record” liderados por los Doctores Hans Nelson y Chris Goldfinger que proponen el desarrollo de una nueva estrategia analítica, sedimentológica, de datación y correlación de las secuencias de turbiditas y hemipelagitas de los márgenes continentales activos de Cascadia y norte de California con el objetivo de comprender el registro paleosísmico durante el Holoceno. La finalidad de la investigación es a) la obtención de un registro que nos permita inferir la periodicidad de los terremotos generadores de turbiditas y por tanto establecer el riesgo sísmico en un área determinada b) la obtención de un registro que permita diferenciar los riesgos geológicos (e.g. sismos, slumps) de otros mecanismos generadores de turbiditas, mediante la metodología de estudio empleada en los testigos de los márgenes de subducción de Cascadia (Oregón) y transformante (atravesado por la falla de San Andrés) del segmento norte de California.

Los objetivos específicos de la investigación recogida en esta memoria de tesis son los siguientes:

1) Desarrollo de una nueva estrategia analítica en el estudio de la cronología de secuencias de turbiditas y hemipelagitas, que consiste en:

a. Estudiar los testigos obtenidos en sistemas de dique-canal para el análisis detallado de los niveles turbidíticos y de los espesores de hemipelagitas, que permitan realizar una estimación del grado de erosión

de las secuencias de hemipelagitas.

b. Obtener la cronología de los eventos turbidíticos usando métodos complementarios: absoluto (radiométrico) y relativo (basado en la corrección del radiométrico teniendo en cuenta el sedimento hemipelagico entre turbiditas)

c. Corregir los márgenes de error de las edades obtenidas por los métodos cronológicos citados anteriormente con los valores de tasas de acumulación obtenidas a través del estudio del grado de erosión de las secuencias de hemipelagitas.

2) Determinar la frecuencia en los eventos turbidíticos, en base a las cronologías obtenidas mediante el nuevo método analítico, y su relevancia para la mitigación de riesgos geológicos mediante el estudio de secuencias turbidíticas y de hemipelagitas en dos márgenes continentales activos, norte de California y Cascadia.

3) Caracterizar sedimentológicamente y de forma detallada y multidisciplinar los eventos turbidíticos en los dos márgenes de estudio para la elaboración de una serie de criterios/patrones que nos permitan distinguir turbiditas generadas por terremotos de turbiditas generadas por otros mecanismos.

4) Sentar las bases para comparaciones futuras entre turbiditas generadas por terremotos en márgenes tectónicamente activos con turbiditas generadas por mecanismos sedimentológicos, en márgenes pasivos. Por ejemplo, durante las investigaciones post-doctorales previstas en un futuro próximo se hará la comparación con turbiditas del margen pasivo del Golfo de Méjico para realizar una modelización sedimentaria predictiva que permita la correlación de eventos turbidíticos a escala regional. Este estudio permitirá establecer diferencias y/o similitudes entre los modelos predictivos generados para las turbiditas Holocenas generadas por terremotos en los márgenes activos de Cascadia y norte de California y las generadas por otros mecanismos en el Golfo de Méjico.

MARCO GEOLÓGICO

El margen continental de Cascadia es parte de una zona de subducción en donde las placas de Gorda y Juan de Fuca se introducen bajo la Norte Americana a una velocidad de 40mm/año en el dominio marino de las costas del norte de California, Oregon y Washington (Fig. 1) (DeMets and Nixon, 1999) . El margen norte de California esta atravesado por la falla de San Andrés en su dominio marino extendiéndose paralelamente a la costa desde Point Arena hasta la triple unión de Mendocino (Fig. 2). La falla de Andrés acumula una tensión de 25mm/año lo que significa aproximadamente el 75 % de el movimiento de la placa Pacifica-Norte Americana sobre 100 Km de área (Argus and Gordon, 1991).

En la cuenca de Cascadia hay numerosos sistemas turbidíticos modernos de cañón/canal que contienen turbiditas depositadas durante el Holoceno y que desde el norte hacia el sur son, Barclay, Juan the Fuca, Quinault, Grays, Willapa, Astoria, Rogue, Smith, Klamath, Trinidad, Eel and Mendocino (Nelson et al., 2000). En este volumen de tesis el estudio sedimentológico y cronológico de los niveles turbidíticos están mas centrados en los canales de Juan de Fuca y Cascadia, y preliminarmente Willapa, por encontrarse un registro turbidítico Holoceno muy continuo y bien correlacionado entre los diferentes canales a partir de edades obtenidas por ¹⁴C (Fig. 1). La Figura 3 ilustra un ejemplo de la morfología y batimetría del sistema canal/cañón turbidítico de Willapa (Goldfineger et al., in press)

De la misma manera el margen norte de California cuenta con numerosos sistemas turbidíticos que desde el norte, empezando en el cabo Mendocino, hasta el sur, acabando en la bahía de Monterey son Gorda, Viscaino, Noyo, Arena, Gualala, Albion, Bodega Cordell, Farallon, Montara, Pioneer and Monterey (Fig.

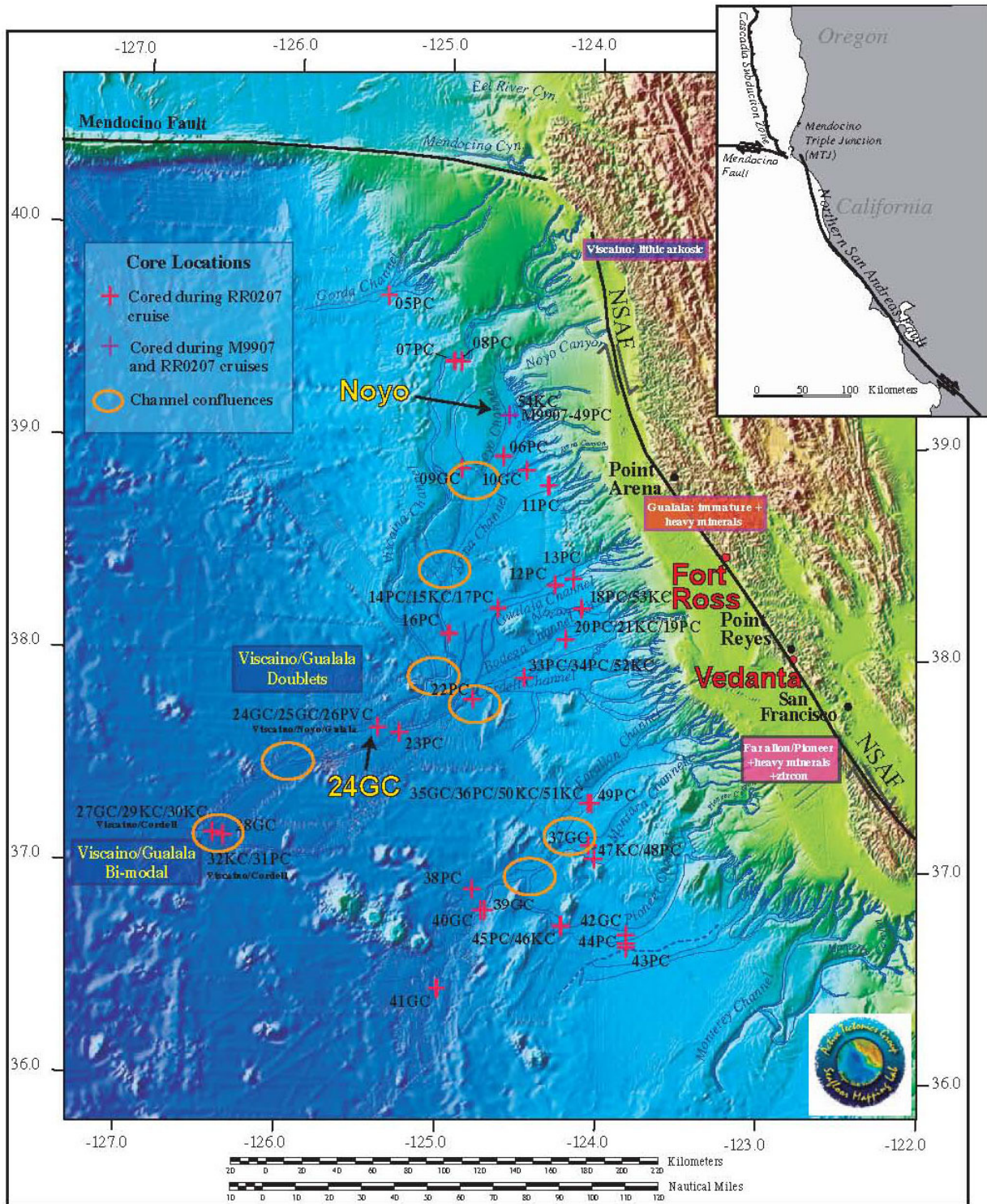


Figura 2. Margen Continental Transformante de California: Sistemas turbidíticos y localización de testigos de sondeo (de Goldfinger et al., 2007).

2) (Goldfinger et al., 2003 a, 2003b; 2007; Gutiérrez-Pastor et al., in press). En este volumen de tesis se estudian mas en detalle las turbiditas del canal de Noyo por estar directamente atravesado, a la altura del cañón, por la falla de San Andrés y por presentar un registro turbidítico muy completo y datado.

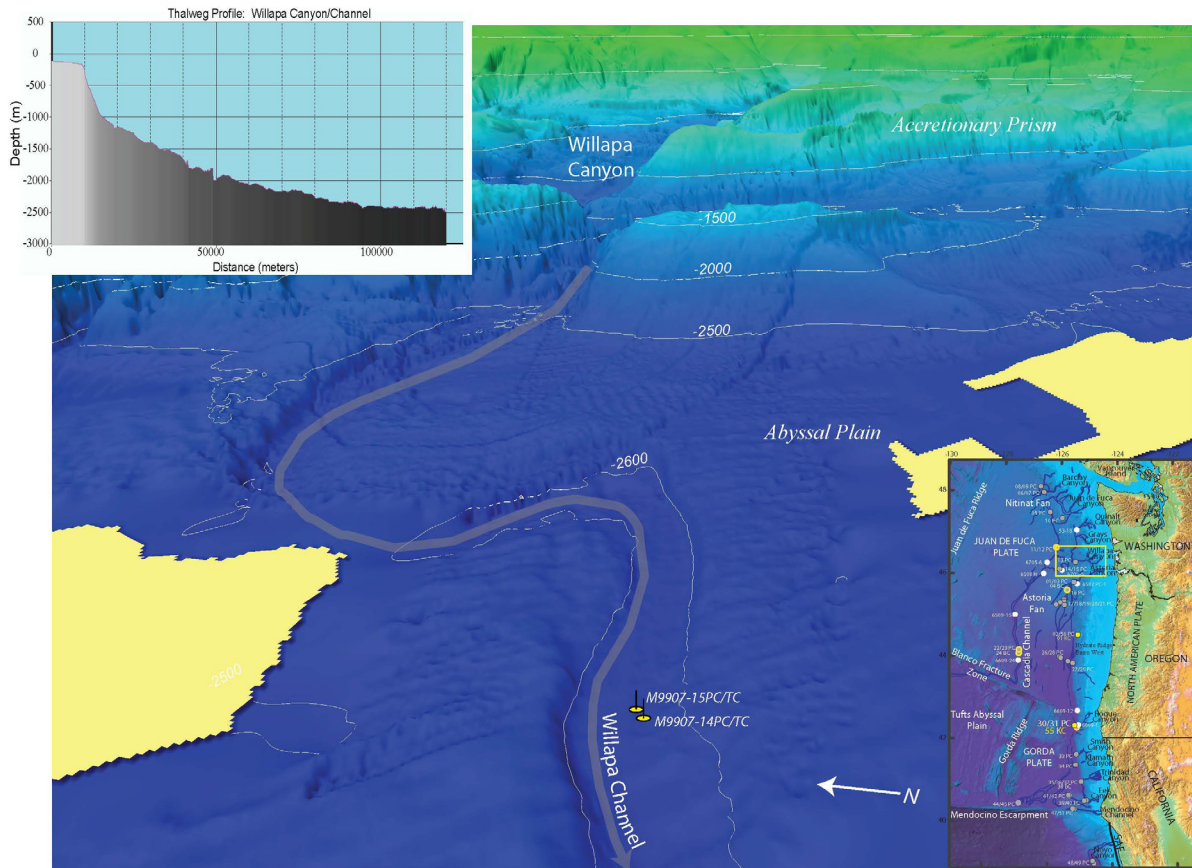


Figura 3. Batimetría, morfología y perfil topográfico del sistema cañón/canal de Willapa, al norte del margen de Cascadia (Goldfinger et al., in press).

MÉTODOS RESUMIDOS

Las metodologías utilizadas para las investigaciones recogidas en esta memoria de tesis doctoral suponen un avance novedoso en el estudio de turbiditas depositadas durante el Holoceno como indicadores de la paleosismicidad. Para este estudio se dispone de una amplia base de datos tanto sedimentológica como batimétrica junto a testigos de sondeos que han sido muestreados y que actualmente están disponibles para su estudio en la litoteca principal del Departamento de Oceanografía de la Oregon State University, Estados Unidos. En los años 1999 y 2002, se realizaron dos campañas oceanográficas en los márgenes continentales de Cascadia y norte de California, respectivamente, para estudios de paleosismicidad. En el margen de Cascadia se recuperaron 44 testigos de pistón (6-8 m), 44 testigos por gravedad (2 m) y 7 testigos de caja (50x50x50 cm) en canales turbidíticos con el potencial de registrar la historia paleosísmica de la cuenca de Cascadia durante el Holoceno (Fig. 1) (Goldfinger et al., 2003a). En el margen norte de California se recuperaron 74 testigos de pistón, gravedad y “kasten” (3 m longitud y 400 cm³) en sistemas de cañón/canal turbidíticos con el mismo objetivo que en la Cuenca de Cascadia (Goldfinger et al., 2007). La localización de los testigos de sedimento se efectuó mediante la cartografía en tiempo real de los sistemas turbidíticos usando swath bathymetry, sidescan sonar backscatter, sistema de GIS actualizado a cada momento y vuelos Fledermause. A los testigos obtenidos se les realizaron una serie de medidas continuas no destructivas utilizando el sistema Geotek, que permite obtener las propiedades físicas de densidad, velocidad y susceptibilidad magnética de los sedimentos. Los sondeos también fueron

fotografiados.

La metodología general de estudio consta de descripción litológica, muestreo para bioestratigrafía (cantidades y relaciones entre foraminíferos y radiolarios para detectar el límite entre el Pleistoceno y el Holoceno), muestreo para cronoestratigrafía (datación por ^{14}C), estratigrafía y mineralogía de las cenizas volcánicas (para detectar la ceniza del Volcán Mazama en el sedimento, que es un marcador en la zona de trabajo), mineralogía de minerales pesados (para verificar el origen del sedimento turbidítico por encima y debajo de las confluencias de canales), análisis granulométrico (para caracterizar sedimentológicamente a las turbiditas), radiografías de rayos X (para analizar la estructuras internas de las turbiditas) y por último, la integración de todos los datos para establecer la correlación de turbiditas registradas en canales turbidíticos separados cientos de kilómetros en el mismo margen continental.

La metodología e instrumentación será explicada con más en detalle en cada manuscrito (capítulos II, III, IV) que acompaña al volumen de tesis, según los objetivos concretos de cada uno. Asimismo, se puede aplicar la metodología paleosísmica y sedimentológica en los testigos de sondeos de otros márgenes continentales, incluso pasivos, como es el del Golfo de Méjico en donde la doctoranda tiene experiencia en turbiditas generadas por mecanismos sedimentológicos por la participación en la campaña 308 “Gulf of Mexico Hydrogeology” y cuyo trabajo está incluido en las perspectivas futuras.

Mi contribución al proyecto de investigación se resume con la participación como miembro de la tripulación científica en las campañas oceanográficas (antes mencionadas) a bordo de los buques Melville (1999) y del Roger Revelle (2002) en los márgenes continentales de Cascadia y norte de California, respectivamente, y con investigaciones posteriores en la Oregon State University e Instituto Andaluz de Ciencias de la Tierra. El trabajo consistió en las siguientes tareas sobre cada testigo de sondeo (Fig. 4):

EN EL BARCO

- 1) Descripción sedimentológica mediante la observación directa del testigo de sondeo
- 2) Análisis de la fracción gruesa (terrágenos y material bioclástico) con lupa de “Visu” en el sedimento hemipelágico subyacente a la turbidita para reconocimiento del límite entre los materiales turbidíticos finos y los hemipelágicos y así facilitar la toma de muestras para ^{14}C
- 3) Estudio de la micropaleontología con lupa de “Visu” para búsqueda del límite Holoceno/Pleistoceno (siendo el Holoceno rico en radiolarios y el Pleistoceno en foraminíferos) y para reconocimiento del sedimento hemipelágico bajo la base de la turbidita
- 4) fotografías de sondeos
- 5) muestreo de sedimento (~ 3 cm de sedimento hemipelágico) para datación por ^{14}C de las turbiditas
- 6) Correlación preliminar de los niveles de turbiditas mediante la integración de la sedimentología, datación, propiedades físicas y mineralogía (logs de susceptibilidad magnética y densidad).

EN EL LABORATORIO POST-CAMPAÑA

Una vez almacenados los testigos de sondeo en cámara frigorífica, se decidió aplicar a la mayoría de testigos de sondeo técnicas de radiografías de rayos-X para conocer mejor las texturas/estructuras internas del sedimento y re-tomar las medidas de las propiedades físicas del sedimento a una más alta resolución (Fig. 5). Tanto en la Universidad de Granada como en la Oregon State University (Corvallis, Oregon,) se trabajó con todo el material disponible con los siguientes objetivos desarrollados en esta memoria:

- 1) Medir con precisión el valor de espesor de sedimento hemipelágico más fiable entre turbiditas mediante la observación directa de testigos de sondeo almacenados en el “Oregon State University Core

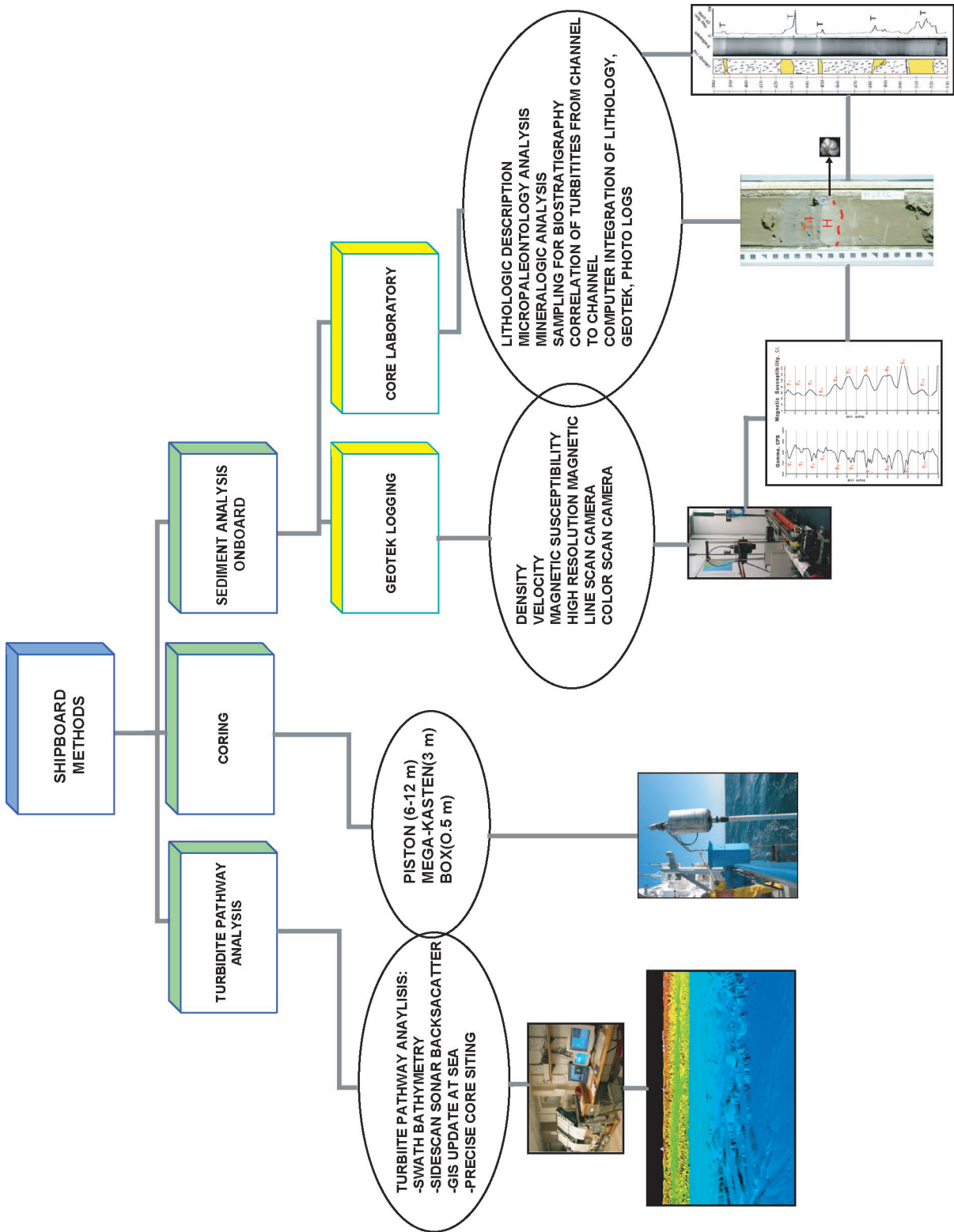


Figura 4. Técnicas paleosísmicas a bordo del Melville (1999) y Roger Revelle (2002) empleadas en los márgenes de Cascadia y norte de California.

Repository” a fin de corregir los errores provocados por la erosión de las corrientes de turbidez.

2) Corregir edades absolutas obtenidas mediante ¹⁴C con los valores de tasa de sedimentación basadas en valores acumulativos de sedimento hemipelágico entre turbiditas

3) Calcular intervalos de recurrencia entre turbiditas usando edades corregidas y compararlas con las edades absolutas.

4) Hacer un análisis granulométrico detallado de turbiditas seleccionadas en los márgenes de Cascadia y Norte de California.

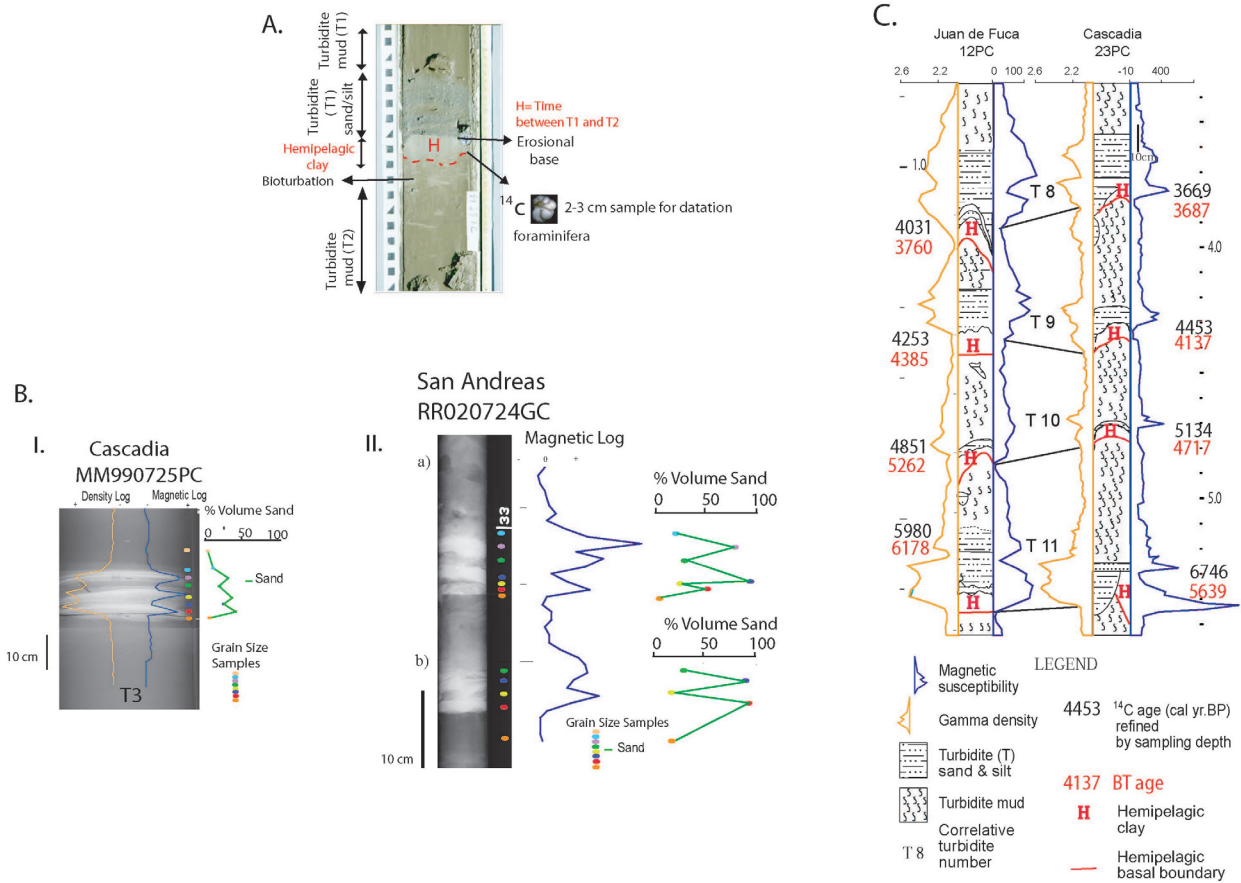


Figura 5. Técnicas paleosísmicas en laboratorios posteriores a las campañas oceanográficas: análisis sedimentológico de la turbidita y hemipelágico, análisis micropaleontológico, granulometría, radiografías de rayos X, alta resolución de las propiedades físicas del sedimento, mineralogía y correlación de turbiditas.

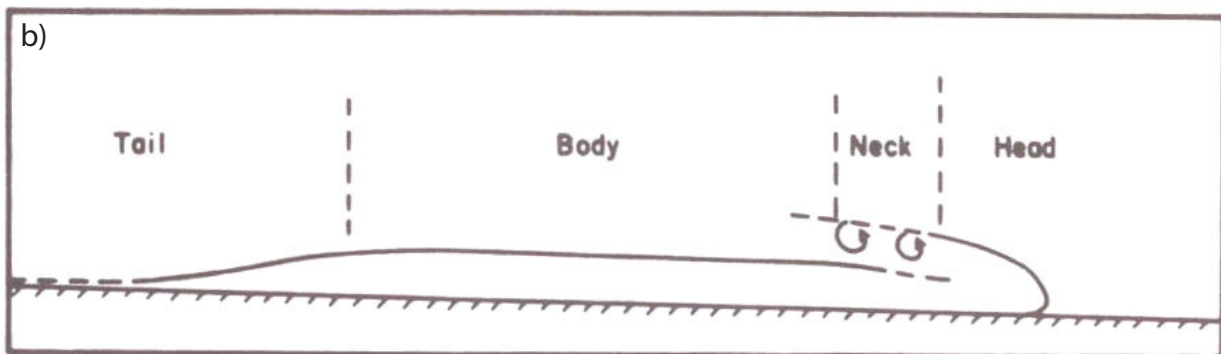
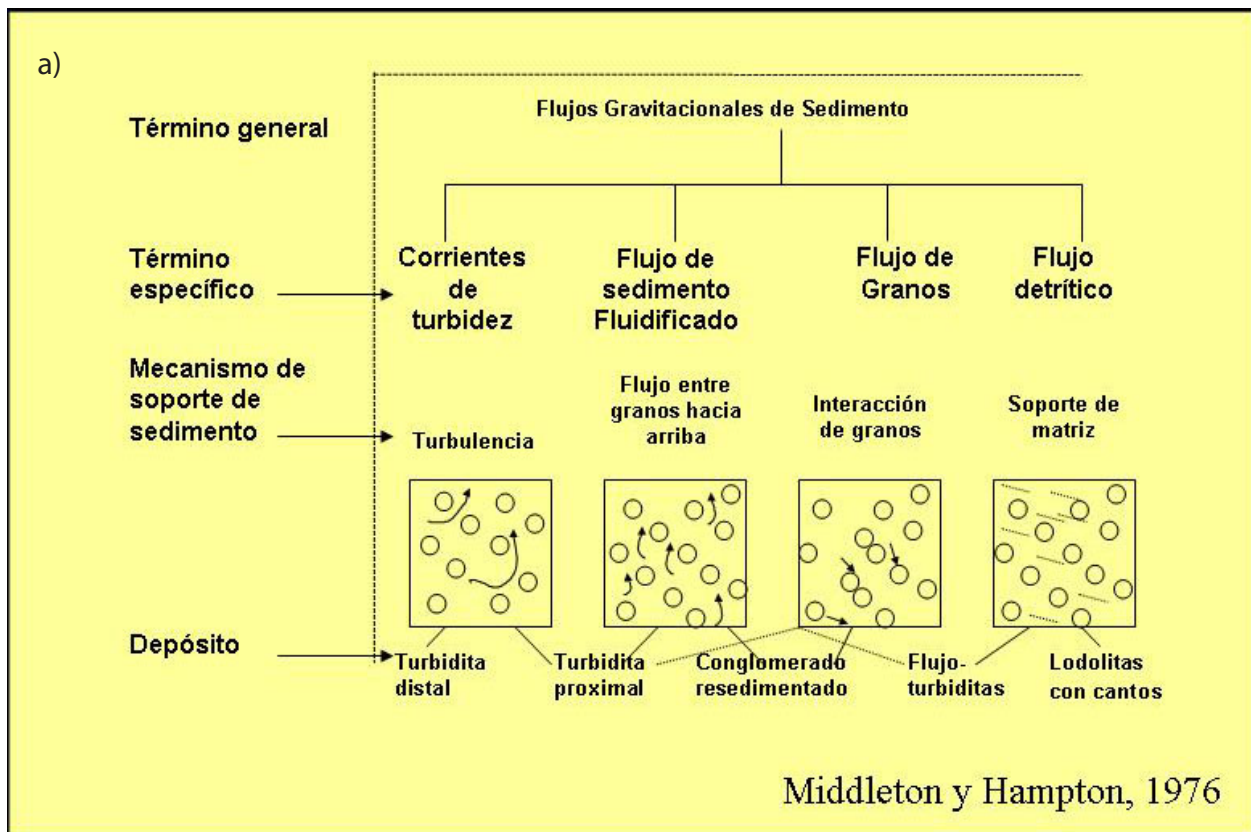
CONCEPTOS BÁSICOS

Al estar esta tesis doctoral enfocada en el estudio de turbiditas como indicadores paleosísmicos durante el Holoceno, se da paso a los conceptos siguientes:

1. CORRIENTES DE TURBIDEZ

El concepto de *corriente de turbidez* fue introducido por Kuenen and Menard (1952), como “Una corriente que fluye como consecuencia de la carga del sedimento que transporta” y más tarde por Middleton (1967) como “una corriente de densidad en la cual la diferencia de densidad entre la corriente y el ambiente fluido (comúnmente agua de mar) es debida a la presencia de sedimento dispersado”. Uno de los trabajos

clave en el estudio del transporte desde la plataforma a las llanuras abisales engloba las corrientes de turbidez en los llamados flujos de sedimentos por gravedad (Middleton y Hampton, 1976). Para Middleton y Hampton (1976) en una corriente de turbidez el sedimento es sostenido principalmente por la componente del flujo turbulento (Fig. 6a). Las corrientes de turbidez en su viaje constan de una cabeza (donde se concentra el sedimento grueso) que produce erosión en el sedimento subyacente, un cuerpo y una cola (material en fino en suspensión) (Fig. 6b) (Middleton y Hampton, 1976). Estas corrientes de turbidez se asocian normalmente a ambientes marinos, tales como abanicos submarinos profundos, aunque también son generadas en ambientes lacustre profundos (Nelson, 1976).



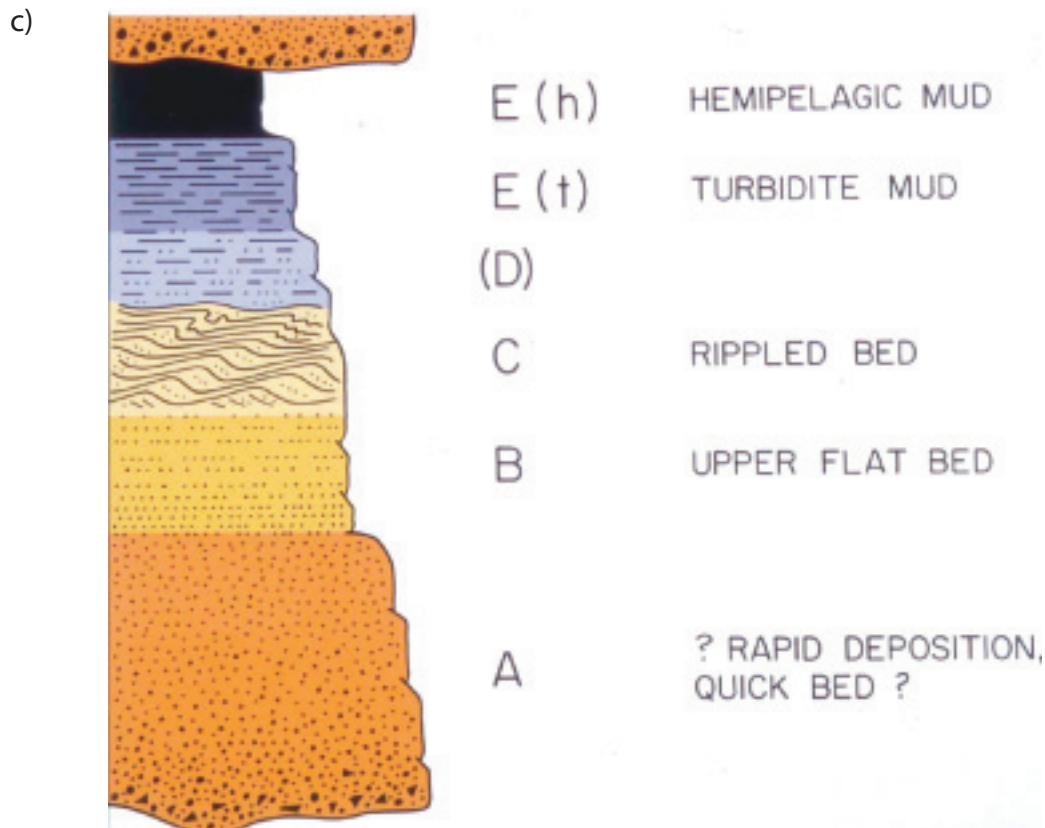


Figura 6. a) Clasificación de los flujos gravitatorios de sedimento (Middleton and Hampton, 1976). b) Corriente de Turbidez: cabeza, cuerpo y cola de una corriente de turbidez (Middleton and Hampton, 1976). c) Secuencia idealizada de una turbidita o secuencia de Bouma modificada por Middleton and Hampton, 1976.

1.1 Turbidita: Las corrientes de turbidez en su camino desde donde se originan hasta donde pierden su capacidad de transporte van depositando el sedimento en suspensión hasta generar los depósitos de turbiditas.

El depósito por gravedad de los granos de sedimento de una corriente de turbidez resulta en una gradación vertical característica de estructuras sedimentarias que caracterizan a una turbidita “típica”, o secuencia de Bouma (Fig. 6c) (Bouma, 1962). Esta secuencia de muro a techo (de mayor a menor energía) consta de arenas masivas sin estructura (Ta), laminación paralela de alta energía en arenas (Tb), ripples de arena/limo (Tc), laminación paralela de baja energía en limos (Td) y lodos de grano fino por decantación de corrientes de baja densidad (Te). La secuencia Ta, Tb, Tc y Td corresponden al cuerpo (“body”) de la turbidita y Te corresponden con la cola (“tail”) de la turbidita.

Los depósitos de turbiditas se encuentran en sistemas deposicionales tanto como niveles individuales de pocos centímetros de espesor como formando abanicos submarinos con volúmenes de millones de kilómetros cúbicos (Suter, 2006). Sea cual sea su ambiente deposicional, tienen en común que son un evento deposicional de corta duración.

1.2 Generación de corrientes de turbidez: Las corrientes de turbidez se generan por diversos mecanismos tales como tormentas, erupciones volcánicas, sobrecarga de sedimento, deslizamientos o/y slumps, flujos hiperpícnicos y terremotos (Inouchi et al., 1996, Shiki et al., 2000, Nakajima and Kanai, 2000). La figura 7 reproduce la generación de una corriente de turbidez en un tanque de laboratorio (Suter, 2006). Son *flujos hiperpícnicos* (“Hyperpycnal Flows”) aquellos que se producen como consecuencia de la diferentes densidades entre un río cargado de sedimentos en suspensión y el océano, de manera que el

río fluye sobre el fondo oceánico debido a que tiene mayor densidad (Fig. 8) (Mulder et al., 2003). En ocasiones, en áreas profundas de la cuenca oceánica, los flujos hiperpícnicos depositan turbiditas. Por ejemplo, durante el Pleistoceno cuando los hielos continentales glaciales se agruparon formando una especie dique, se colapsaron catastróficamente a modo de flujos hiperpícnicos depositando lechos de arena en la cuenca de Cascadia (Normark and Reid, 2003).



Figura 7. Tanque de experimentación para simulación de corrientes de turbidez (Posamentier y Walker, 2006).

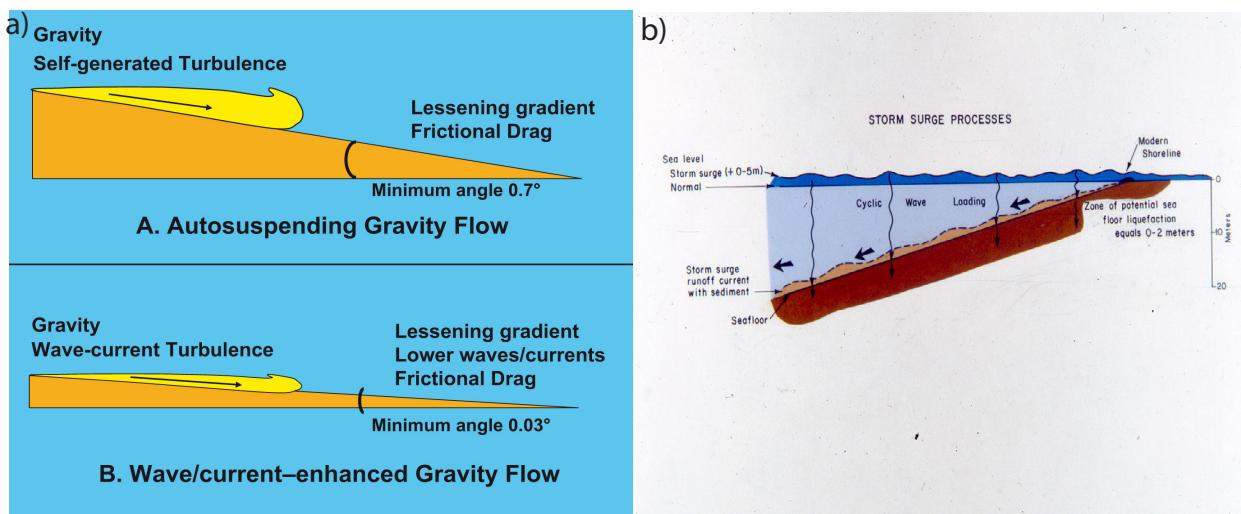


Figura 8. a) Modelo para flujos Hiperpícnicos en plataforma, que producen depósitos de turbiditas (John R. Suter, en Posamentier y Walker, 2006) b) Modelo de generación de corrientes de fondo (Nelson, 1982).

Las corrientes de turbidez originadas por mecanismos estrictamente “sedimentológicos” (e.g. por *sobrecarga de sedimento en taludes* o en regiones con energía de *tormentas* alta, tales como las cabeceras de los cañones submarinos y frentes de lóbulos deltaicos) generalmente ocurren en regiones de rápida sedimentación y durante regímenes de bajo nivel del mar cuando la línea de costa está próxima a las cabeceras de los cañones aumentando la inestabilidad del sedimento (e.g., como es el caso del Pleistoceno) (Piper and Normark, 1983; Reimnitz, 1971).

En periodos de subida del nivel del mar (e.g. el Holoceno), la generación de las corrientes de turbidez por

mecanismos sedimentológicos se ve reducida, por tanto, los *terremotos* se convierten en buenos candidatos como procesos desencadenantes del transporte de sedimento y depósito como turbiditas. Además, las corrientes de turbidez generadas por un evento “instantáneo” como es un terremoto, se caracterizan por ser de baja frecuencia (cada ~100-1000 años) y por depositarse en amplias regiones abisales, como si una manta de sedimento recubriese el fondo oceánico. Tormentas ciclónicas con velocidades mayores a 300 km/h e inundaciones causadas por el fenómeno NIÑO, el cual ocurre con frecuencia de décadas, no han depositado arenas turbidíticas en la cuenca de Cascadia o en el margen norte de California (Nelson et al., 2000, Puig et al., 2004 Goldfinger et al., in press).

2. CORRIENTES DE FONDO (BOTTOM CURRENTS):

Son flujos de agua que re-trabajan e incorporan el sedimento a su paso por el fondo oceánico(Fig. 8b).

2.1 Corrientes de fondo por Tormentas (Storm Surge Bottom Currents): Son corrientes de flujo y reflujos sobre el lecho marino que dan lugar a los depósitos de *Tempestitas*. A diferencia de las turbiditas, las tempestitas se caracterizan por ser típicas de ambientes someros de progradación de deltas, gradación normal, estructuras de “hummocky”, ausencia de la parte basal de la secuencia de Bouma y fauna proximal (Fig. 9a). Las tormentas generan *Arenas gradadas de plataforma* (“Shelf graded sands”) que tienen unas características muy similares a la secuencia típica de una turbidita (Nelson et al., 1982) (*Mimic Turbidites*) (Fig. 9b). En ocasiones es difícil distinguir turbiditas proximales de las tempestitas, aunque existen diferencias como consecuencia de los diferentes mecanismos que las producen (Fig.10). Se especula que depósitos similares a las tempestitas son generados por flujos hiperpícnicos, pero esta afirmación no está

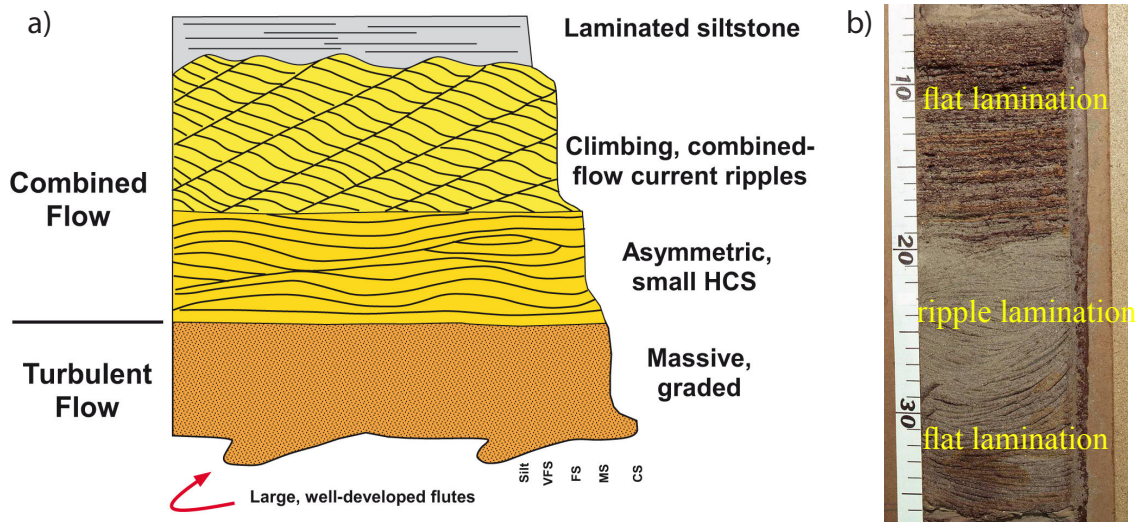


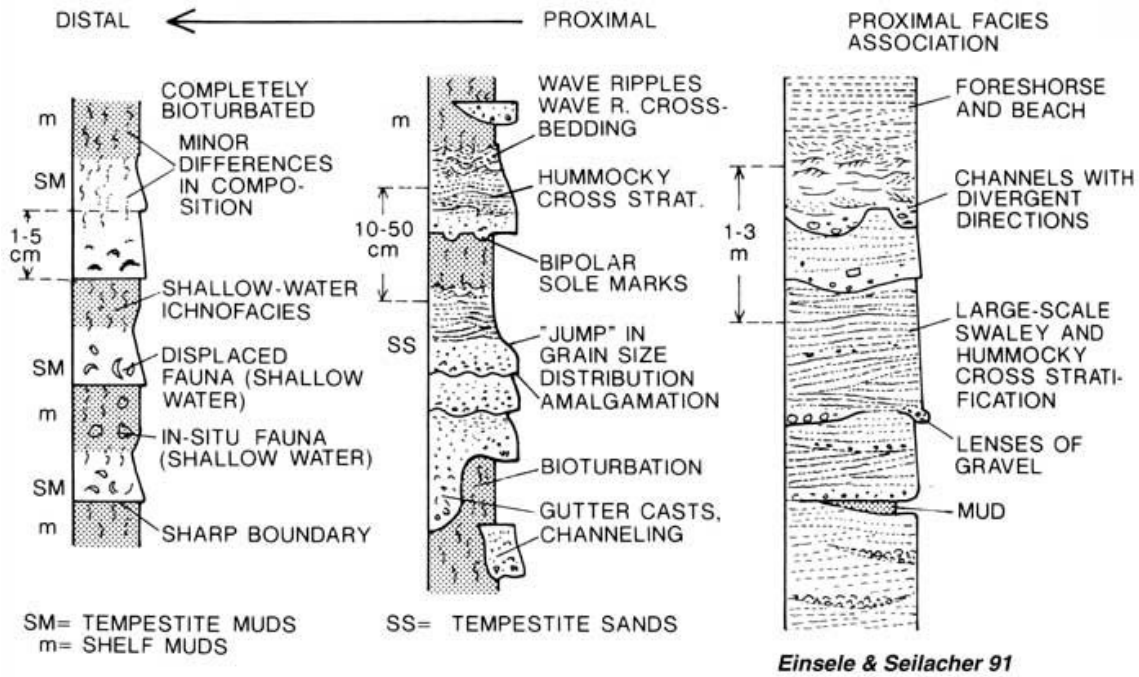
Figura 9. a) Secuencia idealizada de tempestitas (John R. Suter en Posamentier y Walker, 2006) b) Fotografía de testigo de una tempestita (Nelson, 1982).

demostrada de manera contundente.

3. PALEOSISMICIDAD:

Es el estudio de la sismicidad a una extensa escala de tiempo (hasta miles de años) mediante indicadores

TEMPESTITES



TURBIDITES

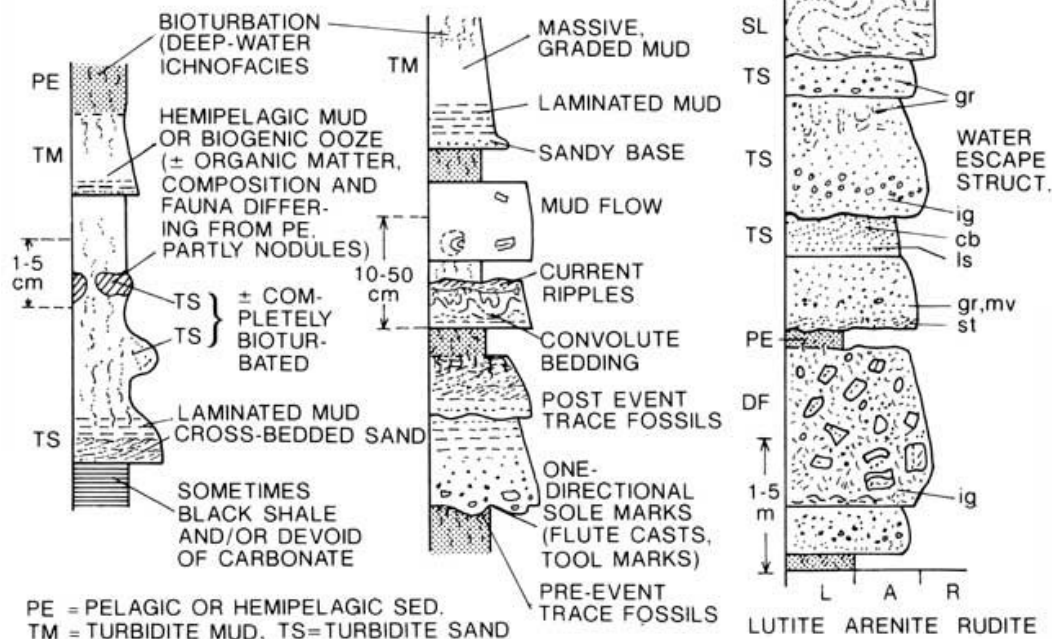


Figura 10. Comparativa de secuencias de turbiditas vs tempestitas (Einsele y Seilacher, 1991).

en el registro sedimentario (e.g. características de depósito o propiedades físicas del sedimento) en márgenes tectónicamente activos (e.g. de subducción, ligado a de fallas transformantes). Hay estudios de paleosismicidad marina que hacen una cartografía de fallas sub-aflorantes y aflorantes en el lecho marino.

3.1 Tierra (Onshore):

Subsidencia Co-sísmica: Rápida subsidencia costera tras un terremoto de elevada magnitud que genera Tsunamis y que es reconocible a través del rápido enterramiento de bosques por la invasión de la Tsunami

generando áreas pantanosas (Fig. 11) (Atwater, 1987; Nelson et al. 1995; Satake et al., 1996; Atwater and Hemphill-Halley, 1997; Kelsey, et al., 2002).

Arenas de Tsunami: Depósitos de olas de Tsunami en zonas costeras de un margen continental (Fig. 12) (Nelson et al., 1995, Satake et al., 1996, Atwater and Hemphill-Halley, 1997, Kelsey, et al., 2002).

3.2. Mar (Offshore):

Seismo-Turbiditas: Turbiditas por cuyas características sedimentarias y propiedades físicas son

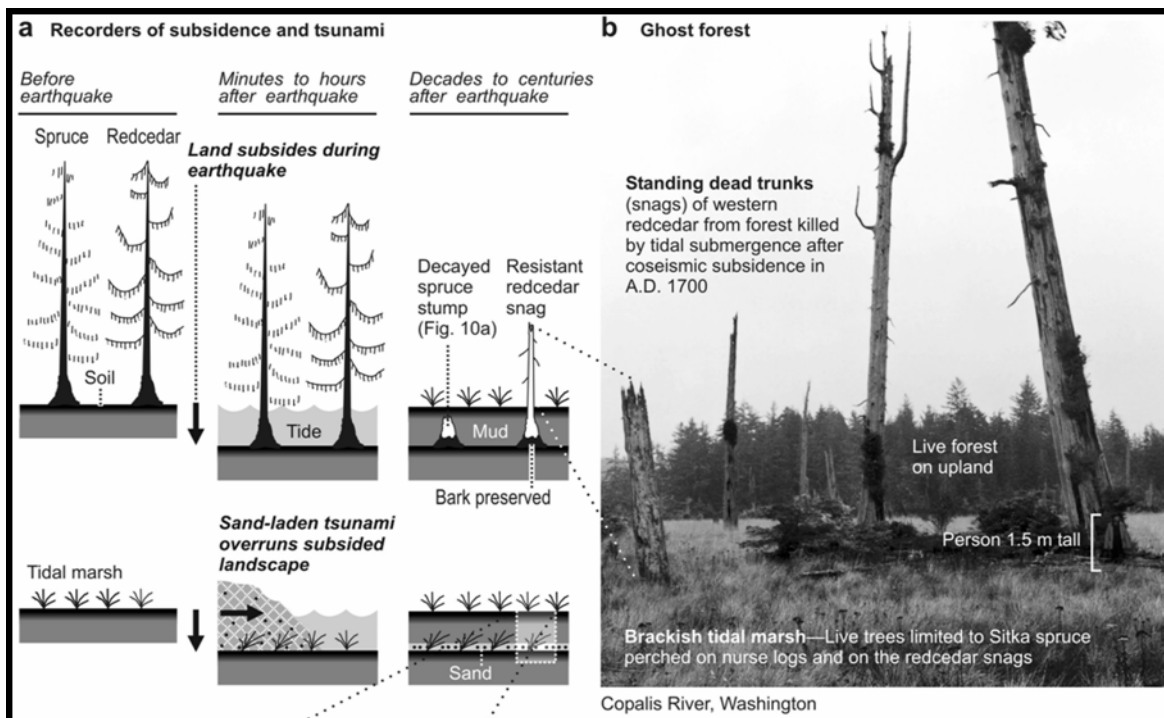
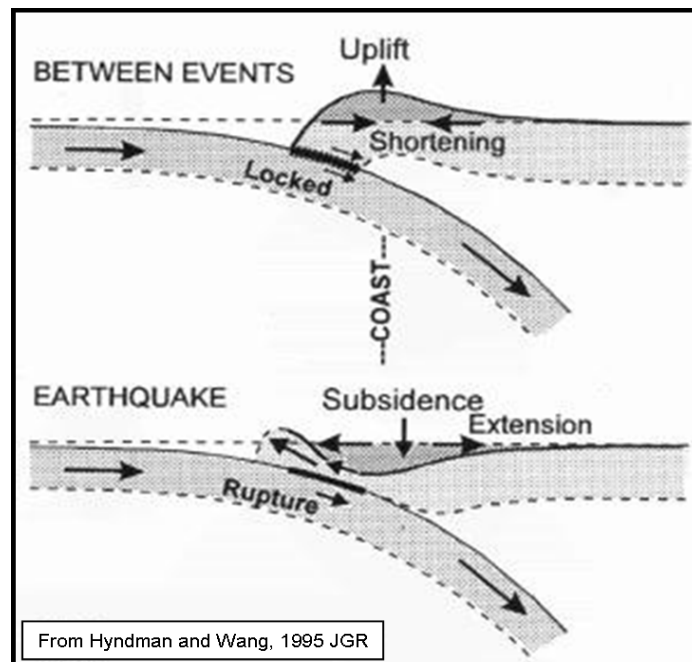


Figura 11. a) Relación esfuerzo-deformación en una zona de subducción antes y después de un terremoto. b) Efectos de la subsidencia co-sísmica: el enterramiento de bosques por la ola de Tsunami genera áreas pantanosas que los salinizan, y por tanto los destruyen (Atwater y Hemphill-Halley, 1997).

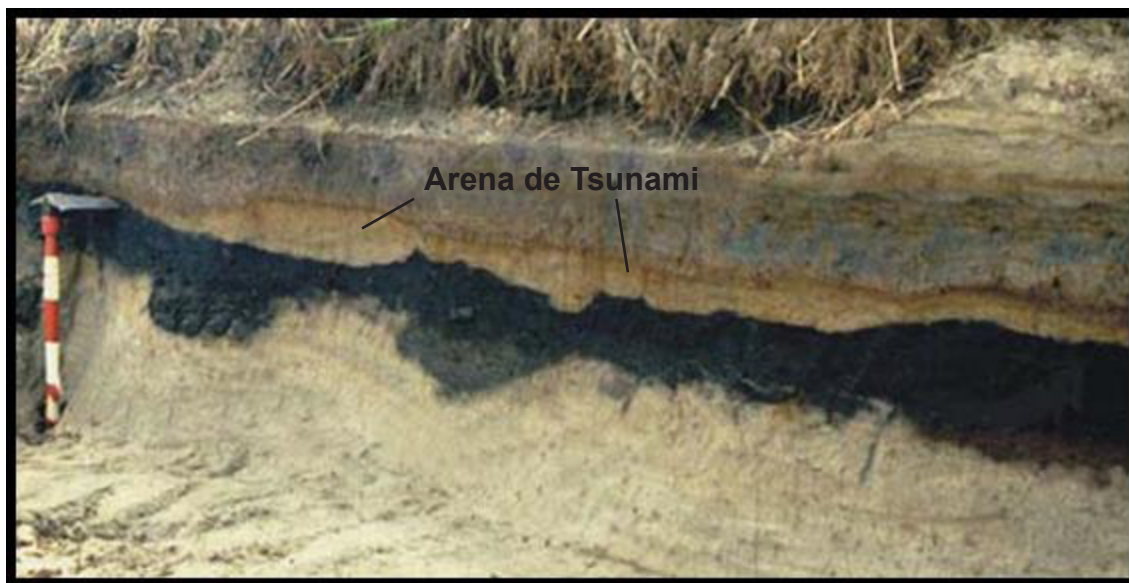


Figura 12. Arena de Tsunami en el río Salmon, Oregon (foto por Allan Nelson, USGS).

atribuidas a ser generadas por terremotos. Se asume que estas turbiditas se depositan por un mecanismo sincrónico, un terremoto de elevada magnitud (8-9Mw), por estar bien correlacionadas entre diferentes sistemas de cañón y canal a lo largo cientos de kilómetros de un margen tectónicamente activo y en régimen de alto nivel del mar. Previos estudios y nuestro trabajo demuestran que la mayoría de las seismo-turbiditas están formadas por múltiples pulsos de arena y limo cada uno asociado a las distintas mineralogías de los cañones tributarios de donde proceden (Fig. 5).

Sedimentación hemipelágica: Entre los niveles de turbiditas en ambientes profundos se produce la *Sedimentación hemipelágica* que genera un depósito continuado partícula a partícula, desde la columna de agua al fondo oceánico, de finos granos de material terrígeno procedente del continente y micro-fauna plantónica y bentónica (Fig. 5).

Tsunamitas: Hay que distinguir las arenas de Tsunami definidas en el apartado previo de las llamadas *Tsunamitas*, que se definen como turbiditas depositadas por olas de Tsunami. Esta creencia de que Tsunamis generan turbiditas no ha sido demostrada y claras evidencias en la cuenca Cascadia demuestran lo contrario. Una ola de Tsunami depositaría turbiditas a lo largo de un margen, paralelamente a la costa tanto en canales y cañones como en áreas entre canales. Sin embargo, grandes Tsunamis generados por grandes terremotos no han depositado turbiditas en estas zonas entre canales, como el caso del gran terremoto de Alaska (1964) de Mw 9 que ocasionó un Tsunami hasta el margen de Cascadia (Nelson et al., 2000; Goldfinger et al., in press).

REFERENCIAS

- Adams, J., 1990, Paleoseismicity of the Cascadia Subduction Zone: evidence from turbidites off the Oregon-Washington margin: *Tectonics*, v. 9, p. 569-583.
- Anastasakis, G.C., and Piper, D.J.W., 1991, The character of seismo-turbidites in the S-1 sapropel, Zakynthos and Strofadhres basins, Greece: *Sedimentology*, v. 38, p. 717-733.

- Argus, D.F., and Gordon, R.G., 1991, Current Sierra Nevada-North America motion from very long baseline interferometry: Implications for the kinematics of the western United States: *Geology*, v. 19, p. 1085-1019.
- Atwater, B.F., 1987, Evidence for great Holocene earthquakes along the outer coast of Washington State: *Science*, v. 236, p. 942-944.
- Atwater, B.F., and Hemphill-Haley, E., 1997, Recurrence intervals for great earthquakes of the past 3500 years at northeastern Willapa Bay, Washington: U.S. Geological Survey Professional Paper 1576, 108 p.
- Beck, C., Mercier de Lépinay, B., Schneider, J.-L., Cremer, M., Çagatay, N., Wendenbaum, E., Boutareaud, S., Ménot, G., Schmidt, S., Weber, O., Eris, K., Armijo, R., Meyer, B., Pondard, N., Gutscher, M.-A., Turon, J.L., Labeyrie, L., Cortijo, E., Gallet, Y., Bouquerel, H., Gorur, N., Gervais, A., Castera, M.H., Londeix, L., de Rességuier, A., and Jaouen, A., 2007, Late Quaternary co-seismic sedimentation in the Sea of Marmara's deep basins: *Sedimentary Geology*, v. 199, p. 65-89.
- Blais-Stevens, A. and Clague, J.J., 2001, Paleoseismic signature in late Holocene sediment cores from Saanich Inlet, British Columbia: *Marine Geology*, v.175, p. 131-148.
- Bouma, A. H., 1962, *Sedimentology of some Flysch Deposits*, Elsevier, Amsterdam, 168 p.
- Carlson, P.R., and Nelson, C.H., 1969, Sediments and sedimentary structures of Astoria Canyon-Fan system: *Journal of Sedimentary Petrology*, v. 39, no. 4, p. 1269-1282.
- DeMets, C. and Dixon, T.H., 1999, New kinematic models for Pacific-North America motion from 3 Ma to present; I, evidence for steady motion and biases in the NUVEL-1A model: *Geophysical Research Letters*, v. 26, p. 1921-1924.
- Duncan, J.R., Fowler, G.A., and Kulm, L.D., 1970, Planktonic Foraminiferan-Radiolarian ratios and Holocene-Late Pleistocene deep-sea stratigraphy off Oregon: *Geological Society of America Bulletin*, v. 81, p. 561-566.
- Einsele, G. and Seilacher, A., 1991. Distinction of tempestites and turbidites. In: Einsele, G., Ricken, W. and Seilacher, A., Editors, 1991. *Cycles and Events in Stratigraphy*, Springer, Berlin, p. 377-382.
- Field, M.E., Gardner, J.V., Jennings, A.E., and Edwards, B.D., 1982, Earthquake-induced sediment failures on a 0.25 degree slope: Klamath River Delta, California: *Geology*, v. 10, p. 542-546.
- Field, M.E., 1984, The Submarine Landslide of 1980 off Northern California: U.S. Geological Survey, Circular 938, p. 65-72.
- Garfield, N., Rago, T.A., Schnebele, K.J., and Collins, C.A., 1994, Evidence of a turbidity current in Monterey Submarine Canyon associated with the 1989 Loma Prieta earthquake: *Continental Shelf Research*, v. 14, no. 6, p. 673-686.
- Goldfinger, C., Grijalva, K., Bürgmann, R., Morey, A. E., Johnson, J. E., Nelson, C. H., Gutiérrez-Pastor, J., Ericsson, A., Karabanov, E., Chaytor, J. D., Patton, J., and Gràcia, E., 2008, Late Holocene Rupture of the Northern San Andreas Fault and Possible Stress Linkage to the Cascadia Subduction Zone, *Earth Bulletin of the Seismological Society of America*, v. 98, No. 2, p. 861–889, doi: 10.1785/0120060411
- Goldfinger, C., Morey, A., Nelson, C.H., Gutierrez-Pastor, J., Jonson, J.E., Karabanov, E., Chaytor, J., and the Shipboard Scientific Party, 2007, Rupture Lengths and Temporal History of Significant Earthquakes on the Offshore and North coast Segments of the Northern San Andreas, *Earth and Planetary Science Letters*, v. 254, p. 9-27.
- Goldfinger, C., and Nelson, C.H., 1999, Holocene Recurrence of Cascadia Great Earthquakes based on the

- Turbidite Event Record: EOS, Transactions of the American Geophysical Union, v. 80, p. 1024.
- Goldfinger, C., Nelson, C.H., and Johnson, J., 2003a, Holocene Earthquake Records From the Cascadia Subduction Zone and Northern San Andreas Fault Based on Precise Dating of Offshore Turbidites, Annual Reviews of Geophysics: v. 31, p. 555-577.
- Goldfinger, C., Nelson, C.H., and Johnson, J.E., 2003b, Deep-Water Turbidites as Holocene Earthquake Proxies: The Cascadia Subduction Zone and Northern San Andreas Fault Systems: *Annali Geofisica*: v. 46, p. 1169-1194.
- Goldfinger, C., Nelson, C. H., Johnson, J. E., Morey, A. E., Gutiérrez-Pastor, J., Karabanov, E., Eriksson, A., Patton, J. Chaytor, J. D., Patton, J., Dallimore A., Gràcia, E., and the Shipboard Scientific Party, in press, Turbidite Event History: Methods and Implications for Holocene Paleoseismicity of the Cascadia Subduction Zone, USGS Professional Paper.
- Grantz, A., Phillips, R.L., Mullen, M.W., Starratt, S.W., Jones, G.A., Naidu, S.S., and Finney, B.P., 1996, Character, paleoenvironment, rate of accumulation, and evidence for seismic triggering of Holocene turbidites, Canada abyssal plain, Arctic Ocean: *Marine Geology*, v. 133, p. 51-73.
- Griggs, G.B., 1969, Cascadia Channel: The anatomy of a deep sea channel [Ph.D. thesis], Oregon State University, Corvallis, OR, 183 p.
- Griggs, G.B., and Kulm, L.D., 1970, Sedimentation in Cascadia Deep-Sea Channel: *Geological Society of America Bulletin*, v. 81, 1361-1384.
- Gutierrez-Pastor, J., Nelson, C.H., Goldfinger, C., Johnson, J. E., Escutia, C., Eriksson, A., Morey, A. E., and the Shipboard Scientific Party, *in press*, Earthquake Control of Holocene Turbidite Frequency confirmed by Hemipelagic Sedimentation Chronology on the Cascadia and Northern California Active Continental Margins, in *External Controls on Deepwater Depositional Systems*: B. Kneller, W. McCaffrey and O. J. Martinsen Eds., SEPM Special publication, v. 92.
- Huh, C.-A., Su, C.-C., Wang, C.-H., Lee, S.-Y., and Lin, I.-T., 2006, Sedimentation in the Southern Okinawa Trough -- Rates, turbidites and a sediment budget: *Marine Geology*, v. 231, p. 129-139.
- Inouchi, Y., Kinugasa, Y., Kumon, F., Nakano, S., Yasumatsu, S., and Shiki, T., 1996, Turbidites as records of intense palaeoearthquakes in Lake Biwa, Japan: *Sed. Geol.*, v. 104, p. 117-125.
- Karlin, R.C., and Abella, S.E.B., 1992, Paleoearthquakes in the Puget Sound region recorded in sediments from Lake Washington, U.S.A.: *Science*, v. 258, p. 1617-1620.
- Karlin, R.E., Holmes, M., Abella, S.E.B., and Sylwester, R., 2004, Holocene landslides and a 3500-year record of Pacific Northwest earthquakes from sediments in Lake Washington: *Geological Society of America Bulletin*, v. 116, p. 94-108.
- Kastens, K.A., 1984, Earthquakes as a triggering mechanism for debris flows and turbidites on the Calabrian Ridge: *Marine Geology*, v. 55, p. 13-33.
- Kelsey, H. M., Witter, R. C. and Hemphill-Haley, E., 2002, Plate-boundary earthquakes and tsunamis of the past 5,500 yr, Sixes River estuary, southern Oregon, *Geological Society of America Bulletin*, v. 114, p. 298-314.
- Kuenen, Ph.H., and Menard, H.W., 1952, Turbidity currents, graded and nongraded deposits. *Journal of Sedimentary Petrology*, v. 22, p. 83-96.
- McHugh, C.M.G., Seeber, L., Cormier, M.-H., Dutton, J., Cagatay, N., Polonia, A., Ryan, W.B.F., and Gorur, N., 2006, Submarine earthquake geology along the North Anatolia Fault in the Marmara Sea, Turkey: A model for transform basin sedimentation: *Earth and Planetary Science Letters*, v. 248, p. 661-

684.

- Middleton, G.V., 1967, Experiments on density and turbidity currents. III Deposition of sediments: Canadian Journal of Earth Sciences, v. 4, p. 475-505.
- Middleton, G.V., and Hampton, M.A., 1976, Subaqueous sediment transport and deposition by sediment gravity flows, in Stanley, D. G., and Swift, D. J., eds., Marine Sediment Transport and Environmental Management: New York, John Wiley, p. 197-217.
- Mulder, T., Syvitski, J. P. M., Migeon, S., Faugeres, J. C., and Savoye, B., 2003, Marine hyperpycnal flows; initiation, behavior and related deposits; a review: Turbidites; models and problems, v. 20, no. 6-8, p. 861-882.
- Nakajima T, and Kanai, Y. 2000. Sedimentary features of seismoturbidites triggered by the 1983 and older historical earthquakes in the eastern margin of the Japan Sea: Sedimentary Geology, v. 135, p. 1-19.
- Nelson, A.R., and Peronius, S.F., 1996, Great earthquake potential in Oregon and Washington - an overview of recent coastal geologic studies and their bearing on segmentation of Holocene ruptures, central Cascadia Subduction zone; in Assessing Earthquake Hazards and Reducing Risk in the Pacific Northwest, Roger, A. M., Walsh, T. J., Kockelman, W. J., and Priest, G. R., eds., USGS Professional Paper 1560, p. 91-114.
- Nelson, C.H., 1968, Marine Geology of Astoria Deep-Sea Fan: Ph.D. Thesis, Corvallis, Oregon State University, 289 p.
- Nelson, C.H., 1976, Late Pleistocene and Holocene depositional trends, processes, and history of Astoria Deep-Sea Fan, northeast Pacific: Marine Geology, v. 20, p. 129-173.
- Nelson, C.H., 1982, Modern shallow-water graded sand layers from storm surges a mimic of Bouma sequences and turbidite systems, Journal of Sedimentary Petrology, v. 52, p. 537-545.
- Nelson, C.H., Carlson, P. R., and Bacon, C. R., 1988, The Mt. Mazama climatic eruption (7626 B.P.) and resulting convulsive sedimentation on the continent, ocean basin, and Crater lake caldera floor in Clifton, H. E., ed., Sedimentologic Consequences of Convulsive Geologic Events: Geological Society of America Special Paper 229, p. 37-56.
- Nelson, C.H., Goldfinger, C., Johnson, J.E., and Dunhill, G., 2000, Variation of Modern Turbidite Systems Along the Subduction Zone Margin of Cascadia Basin and Implications for Turbidite Reservoir Beds, in Weimer, P.W., Nelson, C. H. et al., eds., Deep-water Reservoirs of the World, Gulf Coast Section Society of Economic Paleontologists and Mineralogists Foundation 20 Annual Research Conference, p.714-738.
- Nelson, C.H., Karabanov, E.B., and Colman, S.M., 1995, Late Quaternary Lake Baikal turbidite systems, Russia: in Pickering, K.T., Lucchi, F.R., Smith, R., Hiscott, R.N., Kenyon, N. (eds.): An Atlas of Deep-Water Environments, Chapman and Hall, London, p. 29-33.
- Nelson, C.H., Kulm, L. D., Carlson, P. R., and Duncan, J. R., 1968, Mazama ash in the northeastern Pacific: Science, v. 161, p. 47-49.
- Niemi, T.M., and Ben-Avraham, Z., 1994, Evidence for Jericho earthquakes from slumped sediments of the Jordan River delta in the Dead Sea: Geology, v. 22, p. 395-398.
- Normark, W.R., and Reid, J.A., 2003, Extensive deposits on the Pacific Plate from late Pleistocene North American glacial lake outbursts: Journal of Geology, v. 111, p. 617-637.
- Patton, J.R., Goldfinger, C., Morey, A., Wynn, R.B., Stoner, J., Ikehara, K., Hanifa, U., Djadjadihardja,

- Y.S., Ladage, S., Viscaino, A., and Gracia, E., 2007, Possible Earthquake Generated Turbidites along the Sumatra Margin *Eos Trans. AGU*, v. 88, p. Fall Meet. Suppl., Abstract S24A-05.
- Piper, D.J.W., and Normak, W.R., 1983, Turbidite depositional patterns and flow characteristics; navy Submarine Fan, California Boreland: *Sedimentology*, v. 30, p. 681-694.
- Prentice, C.S., Merritts, D.J., Beutner, E.C., Bodin, P., Schill, A., and Muller, J.R., 1999, Northern San Andreas fault near Shelter Cove, California: *Geological Soc. of America Bulletin*, v. 111, p. 512-523.
- Puig, P., Ogston, A.S., Mullenbach, B.L., Nittrouer, C.A., Parsons, J.D., and Sternberg, R. W., 2004, Storm-induced sediment gravity flows at the head of the Eel submarine canyon, northern California margin: *Journal of Geophysical Research*, v. 109, p. C03019
- Reimnitz, E., 1971, Surf-beat origin for pulsating bottom currents in Rio Balsas Submarine Canyon, Mexico: *Geol. Soc. America Bull.*, v. 82, p. 81-90.
- Satake, K., Shimazaki, K., Tsuji, Y., and Ueda, K., 1996, Time and size of a giant earthquake in Cascadia inferred from Japanese tsunami records of January, 1700: *Nature*, v. 379, p. 246-249.
- Schnellmann, M., Anselmetti, F.S., Giardini, D., and Ward, S.N., 2002, Prehistoric earthquake history revealed by lacustrine slump deposits: *Geology*, v. 30, p. 1131-1134.
- Shiki, T., Kumon, F., Inouchi, Y., Kontani, Y., Sakamoto, T., Tateishi, M., Matsubara, H. and Fukuyama, K., 2000, Sedimentary features of the seismo-turbidites, Lake Biwa, Japan, *Sedimentary Geology*, v. 135, p. 37-50.
- Suter, J. R., 2006, Facies Model Revisited: Clastic Shelves, in *Facies Model revisited* : H. W., Posamentier and R. G., Walker Eds., v. 84, p. 339-397.
- Vizcaino, A., Gràcia, E., Escutia, C., Asiolic, A., Garcia-Orellanad, J., Pallàse, R., Lebreiro, S., and Goldfinger, C., in review, Holocene earthquake record offshore Portugal (SW Iberia): Applying turbidite paleoseismology in a slow-convergence margin: submitted to *Quaternary Science Reviews*.
- Zdanowicz, C.M., Zielinski, G.A., and Germani, M.S., 1999, Mount Mazama eruption: calendrical age verified and atmospheric impact assessed: *Geology*, v. 27, p. 621-624.

A photograph of a sunset over the ocean. The sun is low on the horizon, creating a bright orange and yellow glow that reflects on the water's surface. The waves are dark and textured, with some white foam visible in the foreground. The overall mood is serene and dramatic.

CAPÍTULO II

FRECUENCIA DE SEISMO-TURBIDITAS

Earthquake Holocene Turbidite frequency Confirmed by Hemipelagic Sedimentation Chronology on the Cascadia and Northern California Active Tectonic Continental Margins

Julia Gutiérrez-Pastor¹, C. Hans Nelson¹, Chris Goldfinger², Joel E. Johnson³, Carlota Escutia¹, Andrew Eriksson², Ann E. Morey², and the Shipboard Scientific Party

¹*Instituto Andaluz de Ciencias de la Tierra (IACT) CSIC-UGR
Campus de Fuentenueva s/n 18002 Granada, Spain, juliagp@ugr.es*

²*Oregon State University, College of Oceanic and Atmospheric Sciences
104 Ocean Admin. Bldg., Corvallis OR 97331, USA.*

³*Present address: University of New Hampshire, Department of Earth Sciences 56 College Rd. Durham, NH 03824-3589*

Abstract

This paper analyzes recurrence times of Holocene turbidites as proxies for earthquakes on the Cascadia and northern California active margins of western Northern America. We compare the age, frequency, and recurrence time intervals of turbidites using two methods: (1) radiometric dating, (¹⁴C method) and (2) relative dating, using hemipelagic sediment thickness and sedimentation rates (H method). The two approaches complement each other, and when used together provide a better age framework than ¹⁴C ages alone. Comparison of hemipelagic sediment thickness in several cores from the same site is used to evaluate the erosiveness of turbidity currents and improve the correlation of turbidites and consequent paleoseismic history based only on less complete and unrefined data sets of ¹⁴C turbidite ages along the continental margin. Chronology of hemipelagic sediment thickness provides (1) the best estimate of minimum recurrence times, which are the most important for seismic hazards risk analysis, and (2) the most complete dataset of recurrence times, which shows a normal distribution pattern for paleoseismic turbidite frequencies. We observe that on these tectonically active continental margins, during the sea-level highstand of Holocene time, triggering of turbidity currents is controlled dominantly by earthquakes, and paleoseismic turbidites have an average recurrence time of ~ 550 yr in northern Cascadia Basin and ~ 200 yr along northern California margin. This difference in frequency of turbidites in a subduction zone compared to a transform-fault margin suggests significant differences in earthquake activity that compare favorably with independent paleoseismic indicators.

Key words: Turbidite, Earthquakes, Cascadia, San Andres, Paleoseismicity

1. INTRODUCTION

During the Holocene, deposition of well-correlated turbidites over great spatial length and spanning long time intervals have been studied along the continental margins of the Cascadia Subduction Zone and northern San Andreas Fault of northern California (Adams, 1990; Nelson et al., 2000; Goldfinger et al., 2003a; 2003b; Goldfinger et al., 2007). The correlation of these turbidites implies a method of synchronous triggering. Earthquakes are the best candidates to explain this synchronous phenomenon of turbiditic sedimentation. As discussed by Goldfinger et al. (2003a and 2003b) Goldfinger et al. (2006) and initially approached by Adams (1990), there are numerous possible triggers for turbidity-current generation such as storm-wave loading, tsunamis, sediment loading, hyperpycnal flow, great earthquakes, slab earthquakes, and aseismic accretionary-wedge slip. Despite the difficulty of distinguishing seismo-turbidites from turbidites generated by other triggers, several authors have attempted to define sedimentological features that show this difference (Gorsline et al., 2000; Nakajima and Kanai, 2000; Shiki et al., 2000). Synchronicity of correlative turbidites for thousands of years over areas covering hundreds of kilometers along the margin, however, remains the strongest criterion for testing earthquake triggering of turbidites (Goldfinger et al., 2003a; 2003b; Goldfinger et al., 2006; Goldfinger et al., 2007).

Although the Cascadia Subduction Zone originally was considered a seismic because of the lack of historic or instrumentally recorded seismicity, overwhelming evidence of great earthquakes and tsunamis has been documented at numerous coastal sites along the margin (e.g., Atwater, 1987; Satake et al., 1996). In the past decade, discovery of rapidly buried marsh deposits and associated tsunami sands along the north Pacific Coast of North America has led to the recognition that the Cascadia subduction zone has generated great (Mw 8–9) earthquakes in the past (Atwater, 1987; Nelson et al., 1995). Marine technology allows us to sample Holocene turbidites and determine the age of these deposits along the margin (Goldfinger et al., 2003a, 2003b). The sedimentologic record of turbidites and hemipelagic sediment recovered from multiple turbidite systems is a new proxy for Holocene earthquakes generated along the Cascadia subduction zone (Adams, 1990; Nelson et al., 2000; Goldfinger et al., 2003a; 2003b). This approach is supported by the land sedimentary record (Goldfinger et al., 2006).

The Holocene stratigraphy of submarine channels along the Cascadia margin has long been known to exhibit excellent turbidite marker beds that contain Mazama Ash (MA) from the eruption of Mt. Mazama, which formed Crater Lake, Oregon (Nelson et al., 1968). The calendar age of the eruption of Mt. Mazama has been re-dated at 7627 ± 150 cal. yr B.P. from the GISP-2 ice core in Greenland (Zdanowicz et al., 1999). The confluence test, as described originally in Cascadia Basin by Adams (1990), utilizes the first occurrence of Mazama ash in turbidites as a marker bed and shows synchronicity of turbidite triggering by earthquakes when the number of upstream post-Mazama turbidites in multiple tributaries equals the number of post-Mazama turbidites downstream below the tributary confluences. Correlation of major stratigraphic events is based on the first occurrence of Mazama Ash in turbidites and on the approximate onset of Holocene hemipelagic sediment deposition where the clear change of color in the sediment between the olive-green Holocene and olive-gray Pleistocene deposits is an excellent datum in Cascadia Basin (Table 1, Figs. 1, 2) (Nelson, 1968; Duncan et al., 1970).

Similarly, the turbidite history along the Northern California margin is under investigation (Fig. 1). The tectonic setting of the northern California margin has been widely studied onshore (Brown, 1995; Schwartz et al., 1998; Prentice et al., 1999), and turbidites offshore of this region have also been demonstrated to correlate well with the onshore earthquake record even though no good datum such as the Mazama Ash or

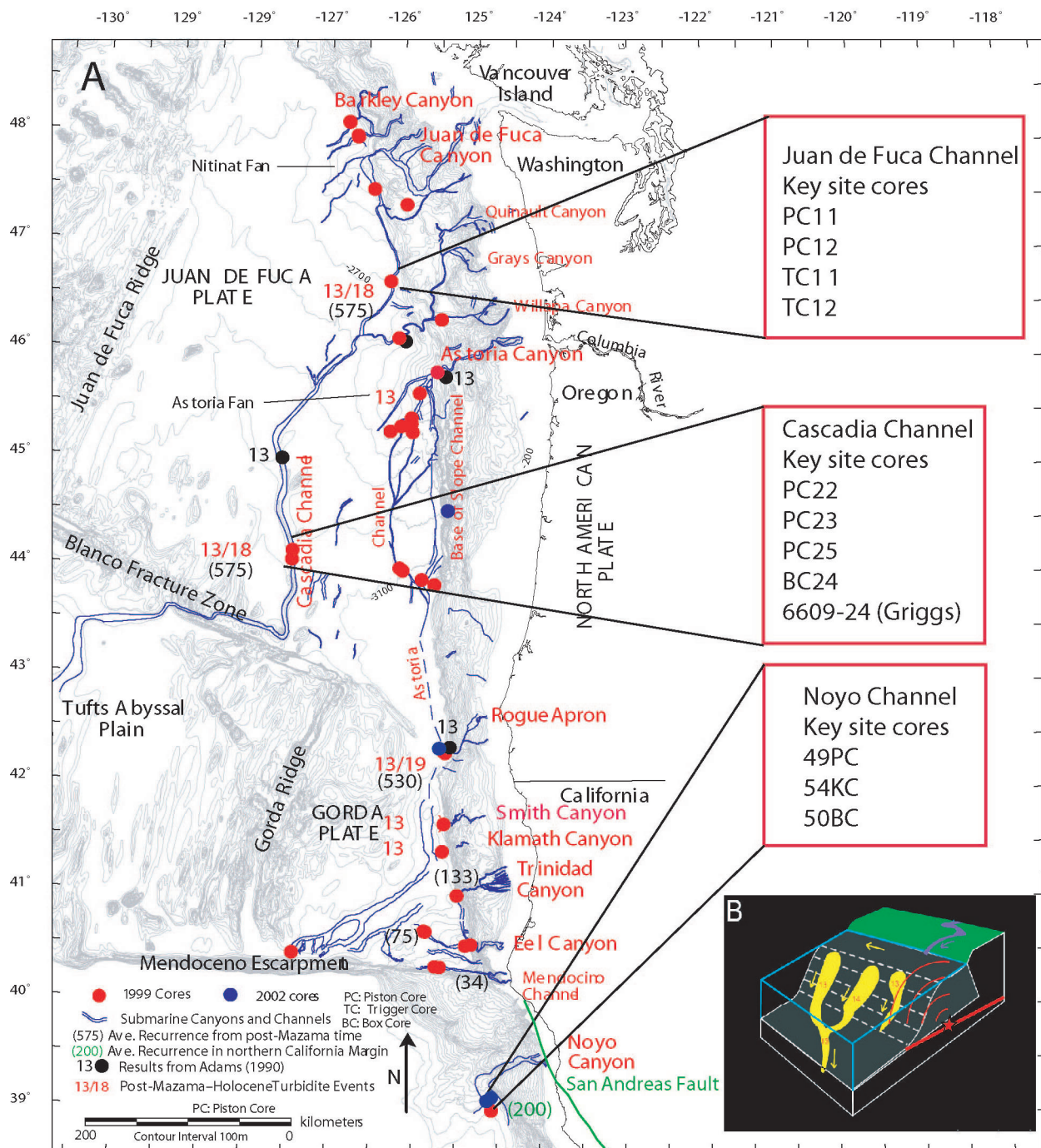


Figure 1. A) Cascadia and northern California margins canyons, channels, 1999–2002 core locations, and main fault systems. The pathways of the major canyons are shown in blue, and the number of post-Mazama and Holocene turbidites are shown in red. Mazama ash was not present in northern Barkley Canyon cores or in the cores south of Rogue Canyon. Average recurrence time of turbidites is shown in black in parentheses next to each core site. Red squares show core locations in the Cascadia and northern California turbidite systems studied in this paper (figure modified from Goldfinger et al., 2003a). B) Synchronicity test at a channel confluence is shown where Washington margin tributary channels merge into the Cascadia Deep-Sea Channel. The number of events downstream should be the sum of events in the tributaries, unless the turbidity currents were triggered simultaneously by an earthquake (Adams, 1990).

color change of Pleistocene to Holocene hemipelagic sediment has been found (Goldfinger et al., 2003a; 2003b; Goldfinger et al., 2007). Since the 1906 rupture, the northern San Andreas Fault has been nearly aseismic, with a few scattered events onshore and offshore (Brown, 1995). The length of past ruptures and segmentation of the northern San Andreas Fault is controversial. Brown et al. (1995), Thatcher et al. (1997), and Prentice et al. (1999) all conclude that abundant evidence for a 1906 rupture exists as far north as the Mendocino Triple Junction. Prentice et al. (1999) estimate a minimum slip rate of 14mm/year for northern San Andreas Fault based on 180 m offset of colluvial deposits dated at $13,180 \pm 170$ cal. yr B.P., with a minimum rupture length of 470 km. Our correlations in the northern California margin are based mainly on ^{14}C ages, heavy mineralogy, and stratigraphic correlation with physical-property proxies (Goldfinger et al., 2007).

Previous papers have established the turbidite paleoseismic history of the Cascadia subduction and northern California margins (Nelson et al., 2000; Goldfinger et al., 2003a; 2003b; Goldfinger et al., 2007). To aid in the analysis of seismo-turbidites, this paper presents a comparison of turbidite ages, frequencies, and recurrence intervals using two methods: (1) radiometric dating, based on radiocarbon ages of foraminifera in the hemipelagic sediment just below each turbidite (^{14}C method), and (2) relative dating, based on the measurement of the time interval between two turbidites, using hemipelagic sediment thickness and sedimentation rate (H method). These two approaches provide complementary semi-independent methods to determine turbidite recurrence times. We focus on the H method to refine turbidite ages, determine the most accurate recurrence time history and frequency of turbidites, and show the dominant control by earthquake triggering in the active tectonic margins of Cascadia and northern California.

	RAW ^{14}C AGES (CAL.YR B.P.)						DATUM
	JUAN DE FUCA (JDF)		CASCADIA (CC)		ROGUE (RA)		(age yr B.P.)
	12PC	11PC	25PC	6609-24*	31PC	6609-13**	average
T1	300 Cal. yr B.P. Nelson et al.(1995), Satake et al. 1996, Atwater et al. (2004)						300
T13	7282	7288	7351	7400			
Sed.rate (cm/1000yr)	11.4	11.6	9	7.8			
Corrected T1 3	7150	7159	7184	7272			7191
T18	9851		9849		9824		
Sed.rate (cm/1000yr)	12.1		8	.3	30.9		
Corrected T1 8	9789		9729		9774		9763
PLEISTOCENE/HOLOCENE					12839	13000	
Corrected P/H					12751	~12750	12750

PC: piston core
T = Turbidite event
Sed. Rate = Sedimentation rate
The P/H boundary is based in faunal color change
Steps to obtain a DATUM using T13 as example :

- 1) age sample thickness = 3 cm
- 2) refining to the middle point of the sample = 1.5 cm
- 3) sedimentation rate at T13 in 12PC at Juan de Fuca = 11.4 cm
- 4) sample depth correction to refine age: $1.5 \text{ cm} * 1000 \text{ yr} / 11.4 \text{ cm} = 131.5 \text{ yr}$ and $7282 \text{ yr} - 131.5 = 7150 \text{ yr}$
- 5) same correction for each core at each site
- 6) average: $7150 + 7159 + 7184 + 7272 / 4 = 7191 \text{ yr} = \text{DATUM}$ M

Table 1. Datums and calculation of average recurrence time between turbidites for Cascadia Basin.

2. GEOLOGICAL SETTING

2.1. Tectonic Setting

The Cascadia margin is part of a subduction zone where three plates interact through the subduction of the oceanic Juan de Fuca and Gorda plates beneath the North American plate off the coast of northern California, Oregon, Washington, and Vancouver Island (Fig. 1). The oblique convergence rate, decreasing

southward, is 40 mm/yr, directed N68°E at the latitude of Seattle (DeMets and Dixon, 1999).

The northern California margin is crossed by the San Andreas Fault where the fault parallels the coast and then proceeds offshore from Point Arena to the Mendocino Triple Junction (Fig. 1). The San Andreas Fault accumulates about 25 mm/year of the 34 mm/year of stress distributed across western California, or approximately 75% of the Pacific–North America Plate motion over a 100-km-wide zone (Argus and Gordon, 1991).

2.2. Turbidite Systems and the Turbidite Record

Numerous modern turbidite systems are found in the Cascadia Basin associated with their canyons, which from north to south are Barclay, Juan de Fuca, Quinault, Grays, Willapa, Astoria, Rogue, Smith, Klamath, Trinidad, Eel and Mendocino (Fig. 1) (Nelson et al., 2000). In the Cascadia margin we focus on two key turbidite systems that we use to apply the turbidite paleoseismic method, specifically, the Juan de Fuca Channel and the Cascadia Channel, where we have the most complete and reliable dataset.

In the northern California margin, this paper focuses on the paleoseismic record inferred from turbidites at the key site of Noyo Channel system only, where the San Andreas Fault crosses and offsets the Noyo canyon head. For our analysis, Noyo Channel has the most complete turbidite record and radiocarbon dataset.

2.2.1. Juan de Fuca Channel (JDF)

The Washington continental margin, within the Cascadia subduction-zone margin, is characterized by a number of submarine canyons and channels (Juan de Fuca, Quinault, Grays, and Willapa) that follow irregular pathways through the accretionary folds of the deformation front along the continental slope (Fig. 1 and Fig. 1 Nelson et al., in press, Anexo 1 de este voumen de tesis).

2.2.2. Cascadia Deep-Sea Channel (CC)

Juan de Fuca and other tributary canyons from the Washington margin join at the southern end of Nitinat Fan on the continental rise to form Cascadia Channel. Cascadia, a deep-sea channel, crosses Cascadia Basin, extends through the Blanco Fracture Zone, and continues hundreds of kilometers into Tufts Abyssal Plain (Nelson et al., 2000; Fig. 1 Nelson et al., this volume). This turbidity-current pathway, traversing 1000 km of Cascadia Basin, has remained open throughout the late Quaternary to the present. This is shown by the presence of the 13 post-Mazama ash (MA) turbidite events (T) in all 1999 cores we have recovered throughout the main channel pathway and those previously examined by Griggs (1969) and Adams (1990). The activity of Cascadia Channel is also verified by the occurrence of the youngest turbidite (T1) with an age of ~ 300 cal. yr B.P. ($362 \pm (284\text{--}443)$ cal. yr B.P. in 23TC and $255 \pm (301\text{--}101)$ cal. yr B.P. in 24BC) comparable to numerous observations of this event by other authors (Fig. 2) (Nelson et al., 1995; Satake et al., 1996; Atwater et al., 2004).

Both the Juan de Fuca tributary and Cascadia channels below the confluence contain 13 post-Mazama turbidites (Fig. 1) (Nelson et al., 2000). We have extended the correlation of turbidites below the T13 first turbidite with Mazama ash so that a total of 18 Holocene turbidites can be correlated in northern Cascadia Basin. Work in progress shows that an additional event, known as T5a, is recorded at more southern sites

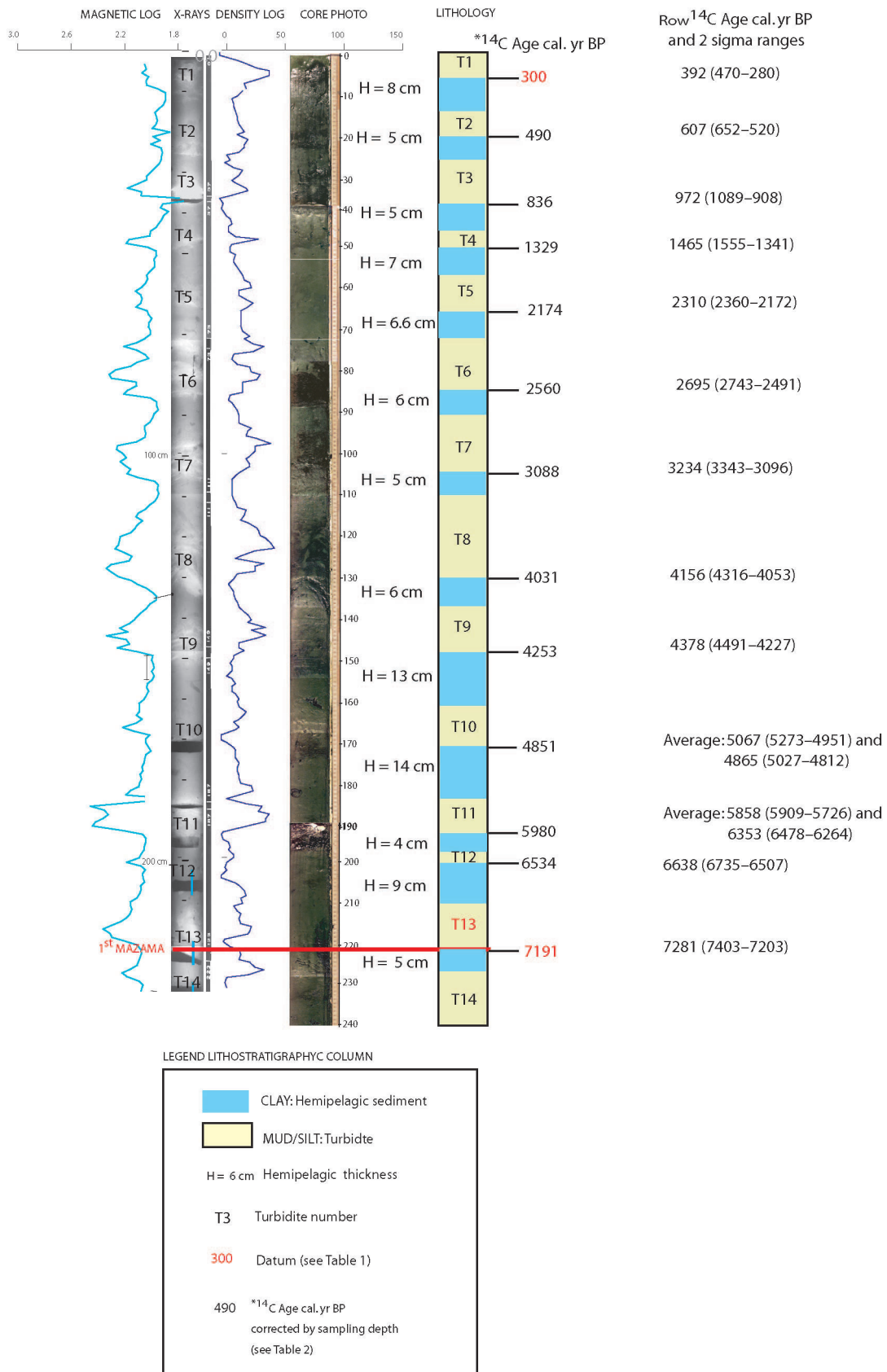


Figure 2. Juan de Fuca Channel 12PC core showing lithology, photographs, and magnetic and density log signatures in light and dark blue, respectively. Coarse-grained sediment pulses in turbidites are exhibited as high density and magnetic peaks and lighter intervals in X-ray radiographs. Note that the first occurrence of Mazama Ash at T13, the main regional datum, is keyed in red. See Figure 5 also for a detailed analysis of turbidite characteristics.

but not found in Juan de Fuca or Cascadia Channels. Our analysis of ^{14}C ages and hemipelagic sediment, however, includes only the 13 post Mazama turbidites for Juan de Fuca Channel, whereas for Cascadia Channel we analyze all 18 Holocene turbidites.

2.2.3. Noyo Channel (NC)

Noyo Channel is found south of Cape Mendocino and extends seaward for more than 200 km from the mouth of the canyon to the end of the pathway, where it has a confluence with Viscaino and Gualala Channels. Our analysis and previous work show that Noyo Channel has a detailed Holocene turbidite record recovered from five cores containing 2–25 turbidites that can be correlated along strike to develop a paleoseismic record (Fig. 1) (Goldfinger et al., 2007).

2.3. Character of Turbidites

In our 1999 cores, as well as the archive cores of Griggs (1969), the characteristic Holocene mud turbidites in Cascadia Channel are thick (40–70 cm) with thin silt bases (1–3 cm) that are interbedded with thin hemipelagic clays of about 2–8 cm thickness (Nelson et al., 2000). Both the 13 post-MA turbidite events and a consistent thickness of hemipelagic interbeds, suggest a Holocene depositional history in the channel with cyclic generation of muddy turbidity currents (Griggs and Kulm, 1970; Adams, 1990). In contrast, intermittent deposits of thick (up to 2 m) graded gravel to sand beds during the late Pleistocene suggest that stronger turbidity currents that probably resulted in channel erosion, nondeposition, or sediment bypass occurred during glacial times in Cascadia Channel (Griggs et al., 1969; Griggs and Kulm, 1970). Juan de Fuca and Noyo Channel contain thinner (10–40cm) and sandier (1–3cm fine sand base) that grade into a mud turbite tail above the sandy turbidite base (Nelson et al., 2000).

3. METHODS

3.1. Core Recovery and Swath Bathymetry

Prior to and during the 1999 and 2002 research cruises, all available swath bathymetry and archive core data sets from the Cascadia and northern California margin were integrated into a GIS database. The bathymetry and sidescan sonar were used to complete an analysis of channel pathways that included physiography, axial gradients, and slope stability/slumping assessments. During the cruises, the Oregon State University wide-diameter (10 cm) coring gear was employed to collect 44 piston cores of 6–8 m length and 44 companion trigger cores (also 10 cm) of 3 m length, as well as seven box cores of 0.5 m length x 0.5 m width in Cascadia Basin. On the northern California margin, 69 piston–trigger pairs and 10 jumbo Kasten cores (of 3 m length and 400 cm³) volume were collected in 2002. Core sites were chosen to take advantage of known depositional segments of channels versus non depositional or erosional segments.

The hemipelagic thickness analysis has been applied to 11 cores: 12PC, 12TC and 11TC at the Juan de Fuca Channel (JDF) key site, and 22PC, 23PC, 25PC, 6609-24PC (Griggs et al., 1969) of the Cascadia Channel (CC) key site, and 49PC, 49TC, 54 Kasten core (KC), and 50 box core (BC), of the Noyo Channel key site on the northern California Margin (Tables 2–4, Appendix 1).

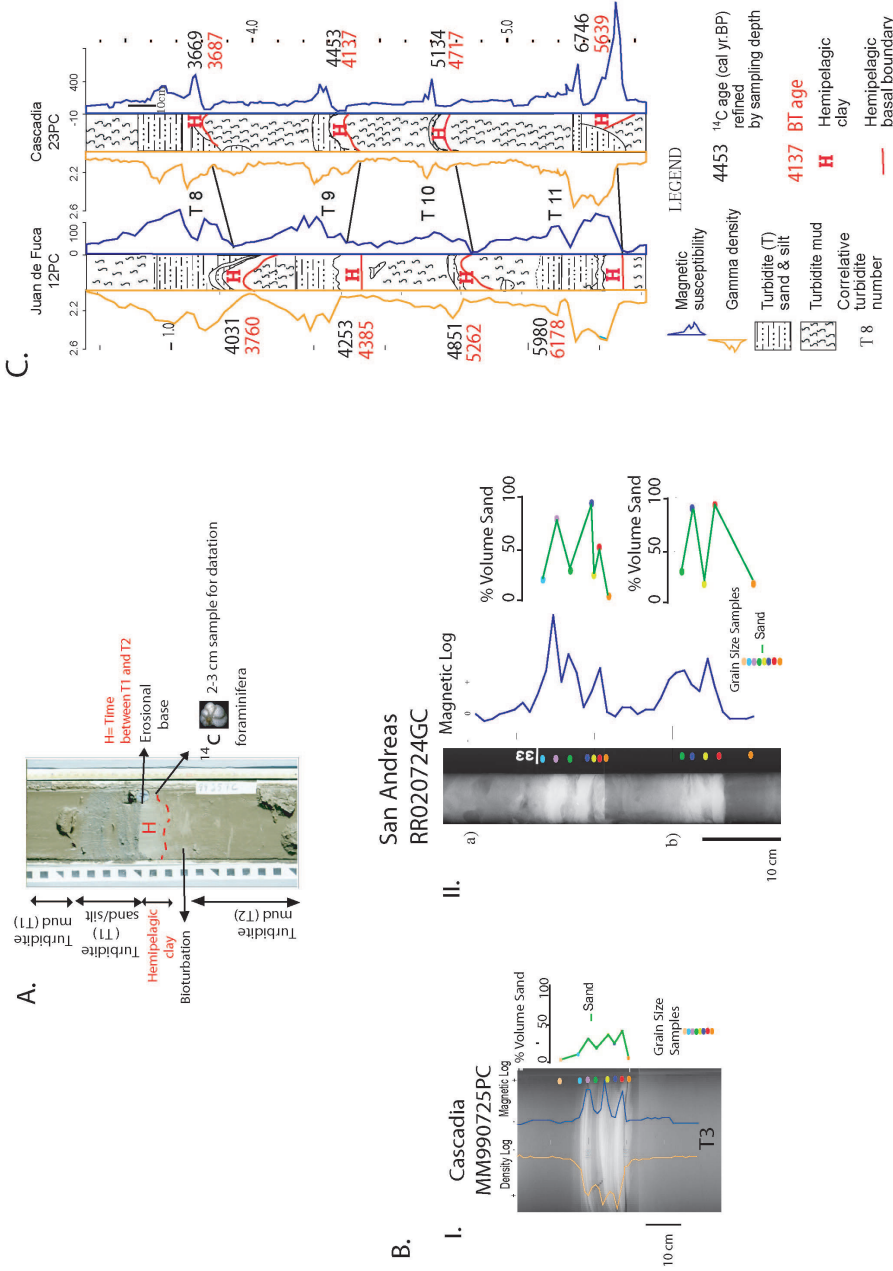


Figure 3. Techniques used for sediment analysis. A) Core photograph identifying the main sediment lithologic types observed in Cascadia and northern California margins. B) examples of grain-size analysis in two cores of Cascadia and northern California margins. B.I: The Cascadia margin grain-size example in the turbidite 3 (T3) of core 25PC (Piston Core). B.II: Grain-size examples in T19 and T20 of core 24GC (gravity core from the northern California margin). Color dots are grain-size sample locations, the green line is the % content of sand for each sample, and blue and orange lines are magnetic and density logs. Grain-size analysis, compared with the X-ray radiography of cores and logs, is used to distinguish turbidite pulses, determine presence or absence of hemipelagic sediment between pulses, and demonstrate that magnetic and density logs can be used as proxies of grain size because there is an excellent agreement between curves (Modified from Goldfinger et al., 2007). C) An example of correlation between two piston cores: 12 PC at Juan de Fuca Channel (JDF) and 23 PC at Cascadia Channel (CC). In the drawing, best hemipelagic thickness (BT) ages (see Hemipelagic Sediment Methology, item 10) are shown in red and ¹⁴C cal. yr B.P. ages are in black. Hemipelagic thicknesses are shown in the drawing with a capital red H at the base of the measured thickness. Correlation of turbidites is based on number of post-Mazama turbidites radiocarbon ages, and magnetic and density log signatures.

3.2. General Sediment Analysis Methods

At sea, we did a thorough lithologic description through macroscopic observations of each core to differentiate accurately between turbidite and hemipelagic sediment thickness. Visually, it was sometimes difficult to distinguish the boundary between the turbidite tail and the overlying hemipelagic sediment (Figs. 2, 3). Higher-latitude cores displayed significant color differences, but some southern cores did not. The sand fraction of turbidite tails are characterized by a high detrital content consisting of plant fragments and micas, while the hemipelagic sediment (clay) is characterized by a high content of microfauna (foraminifera and/or radiolaria), greater bioturbation, and an absence of terrigenous detrital material (Fig. 3A) (Nelson, 1968, 1976). Following the techniques of Nelson (1968), Carlson and Nelson (1969), and Griggs et al., (1969), when the boundary between turbidite and hemipelagic sediment was difficult to differentiate visually, we sampled the sand fraction of the sediment above and below the inferred boundary and counted microfossils and terrigenous grains with a binocular microscope (Fig. 3A). Once the hemipelagic sediment was identified, the number of foraminifera and radiolaria were counted.

Where the sediment color changes abruptly, analysis of the microfauna above and below the stratigraphic boundary between the Holocene and Pleistocene was done, where a predominance of radiolaria in the Holocene compared to a predominance of foraminifera in the Pleistocene is found (Nelson, 1968, 1976; Carlson and Nelson, 1969; Duncan et al., 1970). Based on the clear Pleistocene–Holocene boundary, we can determine the total thickness of the Holocene sediment drape in the Cascadia Basin and compare the cumulative Holocene hemipelagic sediment thickness in channel locations vs. interchannel locations to determine if there has been significant erosion of hemipelagic sediment in channels by Holocene turbidity currents. Holocene hemipelagic sediment thickness in interchannel locations was measured in archive cores (Nelson, 1968, 1976; Duncan et al., 1970) (Fig. 4).

To establish sedimentation rates and determine recurrence time between turbidites, high-resolution ^{14}C ages are required. Accelerator mass spectrometer (AMS) radiocarbon ages provided by the Lawrence Livermore Laboratory in California have been determined from planktonic foraminifera deposited in the hemipelagic sediment that underlies turbidite beds. Because previously deposited planktonic foraminifera can be reworked when they are entrained in the turbidite, the > 0.062 mm sand fraction was sieved and planktonic foraminifera were carefully hand-picked from the top 2–3 cm of the hemipelagic sediment below the base of the turbidite and above any underlying turbidite tail deposit that may have resedimented microfauna (Fig. 3A). This avoids the majority of bioturbation but does not avoid the issue of erosion of hemipelagic sediment. Turbidity currents, in some cases, erode the sea-floor hemipelagic sediment prior to deposition of the turbidite. If the hemipelagic sediment below the turbidite has been eroded, then our ^{14}C age obtained from the hemipelagic sediment will be anomalously old. For this reason, we use multiple cores at each location to determine the most reliable thickness of hemipelagic sediment between set of turbidites. The accurate hemipelagic sediment thickness, when divided by sedimentation rate, represents the recurrence time between deposition of turbidites and provides information to refine ^{14}C ages from core sites where hemipelagic sediment has been eroded. Raw AMS radiocarbon ages have been reservoir corrected and converted to calendar years (cal. yr B.P.) by the method of Stuiver and Braziunas (1993).

The thickness of hemipelagic sediment intervals between turbidites provides a second means of determining time between turbidites for analysis of variance between recurring paleoseismic events. The hemipelagic sedimentation rate at each local core site can be determined by adding up the cumulative thickness of hemipelagic sediment above individual radiocarbon ages and stratigraphic datums such as

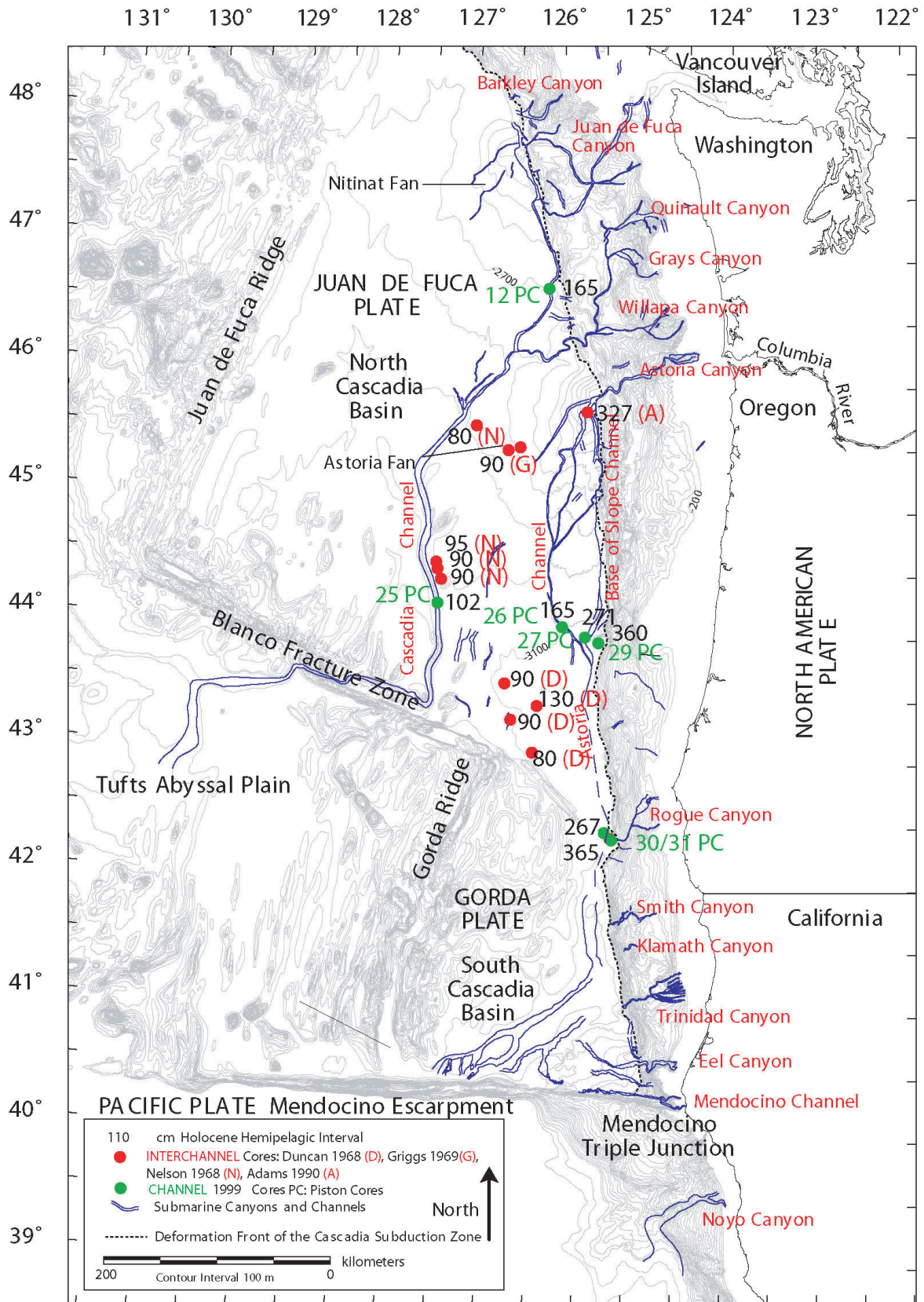


Figure 4. Total thickness of Holocene hemipelagic sediment drape in Cascadia Basin. Green dots, are 1999 channel cores or cores from Rogue Apron with turbidites. Red dots are interchannel archive cores. The source of each archive core is shown by the letter in parenthesis beside the core, as explained in the legend. Black numbers are centimeters of “Holocene hemipelagic sediment thickness” (HHT). Note hemipelagic sediment thickness closer to the slope is greater (about 200–300 cm) than in more distal locations (about 90–100 cm).

the first post-Mazama turbidite (about 7200 cal. yr B.P.) or the Holocene–Pleistocene biostratigraphic color change (12,750 cal. yr B.P.) (Table 1). The average sedimentation rate at each site then equals the cumulative hemipelagic sediment thicknesses above each turbidite or datum age divided by the radiocarbon or datum ages. We measured the cumulative hemipelagic sediment without turbidites above a dated turbidite to calculate sedimentation rates because it is necessary to avoid errors caused by anomalous thin beds that result from the erosion by turbidity currents. We assume that the hemipelagic sediment was deposited at a constant rate during the Holocene, because the thickness of the hemipelagic sediment drape without turbidites is the same in archive interchannel cores as that in our recovered channel cores (see detailed explanation in item 1 of the next section) (Fig. 4). The time between two turbidite events equals the hemipelagic sediment thickness between the two events divided by the average hemipelagic sedimentation rate at each core depth at each specific location. For analysis of variance between events, this time can then be compared with the time between events that has been obtained by calibrated AMS radiocarbon ages BP. The sedimentation rates derived from the ^{14}C ages are of course linked to the H analysis, making the process somewhat circular.

An analysis of turbidites was done to find vitric glass associated with the Mazama eruption, which was originally identified in turbidites throughout Cascadia Basin by Nelson et al., (1968). Mineralogic smear-slide samples from the silt–sand fraction in the turbidites were taken to count volcanic glass shards with a petrographic microscope. X-ray radiography was done in most of the cores from both margins to show grading and internal sedimentary structures of the turbidites and to define hemipelagic compared with turbidite-tail sediment (Figs. 2, 3B.I, 3B.II).

We analyzed physical properties of all cores using the Geotek MST system, collecting gamma density, P-wave velocity and high-resolution magnetic susceptibility series for each core (Figs. 3B, 3C). In many cases, sandy/silty pulses in individual turbidites, without hemipelagic sediment in between, were identified by MST logs (Figs. 3B, 3C). These individual turbidites with multiple coarse-grained pulses within a single bed have been used as criteria by other investigators to identify seismo-turbidites (Gorsline et al., 2000; Nakajima and Kanai, 2000; Shiki et al., 2000). Furthermore, physical-property signatures can help with the stratigraphic correlation. Similar methods have been used in other settings to establish stratigraphic correlation (e.g., Lake Baikal, off Morocco, and the Laptev Sea) (Lees et al., 1998; Wynn et al., 2002; Rivera et al., 2006). The principal use of physical properties, however, is as grain-size proxies. The internal depositional pattern, including sandy intervals, muddy turbidite tails, bioturbated intervals, and hemipelagic clay can be distinguished in the magnetic and density logs in conjunction with the supporting X-ray, image, and Lithologic-log data. This usage is discussed in detail by Goldfinger et al. (2007). To verify the density and magnetic proxies, grain-size analyses were conducted in several turbidites, examples of which are shown for turbidites T3 of piston core (25PC) in Cascadia Basin and T19 and T20 of gravity core (24GC in the northern California margin) (Fig 3B).

4. METHODOLOGY FOR HEMIPELAGIC SEDIMENT

Because ^{14}C ages are lacking for some turbidites, but data on hemipelagic sediment are available for all turbidites, new techniques were used to determine turbidite ages and frequency based on the thickness of hemipelagic sediment between turbidites. These techniques can be used to independently evaluate and refine the AMS radiocarbon (^{14}C) ages through the following steps:

4.1. Evaluation of Maximum Erosion by Turbidity Currents Based on Thickness of Total Holocene Hemipelagic Sediment

To determine if hemipelagic sediment has been systematically eroded below turbidites, we compare the total thickness of Holocene hemipelagic sediment at each key site with the regional thickness of the hemipelagic sediment deposited in Cascadia Basin adjacent to, but unaffected by, turbidity-current pathways. Evaluation of thickness of Holocene hemipelagic sediment drape (HHT) is based on archive interchannel cores at OSU and channel cores recovered during 1999.

Figure 4 shows that along the immediate base of the continental slope of the Cascadia Margin, HHT ranged from 327 cm in a Nelson (1968) interchannel location to 365 cm in a channel location. In southern Cascadia Margin approximately 5–15 km seaward from the base of slope, an HHT of 271 cm compares to 267 cm on the Rogue Apron. About 30 km from the base of slope on the Apron, an HHT of 165 cm compares with 165 cm in Juan de Fuca Channel. A transect at 43° 30' shows a good example of the rapid change in hemipelagic sedimentation rate from 0 to 30 km away from the base of slope (360 cm, 271 cm, and 165 cm) (Fig. 4). This gradient exhibits to a relatively constant hemipelagic sediment thickness of about 90–100 cm westward across the abyssal plain to the longitude of Cascadia Channel. During the Holocene, channel and interchannel cores record the same total thickness of hemipelagic sediment with and without turbidites. Thus, we can assume a constant rate of hemipelagic deposition during the Holocene from proximal to distal locations away from the base of the continental slope.

Because of the lack of core penetration, we cannot measure total hemipelagic thickness up to the Pleistocene–Holocene (P/H) boundary in some of our 1999 Cascadia and Juan de Fuca channel cores. Consequently, we estimate the equivalent amount of hemipelagic thickness that would be deposited at 12,750 cal. yr B.P. using the data on maximum core depth available. In this way, the thickness of the Holocene sediment drape can be mapped in the Cascadia Basin, where there is no recovery of the P/H boundary. For example, in Juan de Fuca Channel we extrapolate to the P/H boundary by using the T13 Mazama datum (7200 cal. yr B.P.). The cumulative hemipelagic sediment thickness above turbidite 13 (T13) is 93.5 cm; thus, $93.5 \text{ cm} \times 12,750 \text{ yr} / 7200 \text{ cal. yr B.P. age} = 165 \text{ cm} = \text{HHT}$ (Fig. 4, Table 2), assuming a constant sedimentation rate (see 12PC location on the map in Figure 4). Similarly, the HHT of 1999 cores 25PC, 26PC, 27PC, 29PC, 30PC, and 31PC are reconstructed.

To utilize the H method it is important to determine whether there has been a significant amount of erosion of hemipelagic sediment on the channel floors. No uniform amount of erosion is found in the Juan de Fuca and Cascadia Channels because the total Holocene hemipelagic sediment thickness (without turbidites) calculated in our cores is about equal to or more than the mapped drape thicknesses from previous studies (Fig. 4) (Duncan, 1968; Nelson, 1968, 1976; Griggs, 1969; Adams, 1990). The 25PC channel core recorded 57.5 cm of hemipelagic sediment measured above T13, and Nelson (1968) recorded an average of 92 cm of HHT ($90 + 90 + 95/3 = 92 \text{ cm}$) based on measurements in three interchannel cores adjacent to the Cascadia Channel for the same interval (Figs. 1, 4, Table 3). Using the 7200 yr T13 Mazama datum, we can calculate the amount of hemipelagic sediment deposited in Nelson (1968) cores above the T13 date as follows: $7200 \text{ yr} / 12,750 \text{ yr} \times 92 \text{ cm} = 52 \text{ cm}$. There is just a 10% difference between the hemipelagic sediment deposited in channel and interchannel locations, showing that the turbidity currents did not erode significantly in the Cascadia Channel vs. nearby interchannel locations. Making similar calculations, an archive interchannel core (Duncan, 1968) closer to the base of slope (50 km) has an HHT of 130 cm and an estimated thickness of 73 cm above T13 (Fig. 4). We can compare the 73 cm sediment thickness above

TURBIDITE	Hemipelagic Thickness (H)				Raw ¹⁴ C age cal.yr B.P.	¹⁴ C age	¹⁴ C Rec.	BT	Acum.BT	Sed rate	Refined sed.rate	Refined Av.sed.rate	BT Rec.	BT Age
	12PC	12TC	11TC	20										
1	80	40	50	300	300	190	57	77	12.7	15.7	14	407	300	
2	50	50	50	607	490	346	50	127	13.0	15.2	14	357	707	
3	50	40	40	972	836(791)	493	45	172	11.7	12.9	14	321	1064	
4	70	70	70	1465	1329	845	70	242	10.5	11.1	12	583	1386	
5	66	60	70	2310	2174	386	68	310	11.5	12.1	12	567	1969	
6	60	50	60	2696	2560	528	60	370	11.4	12.0	12	500	2536	
7	50	50	110	3234	3088	943	80	450	10.8	11.2	12	667	3036	
8	60	90	?	4156	4031	222	75	525	12.0	12.3	12	625	3702	
9	130	100	?	4378	4253	598	115	640	12.9	13.2	13.1	878	4327	
10	140	100	80	4966	4851(4606)	1129	120	760	12.4	12.7	13.1	916	5205	
11	40	160*(80)	180*(90)	6105	5980(5976)	554	85	845	12.7	12.9	13.1	649	6121	
12	90			6638	6534	657	90	935	13.0	13.0	13.1	687	6770	
13	50	50	50	7191	7191		50	985	13.1	13.1	13.1	382	7531	

Table 2. Juan de Fuca Channel (JDF) hemipelagic sediment thicknesses in multiple cores, recurrence times, and age analysis.

TURBIDITE (T)	Hemipelagic Thickness (H)				Raw ¹⁴ C age cal.yr B.P.	¹⁴ C age	¹⁴ C Rec.	BT	Acum.BT	Sed rate	Refined Sed rate	Refined Av.sed.rate	BT Rec.	BT Age
	22PC	23PC	25PC	6609-24										
1	30	60	60	300	300		30	30					300	
2	60	60	70	1503	1360	349	55	85					495	300
3	40	35	10	55	1503		65	150	10.0	11.0	11.1	586	795	
4	55	50	40	55	1828	1709	43	193	10.6	11.3	11.1	387	1381	
5	50	60	60	65	60		53	246					477	1768
6	45	60	60	20	2926	2735(2690)	58	304	10.4	11.1	11.1	523	2245	
7	45	30	55	40			55	359					495	2768
8	60	30	45	30	3836	3669(3533)	47	406	10.6	11.1	11.1	423	3263	
9	60	40	40	75	4620	4453(4273)	45	451	9.8	10.1	10	450	3687	
10	70	40	95	85	5301	5134	58	509	9.6	9.9	9	580	4137	
11	40	25	0	10	6912	6746	83	592	8.6	8.8	9	922	4717	
12	30	20	20	15	6946	6780(6669)	25	617	8.9	9.1	9	278	5639	
13	50	30	25	30	5351	7191	30	647	12.1	9.0	9	333	5917	
14	40	20	45	30	8101	7934	37	684	8.4	8.6	8.6	430	6250	
15		30	30	27	8470	8303	38	722	8.5	8.7	8.6	442	6680	
16		40	25	12			29	751	8.5	8.7	8.6	337	7122	
17		20	40	24			19	770	8.5	8.7	8.6	221	7460	
18							32	802	8.1	8.2	8.6	372	7680	
							30	832				349	8053	

See Text, section New Results:Hemipelagic Methology ,to follow the meaning of each column.

PC: Piston Core, TC: Trigger Core, 6609-24 : Griggs Piston Core, 1969
H and Best Hemipelagic Sediment Thickness (BT) below each T event in mm
Ages below each T event and Recurrence (Rec) in Cal yr. BP
Sedimentation rate (Sed rate) in cm/1000 yr
300 yr, 7191 yr and 9763 yr are T1, T13 and T18 DATUMS (Table 1)
* Double H because T12 missing. Thus, 50% H used to estimate BT
** Sample depth recalculation to refine ¹⁴C age in Cal yr.BP
(791) Ages refined by avoiding the erosion effect

Table 3. Cascadia Channel (CC) hemipelagic sediment thicknesses in multiple cores, recurrence times, and age analysis.

T13 from the Duncan (1968) core with the 93.5 cm at T13 deposited in Juan de Fuca 12PC core, which is located closer to the base of slope (20 km) (Fig. 4, Table 2). Considering the gradation in sedimentation rate and the closer location of 12PC to the base of slope, again no significant erosion of hemipelagic sediment is indicated at this more proximal northern channel location.

4.2. Best Hemipelagic Sediment Thickness (BT)

For this study, the H thickness below turbidites has been measured in Juan de Fuca cores to turbidite T13, in Cascadia cores to turbidite T18, and in Noyo cores to turbidite T25 (Tables 2, 3, Appendix 1). Best hemipelagic thickness (BT) below correlative turbidites from multiple cores at a channel site was calculated by averaging the thickness of the two or three thickest hemipelagic sediment deposits. By using the two or three thickest layers, our error is biased towards maximum thickness and reduces the potential effect of local basal erosion by turbidity currents. By averaging two or three layers we are also reducing the effect of variance in visual core lithology descriptions and visual observations of the geophysical log signatures.

4.3. Hemipelagic Sedimentation Rates Using ¹⁴C Calibrated years Before Present (cal. yr B.P.) Ages

To calculate sedimentation rates down core, we utilize T1 (300 Cal. Yr B.P.), Mazama ash T13 (~ 7200 cal. yr B.P.) and T18 (~ 9770 cal. yr B.P.) age datums, and ¹⁴C ages for individual turbidite events (Tables 1, 2, 3). The sedimentation rate with depth at each site is calculated by subtracting the turbidites and then summing the BT thickness increments above each datum or ¹⁴C age and dividing the thickness of hemipelagic sediment by the age (Tables 1, 2, 3). For example, in T1 of Juan de Fuca Channel we have a total H of 7.7 cm (H above T1 + H between T1 and T2) that we divide between 607 cal. yr B.P. (age below T2). The result is multiplied by 1000 yr to obtain the sedimentation rate of 12.7 cm/1000 yr (Table 2). We use cumulative thickness of BT above turbidites to smooth possible age errors caused by the erosion in individual hemipelagic sediment layers. Sedimentation rates range between 10.5 and 13.1 cm/1000 yr until T13 at Juan de Fuca Channel and between 8.1 and 10.6 cm/1000 yr until T18 at Cascadia Channel. Following, the radiocarbon ages used to obtain these sedimentation rates and age datum calculations have all been refined. To avoid errors in sample depth, the time corresponding to the hemipelagic sediment thickness between the sample mid-point and the base of the turbidite sand has been subtracted, as shown in Fig. 3A and Tables 1, 2, and 3.

4.4. Effects of Hemipelagic Sediment Erosion on ¹⁴C and BT Data: Testing Reliability of Ages

The amount of erosion can be evaluated by comparing all hemipelagic intervals between each correlative turbidite in multiple cores at one site. Any erosion from the top of the hemipelagic layer results in ¹⁴C ages that are anomalously old and recurrence times between turbidites that are anomalously young. Our BT analysis from multiple cores can be used to compensate for differential erosion that has affected H recurrence times. However, for ¹⁴C ages acquired from significantly eroded H intervals, erosion correction is needed for anomalous old ages (Tables 2, 3).

We evaluated the percentage of hemipelagic sediment variation by comparing the hemipelagic sediment measured in the core where the ¹⁴C sample was taken with the BT or maximum thickness for the same turbidite event in all cores at the site. For example, we need to eliminate the effects of erosion of hemipelagic

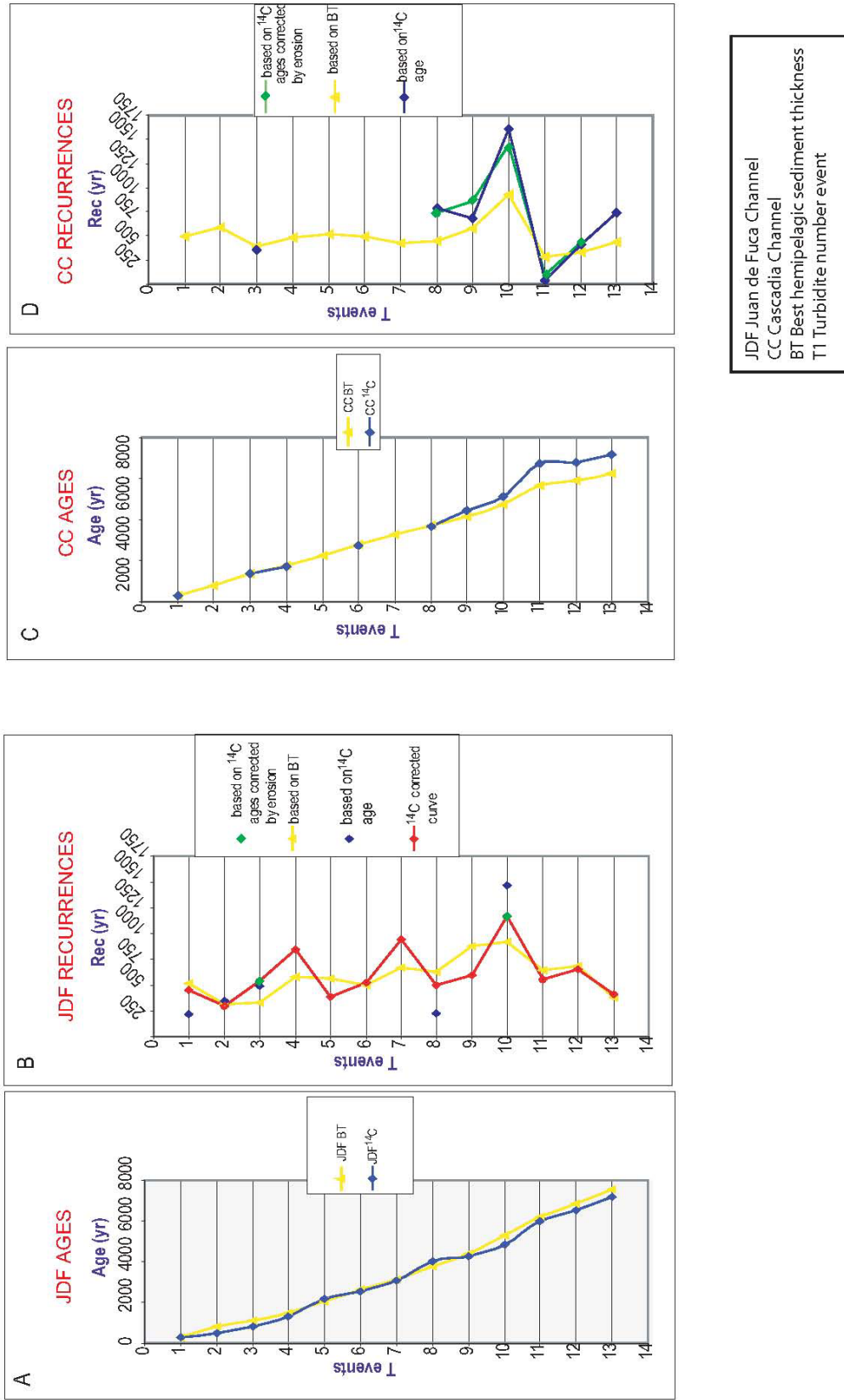


Figure 5. Comparison of age and recurrence times based on AMS radiocarbon age (^{14}C) and averaged hemipelagic sediment thickness, “best thickness” (BT) data sets for T1 to T13 Holocene great earthquakes at Juan de Fuca Channel (JDF) site and Cascadia Channel (CC) on the northern Cascadia margin. A) Plot showing comparative ^{14}C and best hemipelagic thickness (BT) ages vs turbidite (T) events at Juan de Fuca Channel (JDF) (Table 2). After the application of the hemipelagic method to ^{14}C ages to avoid the basal erosion, these two data sets compare well. B) Plot showing turbidite recurrence times at JDF site, for both ^{14}C and BT data sets. After refining calculations based on hemipelagic thickness, agreement of the two independent data sets is considerably improved (Table 2). C) Plot showing comparative ^{14}C and BT ages vs. T events at Cascadia Channel (CC) (Table 3). After hemipelagic-based correction to ^{14}C ages for basal erosion, these two data sets compare well. D) Plot showing turbidite recurrence times at CC site, for both ^{14}C and BT data sets. After corrections based on hemipelagic thickness, agreement of the two independent data sets is improved (Table 3).

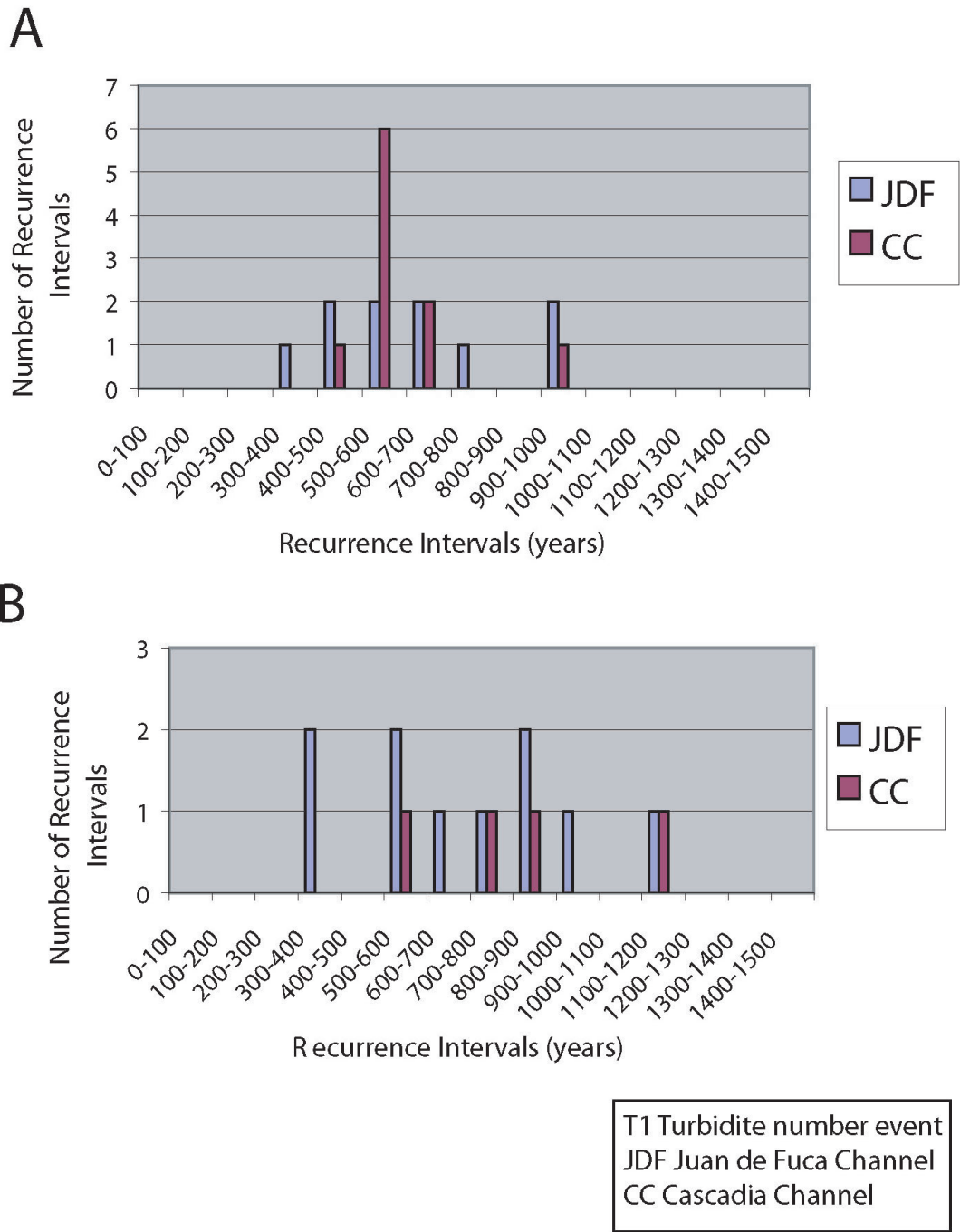


Figure 6. Comparison of the frequency distribution of recurrence times from T1 to T10 turbidite events in Juan de Fuca (JDF) and Cascadia Channel (CC). Histogram A) is based on best hemipelagic sediment thickness (BT), and histogram B) is based on AMS radiocarbon ages (¹⁴C) (Tables 2, 3). Histograms show the number of recurrence times observed in each 100 yr interval class (e.g., 0–100 yr, 100–200 yr) at each site shown in the figure. Note that the maximum (~ 1300 yr) and minimum (~ 300 yr) recurrence times are the same for ¹⁴C and BT, but both extremes are more frequent for the ¹⁴C data set. Comparing both histograms, we can infer that BT data show a major mode of recurrence times from 500 to 600 years and a normal distribution of times, whereas the ¹⁴C recurrence times are more broadly distributed.

sediment on the ¹⁴C age for T3 at Juan de Fuca Channel because the H where the ¹⁴C sample was taken was 12% thinner than the BT for this turbidite T3 (40 mm in 11TC/12TC cores compared to 45 mm of BT for T3 in all cores at this site) (Table 2). We subtract the time corresponding to the 5 mm of sediment thickness. This results in a corrected age of 791 yr, using 11 cm/1000 yr of sedimentation rate. At Juan de

Fuca Channel we eliminated the effect caused by the erosion in the hemipelagic sediment on ^{14}C ages in T3, T10, and T11, obtaining final ages of 791 yr, 4606 yr, and 5976 yr, respectively (Table 2). At Cascadia Channel we did the same recalculation of ^{14}C ages in T6, T8, T9, and T12, obtaining final ages of 2690 yr, 3533 yr, 4273 yr, and 6669 yr, respectively (Table 3). Those ages corrected by erosion have been used to calculate recurrence times shown in Figures 5B and 5D.

4.5. Datum Ages

After refining ^{14}C ages for sampling depth, we find that the first post-Mazama turbidite (T13) occurred at ~ 7200 cal. yr B.P., using ages in 12PC and 11PC from Juan de Fuca Channel and 25PC and core 6609-24 of Griggs (1969) from Cascadia Channel (Table 1, Fig. 1). Utilizing 7200 yr for T13 and 300 cal. yr B.P. (Nelson et al., 1995; Satake et al., 1996) for event T1, the interval of time between both datums is 6900 yr. Dividing 6900 yr by the 12 turbidite events, we obtain a mean recurrence time of 575 yr in northern Cascadia Basin. Using the sedimentation-rate corrections for the nearly identical ^{14}C ages of the T18 datum at key sites Juan de Fuca Channel, Cascadia Channel, and Rogue Apron (RA), we obtain an average age of ~ 9800 yr (Table 1). Based on the time difference between the T13 and T18 datum ages (i.e., 2600 yr /5 T events) equals an average recurrence time interval of 520 yr for the early Holocene in the northern Cascadia margin. In summary, the northern Cascadia margin represented by Juan de Fuca and Cascadia Channels has an average recurrence time of ~ 550 yr for T1 to T18 events during the Holocene.

4.6. Recurrence Times Based on Hemipelagic Sediment

Once the ^{14}C ages are refined for sampling depth and erosion, the sedimentation rates can be recalculated and averaged to estimate recurrence times of turbidite events based on BT.

Recurrence times based on hemipelagic sediment thickness are calculated by dividing BT and our moving-average sedimentation rates for the appropriate interval (Tables 2, 3, 4). As an example, the refined sedimentation rate in T2 of Juan de Fuca Channel is 14 cm/1000 yr and the recurrence time is 407 yr based on the following calculations: (57 cm of BT x 1000 yr) / 14 cm = 407 yr. The maximum BT recurrences times are 916 yr and 922 yr, and the minimum BT recurrences times are 321 yr and 221 yr for Juan de Fuca I and Cascadia Channels, respectively (Tables 2, 3, Figs. 5, 6). The BT recurrence times are shown in a plot of BT recurrence versus turbidite event and compared to ^{14}C recurrence curves for Juan de Fuca and Cascadia key sites (Fig. 5B, 5D). The BT curves are continuous and smoother than the ^{14}C curves at all sites for reasons discussed below, but the temporal patterns of the ^{14}C and BT curves are similar at each key site. Juan de Fuca Channel shows three cycles with maximum times between T11–T10, T8–T7, and T5–T4, with a cluster of more frequent turbidites after each long recurrence time. Cascadia Channel curves are more incomplete because there are some gaps without ages, but we can distinguish a maximum between T11 and T10.

4.7. Recurrence Time based on ^{14}C Age

We calculate turbidite recurrence times based on ^{14}C ages (^{14}C recurrences) by determining the time difference between each pair of turbidites (Tables 2, 3). The ^{14}C recurrences are shown in a plot of recurrence versus turbidite event number (T) for each Juan de Fuca and Cascadia key site (Fig. 5B, 5D). The maximum

^{14}C recurrence times are 1129 yr and 1613 yr, and the minimum ^{14}C recurrences times are 190 yr and 34 yr for Juan de Fuca and Cascadia Channels, respectively, when ages are not corrected for significant H erosion where the ^{14}C sample was taken (see discussion in section 11 below) (Tables 2, 3; Fig. 6).

4.8. Ages of Turbidites Based on Best Hemipelagic Sediment Thickness (BT)

We add the BT recurrence interval times consecutively with depth to determine the age of each turbidite based on hemipelagic sediment thickness (Tables 2, 3). For example, turbidite T2 has a BT age of 707 yr when the time since the last turbidite (300 cal. yr B.P.) (Nelson et al., 1995; Satake et al., 1996) is added to the BT recurrence time of T2 that is 407 yr. Similarly, T3 is 1064 yr when the T2 age of 707 yr is added to the T2 to T3 BT recurrence time of 357 yr, etc. (Table 2). BT and ^{14}C ages are plotted versus T events (Fig. 5). Except for the oldest ages, the independently derived BT and ^{14}C ages have a close correspondence in Juan de Fuca and Cascadia channels. The ^{14}C and BT ages from Juan de Fuca Channel provide the most complete data sets for comparison. At Juan de Fuca Channel, the ^{14}C and BT ages show relatively good agreement, with about half the ages between T1 to T13 exhibiting a difference of ~ 100 yr or less for correlative T events (Table 2, Fig. 5A). Cascadia Channel does not have a complete data set, but between ^{14}C and BT curves we can find less than 100 years difference in T3, T4, T6, and T8 and a difference of hundreds to a thousand years between T9 to T12 (Table 3, Fig. 5C). A gradually greater difference in ^{14}C and H ages most likely takes place down core because age errors are cumulative.

4.9. Analysis of Noyo Independent Hemipelagic Sediment Thickness for ^{14}C Oxcal Age Corrections

The turbidite record for the northern San Andreas Fault, in general, is more difficult to assess, because: (1) there are no good regional datums like Mazama ash or consistent Holocene to Pleistocene faunal changes to correlate turbidites, (2) the turbidites are more difficult to distinguish visually in the upper part of cores because colors are less distinct between the hemipelagic and turbidite tail sediment, and (3) the amount of compaction varies for different coring systems (i.e., we calculated 27% in 49TC, 30% in 54KC, and 17% in 50BC at Noyo Channel, based on differences in thickness for correlated layers in different cores) (Fig. 7, Table 4, Appendix 1). For this reason, we have made alternative calculations for H analysis at Noyo Channel to test calibrated ^{14}C ages that were calculated using the OxCal software to calibrate and refine radiocarbon probability models (<http://www.rlaha.ox.ac.uk/orau/oxcal.html>). Goldfinger et al. (2007) used this method to incorporate external constraints such as sediment thickness, sedimentation rates, and historical data to refine the ^{14}C probability distributions for a given event.

Using OxCal, multiple ages for a given event are taken into consideration, and rather than averaging, iterative Bayesian models are used to narrow the probability distributions for events that are known to correlate, and/or have independent constraints such as the 1906 San Francisco earthquake (Nelson et al., 2000; Ramsey, 2001). Where age data are missing, sedimentation rates and hemipelagic intervals alone can be used. Ages calculated in this way can substitute for undatable events, and serve as a check on the ^{14}C ages. Using ^{14}C ages modified by the OxCal methodology, we have done a parallel H analysis for Noyo Channel, obtaining recurrence times and ages based on hemipelagic sediment thickness (Fig. 7, Table 4, Appendix 1). The basic methodology to obtain these recurrences follows the same techniques used in Cascadia Basin, except that for the Noyo Channel data we do not use cal. yr B.P. ages. Instead, we use ^{14}C ages modified by OxCal with all the constraints included (sampling depth, erosion, and hemipelagic sediment thickness).

TURBIDITE	*H Rec (yr)				Average		OxCal ¹⁴ C Ages	OxCal ¹⁴ C ** Rec
	54KC	49PC	49TC	50BC	* H Rec	H Ages		
1	203	207	203	207	205	97	97	142
2	174	176	174	178	176	302	239	170
3	180	179	180		180	478	409	
4								
5	151	187	188		188	658	559	270
6	151	311	282		296	846	829	348
7	172	206	199		203	1142	1177	202
8	155	231	207		219	1345	1379	260
9	206	148	164		185	1564	1639	240
10	206	215	216		212	1749	1879	270
11	155	207	207		207	1961	2149	210
12	155	215	216		215	2168	2359	260
13	206	169	216		211	2383	2619	180
14	206	169	181		194	2594	2799	

* H Oxcal Recurrences obtained through sedimentation rates using OxCal ages and original H from each core (see Appendix 1).

** Correlative difference between OxCal ages (i.e., 239 yr - 97 yr is 142 yr, the recurrence time between T1 and T2)

Table 4. Noyo Channel hemipelagic sediment thicknesses in multiple cores, recurrence times, and age analysis.

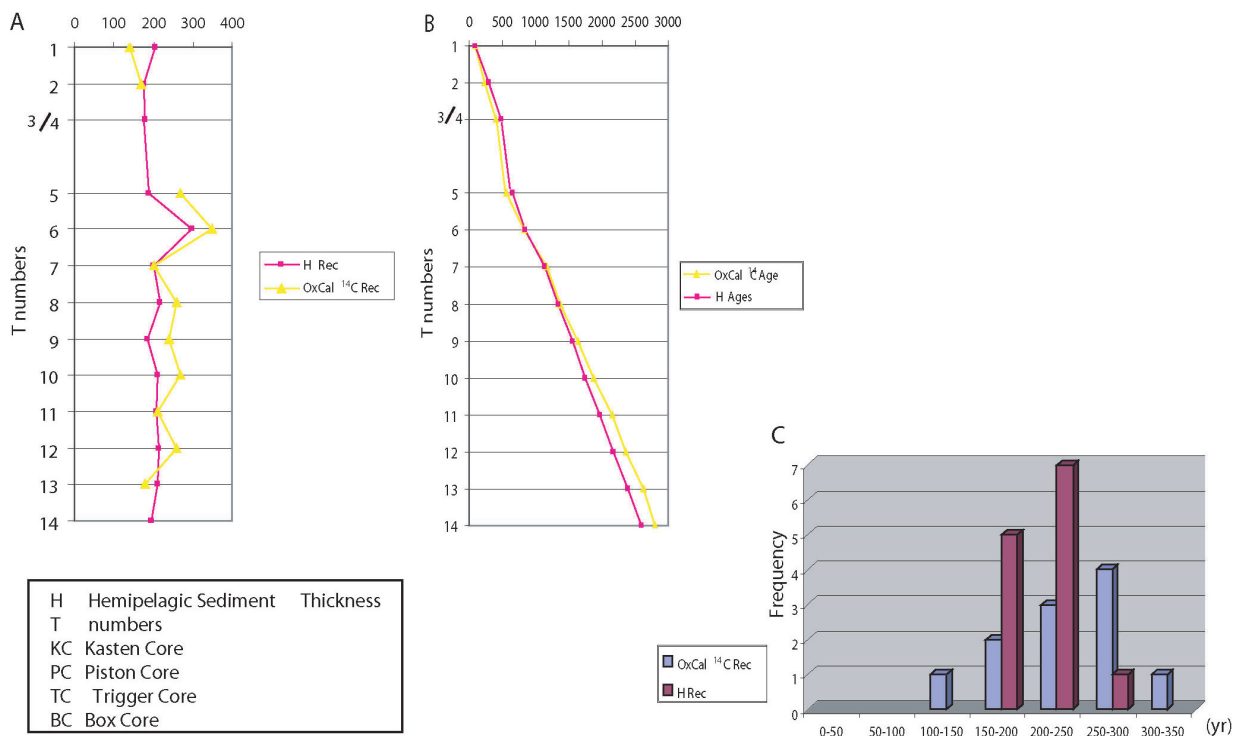


Figure 7. Noyo Channel recurrence analysis based on ¹⁴C ages obtained with the OxCal Software 49PC (piston) and 49TC (trigger), 54 KC (Kasten), and 50BC (box) cores. Plots display results of Table 4. A) Plot showing the hemipelagic sediment recurrence times (H Rec) in dark pink and the OxCal recurrence times (OxCal ¹⁴C Rec) in yellow through 14 correlative turbidites. Note that the hemipelagic sediment recurrence time is an average curve between all the recurrence times obtained in the four cores at Noyo channel (see Table 4 above and Appendix 1). Both curves are in good agreement, but in general, the hemipelagic sediment recurrence times show less variation than ¹⁴C times. B) Plot showing the OxCal ¹⁴C Age in yellow vs. the hemipelagic sediment ages (H Ages) in dark pink through the same 14 turbidites. Note that the H ages are equal or younger from T6 to T14 whereas they are slightly older in T2, T3/4, and T5 (Table 4). C) Histogram showing the distribution of turbidite recurrence frequencies at Noyo Channel for the first 14 turbidite events. Note that the H recurrence bars (H Rec) show a more normal distribution than the OxCal recurrence bars (OxCal ¹⁴C Rec), with maximum, recurrence times of ~ 250 yr and minimum times of ~ 150 yr.

As in Cascadia Basin, the hemipelagic sediment thicknesses were measured between the turbidite events in cores 49 PC/TC, 54KC, and 50BC, and an independent analysis of recurrence interval times for each core was done considering its individual compaction rate. The total H is added to obtain the cumulative H, and

the sedimentation rates are calculated using OxCal ^{14}C ages. The sedimentation rates are calculated using a moving window. The recurrence times were then averaged for each correlative turbidite. In some cases we average the recurrence times from three cores, and in cases where one core has an extreme value the average is based on two cores (except for events one and two, where four recurrences are averaged) (Table 4). To obtain H ages we follow the same procedure used for Cascadia Basin. For OxCal ^{14}C recurrence times, we determine the time between each set of correlative turbidites.

We find that the maximum and minimum H recurrence times are 296 yr and 176 yr, respectively and the maximum and minimum OxCal ^{14}C recurrence times are 348 yr and 142 yr. The average H recurrence time is 207 yr, and the average OxCal ^{14}C recurrence time is 232 yr (Table 4). The pattern of recurrence and age variations down the core for the first 14 events is plotted in Figure 7A and B. Note that events 3 and 4 are considered as one turbidite event because there is an absence of hemipelagic sediment between pulses in a single continuous turbidite.

The recurrence curves show parallel results, suggesting that both data sets are compatible but that H recurrence times have less variation compared to ^{14}C recurrence times. Comparing both data sets, turbidites T2, T7, and T11 exhibit almost equal recurrence times, but the rest of the events have lower values of H recurrence times (about 40–50 yr of difference). The highest frequency of H recurrence times is between 200 and 250 yr (Fig. 7C). The OxCal ^{14}C recurrence times show maximums between 300 and 350 yr, and the distribution of frequencies is lower and broader than H recurrence times. The plot of OxCal ^{14}C age against H age has younger ages from T1 to T5, similar ages from T6 to T8, and older ages from T9 to T14, with an increasing difference down the core, which, as with Cascadia dates, also appears to be related to the cumulative error down core in H ages.

5. DISCUSSION

5.1. Contribution of Analysis of Hemipelagic Sediment Thickness to Paleoseismic Studies

Analysis of hemipelagic sediment thickness contributes significantly to paleoseismic studies in deep-water environments where turbidites can be proxies for earthquakes. The onland coastal paleoseismic record is limited to ~ 7000 yr in the Cascadia Subduction Zone and to ~ 3000 yr on the Northern California margin (Satake et al., 1996; Atwater and Hemphill-Haley, 1997; Kelsey et al., 2002; Niemi et al., 2002) whereas the turbidite stratigraphy provides a 10,000 yr record of earthquake periodicity (Nelson et al., 2000; Goldfinger et al., 2003a; 2003b; Goldfinger et al., 2007). In addition, onshore, paleoseismic studies are commonly based only on ^{14}C ages, and they have no independent method like the hemipelagic thickness analysis to assess reliability of minimum recurrence times between turbidites and to estimate turbidite ages that are undatable by ^{14}C .

How reliable is the hemipelagic-thickness method? In the Cascadia Basin, hemipelagic sediment thickness is consistent throughout the basin relative to the distance from the base of the continental slope. At proximal locations at the base of the continental slope, about 360 cm of hemipelagic sediment was deposited during the Holocene, whereas at distal locations, such as Cascadia Deep Sea Channel, the average thickness is about 100 cm, which is slightly more than numerous interchannel cores without turbidites (~ 90 cm) (Fig. 4). Our analysis of many Cascadia Basin cores also shows that there is only a small percent change in hemipelagic sedimentation rates during Holocene time at any location (Tables 2, 3). The map of Holocene sediment drape demonstrates that the hemipelagic sediment thickness in channel locations

with turbidites and adjacent interchannel locations without turbidites is approximately the same (Fig. 4). An important implication of this study is that during the Holocene there was no significant net erosion of hemipelagic sediment by abyssal-channel turbidity currents. Nevertheless, there is some local erosion below some turbidites, which may have resulted from stronger turbidity currents caused by bigger earthquakes and variable topography of the channel floors.

The hemipelagic-thickness method in Cascadia Basin, along with the turbidite paleoseismic method, may be restricted to times of sea-level highstand because turbidity currents are weaker, contain a smaller and finer sediment load, and are generated in canyon heads distal from river mouths (Fig. 1). In contrast, lowstand turbidites are thicker and coarser grained, and result in significant channel-floor erosion (Nelson, 1976; Nelson et al., 2000). Another reason why this turbidite paleoseismology may work only during highstands is that earthquakes are the primary turbidity-current triggering mechanism whereas during lowstands there may be additional mechanisms, including ignitive turbidity currents, hyperpycnal flows, and random sediment failures in addition to earthquakes (Nelson et al., 2000; Goldfinger et al., 2003a; 2003b; Goldfinger et al., 2006).

On active margins, such as Cascadia and northern California, the hemipelagic-thickness method can be used as a tool to refine turbidite ^{14}C ages, by correcting the effects of erosion of hemipelagic sediment and errors in sample technique that anomalously increase the recurrence times between earthquakes.

5.2. Turbidite Recurrence Times in the Cascadia Subduction Zone

It is of great importance for hazard analysis to define accurate minimum recurrence times for great earthquakes in the Cascadia Subduction Zone. Because of the constant rate of hemipelagic sedimentation in channel versus interchannel locations during the Holocene (e.g., generally 10 cm/1000 yr at Cascadia Channel), minimum ^{14}C recurrence intervals cannot be less than the BT stratigraphic time represented by multiple cores at a key site. For example, the minimum recurrence time based on ^{14}C ages for T11 and T12 in Cascadia Channel is 34 yr, whereas the recurrence interval based on BT is 278 yr (Table 3). Assuming a consistent sedimentation rate of 9 cm/1000 yr between T11 and T12 and having a hemipelagic sediment thickness of 2.5 cm below T11, the stratigraphic time between those turbidites increases almost 250 yr in comparison with the time obtained by considering only uncorrected ^{14}C ages ($6780 - 6746 = 34$ yr, difference between two correlative ^{14}C ages) (Table 3). Thus, it is crucial to refine ^{14}C ages using hemipelagic sediment thickness between turbidites to obtain the most accurate measure of minimum recurrence times.

On the Cascadia Subduction Zone margin, the turbidite events in the Juan de Fuca and Cascadia channels for the past 5000 yr (between T1 and T10) show maximum BT and ^{14}C recurrence times of between ~ 1000 and 1200 yr and minimum recurrence times of ~ 300 –400 yr (Fig. 6). Although both types of data show similar maxima and minima, the BT recurrence times display a more normal distribution with a mode of 500–600 yr compared to the ^{14}C recurrences, which have a broader distribution (Fig. 6). Comparing the hemipelagic-thickness recurrence times (BT recurrences) with the ^{14}C recurrence times for Juan de Fuca and Cascadia Channels from T1 to T13 and from T1 to T18, respectively, in Tables 2 and 3, we can see a difference between the maximum and minimum of ^{14}C recurrence times on the order of a thousand years for both (~ 900 –1500) whereas the difference of BT recurrences are on the order of hundreds of years (~ 600 –700 yr). This demonstrates that when we use data on hemipelagic thickness to correct ^{14}C ages, we smooth the recurrence times by eliminating apparent ^{14}C outliers.

The large number of age dates from cores in Cascadia Basin along with well-constrained stratigraphic

datums allows an accurate measure of turbidity-current recurrence intervals. We found that turbidites occur with an average frequency of ~ 550 yr for the past ~ 7200 yr and ~ 520 yr from 7200 yr to 9800 yr in northern Cascadia Basin. These average recurrence values can be used to compare with other margins with similar tectonic settings. Based on tsunami deposits, Nanayamal et al. (2003) interpret that great earthquakes that rupture ~ 1000 km of the Kurile Trench Subduction Zone also occur approximately every 500 years. In contrast, the historic record of the Nankai Trough Subduction Zone appears to exhibit much more frequent (100–150 yr) and segmented earthquakes (Sugiyama, 1994). Obviously, many more H method studies about earthquake frequency are necessary in other subduction zones, such as Sumatra, to define the variability of earthquake frequency (Gutierrez-Pastor et al., 2005; Nelson et al., 2005).

5.3. Turbidite Recurrence Times on the Northern California Margin

In Noyo Channel, we have been able to obtain and to compare recurrence times based on OxCal ^{14}C ages and hemipelagic sediment thickness (H) where correlations are more difficult to distinguish without regional datums (Table 4, Fig. 7). By using OxCal ^{14}C ages “overlapped” with hemipelagic analysis, we obtain better agreement in turbidite age between H and ^{14}C methods than in Cascadia Subduction Zone Margin, where we use cal yr. B.P. ages. In the northern California Margin, using hemipelagic thickness analysis, we obtain an average recurrence time of ~ 200 yr between turbidite events, maximum times of 296 yr (H recurrence) and 348 yr (OxCal ^{14}C recurrence) and minimum times of 176 yr (H recurrence) and 142 yr (Oxcal ^{14}C recurrence) (Fig. 7C, Table 4). The OxCal ^{14}C recurrence times have greater extremes than those based on analysis of hemipelagic thickness. Similar to Cascadia Basin, the data from California again shows that the larger data base of hemipelagic thickness provides a more normal distribution of recurrence times than ^{14}C ages. The more normal distribution of hemipelagic recurrence times may result in part because the data base from multiple cores and all turbidites is much larger and in part because each ^{14}C recurrence value is based on two ages, each of which can have an error. Consequently, the chances for errors with ^{14}C recurrence times are twice that compared to turbidite recurrence times based on hemipelagic thickness, and could result in additive or subtractive ^{14}C outliers.

We observe that earthquakes on the California margin (~ 200 yr) trigger turbidites more frequently than on the Cascadia margin (~ 500 yr), and this is corroborated by the onland record (Prentice et al., 1999; Knudsen et al., 2002; Kelson et al., 2006; Zhang et al., 2006; Goldfinger, et al., 2007). At Olema, 45 km north of San Francisco, Niemi and Hall (1992) estimate that if the 4–5 m slip event recorded in 1906 is characteristic, the recurrence time for such events would be 221 ± 40 yr. Both our data and 10 new ages from the Vendata site and sites near Fort Ross suggest an average recurrence interval of ~ 200 –230 yr (Goldfinger et al., 2007).

Along the Cascadia margin, the tsunami record at Willapa Bay, Washington, and the onshore record of Sixes Rivers, Oregon, show average recurrence times of great earthquakes for the past 4000 years (533 and 529 yr, respectively) that agree quite closely with those of the turbidite paleoseismic record of the past 4000 yr (~ 520 yr) (Atwater and Hemphill-Haley, 1997; Kelsey et al., 2002; Nelson et al., 2003). Consequently, we have the potential to go back in time using both the turbidite and onshore paleoseismic records to establish a more complete model of earthquake recurrence times to be applied in different active continental-margin settings.

5.4. Global Implications

The Cascadia and northern California continental margins comprise a data base of many cores with numerous ^{14}C turbidite ages. There are many contamination and sampling artefacts that must be noted to obtain the best ^{14}C age. At this point, our study shows that the evaluation of hemipelagic thickness and sedimentation rates together with ^{14}C ages can be an effective method to improve the temporal turbidite history of a continental-margin system. These data are of particular importance where accurate assessment of recurrence-interval statistics is integrated into assessments of seismic hazard. To create a rapid preliminary method to estimate turbidite recurrence times and ages, the hemipelagic analysis can be used with a minimum number of ^{14}C ages. A caveat to this method is that when coastal and turbidite paleoseismic records need to be correlated, both complete ^{14}C and H methods are necessary. The two methods applied to turbidite paleoseismology offer time spans mostly unavailable at land paleoseismic sites and the use of two complementary methods for turbidite ages and frequency.

The analysis of hemipelagic sediment thickness can be applied to different margins with multiple turbidite systems and tributary-channel confluences. The thickness of the Holocene hemipelagic sediment needs to be mapped in areas without turbidites and carefully ^{14}C dated to prove that the amount of hemipelagic sediment deposited is almost equal along the margin and that the sedimentation rate is constant. With the known thickness patterns of the hemipelagic sediment, multiple cores can be utilized to determine the reliability of hemipelagic sediment in channel-floor sites that may be subject to local turbidity-current erosion.

Our studies on the Cascadia and northern California margins suggest that during the Holocene, turbidity currents were weaker and thus hemipelagic sediment is a reliable measure of time. The opposite appears to be the case during the late Pleistocene, because the thick and coarse turbidites indicate stronger and presumably more erosive turbidity currents during times of lower sea level and greater sediment input directly into canyon heads (Nelson, 1968, 1976; Nelson, et al., 2000).

Our study of analysis of hemipelagic sediment thickness has developed the first extensive data set to infer average recurrence times for paleoseismic turbidites on two different types of tectonically active margins. Great earthquakes on the northern California margin are more than twice as frequent on average (200 yr) as those on the northern Cascadia Subduction Zone margin (~ 550 yr). Our data showing two different recurrence frequencies is an important verification of the hemipelagic-thickness and turbidite paleoseismic methods.

6. CONCLUSIONS

On the Cascadia Subduction Zone and northern California continental margins, we define and compare Holocene ages, frequency, and recurrence interval between turbidites with two methods: (1) absolute dating (^{14}C method) and (2) relative dating, based on the measure of time interval between turbidite events, using hemipelagic sediment thickness between two turbidites (H method). Turbidite ages and recurrences times, based on ^{14}C ages or semi-independent hemipelagic thickness ages, generally agree if ^{14}C ages taken from anomalously thin hemipelagic interbeds are corrected for erosion.

The H method is important because (1) deep-sea sedimentation provides an independent time yardstick derived from a constant rate of hemipelagic sediment deposited between turbidites; (2) hemipelagic thickness/sedimentation rate provides a set of turbidite recurrence times and calculated ages to compare

with similar ^{14}C data sets; (3) the evaluation of hemipelagic sediment thickness in multiple cores at the same site can be utilized to evaluate erosion effects, and to refine and test the reliability of radiocarbon ages that look too old for a better correlation of turbidite events and consequent paleoseismic history along the margin; (4) hemipelagic data are available for every turbidite event from multiple cores at each key site compared to a single incomplete set of radiocarbon ages at each key site; (5) hemipelagic data can be used to calculate ages for events that cannot be dated by other methods; and (6) hemipelagic data can be used to constrain radiocarbon age distributions, particularly for (1) minimum recurrence times that are most important for hazards analysis, and (2) where the calibration curves result in broad probability density functions.

From the analysis of hemipelagic sediment thickness in the northern Cascadia Subduction Zone we can conclude that: (1) for the past ~ 7200 cal. yr B.P. whole plate earthquakes take place every ~ 575 yr on average and every ~ 520 yr in the early Holocene (between ~ 7200 and 9800 yr), (2) for the past ~ 5000 yr minimum recurrence times are $\sim 300\text{--}400$ yr and the maximum recurrence times are $\sim 1000\text{--}1200$ yr, and (3) both ^{14}C and hemipelagic data sets have most recurrence times in the 500 to 800 yr range, but the hemipelagic data show a normal distribution of recurrence times from 500 to 600 yr whereas the ^{14}C recurrence times are more broadly distributed.

From the northern California margin hemipelagic analysis we conclude that for the past ~ 2600 yr: (1) frequency of earthquakes in Noyo Channel is ~ 200 yr, (2) the minimum recurrence times are ~ 176 yr based on the H analysis and ~ 142 yr based on the difference between correlative OxCal ^{14}C ages, and (3) the maximum recurrence times are ~ 300 yr based on the H analysis and ~ 350 yr based on the difference between correlative OxCal ^{14}C ages.

The H method indicates that earthquakes on the San Andreas transform fault along the northern California are twice as frequent as on the Cascadia Subduction Zone margin. The H method together with ^{14}C ages may be valuable tools to infer periodicity of earthquakes in different tectonic settings.

Techniques of turbidite paleoseismology and hemipelagic sediment thickness are important to use for analysis of earthquake hazard risk on active margins worldwide. The results obtained in Cascadia Subduction Zone and the California margin off the northern San Andreas Fault can be applied and compared with other active margins as well as passive margins where earthquake triggering is less important.

ACKNOWLEDGMENTS

We wish to thank the crews of the Scripps Institute of Oceanography ships R.V. Melville and R.V. Roger Revelle and the members of the 1999 and 2002 Scientific Parties: Mike Winkler, Pete Kalk, Antonio Camarero, Clara Morri, Gita Dunhill, Luis Ramos, Alex Raab, Nick Pias Jr., Mark Pourmanoutscheri, David Van Rooij, Lawrence Amy, Churn-Chi “Charles” Liu, Chris Moser, Devin Etheridge, Heidi Stenner, Chris Popham, Claire McKee, Duncan MacMillan, Chris Crosby, Susanne Schmid, Eulalia Gracia, Suzanne Lovelady, Chris Romsos, Jason Chaytor, Vincent Rinterknecht, Rondi Robison, David Casas, Francois Charlet, Britta Hinrichsen, Jeremiah Oxford, Miquel Marin, Marta Mas, Sergio Montes, Raquel Villalonga, Alexis Vizcaino, Santiago Jimenez, Mayte Pedrosa, Silvia Perez, Jorge Perez, Andreu Turra, David Lamas, Himar Falcon, and Andres Barranco.

Our special thanks to the Active Tectonics Group at Oregon State and Michela Kashgarian of Lawrence Livermore Laboratory for analysis of ^{14}C ages. James H. Power from the U.S. Environmental Protection Agency at Newport, Oregon, provided the use of the Laser Diffraction Particle Size Analyzer for grain-size

analysis. We gratefully acknowledge funding by the U.S. National Science Foundation (Awards: 0107093 and 0001074) and U.S. Geological Survey for this research (Awards: GRANT00017981, GRANT00018360, 04HQGR0063, 03HQGR0008, 03HQGR0006, 02HQGR0034, 02HQGR0043) and the Ministerio de Educación y Ciencia (Award CGL2006-27096-E/BTE) and Consejo Superior de Investigaciones Científicas (CSIC)-Spain (Award: PI 2006 3 01 021).

REFERENCES

- Adams, J., 1990, Paleoseismicity of the Cascadia Subduction Zone: evidence from turbidites off the Oregon–Washington margin: *Tectonics*, v. 9, p. 569–583.
- Argus, D.F., and Gordon, R.G., 1991, Current Sierra Nevada–North America motion from very long baseline interferometry: Implications for the kinematics of the western United States: *Geology*, v. 19, p. 1085–1019.
- Atwater, B.F., 1987, Evidence for great Holocene earthquakes along the outer coast of Washington State: *Science*, v. 236, p. 942–944.
- Atwater, B.F., Goldfinger, C., and Nelson, C.H., 2004, Onshore–offshore correlation of geologic evidence for great Cascadia earthquakes—Permissive agreement between Washington estuaries and Cascadia deep-sea channel (abstract): *Eos, American Geophysical Union, Transactions*, v. 85, no. 47, Fall Meeting Supplement, Abstract T12B-01.
- Atwater, B.F., and Hemphill-Haley, E., 1997, Recurrence intervals for great earthquakes of the past 3500 years at northeastern Willapa Bay, Washington: U.S. Geological Survey, Professional Paper 1576, 108 p.
- Brown, R.D., 1995, 1906 Surface Faulting on the San Andreas Fault near Point Delgada, California: *Seismological Society of America, Bulletin*, v. 85, p. 100–110.
- Carlson, P.R., and Nelson, C.H., 1969, Sediments and sedimentary structures of the Astoria Submarine Canyon–Fan System, Northeast Pacific: *Journal of Sedimentary Petrology*, v. 39, p. 1269–1282.
- DeMets, C., and Dixon, T.H., 1999, New kinematic models for Pacific-North America motion from 3 Ma to present; I, evidence for steady motion and biases in the NUVEL-1A model: *Geophysical Research Letters*, v. 26, p. 1921–1924.
- Duncan, J.R., 1968, Late Pleistocene and Postglacial Sedimentation and Stratigraphy of Deep-Sea Environments off Oregon: Unpublished Ph.D. Dissertation, Oregon State University, Corvallis, 222 p.
- Duncan, J.R., Fowler, G.A., and Kulm, L.D., 1970, Planktonic foraminiferan–radiolarian ratios and Holocene–Late Pleistocene deep-sea stratigraphy off Oregon: *Geological Society of America, Bulletin*, v. 81, p. 561–566.
- Goldfinger, C., Morey, A., Erhardt, M., Nelson, C.H., Gutiérrez-Pastor, J., Enkin, R., and Dallimore, A. 2006, Cascadia great earthquake recurrence: rupture lengths, correlations and constrained OxCal analysis of event ages: U.S. Geological Survey, Tsunami Sources Workshop, Proceedings, Diggles, J., Geist, E., and Lee, H., eds., CD-ROM, April 21 and 22, 2006.
- Goldfinger, C., Morey, A., Nelson, C.H., Gutierrez-Pastor, J., Johnson, J.E., Karabanov, E., Chaytor, J., Eriksson, A., and the Shipboard Scientific Party, 2007, Rupture lengths and temporal history of significant earthquakes on the offshore and North Coast segments of the Northern San Andreas Fault based on turbidite stratigraphy: *Earth and Planetary Science Letters*, v. 254, p. 9–27.
- Goldfinger, C., Nelson, C.H., and Johnson, J., 2003a, Holocene earthquake records from the Cascadia Subduction Zone and Northern San Andreas Fault based on precise dating of offshore turbidites: *Annual Reviews of Geophysics*, v. 31, p. 555–577.

- Goldfinger, C., Nelson, C.H., and Johnson, J.E., 2003b, Deep-water turbidites as Holocene earthquake proxies: The Cascadia Subduction Zone and Northern San Andreas Fault Systems: *Annali Geofisica*, v. 46, p. 1169–1194.
- Gorsline, D.S., De Diego, T., and Nava-Sanchez, E.H., 2000, Seismically triggered turbidites in small margin basins: Alfonso Basin, Western Gulf of California and Santa Monica Basin, California Borderland: *Sedimentary Geology*, v. 135, p. 21–35.
- Griggs, G.B., 1969, Cascadia Channel: The anatomy of a deep sea channel: Unpublished Ph.D. Dissertation, Oregon State University, Corvallis, Oregon, 183 p.
- Griggs, G.B., Carey, A.G., and Kulm L.D., 1969, Deep-sea sedimentation and sediment–fauna interaction in Cascadia Channel and on Cascadia abyssal plain: *Deep-Sea Research*, v. 16, p. 157–70.
- Griggs, G.B., and Kulm, L.D., 1970, Sedimentation in Cascadia deep-sea channel: *Geological Society America, Bulletin*, v. 81, p. 1361–1384.
- Gutierrez-Pastor, J., Nelson, H.C., Goldfinger, C., and Johnson, J.E., 2005, Holocene turbidite history in the Cascadia Subduction Zone shows the potential to develop paleoseismic methods for the Sumatra and other subduction zones (abstract): Vienna, European Geophysical Union Meeting 05, A07873.
- Kelsey, H.M., Witter, R.C., and Hemphill-Haley, E., 2002, Plate-boundary earthquakes and tsunamis of the past 5500 yr, Sixes River estuary, southern Oregon: *Geological Society of America, Bulletin*, v. 114, p. 29–314.
- Kelson, K., Strieg, A., Koehler, R., and Kang, K., 2006, Timing of Late Holocene Paleearthquakes on the Northern San Andreas Fault at the Fort Ross Orchard Site, Sonoma County, California: *Seismological Society of America, Bulletin*, v. 96, p. 1012–1028.
- Knudsen, K.L., Witter, R.C., Garrison-Laney, C.E., Baldwin, J.N., and Carver, G.A., 2002, Past earthquake-induced rapid subsidence along the northern San Andreas Fault: A new paleoseismological method for investigating strike-slip faults: *Seismological Society of America, Bulletin*, v. 92, p. 2612–2636.
- Lees, J.A., Fowler, R.J., and Appleby, P.G., 1998, Mineral magnetic and physical properties of surficial sediments and onshore samples from the southern basin of Lake Baikal, Siberia: *Journal of Paleolimnology*, v. 20, p.175–186.
- Nakajima, T., and Kanai, Y., 2000, Sedimentary features of seismoturbidites triggered by the 1983 and older historical earthquakes in the eastern margin of the Japan Sea: *Sedimentary Geology*, v.135, p. 1–19.
- Nanayamal, F., Satake, K., Furukawa, R., Shimokawa, K., Atwater, B.F., Shigeno, K., and Yamaki, S., 2003, Unusually large earthquakes inferred from tsunami deposits along the Kuril trench: *Nature*, v. 424, p. 660–663.
- Nelson, A.R., Atwater, B.F., Brobowski, P.T., Bradley, L.A., Clague, J.J., Carver, G.A., Darienzo, M.E., Grant, W.C., Krueger, H.W., Sparks, R., Stafford, T.W., and Stuiver, M., 1995, Radiocarbon evidence for extensive plate-boundary rupture about 300 years ago at the Cascadia subduction zone: *Nature*, v. 378, p. 371–374.
- Nelson, C.H., 1968, Marine Geology of Astoria Deep-Sea Fan: Unpublished Ph.D. Dissertation, Oregon State University, Corvallis, 289 p.
- Nelson, C.H., 1976, Late Pleistocene and Holocene depositional trends, processes, and history of Astoria Deep-Sea Fan, northeast Pacific: *Marine Geology*, v. 20, p. 129–173.
- Nelson, C.H., Goldfinger, C., Gutierrez-Pastor, J., and Johnson, J.E., 2005, Cascadia Subduction Zone: confirmation by onshore records and the Sumatra 2004 Great earthquake (abstract): European

- Geophysical Union Meeting 05, Vienna, A07269.
- Nelson, C.H., Goldfinger, C., Johnson, J.E., and Dunhill, G., 2000, Variation of modern turbidite systems along the subduction zone margin of Cascadia Basin and implications for turbidite reservoir beds, in Weimer, P.W., Nelson, C.H. et al., eds., *Deep-Water Reservoirs of the World: Gulf Coast Section*, SEPM Foundation 20th Annual Research Conference, p. 714–738
- Nelson, C.H., Goldfinger, C., Johnson, J.E., and Gutierrez- Pastor, J., 2003, Holocene history of great earthquakes in the Cascadia Subduction Zone based on the turbidite event (abstract): *Eos*, v. 84, no. 46, Fall Meeting Supplement, Abstract S421-05.
- Nelson, C.H., Kulm, L. D., Carlson, P. R., and Duncan, J. R., 1968, Mazama ash in the northeastern Pacific: *Science*, v. 161, p. 47–49.
- Niemi, T.M., and Hall, N.T., 1992, Late Holocene slip rate and recurrence of great earthquakes on the San Andreas Fault in northern California: *Geology*, v. 20, p. 195–198.
- Niemi, T.M., Zhang, H., Generaux, S., Fumal, T., and Seitz, G.G., 2002, A 2500-year record of earthquakes along the Northern San Andreas Fault at Vedanta Marsh, Olema, CA: Geological Society of America, Cordilleran Section, 98th Annual Meeting (May 13–15, 2002), Abstracts with Programs, v. 34, no. 5, p. 70.
- Prentice, C.S., Merritts, D.J., Beutner, E.C., Bodin, P., Schill, A., and Muller, J.R., 1999, Northern San Andreas fault near Shelter Cove, California: Geological Society of America, Bulletin, v. 111, p. 512–523.
- Ramsey, C.B., 2001, Development of the Radiocarbon Program OxCal: *Radiocarbon*, v. 43, p. 355–363.
- Rivera, J., Karabanov, E.B., Williams, D.F., Buchinskyi, V., and Kuzmin, M., 2006, Lena River discharge events in sediments of Laptev Sea, Russian Arctic: *Estuarine Coast and Shelf Science*, v. 66, p. 185–196.
- Satake, K., Shimazaki, K., Tsuji, Y., and Ueda, K., 1996, Time and size of a giant earthquake in Cascadia inferred from Japanese tsunami records of January, 1700: *Nature*, v. 379, p. 246–249.
- Schwartz, D.P., Pantosti, D., Okumura, K., Powers, T.J., and Hamilton, J.C., 1998, Paleoseismic investigations in the Santa Cruz mountains, California: Implications for recurrence of large-magnitude earthquakes on the San Andreas Fault: *Journal of Geophysical Research*, v. 103, p. 17,985–18,001.
- Shiki, T., Kumon, F., Inouchi, Y., Kontani, Y., Sakamoto, T., Tateishi, M., Matsubara, H., and Fukuyama, K., 2000, Sedimentary features of the seismo-turbidites, Lake Biwa, Japan: *Sedimentary Geology*, v. 135, p. 37–50.
- Stuvier, M., and Braziunas, T.F., 1993, Modeling atmospheric ^{14}C influences and ^{14}C ages of marine samples to 10,000 BC: *Radiocarbon*, v. 35, p. 137–189.
- Sugiyama, Y., 1994, Neotectonics of Southwest Japan due to the right-oblique subduction of the Philippine Sea Plate: *Geofisica Int.*, v. 33, p. 53–76.
- Thatcher, W., Marshall, G., and Lisowski, M., 1997, Resolution of fault slip along the 470 km long rupture of the great 1906 San Francisco earthquake: *Journal of Geophysical Research*, v. 102, p. 5353–5367.
- Wynn, R.B., Weaver, P.P.E., Masson, D.G., and Stow, D.A.V., 2002, Turbidite depositional architecture across three interconnected deep-water basins on the north-west African margin: *Sedimentology*, v. 49, p. 669–695.
- Zdanowicz, C.M., Zielinski, G.A., and Germani, M.S., 1999, Mount Mazama eruption: calendrical age verified and atmospheric impact assessed: *Geology*, v. 27, p. 621–624.
- Zhang, H., Niemi, T., and Fumal, T., 2006, A 3000-year record of earthquakes on the Northern San Andreas Fault at the Vedanta Marsh site, Olema, California: *Seismological Research Letters*, v. 77 p. 356-357.

APPENDIX 1. ANALYSIS OF NOYO CHANNEL HEMIPELAGIC SEDIMENT THICKNESS

TURBIDITE	54KC H (cm)	Acumul. H	Oxcal ¹⁴ C ages	Sed rate	Grouping Sed. rates	Recurrence times
	0.9	0.9				
1	6.4	7.3	97	30.5	31.6	203
2	5.5	12.8	239	31.3	31.6	174
3 & 4	5.7	18.5	409	33.1	31.6	180
5	3.5	22	559	26.5	23.2	151
6	3.5	25.5	829	21.7	23.2	151
7	4	29.5	1177	21.4	23.2	172
8	3	32.5	1379	19.8	19.4	155
9	4	36.5	1639	19.4	19.4	206
10	4	40.5	1879	18.8	19.4	206
11	3	43.5	2149	18.4	19.4	155
12	3	46.5	2359	17.8	19.4	155
13	4	50.5	2619	18.0	19.4	206
14	4	54.5	2799		19.4	206

TURBIDITE	49PC H (cm)	Acumul. H	Oxcal ¹⁴ C ages	Sed. rate	Grouping Sed. rates	Recurrence times
	1.1	1.1				
1	7.5	8.6	97	36.0	36.3	207
2	6.4	15	239	36.7	36.3	176
3 & 4	6.5	21.5	409	38.5	36.3	179
5	6.8	28.3	559	34.1	36.3	187
6	10.1	38.4	829	32.6	32.5	311
7	6.7	45.1	1177	32.7	32.5	206
8	7.5	52.6	1379	32.1	32.5	231
9	4.5	57.1	1639	30.4	30.4	148
10	6.4	63.45	1879	29.5	29.5	215
11	6.1	69.546	2149	29.5	29.5	207
12	6.4	75.896	2359	29.0	29.5	215
13	5	80.896	2619	28.9	29.5	169
14	5	85.896	2799		29.5	169

TURBIDITE	49TC H(cm)	Acumul. H	Oxcal ¹⁴ C ages	Sed rate	Grouping Sed. rates	Recurrence times
	0.9	0.9				
1	6.4	7.3	97	30.5	31.6	203
2	5.5	12.8	239	31.3	31.6	174
3 & 4	5.7	18.5	409	33.1	31.6	180
5	5	23.5	559	28.3	26.6	188
6	7.5	31	829	26.3	26.6	282
7	5.3	36.3	1177	26.3	26.6	199
8	5.5	41.8	1379	25.5	26.6	207
9	4	45.8	1639	24.4	24.4	164
10	5	50.8	1879	23.6	23.2	216
11	4.8	55.6	2149	23.6	23.2	207
12	5	60.6	2359	23.1	23.2	216
13	5	65.6	2619	23.4	23.2	216
14	4.2	69.8	2799		23.2	181

TURBIDITE	50BC H(cm)	Acumul. H	Oxcal ¹⁴ C ages	Sed rate	Grouping Sed. rates	Recurrence times
	0.9	0.9				
1	6.4	7.3	97	30.5	30.9	207
2	5.5	12.8	239	31.3	30.9	178
3 & 4			409			
5			559			
6			829			
7			1177			
8			1379			
9			1639			
10			1879			
11			2149			
12			2359			
13			2619			
14			2799			

KC: Kasten Core
 PC: Piston Core
 TC: Trigger Core
 BC: Box core

H: Hemipelagic Sediment Thickness
 Sedimentation rate (Sed rate) in cm/ 1000 yr
 Oxcal¹⁴C ages (see Table 4 and Golfinger et al., in prep)



CAPÍTULO III

PALEOSISMICIDAD EN EL MARGEN DE CALIFORNIA

Rupture Lengths and Temporal History of Significant Earthquakes on the Offshore and North Coast Segments of the Northern San Andreas Fault Based on Turbidite Stratigraphy

Chris Goldfinger¹, Ann Morey¹, C. Hans Nelson², Julia Gutiérrez-Pastor², Joel E. Johnson³, Eugene Karabanov⁴, Jason Chaytor¹, Andrew Eriksson¹, and the Shipboard Scientific Party

¹*Oregon State University, College of Oceanic and Atmospheric Sciences
104 Ocean Admin. Bldg., Corvallis OR 97331, USA. gold@coas.oregonstatet.edu*

²*Instituto Andaluz de Ciencias de la Tierra (IACT) CSIC-Univ. de Granada
Campus de Fuentenueva s/n 18002 Granada, Spain odp@ugr.es*

³*Present address: University of New Hampshire, Department of Earth Sciences 56 College Rd. Durham, NH 03824-3589*

⁴*University of South Carolina, Dept. of Geological Sciences, Columbia, SC, 29208,*

Abstract

74 piston, gravity and jumbo Kasten cores were collected from channel and canyon systems draining the northern California continental margin to investigate the record of periodic Holocene turbidites for possible connection to large magnitude earthquakes on the adjacent Northern San Andreas Fault. Poorly known channel systems were mapped with multibeam sonar to define pathways and channel confluences. Cores sampled all major and many minor channel systems extending from Cape Mendocino to just north of Monterey Bay. Sampling both along and across channels was done, and particular attention was paid to channel confluences, as these areas afford opportunities to test for synchronous triggering of turbidity currents. While at sea, all cores were scanned using a GEOTEK multisensor core logger (MSCL), which collects high-resolution photography, P-wave velocity, gamma-ray density, and magnetic susceptibility data from the unsplit cores. Lithology was logged visually, and cores were later imaged with X-radiography.

We use ¹⁴C ages, relative dating tests at channel confluences, and stratigraphic correlation using physical properties to determine whether turbidites deposited in separate channel systems are correlative, implying they were triggered by a common event. These tests can, in most cases, separate earthquake triggered turbidity currents from other possible sources. The late Holocene turbidite record off northern California passes these tests for synchronous triggering, and can be correlated with multiple proxies from site to site between Noyo Channel and the latitude of San Francisco. Preliminary comparisons of our event ages with existing and in progress work at onshore coastal sites show good correlation, further circumstantial evidence that the offshore record is primarily earthquake generated. During the last ~2800 years, 15 turbidites are recognized, including the great 1906 earthquake. Their chronology establishes an average repeat time of ~200 years, similar to the onshore value of ~230 years. Along-strike correlation suggests that at least 8 of the youngest 10 of these events ruptured the 320 km distance from the Mendocino Triple Junction to near San Francisco.

Keywords: Paleoseismology, turbidite, Northern San Andreas Fault

1. INTRODUCTION

Recent rapid advances in Global Positioning System (GPS) technology now make it possible to measure crustal strain accumulation at plate boundaries with a high degree of certainty in only a few years. However, real-time strain measurements typically represent a fraction of one strain cycle. Fundamental questions about clustering, the applicability of slip-predicable or time-predicable models and the nature of long term stress interactions (e.g. [1,2]) remain largely unanswered because we rarely have a long enough earthquake record. What is needed most is recurrence data for more fault systems and over longer spans of time, so that meaningful statistical conclusions can be drawn. Paleoseismology has the potential to address these questions by directly using the larger time span available through the geologic record and precise dating techniques. In the past decade, discovery of rapidly buried marsh deposits and associated tsunami sands along the northern Pacific Coast of the US has led to the recognition that the Cascadia Subduction Zone, once thought aseismic due to low instrumental seismicity, has generated great (Mw 8-9) earthquakes in the past (e.g. [3,4]) and spurred the development of *off-fault* paleoseismology.

We have been using the marine turbidite record as a proxy for earthquake recurrence in both Cascadia and on the Northern San Andreas Fault (NSAF) [5,6]. Turbidite paleoseismology and other off-fault techniques must of course demonstrate that the events recorded are earthquake-triggered. Marine records are more continuous and extend further back in time than land records in most cases, and are actually more precise in the early to mid Holocene due to the abundance of datable foraminifera. In recent years, turbidite paleoseismology has been attempted in Cascadia [5,6,7], Puget Sound [8], Japan [9,10,11], the Mediterranean [12], the Dead Sea [13], northern California [14,15] and the Arctic ocean [16], and is a technique that is evolving as a precise tool for seismotectonics.

In 1999-2002, we collected 74 piston, gravity and jumbo Kasten cores from channel/canyon systems draining the northern California margin adjacent to the onshore and nearshore NSAF (Fig. 1). We mapped channel systems with a Simrad EM-120 multibeam sonar, collecting both high-resolution bathymetry and backscatter data essential for analysis of channel morphology, sedimentation patterns, and core siting. These data were processed and merged with existing multibeam data.

During the cruise, we sampled all major and many minor channel systems extending from Cape Mendocino to just north of Monterey Bay (Fig. 1). Sampling both down and across channels in some cases was done, and particular attention was paid to channel confluences, as these areas afford opportunities to test for synchronous triggering of turbidity currents.

These cores have yielded a turbidite record that is in good agreement with the shorter land record of Holocene NSAF earthquakes. Despite the intense scientific study of the NSAF stemming from the great seismic hazards to San Francisco, a reliable event history for this fault extending back through the Holocene has yet to be established. This is particularly true for the segments of the NSAF near and north of San Francisco. Establishment of an offshore record, reconciled with the land paleoseismic record, offers the opportunity to investigate long term earthquake behavior, stress interactions with other fault systems, and enables the use of these parameters in probabilistic hazard models.

In this paper we present preliminary results from the offshore turbidite event record along the NSAF extending to ~3000 years BP. We detail results from multiple tests of synchronous triggering, a key requirement for earthquake origin, as well as a comparison with onshore paleoseismic data. Finally, we

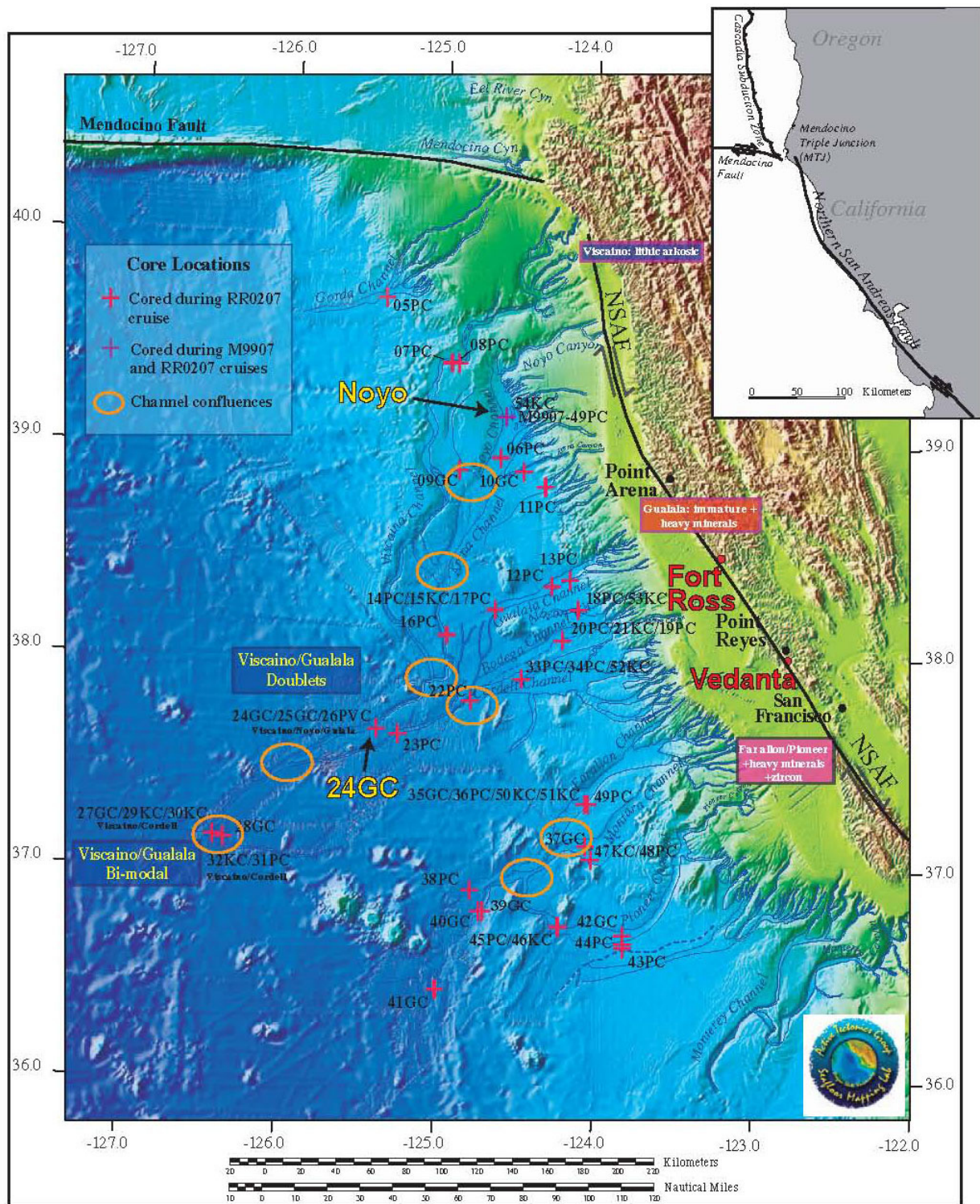


Figure 1. Core locations from 1999 and 2002 cruises on R/V Melville and Roger Revelle. Bathymetric and topographic data compiled by OSU from NASA land data, archive and newly collected marine survey data during these cruises. Channel systems mapped from the new bathymetric grid and sidescan data. Core numbers are referred to in the text. Noyo Cores (including 49PC from Melville 1999 cruise) and 24GC, discussed in text are also shown in yellow. Offshore provenance from heavy mineral analyses are indicated in boxed text. At the confluence upstream of 24GC, Viscaino and Gualala mineralogies mix and result in stacked pulses, reflecting source mineralogies. Onshore paleoseismic sites Vedanta and Fort Ross are shown in red.

examine the origins of detailed stratigraphic correlations, and the potential for extracting earthquake rupture information from the stratigraphic record.

2. GEOLOGICAL SETTING AND BACKGROUND

2.1. NSAF Seismotectonic Setting

The San Andreas Fault (SAF) is probably the most intensively studied transform system in the world. Extending along the west coast of North America, from the Gulf of California to Cape Mendocino, the SAF is the largest component of a complex and wide plate boundary that extends eastward to encompass numerous other strike-slip fault strands and interactions with the Basin and Range extensional province. The Mendocino Triple Junction (MTJ) lies at the termination of the northern San Andreas, and has migrated northward since about 25-28 Ma [17]. As the triple junction moves, the former subduction forearc transitions to right lateral transform motion and the SAF continues to lengthen.

West of the Sierra Nevada block, three main fault systems accommodate ~75% of the Pacific-North America plate motion, distributed over a 100 km wide zone [18]. The Eastern California Shear Zone carries the remaining plate motion [18,19]. The NSAF accommodates about 25 mm/yr of the ~34 mm/yr distributed across northwestern California. Most of the remainder is taken up on the parallel Hayward-Rogers Creek, Calaveras, Maacama and Bartlett Springs Faults (Fig. 1). South of San Francisco, the NSAF bifurcates to include the San Gregorio fault, joining the Northern San Andreas at Olema. Between San Francisco and Cape Mendocino, the main strand of the San Andreas is a relatively simple system. Several uncertain faults exist off shore, but the age and activity of these faults is unknown [20]. Since the 1906 rupture, the main NSAF has been nearly aseismic [21], with only a few small events near Pt. Arena. Seismicity has been greater near the MTJ, and on the Maacama and Bartlett Springs faults to the east [22] (Castillo and Ellsworth, 1993).

2.2. Northern San Andreas Onshore Paleoseismicity

The NSAF system has been divided into segments based on its historical record of earthquake behavior. All four northern segments (north of the creeping section at San Juan Bautista: Santa Cruz Mountain, Peninsula, North Coast, and Offshore [23]) ruptured in the 1906 Mw 7.9 earthquake, extending from the San Juan Bautista north to the Mendocino Triple Junction [24,25,26]. The minimum rupture length for this event is estimated to be ~470 km [27].

The paleoseismology of the NSAF has been investigated at Olema, 45 km north of San Francisco, at Dogtown, close to the Olema site, at Point Arena, Fort Ross, at several sites on the San Francisco Peninsula, and at Arano and Grizzly Flats in the Santa Cruz mountains. At the Vedanta site (Fig. 1) near Olema, Niemi and Hall [28] found a maximum late Holocene slip rate of 24 ± 3 mm/yr, in fair agreement with geodetic data [29]. They estimate that if the 4-5 m slip event recorded in 1906 is characteristic, the recurrence time for such events would be 221 ± 40 yrs. The average slip per event at Point Arena similarly implies a recurrence time of 200-400 yrs [30]. Recently, 10 new ages from the Vedanta site [31] and sites near Fort Ross [32] (Fig. 1), suggest a recurrence interval of ~200 years, and timing of the penultimate event on the North Coast and Offshore segments at ~AD 1700-1750.

A controversial aspect of NSAF tectonics has been whether the fault is seismically segmented, or whether the long 1906 rupture was characteristic, or perhaps a mix of both. The consistent slip rates found north

of the Golden Gate, slow to about 17 mm/yr south of the Golden Gate. This, and a lower 1906 co-seismic slip south of the Golden Gate [33,34,35] led investigators to conclude that the fault is segmented near the Golden Gate. Schwartz et al. [27] argues that the segmentation is a reflection of the offshore San Gregorio Fault absorbing some of the slip [36,37], correspondingly reducing the slip-rate on the main SAF. They argue that the through-going rupture in 1906 (and perhaps previous events) was not segmented, and further, that the penultimate event ruptured approximately the same distance and magnitude as the 1906 event. Fumal et al. [38] however, reports that the Santa Cruz Mountain segment has a more frequent recurrence interval (~100 years) than is evident for the North Coast and Peninsula segments.

3. TURBIDITE METHODOLOGY AND ANALYTICAL METHODS

3.1. *Turbidite Methodology and Application to Cascadia and the San Andreas*

3.1.1. *Identifying Earthquake-Triggered Turbidites*

The Grand Banks earthquake of 1929 in the northwest Atlantic clearly demonstrated the association between earthquakes and turbidity currents [39], however other plausible triggers for turbidity currents include: 1) storm or tsunami wave loading; 2) sediment loading; and 3) storm (hyperpycnal) discharges. Investigators have attempted to distinguish seismic turbidites from storm, tsunami, and other deposits [9,10,11], arguing that seismo-turbidites can in some cases be distinguished sedimentologically. They observe that known seismically triggered turbidites in the Japan Sea and Lake Biwa (western Honshu, Japan) are distinguished by wide areal extent, multiple coarse-fraction pulses, variable provenance, and greater depositional volume than events triggered by other mechanisms. These investigators observed that known earthquakes caused multiple slump events in a canyon system, generating multiple pulses resulting in an amalgamated turbidite also including reverse grading and cutouts (Fig. 2).

Similar observations regarding areal extent and volume have been made for the Santa Monica and Alfonso Basins of the California Borderland and Gulf of California respectively [40]. In general, these investigators observe that known storm sediment surges are thinner, finer grained and have simple normally graded Bouma sequences.

In this paper, we do not attempt to distinguish between triggering mechanisms sedimentologically, but use a spatial and temporal pattern of event correlations to establish synchronous triggering within individual canyons along 320 km of coastline. Synchronicity of event records in separated canyons, over a wide region, is difficult to attribute to non-earthquake sources which are limited spatially and temporally to single canyons. Possible exceptions include storm wave loading and hyperpycnal flow, which also occur over large areas and short time scales.

Hyperpycnal flow, or direct turbid injection from rivers, can produce turbidity currents, and can even mimic earthquakes in that they may affect several rivers over a span of days. This certainly occurred during periods of lowered sea level during the Pleistocene, when there was direct connection between rivers and offshore canyons. However, sea level-rise in the Holocene isolated most west coast canyons from their rivers [41,42]. Holocene sediment input is generally distributed across the shelf, not directly injected in the canyons, with some narrow-shelf exceptions such as the Eel, Mendocino, Viscaino, and Monterey Canyons [43,44,45] (Fig. 1).

Tsunamis and storm waves may also conceivably act as regional triggers of turbidity currents. Storm

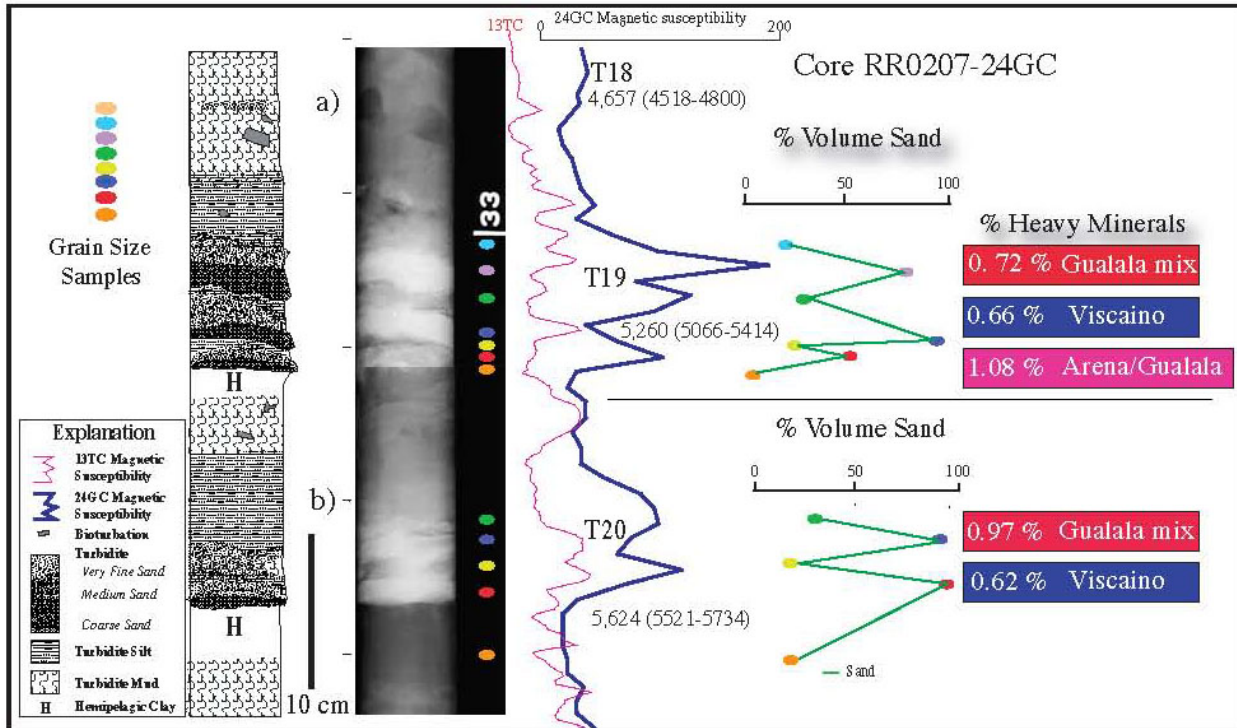


Figure 2. Grain Size analysis, magnetic susceptibility/density signatures and X- radiography in turbidites T19 and T20 in core 24GC below the Gualala-Noyo-Viscaino channel confluence (Base of T18 is also shown; see Figure 1 for location). Light tones in the x-radiograph represent dense sand/silt intervals, darker gray tones represent clay/ mud. Colored dots are grain size samples. Blue trace is the magnetic susceptibility signature. Green plot is percent sand (obtained with Coulter laser counter method). The good correspondence between grain size, density, and magnetic susceptibility for the lithologies in NSAF cores is apparent, and permits use of density and magnetics as mass/ grain size proxies due to the large number of analyses that would otherwise be required. These typical turbidites are composed of 1-3 fining upward sequences, each truncated by the overlying “pulse”. No hemipelagic exists between pulses, indicating the three pulses were deposited in a short time interval. Only the last pulse has a fine tail, indicating final waning of the turbidity current. We interpret these signatures as resulting from a single multipulse turbidity current. Number of coarse pulses commonly remains constant in multiple channel systems for a given event. “H” denotes hemipelagic sediment between turbidites. Correlative magnetic susceptibility trace for Gualala core 13TC is also shown, as are correlative 14C ages projected from core 54KC in Noyo Channel. Source provenance affinity for each sand pulse is shown to the right, and keyed to source regions in Figure 1. This shows the arrival of discrete source pulses with a dominant lithology from multiple channel systems.

waves can induce sediment resuspension by either erosion due to shear stress induced by orbital motion from the waves, or from fluidization of near surface sediments due to cyclic pressure changed during repeated wave passage. Our calculations [based on 46] using historical and predicted maximum wave data [47] suggest that extreme storm waves common in the NE Pacific have the potential to both erode and liquefy sediments at canyon head depths of ~120-150 m. Nevertheless, we see no evidence of such material reaching the abyssal plain, indeed there is nothing but hemipelagic sediment overlying the turbidite triggered by the AD 1700 Cascadia earthquake [5,6] and the 1906 NSAF event. Puig et al. [44] and other investigators have shown that this process occurs, but also that such flows generally settle in the canyons in 200-500 m depth where the resuspending force dies out. We note that the tsunami from the 1964 Alaska Mw 9.0 event also did not result in deposition of turbidites in abyssal plain channels in Cascadia Basin [5,6,7]. For these reasons, it appears that synchronous widespread deposition of turbidites on the abyssal plain, at least during high sea level, is best explained by a proximal great earthquake source.

3.1.2. Tests of Synchronous Triggering and Correlative Deposition of Turbidites

Unlike Cascadia, the northern California margin does not appear to have a regional stratigraphic datum like the Mazama ash deposited along the Cascadia margin [5,6], thus correlating events and testing for event origin depends heavily on stratigraphic correlation of other datums and radiocarbon ages. A key test of synchronous triggering has become known as the “confluence test”. In Cascadia Basin channels, Adams [7] observed that most cores contained 13 turbidites overlying the Mazama ash (which was included in the 13th). Cores from Juan de Fuca Canyon, Willapa, Grays, and Quinault Canyons also contain 13 turbidites and include the Mazama ash (several additional events appear in the most proximal canyon sites). The correlative turbidites in Cascadia channel lie downstream of the confluence of those channels. If these events had been independently triggered, with more than a few hours separation in time the channels below the confluence should contain from 26 turbidites not 13 as observed. This simple observation demonstrates synchronous triggering of turbidity currents in tributaries the headwaters of which are separated by 50-150 km. Similar inferences about regionally triggered synchronous turbidites in separate channels elsewhere have been reported [9,11,40,48].

We have begun to apply this “confluence test” to the NSAF turbidite data. In the NSAF system, channel mapping shows that there are eight major confluences available (Fig. 1). Here a modified confluence test is applied to ~6000 years of turbidite record observed in multiple systems meeting at multiple confluences. We have been able to distinguish three heavy mineral provenances in the cores, well linked to the onshore source geology (Fig. 1). Using these three heavy mineral suites allows us to distinguish the various dominant sources of the stratigraphy within turbidites both up and downstream from confluences, and test for synchronous or asynchronous arrival at confluences by observing the stacking of turbidites and their provenance components. As in the original confluence test, a sequence of turbidites should show little change in stratigraphy downstream of confluences if the multiple source canyons were triggered simultaneously, but may show the arrival and blending of the separate provenance components.

3.2. Analytical Methods

3.2.1. Stratigraphic Correlation and Event “Fingerprinting”

We carried out extensive sampling of the physical properties of the cores to establish the stratigraphy reflected in the cores. This has allowed us to identify characteristic stratigraphic “fingerprints” for turbidite sequences that are a result of the grain size distribution of individual events. Because this property has allowed stratigraphic correlation along hundreds of km of coast, we discuss the methods and implications in detail.

While at sea, all cores were scanned using a GEOTEK MSCL, collecting P-wave velocity, gamma-ray density, and magnetic susceptibility data from the unsplit cores. Cores were then split to collect high-resolution line-scan imagery. Subsequently, high-resolution magnetic susceptibility data were collected from each core using a point probe (Bartington MS2E high-resolution surface sensor) at 1 cm intervals, and imaged with X-radiography (e.g. Fig. 2). Selected grain size analyses were performed with a Coulter laser counter.

Initially these data were used to correlate stratigraphy between cores at single sites, which typically have 4-6 cores. This makes use of the trigger cores (collected 1 m apart from the linked piston cores), and

helps identify missing upper sections, an occasional problem with piston cores. The correlation is done using primarily magnetic susceptibility (MS) and density, much as e-logs are correlated in the oil industry [49,50]. Physical property correlations of this type are also common practice with academic and ODP/IODP cores (e.g. [51]) and have recently come into use for paleoseismology (i.e. [8,52,53,54,55,56]). In addition to local site correlation, we have found that it is possible to correlate unique physical property signatures of individual turbidites from different sites within individual channels. This suggests that the processes controlling deposition of the turbidite maintain consistency for some considerable distance within a channel. We have also found it possible to correlate event signatures not only down individual channels and past confluences, but between channel systems separated by considerable distance, some of which never meet. These turbidite “fingerprints” form the basis of long-distance correlations, and are beginning to be recognized and used for regional correlation (e.g. Lake Baikal [57], off Morocco [58], Cascadia [59], the Laptev Sea: Russian Arctic [60] and elsewhere). Recently, the “event signatures” of Cascadia turbidites have been linked to coastal fjord records on Vancouver Island [61,62].

Figure 2 shows a single representative turbidite in core 24GC, located below two channel confluences (Fig. 1); illustrating the multiple fining-upward sequences (Bouma A-C) that compose each turbidite. Typically, these sequences have only one fine tail (Bouma D) associated with waning of the turbidity current. The signatures we are correlating are comprised of these stacked coarse pulses. This figure shows in detail that the magnetic susceptibility, density, and grain size trends within each event are closely correlated. This is straightforward but important because we can in most cases use the high-resolution density and magnetic data as grain size proxies, at least for lithologies along the NSAF system [63,64,65]. In detail, the magnetic susceptibility (MS) signal is associated with terrestrial silt-sized magnetic minerals, but often we see sand at the turbidite base. The sand may be non-magnetic quartz sand, so the MS peak does not always correlate with a maximum of grain size. Also in thick turbidite beds, separation of grains according to specific gravity (or mineral density) can dominate, resulting in fine silt heavy mineral lamina located below medium quartz silt or sand. We find, however, that this approximation is reasonable in most cases (using both density and MS reduces this problem), and the differences are not critical to observing a recognizable “fingerprint” for many turbidites.

On close inspection of physical property logs, we sometimes see a remarkable similarity between correlative turbidites that are separated by as much as 500 km (Cascadia) and 280 km (NSAF). Figure 3 shows several typical examples of correlative events in detail along strike over a distance of 280 km. We see a general correspondence of relative turbidite size downcore that is reflected in separate channels, as well as correlable details such as the number of coarse sandy pulses (density and magnetic peaks). For example, Cascadia turbidite events T5, T10, and T12 are small events in all cores, T11 and T16 are very large events in all cores, and other many events follow similar size patterns across the margin. We observe similar patterns along the NSAF margin, where size trends, and individual characteristics persist over large distances. Figure 3b also shows the evolution of a single event down channel over a distance of 74 km, showing the gradual merging of two sand pulses into a bimodal grain distribution. Stratigraphic correlation has the potential to establish links of individual events between core sites, independent of radiocarbon ages. Possible explanations for the correlation signatures are discussed in a subsequent section.

3.2.2. Radiocarbon Analysis

To date the turbidites, we extract planktic foraminifers from the hemipelagic sediment below each

Turbidite Characteristics

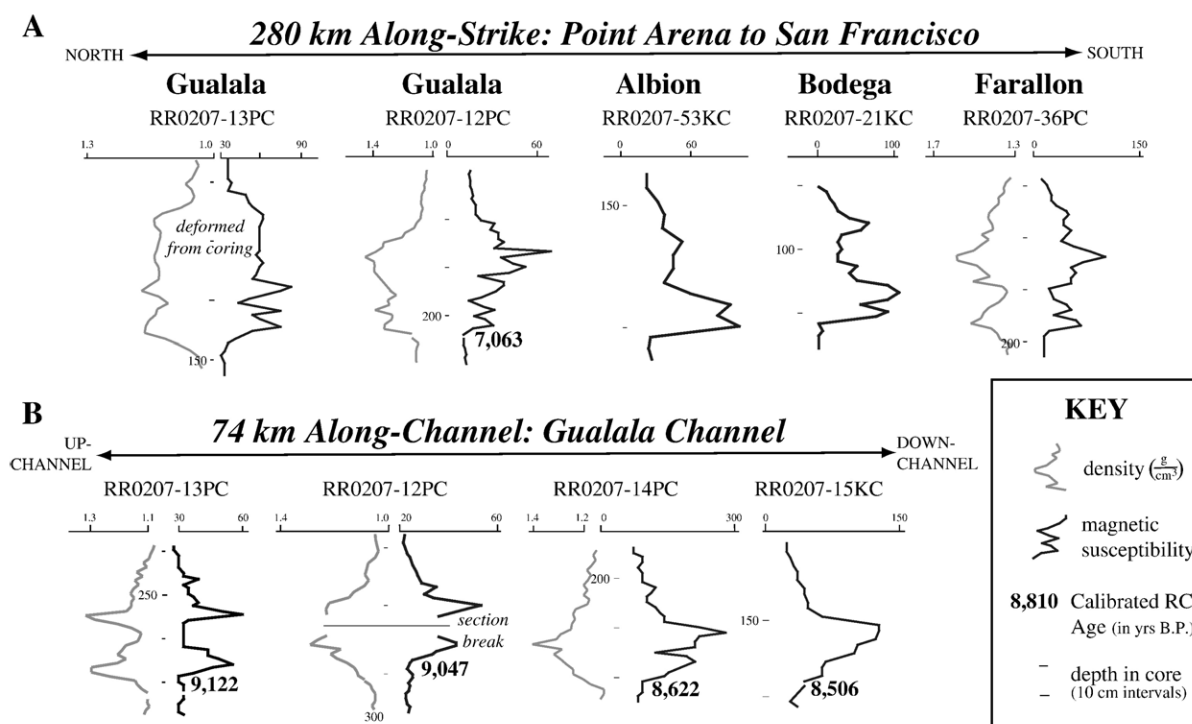


Figure 3. A. Representative physical property details of a single correlative turbidite along 280 km of margin parallel to the NSAF. See Figure 1 for core locations. Along-strike series shows typical variability of the same event in five separate channels above any channel confluences. B. Representative physical property series of a single turbidite from proximal to distal position along 74 km of Gualala Channel. This example shows the merging of separate pulses with distance from the source.

turbidite. We do this because the boundary between the top of the turbidite tail and the hemipelagic sediment is difficult to identify and bioturbation is concentrated at this boundary, possibly because the organic material brought down in the turbidite tail results in a benthic “bloom” [66]. To evaluate the effect of foraminifera shell size on the radiocarbon age in a single sample, we divided the foraminifers into large ($> \sim 350$ microns) and small ($< \sim 350$ microns) groups. The resulting ages are within 45 radiocarbon years of each other, suggesting foraminifer size is not a factor. The close match in ages between land and marine events observed in both Cascadia and on the NSAF also suggests that neither bioturbation [67,68] nor basal erosion significantly biases ^{14}C ages derived from planktic foraminifers.

To correct the ages for the thickness of the sample, we determined hemipelagic thickness between turbidites using visual observations of color change, X-radiography, mineralogic content, and high-resolution physical property data (Fig. 2). We also examined all turbidite bases to estimate the degree of basal erosion. An erosional index (EI) was estimated by examining the morphology of the turbidite bases, which can tell us that erosion occurred, though it may not correlate with the amount of erosion, and may miss laminar erosion. We then averaged thickness determined from multiple methods, and averaged the two or three thickest layers out of a typical four at a given site. We infer that differential erosion is the most likely source of variability at any site, and by taking the thickest layers we attempted to reduce its influence. By averaging the thickest layers we also reduce the effect of variance in observations, which range between ± 0.5 to 1 cm.

Using a moving window average sedimentation rate, we corrected the original AMS ages by subtracting

the time corresponding to the thickness of the sample interval. Hemipelagic thickness was then converted to time for input into OxCal calibration software [69,70]. A sedimentation rate regression analysis was employed to flag erosion at a given interval, and provide a check for consistency downcore, as sudden hemipelagic sedimentation rate changes in the marine environment are relatively rare (see Elect. Supl). Outliers in this analysis are most likely caused by basal erosion because ages appear to be older, with less sediment thickness between events than expected.

Figure 4 illustrates the main steps used to combine ^{14}C age and hemipelagic sedimentation constraints. Since the calculated sedimentation rates are also dependent on the radiocarbon ages, and on basal erosion, there is some unavoidable circularity in this process, however analysis of multiple cores at each key site can address these issues quite well.

We used the Bayesian methods within OxCal to take advantage of multiple ages (if within analytical error of one another), included constraints imposed by the time represented by hemipelagic sediment between events, and in one case used historical information to restrict ages. Where age data are missing, sedimentation rates alone can be used to model event ages, which we have done for several events in our time series due to scarcity of foraminifers in those intervals.

Figure 4 shows a detailed example using OxCal with hemipelagic sedimentation and historical constraints for the 1906 and the penultimate earthquakes. Using this well-known event, and time constraints provided by the hemipelagic sediment deposited in the interseismic period, OxCal returns the calendar age of the 1906 earthquake to within a few years (Fig. 4). The penultimate event is similarly constrained to a narrower time window than obtained by simple calibration.

The age constraints provided by uniform sedimentation between events are quite strong, in fact somewhat too strong, since the inter-event hemipelagic sediment can account for nearly 100% of the time in a given core (the turbidites themselves representing zero time). While this is good, in a statistical sense, there is no temporal “room” left for the probability density function (PDF) required to describe the ^{14}C event age. For this reason, we presently relax the hemipelagic constraint to 75% of the time represented to allow for overlap of the hemipelagic time interval with the PDF for each turbidite age in OxCal.

In our age series, we apply a reservoir correction that is linearly interpolated between the nearest points available in the Marine04 database [71], which are at San Francisco (R 271+/-) and Coos Bay (R 402+/-). Because the database is largely limited to the 20th century, time variation of the reservoir age is usually ignored because little data on the time history is available. We do not yet know whether time and space variable reservoir age issues will be significant offshore northern California, however we suspect it will show similar variability as along the Cascadia margin [72,73,74].

4. RESULTS: NORTHERN SAN ANDREAS TURBIDITE RECORD

4.1. Confluences and Mineralogy

Figure 2 shows the stratigraphy of two typical NSAF turbidites in core 24GC below several confluences of Viscaino, Noyo, and Gualala Channels (confluences “A”, “B”, and “C” in Fig. 1). At this site, we find that the multiple coarse pulses which also reveal the heavy mineral assemblage from individual canyon sources, stacked vertically in order of arrival at the core site. The turbidites at this site also have no hemipelagic sediment between the sand pulses, indicating little time passage between deposition of each

Estimating Calendar Ages: four methods to estimate the age of a known event

(example from Noyo Canyon, 1906 San Andreas Fault earthquake)

We show this example because the upper-most event is known to be the 1906 earthquake, the penultimate event is dated at multiple land sites, and the reservoir correction is known for the 20th century. The upper-most event can be dated using the following methods:

1. Calibrate the RC date for the upper-most event: **1913 (1898-1940)**
2. Date of coring (1999) minus H_1' : **1916**
3. Age of calibrated penultimate event (1724(1647-1819)) plus H_2' : **1861 (1784-1956)**

Or, use the Sequence option in OxCal with all available data (preferred option):

4. Constrain calibrated upper-most and penultimate ages using all available data in panel to the left: **1902 (1845-1910)**

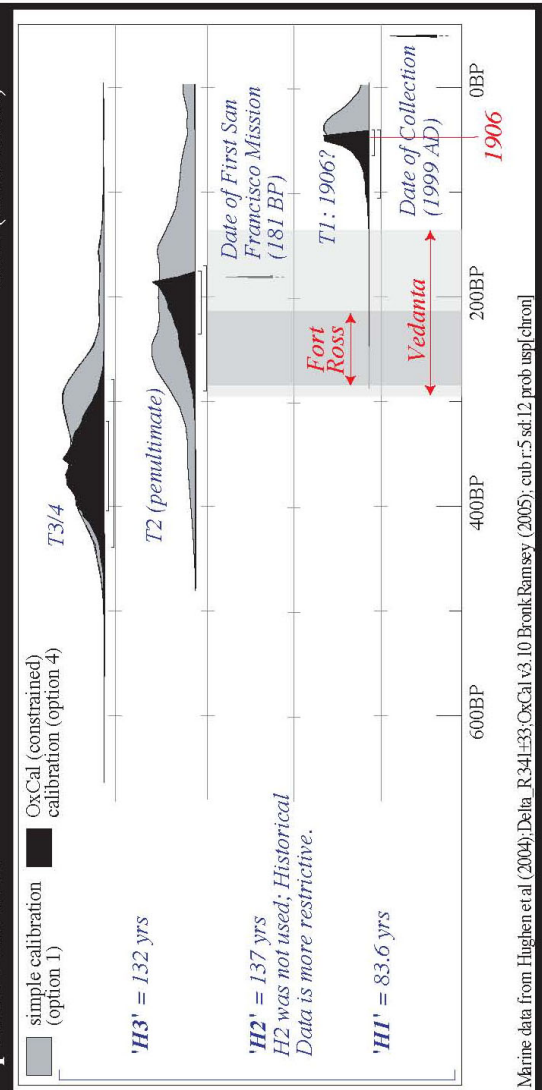
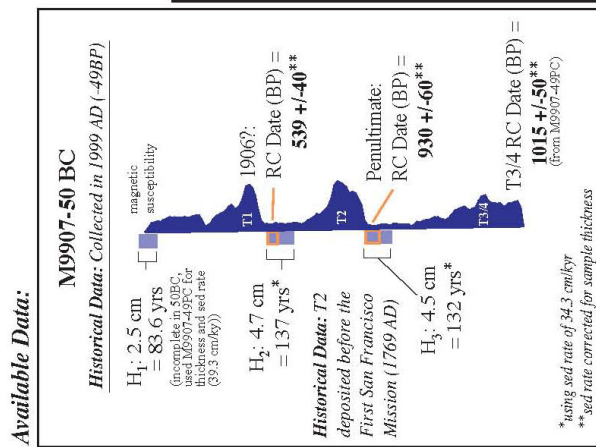


Figure 4. OxCal methods test using the well constrained 1906 earthquake and associated paleoseismic data onshore and offshore. The left panel shows the hemipelagic (H) data determined from visual observation, physical property data mineralogy and x-radiography. H data is then input to OxCal and with raw 14C ages are converted to time via sedimentation rate curves developed for each site. Right panel shows four ways to calculate the age of the 1906 earthquake, with the preferred method being the use of underlying and overlying hemipelagic intervals, historical data (no written record of an earthquake between the date of the first San Francisco Mission built in 1769 and 1838), and 14C ages together. This method yields 1902 (1845-1910) for the 1906 event. The Fort Ross and Vedanta mean age and range for the penultimate event is shown, along with the OxCal solution for that event, calculated using the preferred method. The turbidite result 1660-1769 (~1760 peak) for the penultimate event is in good agreement with NSAF paleoseismic sites on land: Fort Ross = 1710 (1610-1810), Vedanta = 1711 (1695-1720) [28,32].

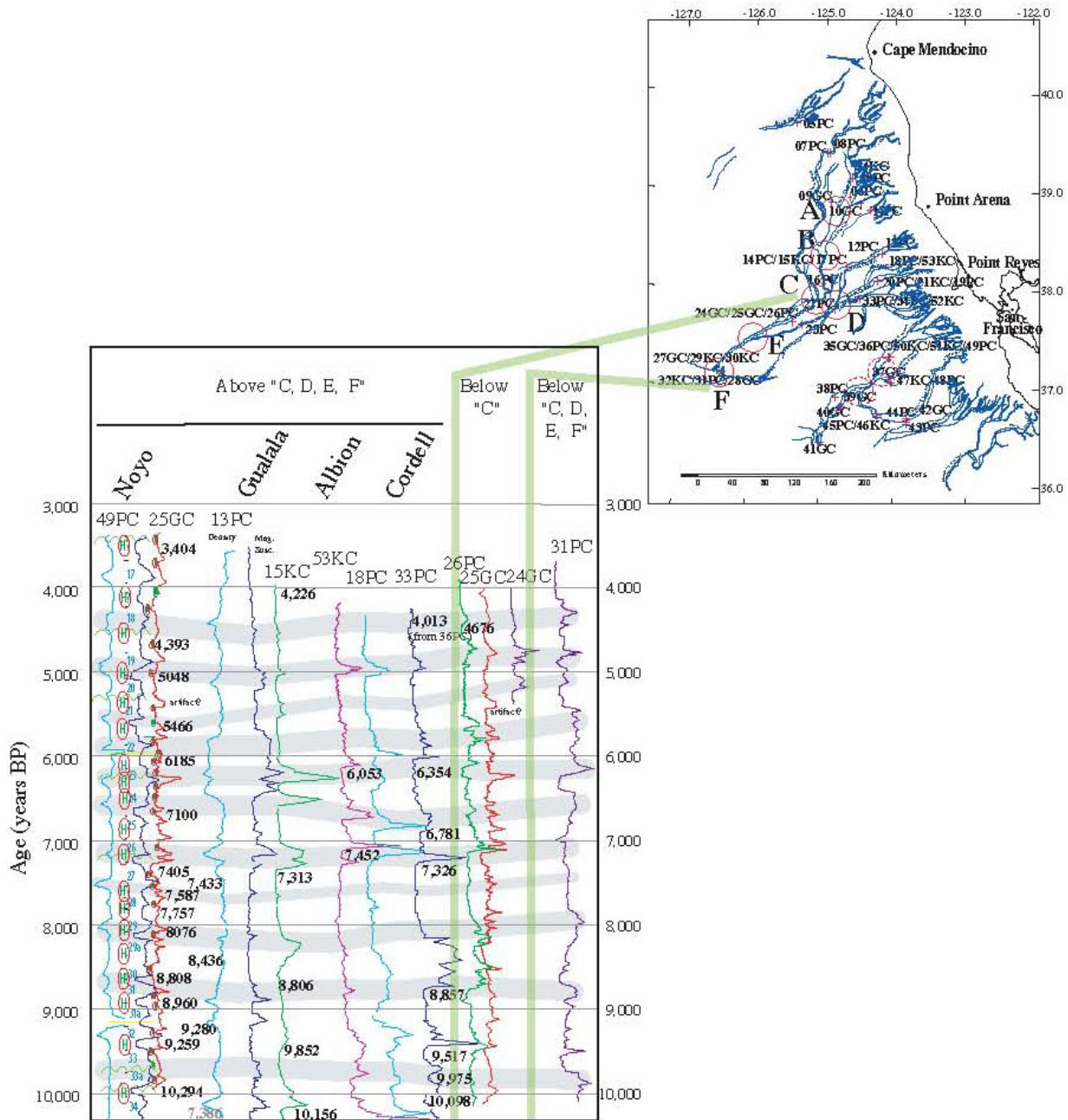


Figure 5. “Confluence Test” as applied to the central NSAF margin channel systems for the period ~4000-10,000 ybp. Inset map shows eight confluences (southern two dashed, not yet tested). The correlation figure uses magnetic susceptibility records from six cores at four sites above confluence “C” (representative lithologic log for 13PC shown, 13PC gamma density shown in light blue). Magnetic susceptibility for three cores below confluence “C”, and one core below confluences “B”, “C”, “D”, and “E” are also shown. Green bars separate these three core sets, and are linked to the map. Core 25GC (red) also shown alongside 49PC with hemipelagic intervals (circled H) shown between turbidites. Magnetic trace for 49PC shows disturbance by sampling, density trace is shown for comparison. Mismatching hemipelagic intervals shown green, all others in red. Green wavy lines are known erosive bases. Turbidite numbers shown on 49PC in green. Peak radiocarbon ages are shown without ranges to reduce clutter, ranges are given for upper 14 events on Figure 7. Color bands show correlation ties for key turbidites. While some details of each of the correlated turbidites vary from site to site as would be expected, the stratigraphy represented by these turbidites remains largely unaffected by passage through the confluences with other channels. The total number of turbidites is nearly constant, indicating that turbidite arrival at confluences from separate channel systems was most likely synchronous. See figure 6 for mag. sus. and density scales. Color scheme matches events in Figures 6 and 7 for events common to both figures.

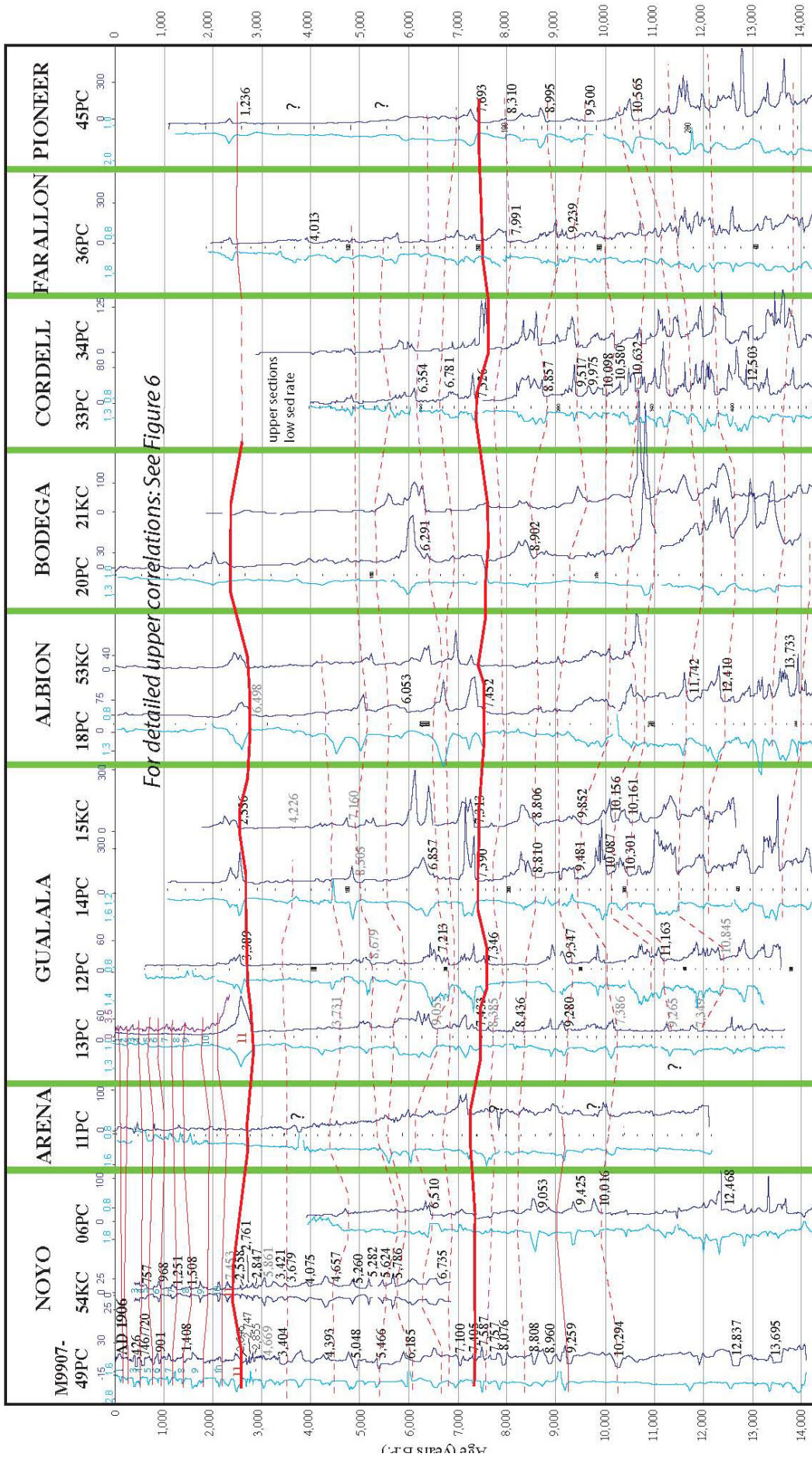


Figure 6. In progress Holocene correlation diagram for NSAF system cores. Light blue traces are gamma density, dark blue traces are magnetic susceptibility. (Kasten cores “KC” do not have associated density data as they are too large for the scanner). This correlation is approximately oriented in a 14C age framework, with some vertical stretching of cores based on differing sedimentation rates. Peak probability calendar ages corrected for sample thickness are shown in black (gray if questionable) below the dated turbidite, 2 sigma range omitted for clarity. Upper ~2500 years of data shown in Figure 7 using 3 mm high-resolution magnetic susceptibility data. Significant correlation horizons, are shown, but not all individual events are depicted to reduce clutter. Color scheme matches events in Figures 5 and 7 for events common to both figures.

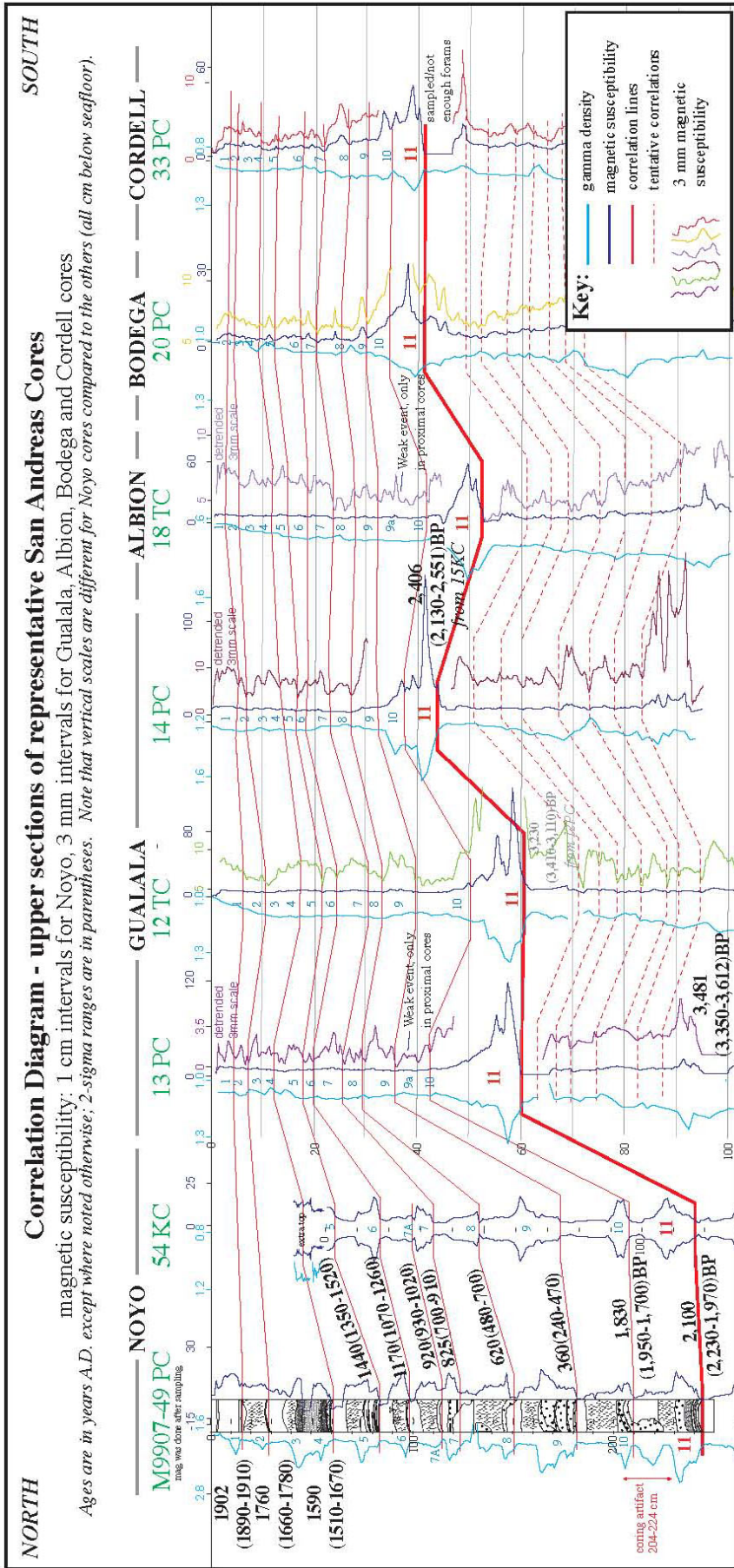


Figure 7. Correlation diagram for the uppermost ~ 3000 years in NSAF system cores. Channel locations shown in Figure 1. Light blue traces are Gamma density, dark blue are magnetic susceptibility. 1 cm resolution magnetic susceptibility data are shown for Noyo cores, and 3 mm high-resolution signal resolved with this resolution. The 3 mm magnetic susceptibility data is stretched horizontally (variable colored traces) to show the low amplitude signal resolved with this resolution. Event numbers in blue at core centers. NSAF cores all have a number of relatively thick events that serve as excellent datums, and are the basis for our regional correlations in Figure 6. The uppermost of these marker events, a very distinctive multipulse event dated at ~ 2100 ybp, is shown labeled “11” in red. Gualala, Albion, Bodega and Cordell and 54KC core tops have been vertically expanded for viewing to offset low sedimentation rates in the upper 2100 years for all cores. OxCal age peaks and ranges shown on cores 49PC and 54KC at left; these ages do not match figure 6 ages, for which data are insufficient for OxCal analysis. Gualala ages have been corrected for sample thickness only. Correlation for weak events T7a and T9a uncertain and not shown beyond Noyo Channel. T7a is datable, and included in our time series; T9a appears to be limited to two adjacent proximal core sites, and is not included in the recurrence statistics. 49PC high-resolution magnetic trace is punctuated by sample voids, indicated by yellow squares. Color scheme matches events in Figures 5 and 6 for events common to both figures.

pulse (the alternative, removal by erosion, is possible, but would have to occur in each turbidite at every correlative site). Further downstream, we observe bimodal heavy mineral coarse fractions, with mineralogic peaks representing the separate provenance components (Fig. 3 [75,76]). Figure 2 also shows the magnetic susceptibility trace for the same two correlative turbidites, upstream of the confluences, in core 13TC. We observe no significant change in the stratigraphy between these two sites, despite input from multiple sources at the confluences. Further downstream at the site of core 31PC, we find that individual turbidites have the same stacking of coarse pulses, but the provenance input is less distinct, suggesting further mixing downstream. Figure 5 shows our stratigraphic correlation detail for a series of cores upstream, near, and downstream of the confluences of Viscaino, Noyo, Gualala, Albion, and Cordell Channels.

We show the time period from ~3500 ybp to ~10,000 yr bp because the upper section is poorly preserved in some of the downstream cores. The downstream cores have, as yet, only a few dated turbidites, in part due to the low foram abundance at water depths in excess of 3500 m at these sites. The section ages are bounded by several late Pleistocene ages (not shown in Figure 5), and the age of 4676 (4525-4810) ybp for T18 in core 26PC which we use to constrain the upper part of the correlation.

While additional ^{14}C ages are still needed, we can test for synchronicity by carefully matching events between upstream cores at Noyo and Gualala Channels and correlative events in the downstream cores in this time range. We matched the stratigraphy and checked for presence/absence of hemipelagic sediment between events (or an erosive event that removed it) as well as the multiple cues used in physical property correlation. We observe that upstream (49PC) and downstream cores (e.g. 25GC) both contain 22 events in this time range. Differences between the two are minor, and appear mostly attributable to local basal erosion. Figure 5 includes correlation with core 31PC, which is actually below a total of four confluences, with input from a total of six channels, while cores 24GC, 25GC, and 26PC each sample three channels. The good correlation between these cores suggests that input mixing at each confluence has little effect on the stratigraphy of the turbidites, even though the number of sources increases at each confluence. We infer that synchronous triggering is the only viable explanation for this, and are unable to suggest an alternative. Non-synchronous triggering should produce an amalgamated record that increases in complexity below each confluence, with only partial correlations if any, for the synchronous events. The mixing and stacking of the provenance components further suggests synchronous arrival at the confluence. From these results we infer that the sites included in this analysis pass a strict test of synchronicity, and are most likely of earthquake origin. Further analysis of the remaining confluence sites is in progress. A similar use of mineralogic provenance to fingerprint source channels and test for earthquake origin has been used in the Sea of Japan by Shiki et al. [10].

4.2. Stratigraphic Correlation

We have made a preliminary correlation of events along the length of the NSAF margin using subsurface correlation of the physical property logs as described above. This has been hampered somewhat by the fact that the turbidite signal for most of the NSAF channels is subdued by comparison to Cascadia. This is not surprising, given smaller earthquakes and greater epicentral distance to the canyons. The correlation is made within a ^{14}C age framework, with some vertical stretching of cores required due to varying sedimentation rates.

Figure 6 shows the regional correlation of turbidite stratigraphy spanning the Holocene, and Figure 7 shows the upper ~2100 years of record, making use of high-resolution magnetic susceptibility data (3 mm

spacing, point sensor). We focus here on the upper 2100 years of the record; the analysis of earlier periods in the Holocene is the subject of ongoing investigation. Our Noyo Canyon cores, 49PC and companion Kasten core 54KC, are particularly important because unlike all the other channel systems, Noyo Canyon is actually cut by the NSAF, and has an epicentral distance of zero. Most likely for this reason, the turbidite record there is expanded in thickness, making investigation of the details of each event much clearer in those cores. Cores to the south have much reduced sedimentation rates, even though they are closer to the Russian River source, the largest river along the North Coast section of the NSAF. We speculate that the low hemipelagic sedimentation rates might be related to capture of much of the Russian River drainage and diversion into the San Joaquin Valley, which may have occurred during the Holocene [77]. By comparison to the robust Noyo record, most of the events along the NSAF in other channels are subdued, and indeed the upper 10 events shown in these figures are very fine silt turbidites not visible to the naked eye. Their unique signatures in the physical property data, however, allow good correlation between sites. We have collapsed a much larger set of core records onto the representative correlation diagrams shown in Figures 6 and 7. A key stratigraphic datum in this correlation is T11, which is a robust event correlated and visible as a sandy turbidite in all cores, dated at 2574 (2397-2681) ybp in Noyo Channel, and 2256 (2080-2401) ybp in Gualala Channel. We suspected that the original ^{14}C age for this event (~ 2600 ybp) was too old (possible basal erosion) and have used constraints from hemipelagic sedimentation rates surrounding this interval to estimate the ~ 2100 ybp age in Figure 7.

As in Cascadia, correlation of individual events based on the grain size distribution represented by the magnetic and density data are possible both along strike and down channel. Robust event “signatures” that can be recognized both within single channels, between multiple channel systems, and above and below confluences support the inference that they in fact represent the same source events, independent of other methods. We observe that the correlated events retain their essential character, typically made up of a stack of coarse pulses, for considerable distances along the margin. The “signatures” are observed to evolve downstream where coarse pulses merge with distance from the margin. The event “signatures” also evolve to some extent along strike in some cases, although in other cases stratigraphic sections at opposite ends of the fault system match as well as close neighbors. These properties can be observed through close inspection of Figures 3-7.

4.3. Radiocarbon Time Series and Comparison to Onshore Paleoseismic Sites

In terms of event ages and their distribution in time, the youngest 15 events have a mean repeat time of ~ 200 years, with a standard deviation of 60 years. Using peak PDF values for event ages, the minimum interval value is ~ 95 years between T7a and T7 and T12a and T12, and the maximum value is ~ 270 years between T5 and T6 and T10-T11 (we refer to the third event as “T3-4” because it is a doublet that may yet prove to be two events). We find these values reasonably consistent with previous paleoseismic data onshore. The ages shown in Figure 8 include 11 ages reported by Zhang et al. [31] from the Vedanta Marsh site, and 5 ages reported by Kelson et al. [32] from sites at Fort Ross.

These results indicate that the penultimate event occurred $\sim \text{AD } 1700\text{-}1750$ north of San Francisco, and that the age correspondence is good for the last ~ 2300 years when comparing Noyo Canyon marine ages to Vedanta and Fort Ross land ages. For a given time interval, we see approximately the same total number of events (± 1) onshore and offshore, suggesting either a coincidence, or that land and marine sites are recording the same events. Further support for a linkage between the turbidite series presented here and

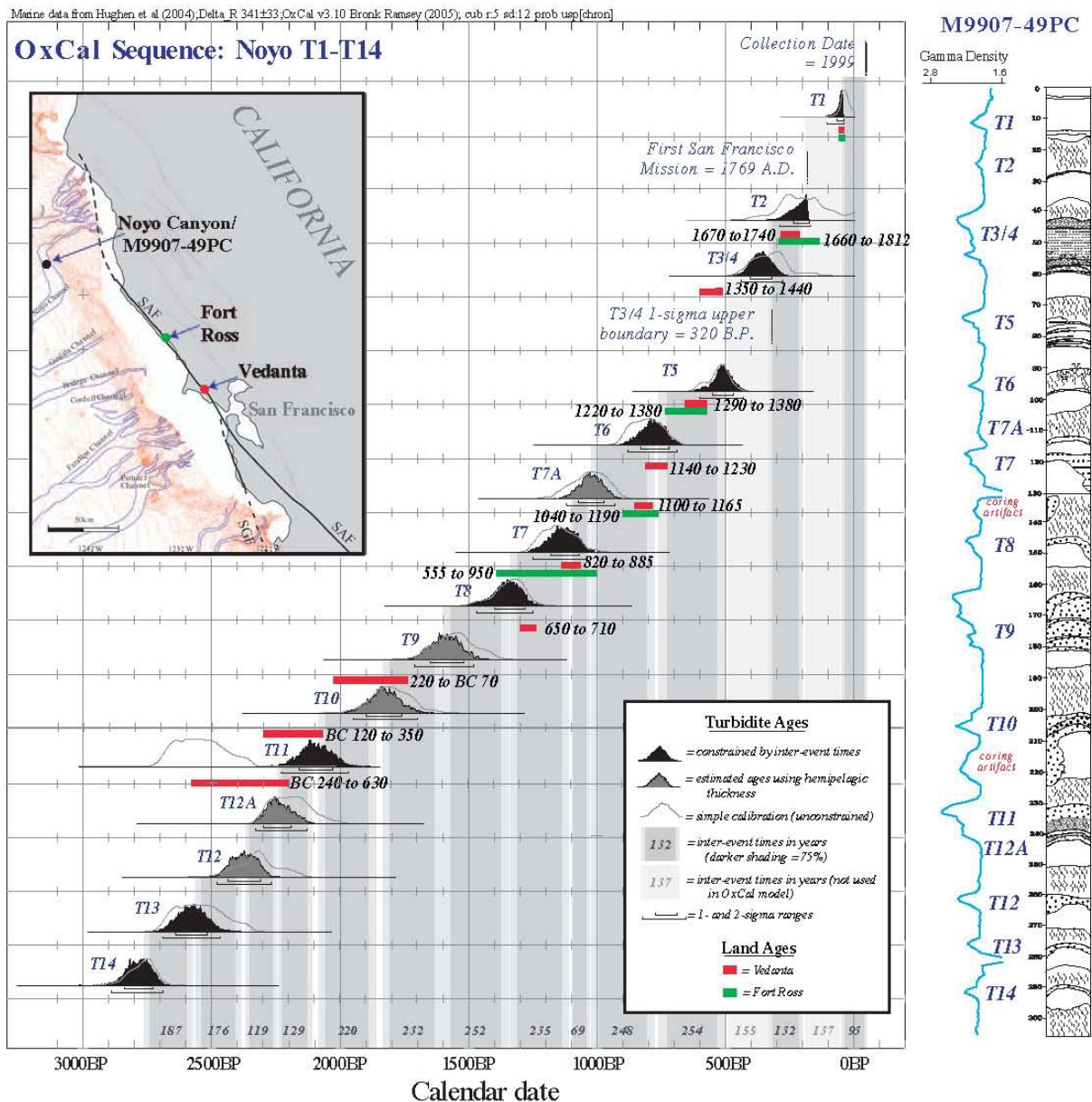


Figure 8. OxCal age model for the youngest 15 events in the NSAF offshore system, and comparison to onshore ages. Inter-event times based on hemipelagic sediment thickness (represented by gray bars) were used to constrain original ^{14}C calendar age distributions (gray traces) using the SEQUENCE option in OxCal. Inter-event times were estimated by converting hemipelagic sediment thickness between each pair of events to time using the sedimentation rate. Events dated more than once were combined in OxCal prior to calibration if results were in agreement; if not in agreement, the younger radiocarbon age was used in the final model. Five ages are calculated from sedimentation rates where not enough forams were present for ^{14}C dating. The resulting probability distributions (filled black, grey for undated events) are mostly in good agreement with land ages from Fort Ross except for T3-4 and T7a (green lines; [32]) and Vedanta (red lines; [31]). See inset for geographic locations. See Electronic Supplement for OxCal input data and sedimentation rate curves.

onshore earthquakes, is the good correspondence between land and turbidite recurrence intervals, which are 200 years and 230 years for marine and land ages respectively. Individually, most ages except Noyo T3-4 (a doublet) and T7a have significant overlap of age ranges (Fig. 8). In addition, our event T3-4 was not reported at Fort Ross, and our event T9 was apparently not observed at Vedanta. Nevertheless, our preliminary stratigraphic correlation and age series, taken together, suggests that the previous 11 events may be correlated from Noyo Canyon to at least to the latitude of Vedanta, just north of San Francisco. If

correct, our initial along-strike correlations imply rupture lengths for many (or most) events of > 250 km.

5. DISCUSSION

We concluded that along-strike physical property correlations, supported by application of the “confluence test” and good correspondence with land paleoseismic dates both in individual matching, and total number of events, supports the use of offshore turbidites as paleoseismic indicators for the NSAF. We suggest several other lines of evidence that support this conclusion. First, the recurrence interval overall is consistent with other paleoseismic evidence from the North Coast segment of the fault, such as Prentice [30], Zhang et al. [31], and Kelson et al. [32]. Second, the mean recurrence interval changes abruptly (more than doubling) at the MTJ, from a value consistent with NSAF earthquakes south of the MTJ, to a value consistent with Cascadia earthquakes north of the MTJ [61]. We can think of no other reason for such a rate change, and indeed if such a change were due to external factors such as storm frequency or sediment loads, the frequency should increase northward, not southward as observed. Third, we observe that the thickness of the turbidites decreases southward as the shelf widens and the distance from the canyon heads to the fault increases (see Fig.1). This occurs despite closer proximity to the main sediment sources, the Russian River and San Francisco Bay, which are to the south. This relationship suggests that epicentral distance, and not sediment supply, is the controlling factor for turbidite size, at least during Holocene high sea-levels. This observation also supports our primary inference of earthquake origin, and is consistent with observations in Cascadia where robust turbidites are found in channels fed by small sediment sources, such as the Mendocino Channel fed by the Mattole River [78].

Physical property correlations often reveal detailed correlatable patterns that were unexpected. The magnetic-density event signatures we see are created by sand rich layers, mostly in the base of the turbidite. These layers include heavy (dark) minerals such as magnetite and hematite, which are largely responsible for the signatures. This is clear from the high-resolution imagery and x-rays, which show an obvious correlation between, density, magnetic susceptibility, and the coarse stringers in the turbidites [61] (Fig. 2). The correlation of these signatures indicates that the integrity of the signatures, and thus the pattern of coarse fraction deposition, is maintained to some extent over time and distance during the turbidity current. One might expect that such correlation could be due to details of how the turbidity current initiated in the canyon’s upper reaches. An earthquake, unlike other triggers for submarine landslides, is likely to trigger multiple failures along the length of a canyon. Thus the turbidity current could contain multiple inputs, each containing a coarse fraction pulse, which coalesce down-channel (this could also be due to retrograde landsliding). This could explain the persistent pattern we see within channels as reflecting an original multiple source input. But we are still left with the problem: Why do they correlate beyond an individual channel system, to other channels with different pathways?

The fact that they correlate at all is strong evidence that the turbidity currents were earthquake generated, and is robust regardless of the reasons for the correlation. Japanese investigators have similarly shown that the only plausible mechanism for multiple, simultaneous, regional landslide triggering, is an earthquake (see also [8]). We further suggest then that the only plausible commonality between correlative turbidites in separate channels is the original earthquake itself. In the case of the NSAF, we find that turbidites correlate across channels where the mineralogy is different, the physiography is different, the sediment sources are different, and the underlying geology is different. We postulate that the physical property signatures may record elements of the unique shaking signal imparted to the sediment failure region by

the earthquake itself, in effect the physical property signatures may be crude paleoseismograms, imparting some information about magnitude, source character, or aftershocks to the depositional history of each turbidite [79,80]. This may be a controversial interpretation, but we are led to it out of a need to explain the observed data. This topic is the focus of another paper that makes use of both NSAF and Cascadia data (Goldfinger et al., in preparation), and will be tested experimentally in the near future.

The direct tie between events at widely separated sites implies, we infer, that this method can be used to link events separated in space directly, independent of but strengthened by ^{14}C dating. This method has the potential to overcome the largest issue in paleoseismology, the linking of events along strike via radiocarbon dating, with its inherent errors, to determine rupture length and segment recurrence values.

Our data, and those from Vedanta and Fort Ross, suggest an age near AD 1700-1750 for the NSAF penultimate event. While Vedanta and Fort Ross are sufficiently distant from Cascadia to preclude confusion, the Noyo Canyon offshore site is much closer at 90 km. The ^{14}C ages cannot distinguish the penultimate NSAF from the Cascadia AD 1700 event. However this event, as with most of the other 10

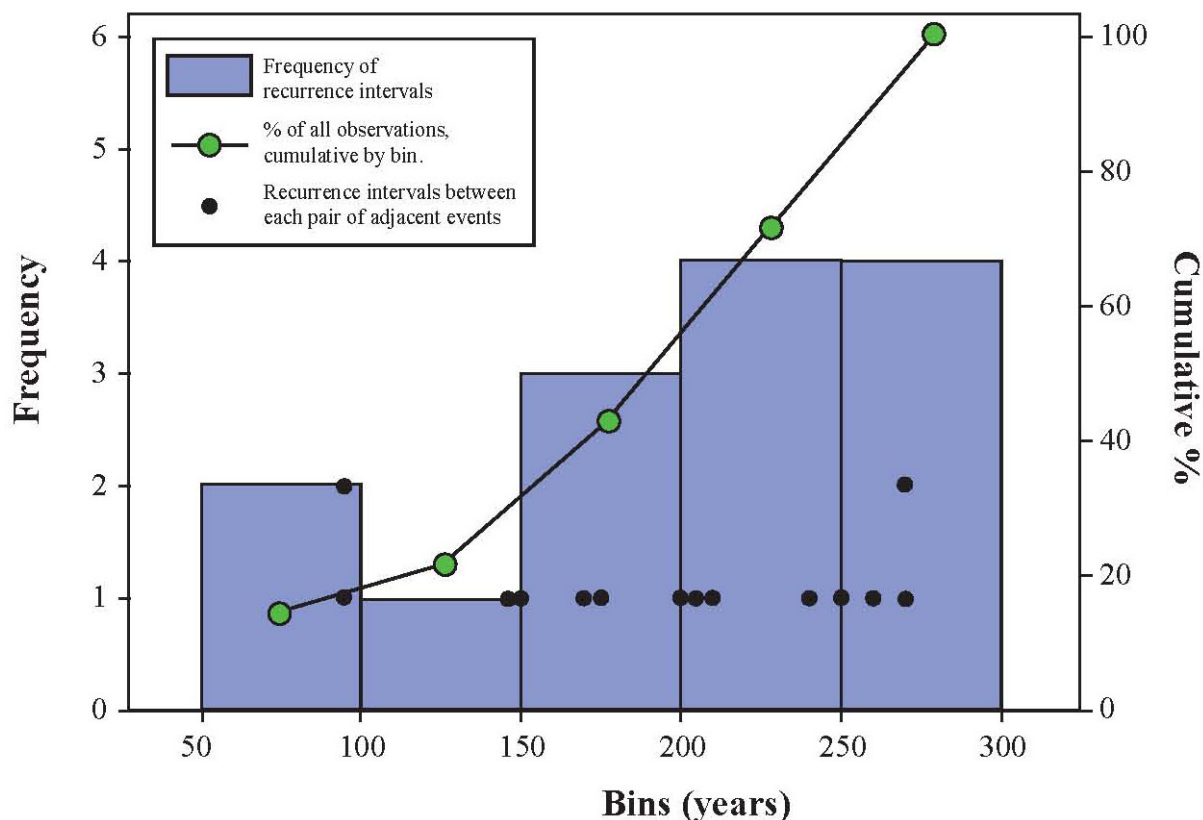


Figure 9. Histogram showing the frequency of recurrence intervals within each bin (purple bars), with cumulative percent of all inter-event times ($n=14$) shown at the midpoint of each bar (circles filled in green). The actual data (black circles, each circle representing one recurrence interval) show the majority of recurrence times (8 out of 14) are between 150 and 250 years.

events discussed here, can be correlated well to the south, making it unlikely that the Cascadia record is confused in the NSAF record.

A related question of importance for the NSAF is the minimum magnitude and triggering distance from the earthquake hypocenter. Shiki et al. [10] observed that earthquakes less than $M_w=7.4$ do not trigger turbidity currents in the Japan Sea or Lake Biwa, and similarly cores taken before and after the 1992 M_w 7.1 Petrolia earthquake in the canyon source area do not include this event [78]. Several NSAF events

that are well recorded in Noyo Channel are much more weakly represented in channels to the south, while others are robust in all channels. We suspect that there are probably smaller events not represented in the offshore data, and that they may similarly be unrepresented in the onshore data. Observations of turbidites from small events may also simply be a function of the resolution of the observations. We do not presently understand why some events such as T11 in the NSAF record, are much larger than others, particularly considering that the 1906 earthquake was likely near the maximum magnitude for that fault segment.

With a long paleoseismic record we can draw some preliminary conclusion about the distribution of recurrence intervals with time. A frequency histogram for the binned repeat intervals for the 15 earthquake series of Figure 8 is shown in Figure 9. While preliminary, this suggests the majority of repeat intervals lie between 150 and 250 years. The minimum rupture lengths of ~320 km established from the turbidite data presented here imply magnitudes of 7.8-8.2 for these events based on empirical rupture length magnitude relationships [81]. Future work will test the full rupture length south of San Francisco for these events.

Finally, long paleoseismic records in both Cascadia and the NSAF offer many opportunities to investigate clustering and fault interaction. Given the close connection between the NSAF and Cascadia, it might be surprising if we did not see a temporal connection. The close temporal correspondence between the NSAF penultimate event ~AD 1700 and the Cascadia AD 1700 event is striking, and suggestive of stress triggering. Testing this hypothesis is the subject of ongoing investigation.

6. CONCLUSIONS

We have tested the turbidite record along the NSAF for synchronous triggering of turbidity currents as a method for determining the origin of these deposits, whether from earthquake, or other sources. We have used ^{14}C ages, relative dating tests at channel confluences, and direct correlation of physical properties to determine whether turbidites deposited in separate channel systems are correlative, that is, they were triggered by a common event. The NSAF late Holocene turbidite record examined thus far has passed these tests, and can be correlated with multiple proxies along multiple canyon systems from the MTJ to offshore San Francisco. The inference of earthquake origin is further supported by an abrupt change in turbidite recurrence interval at the Mendocino Triple Junction, from ~200 years, a value consistent with onshore NSAF earthquakes to the south, to a value of ~520 years consistent with the Cascadia subduction zone to the north.

Preliminary comparisons of our event ages with existing and in progress work at onshore coastal sites show good correspondence, further circumstantial evidence that the offshore record is primarily earthquake generated. During the last ~2100 years, we observe 11 most likely correlative turbidites, including one likely generated by the 1906 earthquake, that can be traced between Noyo Canyon, near the MTJ, and Cordell Channel near Point Reyes. Using combined constraints from physical property correlation, radiocarbon ages, and inter-event sedimentation, we conclude that it is likely that at least 8 of 11 events recorded both onshore and offshore in the past 2100 years have rupture lengths of at least 250 km, and extend from the MTJ region to near the latitude of San Francisco.

ACKNOWLEDGEMENTS

We thank the officers and crew of the Scripps vessels R.V. Melville and Revelle. We thank the members of the 1999 and 2002 Scientific Parties: Mike Winkler, Pete Kalk, Antonio Camarero, Clara Morri, Gita

Dunhill, Luis Ramos, Alex Raab, Nick Pisijs jr., Mark Pourmanoutscheri, David Van Rooij, Lawrence Amy, Churn-Chi “Charles” Liu, Chris Moser, Devin Etheridge, Heidi Stenner, Chris Popham, Claire McKee, Duncan McMillan, Chris Crosby, Susanne Schmid, Eulalia Gracia, Suzanne Lovelady, Chris Romsos, Vincent Rinterknecht, Rondi Robison, David Casas, Francois Charlet, Britta Hinrichsen, Jeremiah Oxford, Miquel Marin, Marta Mas, Sergio Montes, Raquel Villalonga, Alexis Vizcaino, Santiago Jimenez, Mayte Pedrosa, Silvia Perez, Jorge Perez, Andreu Turra, David Lamas, Himar Falcon, and Andres Baranco. We thank David Schwartz, Mary Lou Zoback, Tom Fumal, Tina Niemi and many others for insightful discussions on the NSAF, and two anonymous reviewers for numerous improvements to the paper. We gratefully acknowledge funding by the U.S. National Science Foundation, Earth Sciences Division, and the U.S. Geological Survey National Earthquake Hazards Reduction Program.

REFERENCES

- [1] R.S. Stein, G.C.P. King and J. Lin, Change in failure stress on the southern San Andreas fault system caused by the 1992 M 7.4 Landers earthquake: *Science*, 199 (1992).
- [2] S.N. Ward and S.D.B. Goes, How regularly do earthquakes recur? A synthetic seismicity model for the San Andreas fault: *Geophysical Research Letters*, 20, no. 19 (1993) 2131-2134.
- [3] B.F. Atwater, Evidence for great Holocene earthquakes along the outer coast of Washington State: *Science*, 236 (1987) 942-944.
- [4] A.R. Nelson, B.F. Atwater, P.T. Brobowski, L. Bradley, J.L. Clague, G. A. Carver, M. Darienzo, W. C. Grant, H.W. Krueger, R. Sparks, T. Stafford, and M. Stuiver, Radiocarbon evidence for extensive plate boundary rupture about 300 years ago at the Cascadia subduction zone: *Nature*, 378 (1995) 371-374.
- [5] C. Goldfinger, C.H. Nelson, J. Johnson, Holocene Earthquake Records From the Cascadia Subduction Zone and Northern San Andreas Fault Based on Precise Dating of Offshore Turbidites *Annual Reviews of Geophysics*, 31 (2003a) 555-577.
- [6] C. Goldfinger, C.H. Nelson and J.E. Johnson, Deep-Water Turbidites as Holocene Earthquake Proxies: The Cascadia Subduction Zone and Northern San Andreas Fault Systems: *Annali Geofisica*, 46 (2003b) 1169-1194.
- [7] J. Adams, Paleoseismicity of the Cascadia subduction zone: evidence from turbidites off the Oregon-Washington margin: *Tectonics*, 9 (1990) 569-583.
- [8] R.E. Karlin, M. Holmes, S.E.B. Abella, and R. Sylwester, Holocene landslides and a 3500-year record of Pacific Northwest earthquakes from sediments in Lake Washington: *Geological Society of America Bulletin*, 116, no. 1-2 (2004) 94-108.
- [9] Y. Inouchi, Y. Kinugasa, F. Kumon, S. Nakano, S. Yasumatsu and T. Shiki, Turbidites as records of intense palaeoearthquakes in Lake Biwa, Japan: *Sed. Geol.*, 104 (1996) 117-125.
- [10] T. Shiki, F. Kumon, Y. Inouchi, Y. Kontani, T. Sakamoto, M. Tateishi, H. Matsubara and K. Fukuyama, Sedimentary features of the seismo-turbidites, Lake Biwa, Japan: *Sed. Geol.*, 135 (2000) 37-50.
- [11] T. Nakajima and Y. Kanai, Sedimentary features of seismoturbidites triggered by the 1983 and older historical earthquakes in the eastern margin of the Japan Sea: *Sedimentary Geology*, 135, (2000) 1-19.
- [12] K.A. Kastens, Earthquakes as a triggering mechanism for debris flows and turbidites on the Calabrian Ridge: *Marine Geology*, 55 (1984) 13-33.
- [13] T.M. Niemi and Z. Ben-Avraham, Evidence for Jericho earthquakes from slumped sediments of the Jordan River delta in the Dead Sea: *Geology*, 22 (1994) 395-398.

- [14] M.E. Field, The Submarine Landslide of 1980 off Northern California: U. S. Geological Survey, Circular 938 (1984) 65-72.
- [15] N. Garfield, T.A. Rago, K.J. Schnebele and C.A. Collins, Evidence of a turbidity current in Monterey Submarine Canyon associated with the 1989 Loma Prieta earthquake: *Continental Shelf Research*, 14, no. 6 (1994) 673-686.
- [16] A. Grantz, R.L. Phillips, M.W. Mullen, S.W. Starratt, G.A. Jones, S.S. Naidu and B.P. Finney, Character, paleoenvironment, rate of accumulation, and evidence for seismic triggering of Holocene turbidites, Canada abyssal plain, Arctic Ocean: *Marine Geology*, 133 (1996) 51-73.
- [17] W.R. Dickinson, and W.S. Snyder, The geometry of the triple junctions related to San Andreas transform: *Journal of Geophysical Research*, 84, (1979) 561-572.
- [18] D.F. Argus and R. G. Gordon, Current Sierra Nevada-North America motion from very long baseline interferometry: Implications for the kinematics of the western United States: *Geology*, 19 (1991) 1085-1019.
- [19] J.W. Sauber, W. Thatcher, S.C. Solomon and M. Lisowski, Geodetic slip-rate for the eastern California shear zone and the recurrence time for Mojave Desert earthquakes: *Nature*, 367 (1994) 264-266.
- [20] C.W. Jennings, New fault map of California and adjacent areas: *California Geology*, 48, no. 2 (1995) 31-42.
- [21] M.L. Zoback, R.C. Jachens and Olson, J. A., Abrupt along-strike change in tectonic style: San Andreas fault zone, San Francisco Peninsula: *Journal of Geophysical Research*, v. 104 (1999) 10719-10742.
- [22] D.A. Castillo and W. L. Ellsworth, Seismotectonics of the San Andreas Fault System between Point Arena and Cape Mendocino in Northern California: Implications for the Development and Evolution of a Young Transform: *Journal of Geophysical Research*, 98, no. 4 (1993) 6543-6560.
- [23] Working Group on California Earthquake Probabilities, Earthquake Probabilities in the San Francisco Bay Region: 2003 to 2032: U.S. Geological Survey Open-File Report 03-214, 235 p., 2003.
- [24] A.C. Lawson, The California Earthquake of April 18, 1906, report of the State Earthquake Investigation Commission: Carnegie Institution of Washington, Publication 87 Volumes I and II, 1908 (reprinted 1969), Washington, D.C.
- [25] R.D. Brown, 1906 Surface Faulting on the San Andreas Fault near Point Delgada, California: *Bulletin of the Seismological Society of America*, 85, no. 1 (1995) 100-110.
- [26] C.S. Prentice, D.J. Merritts, E.C. Beutner, P. Bodin, A. Schill, and J.R. Muller, Northern San Andreas fault near Shelter Cove, California: *Geological Soc. of America Bulletin*, 111 (1999) 512-523.
- [27] D.P. Schwartz, D. Pantosti, K. Okumura, T.J. Powers and J.C. Hamilton, Paleoseismic investigations in the Santa Cruz mountains, California: Implications for recurrence of large-magnitude earthquakes on the San Andreas fault: *Journal of Geophysical Research*, 103 no. 8 (1998) 17985-18001.
- [28] T.M. Niemi and N.T. Hall, Late Holocene slip rate and recurrence of great earthquakes on the San Andreas fault in northern California: *Geology*, 20 (1992) 195-198.
- [29] P. Segall, Integrating geologic and geodetic estimates of slip rate on the San Andreas fault system: *International Geology Review*, 44 no. 1 (2002) 62-82.
- [30] C.S. Prentice, Earthquake Geology of the Northern San Andreas Fault near Point Arena, California: [Ph.D. thesis], California Institute of Technology, Pasadena, California, 252 p., 1989.
- [31] H. Zhang, T. Niemi and T. Fumal, A 3000-year Record of Earthquakes on the Northern San Andreas Fault at the Vedanta Marsh Site, Olema, California *Seismological Research Letters*, 77 no. 2 (2006) 248.

- [32] K. Kelson, A. Strieg, R. Koehler and K. Kang, Timing of Late Holocene Paleoearthquakes on the Northern San Andreas Fault at the Fort Ross Orchard Site, Sonoma County, California: *Bulletin of the Seismological Society of America*, 96, no. 3 (2006) 1012-1028.
- [33] P. Segall and M. Lisowski, Surface displacement in the 1906 and 1989 Loma Prieta Earthquakes: *Science*, 250 (1990) 1241-1244.
- [34] W. Thatcher, G. Marshall and M. Lisowski, Resolution of fault slip along the 470 km long rupture of the great 1906 San Francisco earthquake: *Journal of Geophysical Research*, 102 (1997) 5353-5367.
- [35] C.S. Prentice and D.J. Ponti, Coseismic deformation of the Wrights tunnel during the 1906 San Francisco earthquake: a key to understanding 1906 fault slip and 1989 surface ruptures in the southern Santa Cruz Mountains, California: *Journal of Geophysical Research*, 102 (1997) 635-648.
- [36] K.B. Clahan, Paleoseismic characteristics of the San Andreas Fault, Woodside, California, MS thesis, San Jose State University, San Jose, CA, (1996) 96 pp.
- [37] J.C. Clark, Neotectonics of the San Gregorio fault zone; age dating controls on offset history and slip rates, USGS NEHRP Final Technical Report, 1999.
- [38] T. Fumal, T. Niemi and H. Zhang, High Resolution Paleoseismic Records at Three Sites on the Northern San Andreas Fault: *Seismological Research Letters*, 77, no. 2 (2006) 269.
- [39] B.C. Heezen and M. Ewing, Turbidity currents and submarine slumps, and the 1929 Grand Banks earthquake: *American Journal of Science*, 250 (1952) 849-873.
- [40] D.S. Gorsline, T. De Diego and E.H. Nava-Sanchez, Seismically triggered turbidites in small margin basins: Alfonso Basin, Western Gulf of California and Santa Monica Basin, California Borderland: *Sedimentary Geology*, 135 (2000) 21-35.
- [41] R.W. Sternberg, Transport and accumulation of river-derived sediment on the Washington continental shelf, USA, *Jour. of Geol. Soc. London*, 143 (1986) 945-956.
- [42] C. Goldfinger and C.H. Nelson, Holocene Recurrence of Cascadia Great Earthquakes based on the Turbidite Event Record: *Nature*, in revision, 2005.
- [43] C.K. Sommerfield, D.E. Drake and R.A. Wheatcroft, Shelf record of climatic changes in flood magnitude and frequency, north-coastal California: *Geology*, 30, no. 5 (2002) 395-398.
- [44] P. Puig, A.S. Ogston, B.L. Mullenbach, C.A. Nittrouer, J.D. Parsons and R.W. Sternberg, Storm-induced sediment gravity flows at the head of the Eel submarine canyon, northern California margin: *Journal of Geophysical Research*, 109 (2004) C03019.
- [45] C. K. Paull, P. Mitts, P., W. Ussler III, R. Keaten, and H. G. Greene, Trail of sand in upper Monterey Canyon: Offshore California: *Geol Soc Am Bull*, 117, no. 9-10 (2005) 1134-1145.
- [46] O.S. Madsen, Spectral wave-current bottom boundary layer flows: *Coastal Engineering 1994, Proceedings, 24th International Conference, Coastal Engineering Research Council / ASCE*, (1994) 384-398.
- [47] S. Caires, and A. Sterl, 100-year return value estimates for ocean wind speed and significant wave height from the ERA-40 data: *J. Climate*, 18, no. 7 (2005) 1032-1048.
- [48] O.H. Pilkey, Basin plains; Giant sedimentation events: *Spec. Pap. Geol. Soc. Am.*, 229 (1988) 93-99.
- [49] D.G. McCubbin, Barrier-Island and Strand-Plain Facies. *In: Sandstone Depositional Environment*. P.A. Scholle & D. Spearing, eds., The AAPG, Tulsa, Oklahoma (1982) 247-279.
- [50] R. Lovlie, and P. Van Veen, Magnetic susceptibility of a 180 m sediment core: reliability of incremental sampling and evidence for a relationship between susceptibility and gamma activity, *in Turner, P., and Turner, A., eds., Palaeomagnetic applications in hydrocarbon exploration and production: Special*

- Publication, 98, Geological Society, London, (1995) 259-266.
- [51] K. Fukuma, Origin and applications of whole-core magnetic susceptibility of sediments and volcanic rocks from Leg 152: Proceedings of the Ocean Drilling Program: Scientific Results, 152 (1998) 271-280.
- [52] A.L. Abdelayem, K. Ikehara and T. Yamazaki, Flow path of the 1993 Hokkaido-Nansei-Oki earthquake seismoturbidite, southern margin of the Japan Sea north basin, inferred from anisotropy of magnetic susceptibility: *Geophys. Jour. Int.*, 157 (2004) 15-24.
- [53] G. St-Onge, T. Mulder, D.J.W. Piper, C. Hillaire-Marcel and J.S. Stoner, Earthquake and flood-induced turbidites in the Saguenay Fjord (Québec): a Holocene paleoseismicity record: *Quaternary Science Reviews*, 23, (2004) 283-294.
- [54] J.T. Hagstrum, B.F. Atwater and B.L. Sherrod, Paleomagnetic correlation of late Holocene earthquakes among estuaries in Washington and Oregon: *G3*, 5 (2004) doi:10.1029/2004GC000736.
- [55] H. Iwaki, A. Hayashida, N. Kitada, H. Ito, S. Suwa and K. Takemura, Stratigraphic correlation of samples from the Osaka Bay off Kobe based on magnetic properties and its implication for tectonic activity of the Osaka-wan fault for the last 6300 years: *Eos Transactions American Geophysical Union*, 84 (2004) GP41C-0053 F554. [53] J.A. Lees, R. J. Fowler and P.G. Appleby, Mineral magnetic and physical properties of surficial sediments and onshore samples from the southern basin of Lake Baikal, Siberia: *Journal of Paleolimnology*, 20, no. 2 (1998) 175-186.
- [56] M. Schnellmann, F.S. Anselmetti, D. Giardini and S.N. Ward, Prehistoric earthquake history revealed by lacustrine slump deposits: *Geology*, 30 no. 12 (2002) 1131-1134.
- [57] J. A. Lees, R. J. Fowler, and P. G. Appleby, Mineral magnetic and physical properties of surficial sediments and onshore samples from the southern basin of Lake Baikal, Siberia: *Journal of Paleolimnology*, 20, no. 2 (1998) 175-186.
- [58] R.B. Wynn, P.P.E. Weaver, D.G. Masson and D.A.V. Stow, Turbidite depositional architecture across three interconnected deep-water basins on the north-west African margin: *Sedimentology*, 49 no. 4 (2002) 669-695.
- [59] C. Goldfinger, C.H. Nelson, J.E. Johnson, M.A. Arsenault, A. Eriksson, E. Karabanov and J. Chaytor, Physical Property Correlations from Cascadia and Northern San Andreas Great Earthquakes: What Are They Telling Us About The Triggering Events? Submitted to *Geophysical Research letters* (submitted 2006).
- [60] J.Rivera, E.B. Karabanov, D.F. Williams, V. Buchinskyi, M. Kuzmin, Lena River discharge events in sediments of Laptev Sea, Russian Arctic. *Estuarine Coastal and Shelf Science*, 66 (2006) 185-196.
- [61] C. Goldfinger, A. Morey, M. Erhardt, C.H. Nelson, J. Gutierrez-Pastor, R. Enkin and A. Dallimore, Cascadia Great Earthquake Recurrence: Rupture Lengths, Correlations and Constrained OxCal Analysis of Event Ages, proceedings of the USGS Tsunami Sources Workshop, Diggles, Geist, and Lee, eds. (2006), CD-ROM, April 21 and 22, 2006.
- [62] A. Dallimore, R.E. Thomson and M.A. Bertram, Modern to late Holocene deposition in an anoxic fjord on the west coast of Canada: Implications for regional oceanography, climate and paleoseismic history: *Marine Geology*, 219, no. 1 (2005) 47-60.
- [63] C. Goldfinger, C.H. Nelson, J. E. Johnson, and A. Morey, Physical Property Correlations and Radiocarbon Ages Illuminate Cascadia Earthquake Recurrence Patterns, *Eos Trans. AGU*, 84(46), (2003c) Fall Meet. Suppl., Abstract S42A-0144.
- [64] A. Morey, C. Goldfinger, C.H. Nelson, J. Chaytor, J.E. Johnson and A. Ericsson, TI: Turbidite Based

- Earthquake Record Along the Northern San Andreas Fault , *Eos Trans. AGU*, 84(46), Fall Meet. Suppl., Abstract T51C-02 (2003d).
- [65] R.B. Wynn and D.G. Masson, Canary Islands landslides and tsunami generation. In: Proc. 1st Int. Symposium on Submarine Mass Movements and their Consequences (Ed. by J. Mienert and J. Locat), Kluwer, Dordrecht, 325-332, 2003.
- [66] C.R. Smith, R.H. Pope, D.J. DeMaster and L. Magaard, Age-dependent mixing of deep-sea sediments. *Geochimica et Cosmochimica Acta* 57: (1993) 1473-1488.
- [67] R.A. Wheatcroft, Experimental tests for particle size-dependent bioturbation in the deep ocean. *Limnology and Oceanography* 37: (1992) 90-104.
- [68] J. Thomson, G.T. Cook, R. Anderson, A.B. Mackenzie, D.D. Harkness, I.N. McCave, Radiocarbon Age Offsets In Different-Sized Carbonate Components Of Deep-Sea Sediments, *Radiocarbon*, 7 no. 2 (1995) 91-103.
- [69] C.B. Ramsey, Radiocarbon calibration and analysis of stratigraphy: The OxCal program: *Radiocarbon* 37, no. 2, (1995) 425-430.
- [70] C.B. Ramsey, Development of the Radiocarbon Program OxCal: *Radiocarbon*, 43 (2001) 355-363.
- [71] P.J. Reimer, M.G.L. Baillie, E. Bard, A. Bayliss, J.W. Beck, C.J.H. Bertrand, P.G. Blackwell, C.E. Buck, G.S. Burr, K.B. Cutler, P.E. Damon, R.L. Edwards, R.G. Fairbanks, M. Friedrich, T.P. Guilderson, A.G. Hogg, K.A. Hughen, B. Kromer, F.G. McCormac, S.W. Manning, C.B. Ramsey, R.W. Reimer, S. Remmele, J. R. Southon, M. Stuiver, S. Talamo, F.W. Taylor, J. van der Plicht and C.E. Weyhenmeyer. IntCal04 Terrestrial radiocarbon age calibration, 26 - 0 ka BP. *Radiocarbon* 46: (2004) 1029-1058.
- [72] L. Ingram, Holocene Climate Change Recorded in Radiocarbon Age Differences Between Shell and Charcoal From a Shell mound Near San Francisco Bay: *Eos Trans. American Geophysical Union*, 78, 1997.
- [73] L. Anderson, M. B. Abbott, and B. P. Finney, Holocene Climate Inferred from Oxygen Isotope Ratios in Lake Sediments, Central Brooks Range, Alaska: *Quaternary Research*, 55 (2001) 313-321.
- [74] R.T. Patterson, A. Prokoph, A. Dallimore, R.E. Thomson, D.M. Ware and C. Wright, Impact of abrupt Holocene climate change and solar cyclicity on fish population dynamics in the NE Pacific: Geological Society of America Abstracts with programs, 2001.
- [75] C. Goldfinger, C.H. Nelson, J.E. Johnson, M.A. Arsenault, A. Eriksson, E. Karabanov and J. Chaytor, Physical Property Correlations from Cascadia Great Earthquakes: What Are They Telling Us About The Triggering Events? *Eos Trans. AGU*, 85 (2004) (47), Fall Meeting Supl. Abstract OS21E-01.
- [76] A. Morey, C. Goldfinger, C.H. Nelson, J. Chaytor, J.E. Johnson, and A. Eriksson, Turbidite Based Earthquake Record Along the Northern San Andreas Fault , *Eos Trans. AGU*, 84 (46), Fall Meet. Suppl., (2003) Abstract T51C-02.
- [77] J.D. Hopkirk, Endemism in fishes of the Clear Lake region of Central California, Contributions from the Museum of Vertebrate Zoology of the University of California: Berkeley, University of California Press, 1973, 135 pages and plates.
- [78] C.H. Nelson, C. Goldfinger, J.E. Johnson and G. Dunhill, Variation of modern turbidite systems along the subduction zone margin of Cascadia Basin and implications for turbidite reservoir beds, *in* Deep-water Reservoirs of the World, GCSSEPM 20th Annual Research Conference, p. 31 pp., 2001.
- [79] C. Goldfinger, C.H. Nelson and J.E. Johnson, Deep-Water Turbidites as Holocene Earthquake Proxies: The Northern San Andreas Fault System, San Andreas Fault Workshop: USGS, Menlo Park California, 2004.

- [80] C. Goldfinger, A. Morey and H. Nelson, Deep-Water Turbidites as Holocene Earthquake Proxies along the Northern San Andreas Fault System: *Seismological Research Letters*, 77 no. 2 (2006) 195-196.
- [81] D.L. Wells, K.J. Coppersmith, New empirical relationships among magnitude, rupture length, rupture width, rupture area, and surface displacement: *Bulletin of the Seismological Society of America*, v. 84; no. 4 (1994) 974-1002.



CAPÍTULO IV

CARACTERIZACIÓN SEDIMENTOLÓGICA DE SEISMO-TURBIDITAS

Sedimentology of Seismo-Turbidites off the Cascadia and Northern California Active Tectonic Continental Margins, Northeast Pacific Ocean

Julia Gutiérrez-Pastor¹, C. Hans Nelson¹, Carlota Escutia¹, Chris Goldfinger², Andrew Eriksson²

¹Instituto Andaluz de Ciencias de la Tierra (IACT) CSIC-UGR

Campus de Fuentenueva s/n 18002 Granada, Spain, juliagp@ugr.es

²Oregon State University, College of Oceanic and Atmospheric Sciences

104 Ocean Admin. Bldg., Corvallis OR 97331, USA.

Abstract

The sedimentologic characteristics of Holocene turbidites, along the active tectonic continental margins of the Cascadia Subduction Zone (Washington, and Oregon offshore) and the northern San Andreas Fault (California offshore), help to identify their origin by seismic triggering of great earthquakes. Based on visual core descriptions, grain size analysis, X-ray radiographs, mineral analysis and physical properties, we observe that at the proximal channel sites of Juan de Fuca and Willapa Channels turbidite bases are generally uni-pulsed, with typical fining upward grain size. The absence of many tributary canyon heads and the simple morphology of a single channel without confluences of tributary channels usually result in turbidites that are uni-pulsed. Some multi-pulsed turbidites, however, are found in both Juan de Fuca and Willapa Channels, and these correlate with the thickest turbidites in other Cascadia Basin Channels, which suggests that the strongest great earthquakes may cause multi-pulsed turbidites in proximal channels. These multi-pulsed turbidites appear to record the shaking signature of the strongest earthquakes. Downstream in Cascadia Channel, below the confluence of Juan de Fuca and Willapa tributary channels, individual turbidites, that are correlative with upstream uni-pulsed turbidites, become multi-pulsed, thicker and coarser grained. The multi-pulsed turbidites of Cascadia Channel result from amalgamated pulses generated by synchronous earthquake triggering of turbidity currents in the tributary canyons and channels.

Along the northern California margin in proximal channels turbidite are uni or multi-pulsed, but most commonly multi-pulsed because there are multiple upstream tributary canyons that join at the base of the continental slope. In both Cascadia and California margins, below channel confluences, turbidites are multi-pulsed without hemipelagic sediment in between. The coarser-grained sand/silt pulses, with incomplete truncated Bouma sequences, deposit from multiple tributary canyon and channel inputs. Because no hemipelagic sediment exists between pulses, and each pulse has a distinct mineralogy from a different tributary canyon, we interpret that these individual amalgamated turbidites result from several turbidity currents fed by multiple tributary canyons with synchronous triggering by a great earthquake. Hence, earthquake triggering and stacking of multiple coarse grained pulses become an alternative explanation for the amalgamated turbidite beds in active tectonic margins, in addition to other classic explanations for amalgamated turbidites.

Previous work and this study demonstrate that the number and character of coarse pulses for an individual turbidite commonly remains constant in multiple channel systems along a continental margin. This suggests that the earthquake shaking or aftershock signature is often preserved, especially for the strongest great earthquakes. Consequently, both downstream confluences and the strongest great earthquakes may

contribute to multiple pulses that are typical for seismo-turbidites. The detailed analyses of the turbidites recovered in the Cascadia and northern California margins reveals common sedimentological characteristics of turbidites triggered by earthquakes that can be used to distinguish seismo-turbidites in other active tectonic margins around the world.

Keywords: seismo-turbidite, sedimentology, earthquakes, Cascadia Subduction Zone, San Andreas Fault, continental margins

(To be submitted to Marine Geology in June, 2009)

1. INTRODUCTION

Marine and onshore paleoseismic records are being studied along the Cascadia subduction zone margin and northern California transform fault margin. The onshore area of the Cascadia margin has abundant paleoseismic evidence for rapid coastal subsidence that records buried marsh deposits and tsunami records (e.g. Atwater, 1987; Atwater et al., 1995; Darienzo and Peterson, 1990; Nelson et al., 1995; Satake et al., 1996; 2003). The northern California margin, associated with the active San Andreas Fault, also has an onshore paleoseismic record based on the geodetic data and fault offset history (Kelson et al., 2006; Niemi and Hall, 1992; Prentice, 1999; Schwartz et al., 1998; Segall, 2002; Zhang, et al., 2006). Along offshore margins, the paleoseismic record is recorded as turbidites in canyon and basin floor channel turbidite systems. We and Adams (1990) have demonstrated the synchronous seismic triggering of well-correlated individual turbidites from different canyon and abyssal basin channel sites for hundreds of kilometers along these active margins (Nelson et al, 2000; Goldfinger et al., 2003a; 2003b; 2006; 2007; 2008, Gutierrez-Pastor et al., in press). The synchronicity of turbidites in such active margins has been proved by the same number of turbidites recorded in tributary canyons above and downstream channels below confluences and by synchronicity of turbidites in different turbidite systems that are separated by hundreds of kilometre along the same margin. In previous papers, we have discussed but discounted other possible triggers for turbidity current generation such as storm wave loading, tsunamis, sediment loading, hyperpycnal flow and aseismic accretionary wedge slip (Nelson et al., 2000; Goldfinger et al., 2003a, 2003b; 2006; 2007; 2008, Gutierrez-Pastor et al., in press).

Because both Cascadia and northern California margins have recorded a Holocene history of turbidites mainly triggered by great earthquakes, they are ideal places to develop a turbidite sedimentological model to characterize their seismic triggering. Until now in these margins the turbidite studies have been focused on the correlation of turbidites triggered by earthquakes based on stratigraphic datums (Adams, 1990; Nelson et al., 2000), AMS radiocarbon ages and physical properties (Goldfinger et al., 2003a; 2003b; 2006; 2007; 2008) and recurrence time intervals determined by hemipelagic sediment thickness and sedimentation rates (Gutierrez- Pastor et al., in press). In this paper we analyze the detailed sedimentologic characteristics of turbidites from Cascadia and northern California margins by using a wide variety analyses. Several authors in other areas have attempted to define sedimentologic differences between turbidites triggered by earthquakes and turbidites triggered by other mechanisms (Gorsline et al., 2000; Nakajima and Kanai, 2000; Shiki et al. 2000). In our research, we add further observations to characterize turbidites generated by great earthquakes, for which we use the term seismo-turbidites. We study the sediment lithology using visual core descriptions, photos, x- ray imagery, quantitative grain size analyses, mineralogical

analysis and physical properties of high-resolution magnetic susceptibility and density. Finally, we develop a sedimentological model in space and time for seismo- turbidites that provides information about the triggering, source, mechanisms of deposition and even magnitude of earthquakes. This model can be help to distinguish seismo-turbidites in other active tectonic margins.

2. GEOLOGICAL SETTING AND TURBIDITE SYSTEMS

2.1. Cascadia Continental Margin

The Cascadia margin is part of a subduction zone generated when the Gorda and Juan de Fuca plates are thrust under the North American plate (Fig. 1). Cascadia Basin is the abyssal seafloor off northern California, Oregon, Washington, and Vancouver Island along the subduction zone. Great Earthquakes (>8Mw) from the Cascadia subduction zone have generated paleoseismic turbidites offshore. and tsunami sands and buried marshes onshore (Adams, 1990; Atwater, 1987; Atwater and Hemphill-Haley, 1997; Kelsey et al, 2002; Goldfinger et al., 2003 a, 2003b; Nelson et al., 1995; Nelson et al., 2000; Satake et al., 1996).

A wide variety of modern turbidite systems all containing correlative, synchronously triggered turbidites are found in the Cascadia Basin (Nelson et al., 2000). The Rogue Apron is an example of a small-scale (~ 5-10 km diameter) base-of-slope sand-rich apron system without evident channels (Nelson et al., 2000; Wolf and Hammer, 1999). The Astoria Fan is a a channelized submarine fan that funnels sediment into depositional lobes. Cascadia Channel is a deep-sea channel system fed by multiple tributary canyons, and extends for hundreds of kilometers across Cascadia Basin. Plunge pools and dune fields associated with canyon mouths such as those of the Trinidad and Eel systems are other atypical turbidite systems (Nelson et al., 2000).). For our detailed sedimentological analysis, we have selected a well correlated turbidite event within the Juan de Fuca and Willapa Channels that are tributary channels to the Cascadia Channel.

2.2. Northern California Continental Margin

Along the continental margin of northern California, the San Andreas Fault extends from San Francisco, where the fault parallels the coast and then further north underlies the margin until the Mendocino Triple Junction (Fig. 2). The earthquake history onshore has been well studied in coastal areas such as Olema, Point Arena, Vandata, Fort Ross and several places on the San Francisco Peninsula (Prentice, 1999, Niemi and Hall, 1992; Segall, 2002; d'Alessio et al., 2005; Zhang et al., 2006; Kelson et al., 2006). The earthquake history also has been recorded in several turbidite systems offshore along the northern California margin (Goldfinger et al., 2007; Gutierrez-Pastor et al., in press).

Along the northern California margin there are numerous canyon/channel systems containing earthquake-triggered synchronous Holocene turbidites. From the north, beginning at Cape Mendocino, to the south at Monterey Bay, the canyons and channels are: Gorda, Viscaino, Noyo, Arena, Gualala, Albion, Bodega Cordell, Farallon, Montara, Pioneer and Monterey (Fig. 2) (Goldfinger et al., 2003 a; 2003b; 2007; Gutierrez-Pastor et al., in press). The turbidite channels join together creating downstream confluence pathways. Noyo Channel, which is found south of Cape Mendocino, extends seaward for more than 200 km from the mouth of the canyon where it has a confluence with Viscaino and Gualala Channels (Fig. 2). Southern Point Arena and Gualala canyons join at the base of the continental slope to form a channel that

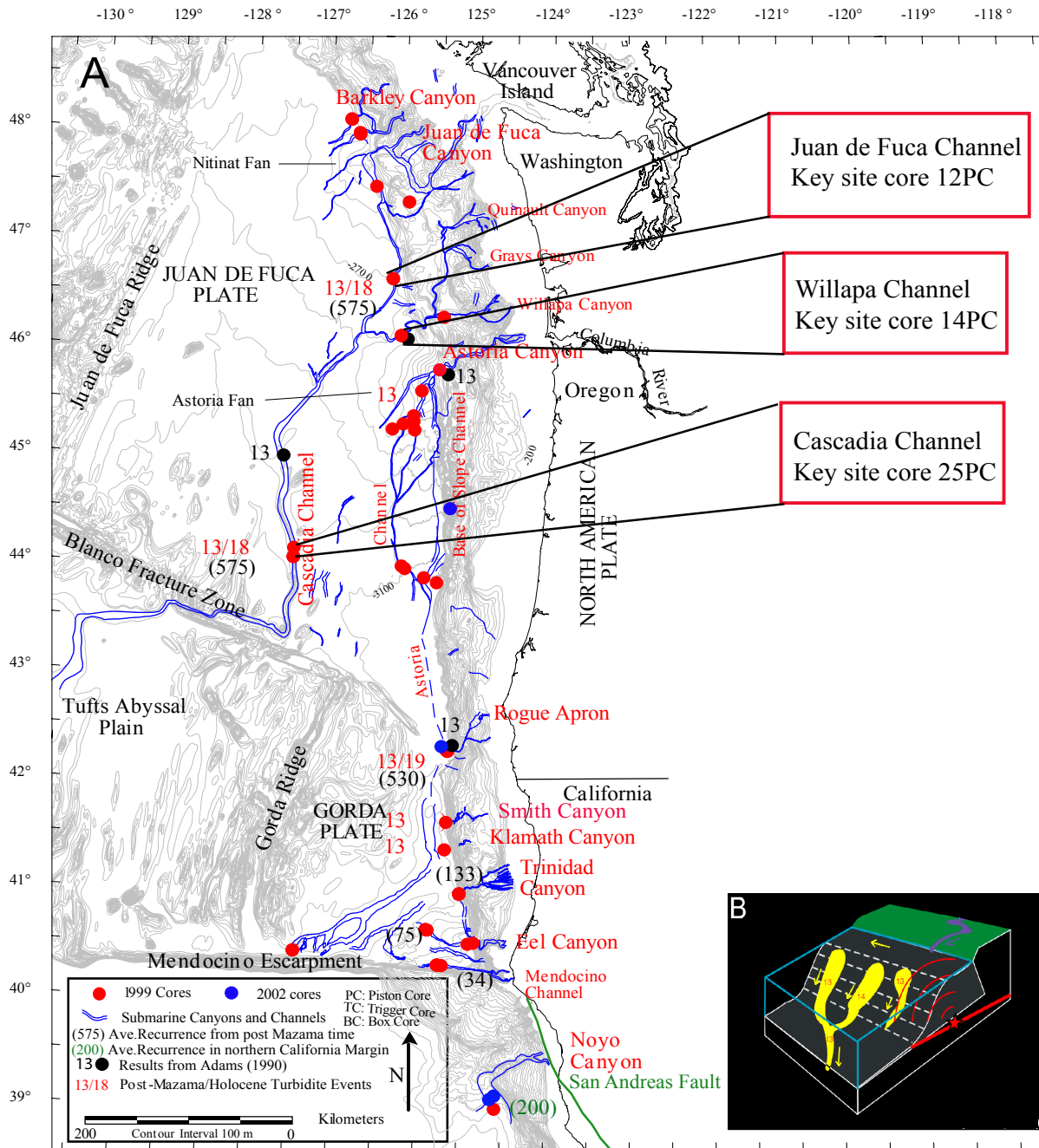


Figure 1. The Cascadia margin turbidite systems, core locations and the geological setting of the active tectonic continental associated with the Cascadia Subduction Zone made up of the Juan de Fuca and Gorda Plates (modified from Goldfinger et al., 2008).

extends 100 km until its confluence with Noyo and Viscaino Channels. Similarly, north of the Noyo Channel, the Viscaino channel is formed by multiple tributaries that meet to develop the main channel traveling more than 200 km until a confluence with Noyo, Gualala and Cordell. For our sedimentological characterization, we have selected turbidites from the Noyo, Gualala and channels downstream from confluences to examine representative turbidites from tributary source channels and below their confluence.

3. SEDIMENT ANALYSIS METHODS

During the 1999 and 2002 cruises for paleoseismic studies, cores were recovered from several turbidite

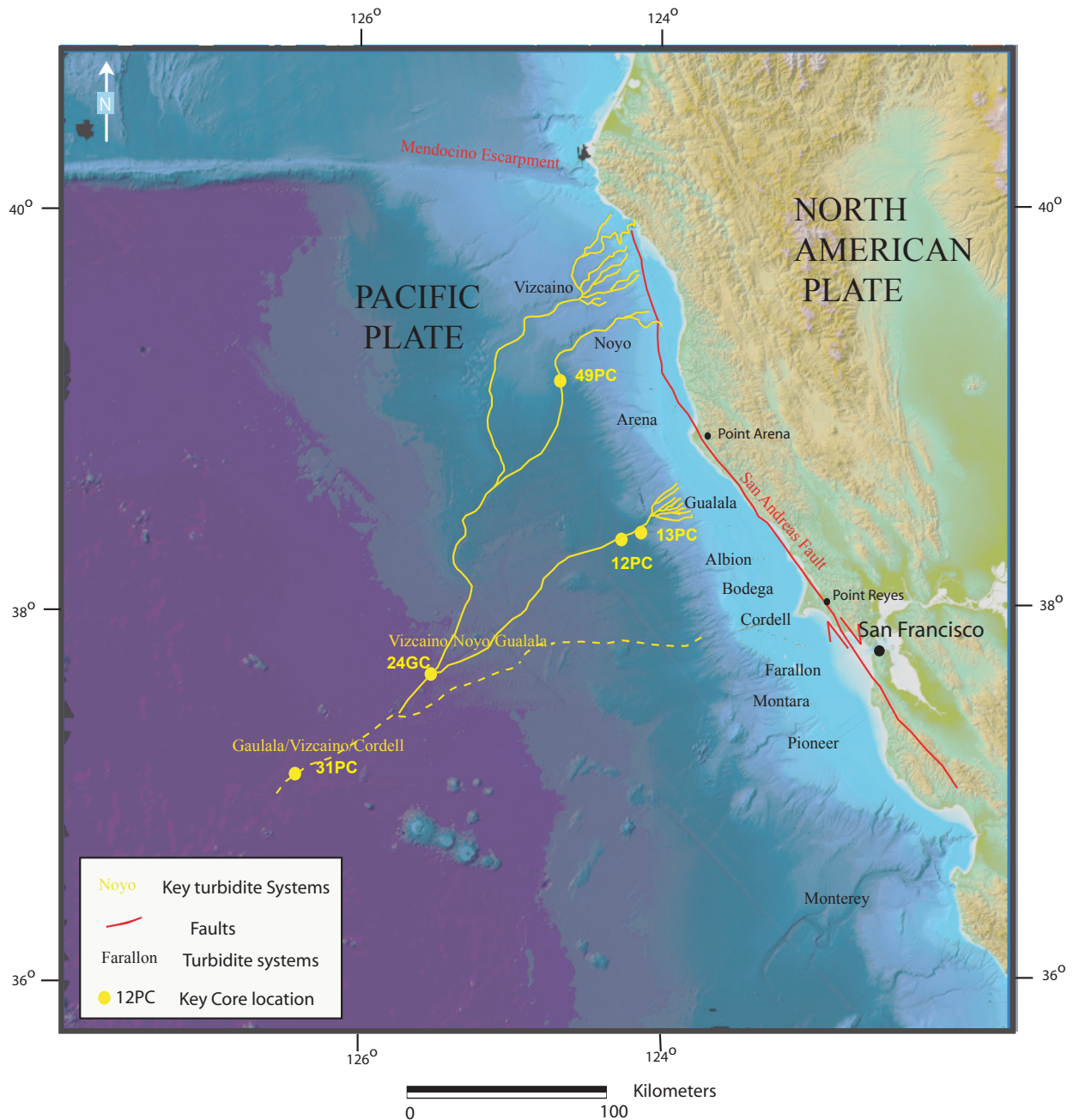


Figure 2. Northern California margin turbidite systems, core locations and geological setting of the active tectonic margin associated with the northern San Andreas Fault.

systems along the Cascadia and northern California margins. The core locations were selected carefully in channel pathways integrating all available swath bathymetry and archive cores in a GIS data base. This allowed exploring in real time the ocean floor using advanced side scan sonar and Fledermaus fly-throughs. Core sites were chosen to take advantage of known depositional segments of channels versus non-deposition or erosional segments to capture the most complete turbidite record.

During the cruises, the Oregon State University wide diameter (10 cm) coring gear was employed to collect 44 piston cores of 6- 8m length and 44 companion trigger cores (also 10 cm) of 2 m length, as well as seven box cores of 0.5m length x 0.5m width in Cascadia Basin. On the northern California margin, 69 piston/trigger pairs and 10 jumbo Kasten cores (of 3m length and 400 cm³) were collected in 2002.

On board the ship, turbidites versus hemipelagic sediment were logged by visual core lithologic analysis

(Fig. 3A). Color photos of each core were taken to complement the visual core observations. Analysis of the sand fraction (> 62 microns) of the hemipelagic sediment using a binocular microscope was done to determine the micro fauna content (foraminifera and radiolarian), main lithology of the sand grains, plants fragments and micas. This analysis was done to distinguish the hemipelagic sediment from the turbidite tail and also to determine the Holocene/Pleistocene boundary. In addition, hemipelagic sediment thickness was measured to calculate accurate sedimentation rates for estimation of turbidite recurrence time intervals (Gutierrez-Pastor et al., in press)

To help the turbidite identification, the Multisensor Core Logger (MSCL) from Geotek was used to obtain continuous measurements of the physical properties (density, p-wave velocity and high-resolution magnetic susceptibility (MST) for each core (Figs. 3B and 3C). The physical properties measurements have been very useful as proxies for grain size to identify turbidites with sandy/silty multiple pulses without hemipelagic sediment in between pulses. A semi-quantitative mineralogical analysis was done with smear slides from critical turbidites to identify the Mazama Ash content (Mazama Ash Datum: 7627 ± 150 cal yr B.P) in the Cascadia margin and the sand/silt provenance of tributary canyons in the northern California margin (Zdanowicz et al., 1999). Between two to three centimeters of hemipelagic sediment were sampled below the base of each turbidite bed to obtain planktonic foraminifera for radiocarbon ages (Fig. 3A). Ages were obtained from foraminifera using Accelerator Mass Spectrometry (AMS) methods at the Lawrence Livermore Laboratory. X-ray radiographs were taken in many cores from both margins to show grading and internal sedimentary structures of the turbidites and to distinguish the lighter intensity hemipelagic sediment from the turbidite tail mud (Fig. 3B).

Grain size analyses for selected turbidites from both Cascadia and Northern California margins were performed with a laser diffraction particle size analyser using the Beckman-Coulter recommended procedure (Blott and Pye, 2006). With this method we have measured the size distribution of particles in the range of 0.4 microns to 850 microns. Prior to the measurements, we treated the ~ 10 g samples with hydrogen peroxide to remove the organic matter. The results are shown in granulometric curves that reflect the variations of grain size in each part of the individual turbidites. The grain size analyses were done to distinguish individual turbidites with complex multiple pulses of coarse grain size from turbidites with simple fining upward gradation, and to identify the different parts of the turbidite (base, turbidite body and tail) and the hemipelagic sediment just below the turbidite base. Also, we wanted to recognize associated grain size patterns in turbidites triggered by earthquakes compared with turbidites triggered by other mechanisms.

Broad mineral provenance bins were determined from standard heavy-mineral analysis techniques (Goldfinger et al., 2007). We sieved the sand fraction from selected turbidites, and separated the heavy minerals with tetrabromoethane (specific gravity is 2.9), separating light and heavy fractions. The grain mounts of the heavy minerals were then counted for at least 300 grains, 200 being true heavy minerals. All the physical property logs, X-ray radiographs, lithologic log data, together with mineralogical and grain size analyses have been integrated to compare the sedimentological characteristics of the turbidites.

4. PALEOSEISMIC TURBIDITE RECORD: PREVIOUS RESULTS

Along the Cascadia and northern California margins, turbidites have been recognized in 1999, 2002 and archive cores (Nelson, 1968; 1976; Griggs, 1969; Duncan, 1970) The turbidites exhibit a turbidite base, that contains one or multiple pulses of sand and/or silt at a centimeter scale, and, a turbidite tail above, that is

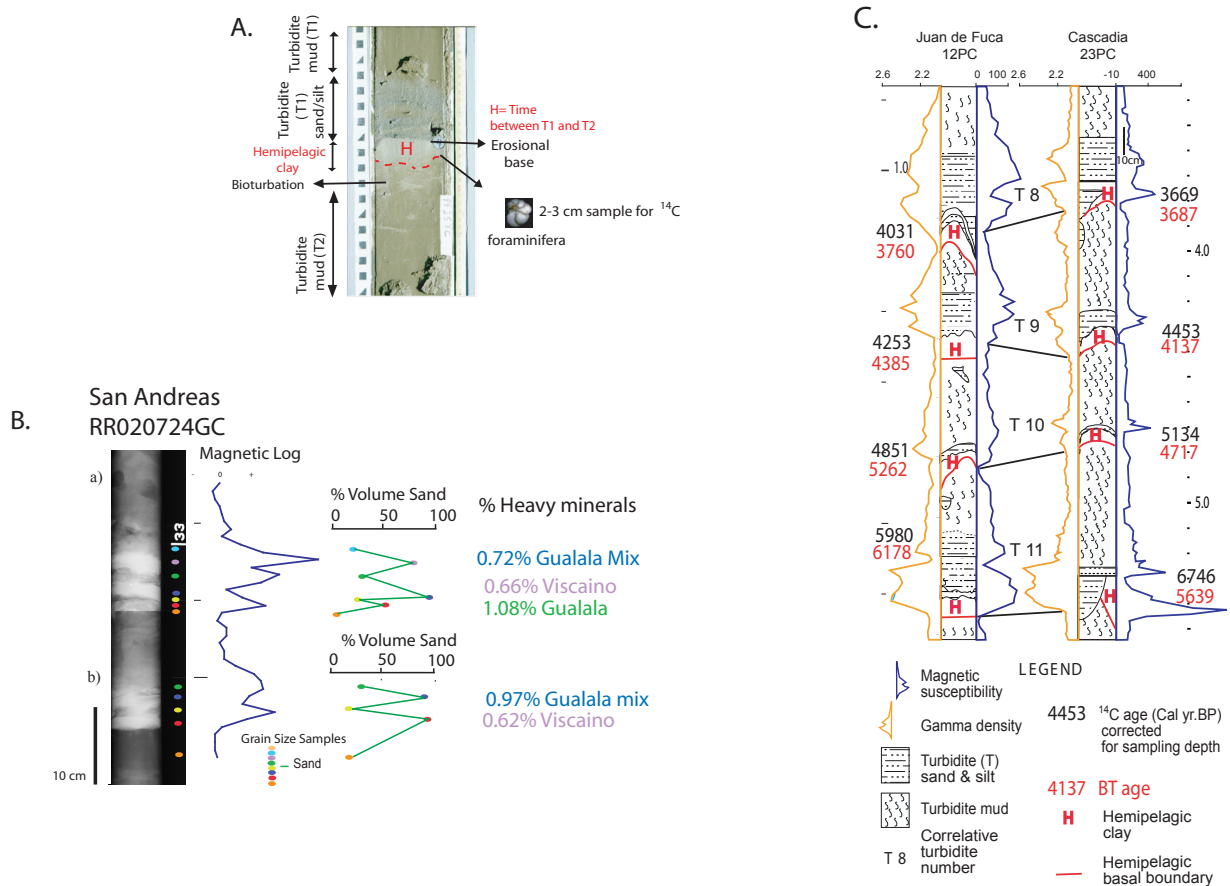


Figure 3. Analysis of core sections. 3A. Definition of turbidite versus hemipelagic sediment sequences. 3B. X-rays, physical properties, grain size samples and mineralogy of 24GC of the northern California margin. 3C. Example of turbidite correlations along the Cascadia margin based on lithology, physical properties and radiocarbon ages.

composed of a frequently bioturbated interval of mud (silt and clay).

Turbidites are emplaced over the hemipelagic sediment that is composed of intensely bioturbated clay with a coarse fraction of dominant microfauna tests (foraminifera and radiolaria) in distal sites and with more abundant terrigenous (up to 50%), such as plant fragments and micas, and less abundant microfauna (less than 50%) in proximal sites near the base of the continental slope (Fig. 3A) (Nelson, 1976). Following the techniques of Nelson (1968; 1976), when the boundary between turbidite and hemipelagic sediment was difficult to differentiate visually, we sampled the sand fraction of the sediment above and below the inferred boundary and counted microfossils and terrigenous grains with a binocular microscope (Fig. 3A). Once the hemipelagic sediment was identified by the dominance of planktonic tests, the number of foraminifera (dominance = Pleistocene) and radiolarian (dominance = Holocene) were counted. Nelson et al. (2000) described the Holocene turbidites in Cascadia Channel as muddy, with a thickness between 40 and 70 cm. The turbidites consist of thin silt bases (1-3 cm) overlain by a mud tail that is separated from the above turbidite by hemipelagic clays of approximately 2-8 cm thickness. In Juan de Fuca Channel, Holocene high-stand turbidites are thinner (10-40cm) and sandier (1-3cm fine sand base) than those in Cascadia Channel and they grade into a mud turbidite tail above the sandy turbidite base (Nelson et al., 2000).

Along the Cascadia margin, Holocene turbidites have been deposited synchronously in different channels separated by hundreds of kilometers, when the sea level was high and turbidite deposition was

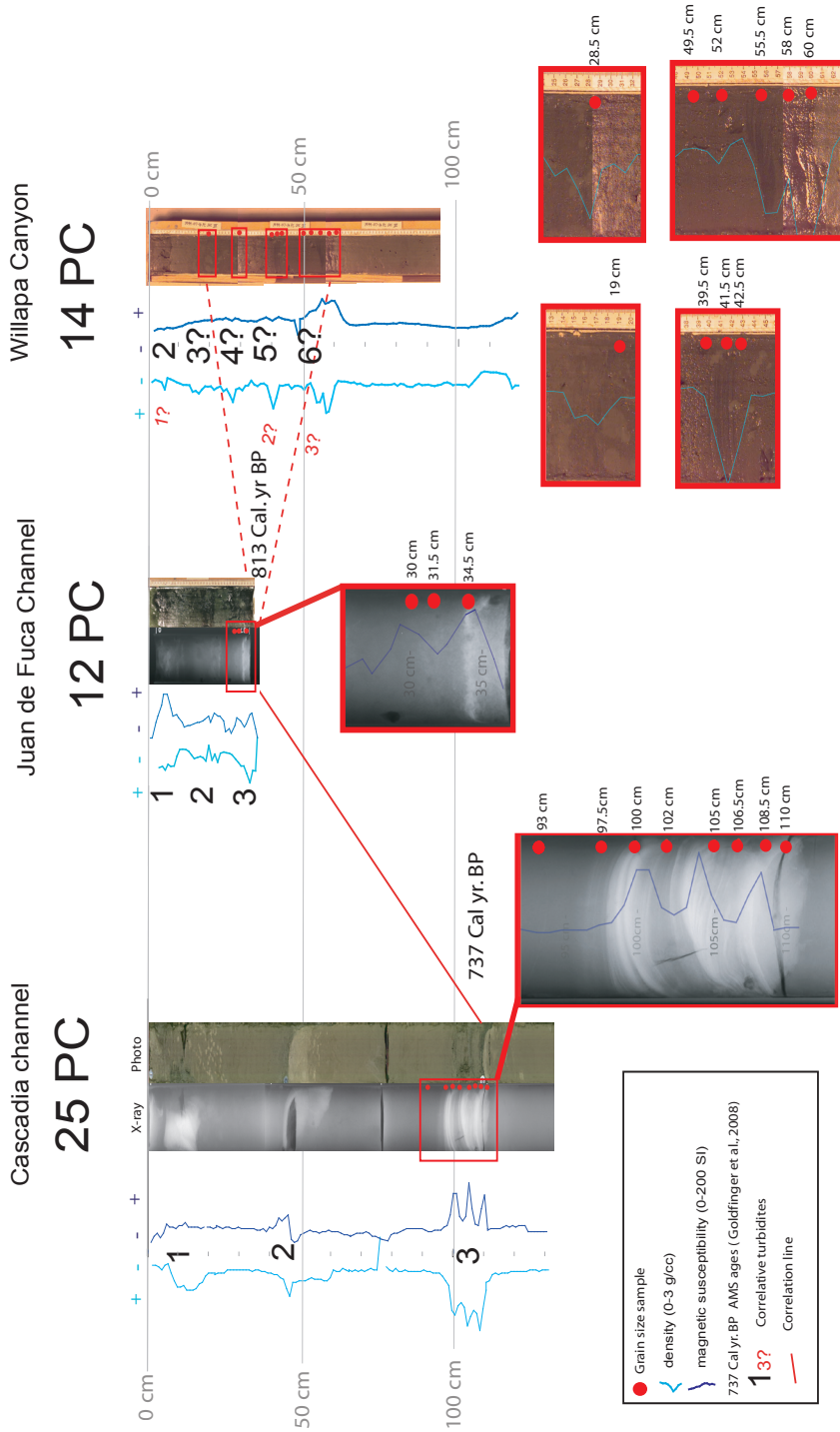


Figure 4. Cascadia margin core sections of 12PC at Juan de Fuca Channel, 25 PC at Cascadia Channel and 14PC at Willapa Channel. Core photos, X-ray radiographs and physical properties (density and magnetic signatures) are represented to show the correlation of the turbidite 3 (T3) in the Cascadia margin channels. Red dots are grain size samples. Numbers down the core sections show the correlative turbidites. For Willapa Canyon the black numbers correspond with the Goldfinger et al. (2008) turbidite correlations based on the shape of physical properties. Red numbers are the inferred correlative turbidites based on core observations, grain size analysis and physical properties.

not expected. Great earthquakes on the subduction zone are the best candidate to explain the synchronicity of turbidite triggering in such a wide area during the Holocene time. To show synchronicity of turbidite triggering by earthquakes, the confluence test postulated by Adams (1990) utilizes the first occurrence of Mazama ash (7627 ± 150 cal yr B.P) in a turbidite as a marker bed; synchronous triggering is shown when the number of upstream post-Mazama ash (MA) turbidites in multiple tributaries equals the number of post (MA) turbidites downstream below the tributary confluences. In Cascadia Basin, both the Juan de Fuca and other tributary channels and the Cascadia Channel below the confluence contain 13 post-MA turbidites (Fig. 1) (Adams, 1990; Nelson et al., 2000). This test is supported by turbidite correlations based on ^{14}C ages and correlative physical properties between sample sites that are separated by several hundred kilometers along the Cascadia margin (Figs. 1 and 3C) (Goldfinger et al., 2003a, 2003b; 2008). We have extended the correlation of turbidites below the T13 post MA turbidites so that a total of 18 Holocene turbidites can be correlated in northern Cascadia Basin. To help extend the correlation in time, the Holocene/Pleistocene boundary has been determined by the dominance of radiolaria in the Holocene versus the dominance of foraminifera sediment in the Pleistocene sediment and by a clear change in the sediment color (Gutierrez-Pastor et al., in press).

In the northern California margin, Noyo Channel has been studied in detail because its Noyo Canyon source is underlain by the San Andreas Fault and thus sedimentary processes are affected directly by earthquakes associated with the canyon (Fig. 2). The channel also has a good Holocene turbidite record recovered from five cores containing 2-25 turbidites that can be correlated along strike (Fig. 2) (Goldfinger et al., 2007). In the Noyo Channel, as in other turbidite channels of the northern California margin, correlations have been based mainly on ^{14}C ages, heavy mineralogy and stratigraphic correlation with physical property proxies. Examples are shown in figures 3B. and 3C for the northern California and Cascadia margins respectively (Goldfinger et al., 2003a; 2003b; 2007; 2008; Gutierrez-Pastor et al., in press).

The northern California margin also has a turbidite paleoseismic history. In general, along the northern California margin, turbidites exhibit a uni-pulse or multi-pulsed coarse silt or sand bases into the cm scale and a big muddy tail. Ages of turbidites offshore from this region have also been demonstrated to correlate well with the onshore paleoseismic record even though no good datum such as the Mazama Ash or color and sediment compositional change of Pleistocene to Holocene hemipelagic sediment has been found (Goldfinger et al., 2003a; 2003b; 2007, Gutierrez-Pastor et al., in press). The confluence test also has been applied to the northern California Margin and indicates an equal number of correlative turbidites above and below channel confluences. Individual turbidites below confluences contain multiple coarse grained-pulses with different heavy mineral compositions correlated to tributary canyon mineral provenances (Fig. 3B). For example, Fig.3B shows an interval of the 24 GC gravity core below the Gualala, Viscaïno and Noyo confluence that has two multi-pulsed turbidites with each pulse containing a different heavy mineral content that can be correlated to a specific tributary canyon (Goldfinger et al., 2007). The heavy mineral assemblages from individual canyon sources are stacked vertically in order of arrival at the core site. The absence of hemipelagic sediment within the individual turbidite shows that little or no time passed between depositions of each pulse. Further explanation is provided in the results section of this paper.

5. RESULTS: SEDIMENTOLOGIC CHARACTERIZATION OF TURBIDITES

5.1. Cascadia Margin.

In Cascadia Basin 13 Holocene turbidities overlying the first occurrence of Mazama ash have been well correlated based on AMS radiocarbon ages, physical properties and visual core observations (Nelson et al., 2000; Goldfinger et al 2003a; 2003b; 2008, Gutierrez -Pastor et al., in press). To characterize turbidites we have selected one correlative turbidite from three different turbidite channels: 1) the tributary Juan the Fuca Channel in a proximal location of northern Cascadia Basin, 2) the Willapa Channel, another proximal tributary channel to Cascadia Channel, and 3) the Cascadia Channel below a confluence of these two channels in a downstream distal site (Fig. 1). The samples consist of turbidite number 3 (T3) of Piston core (PC) 12 in Juan de Fuca Channel, T3 of 14PC in Willapa Channel and T3 of 25PC in Cascadia Channel (Fig. 4). Our goal is to see how the sedimentologic features in the same correlative turbidite vary from proximal to distal in a channel and downstream from a confluence of several tributary canyons or channels.

5.1.1. Turbidite 3 in Juan De Fuca Channel

Visual core observations suggest that T3 in Juan de Fuca Channel has a sand/silt thickness of 9 cm with two pulses shown by the magnetic log compared with the one fining-up pulse shown by the grain size and density log, a muddy tail of 5 cm and hemipelagic sediment below of 5 cm, as shown by the dark homogeneous color of the X-ray. An incomplete “Bouma set of sedimentary structures” (Tc or Td) with the typical fining upward sequence is observed (Tables 1A and 1B) (Bouma, 1962). No significant sedimentary structures are found. The X-ray radiograph shows a light intensity of the X-ray for the silt lamina that coincide with the highest value peak in the magnetic log signature for the base of the turbidite (Fig. 4).

Three grain size samples have been processed at 34.5 cm, 31.5 cm and 30 cm. Grain size distribution curves have been calculated for each sample representing the % and cumulative % of grain sizes in volume (Appendix 1A). The grain size is in a phi (ϕ) scale ($\phi = \log_2 \text{ mm}$) with the lower values corresponding to the coarser grain size of the sediments (1-4 ϕ = sand, 4-8 ϕ = silt and 8-10 ϕ = clay) (Table 1C). In table 1A the key percentiles (d50 and d90) of each curve and the % volume of sand, silt and clay are shown. D50 is the median grain size for a specific sample. D90 is the maximum grain size in the sample. The T3 appears as a single bed with d50 between medium and fine silt. The largest grain size transported by the turbidity current (d90) is very fine sand (Table 1A).

In the base of T3, silt lamina at 34.5 cm are represented by a curve mode going to the right toward coarser values and by the high content of silt (63%) and sand (21%) (Appendix 1A, Table 1A). Curves representing samples at 31.5 and 30 cm show broader mode distribution with a progressive decrease in the sand content and also with a progressive increase in the silt/clay content. The slightly increased silt content (66%) at 30 cm compared with 31.5 cm (64%) can be correlated with the peak in the magnetic log signature.

5.1.2. Turbidite 3 in Cascadia Channel

In Cascadia Channel T3 from core 25PC can be divided into two main intervals, the first one from ~109 cm to ~97 cm that is composed of three sandy/silty pulses at 109-108 cm, 105-104 cm and 101-97 cm, and the second interval from 97 cm to 52 cm that is composed of dark turbidite mud. The base of the bed is a sharp contact just above ~1 cm of light colored hemipelagic clay. The X-ray radiograph shows some parallel lamination for the deepest pulse, convolute lamination (ripples) for the middle pulse, and parallel

GRAIN SIZE ANALYSIS

	T3 Sample Depth	d50 (φ)	d90 (φ)	% Sand	% Silt	% Clay	Interpretation
Juan de Fuca 12 PC	34 cm	5.3	3.3	21	63	16	Bouma Tc or Tb, silty turbidite
	31.5 cm	6.3	3.2	15	64	21	Bouma Te, turbidite mud (tail)
	30 cm	6.5	3.9	10	66	24	turbidite mud, Te
Cascadia 25 PC	110 cm	7	4.5	6	65	29	hemipelagic with high detrital content
	108.5 cm	4.3	2.4	43	49	8	Bouma Tb, sandy/silty lamination, bi-modal turbidite mud
	106.5 cm	5.2	2.9	26	61	13	
	105 cm	4.3	2.3	38	56	6	sandy Tc, Ripples, subtle bi-modal turbidite mud
	102 cm	5.6	3.2	19	66	15	
	100 cm	4.9	2.4	19	66	15	Bouma Td, silty lamination, bi-modal Td, subtle lamination
Willapa 14PC	97.5 cm	6.4	3.7	11	67	22	
	93 cm	6.8	4.8	4	72	24	
	60 cm	3.6	2.2	54	35	11	Bouma Ta, sand with shell and forams, subtle bi-modal Tc? High silt content, bi-modal
	58 cm	5.9	2.7	29	54	17	
	55.5 cm	3.7	2.4	55	35	10	Tb? High sand content, bi-modal
	52 cm	5.9	2.8	30	52	18	Tc?, bi-modal
	49.5 cm	5.7	2.9	30	52	18	Tc, bi-modal
	42.5 cm	3.6	2.5	59	31	10	T2/5? sandy base (base of bed), Tb?
	41.5 cm	4.8	2.7	41	44	15	~ = sandy/silty content (middle), bimodal Tb, or Tc?
	39.5 cm	5.9	2.3	27	54	19	silty upper part of the bed, bi-modal, Td?
28.5 cm	3.6	2.8	66	29	5	T4 sand layer	
19 cm	4.8	2.8	38	47	15	T3? silt/sand layer, subtle bi-modal	

TABLE 1.B. d50 is the median, showing the most representative grain size in the sample

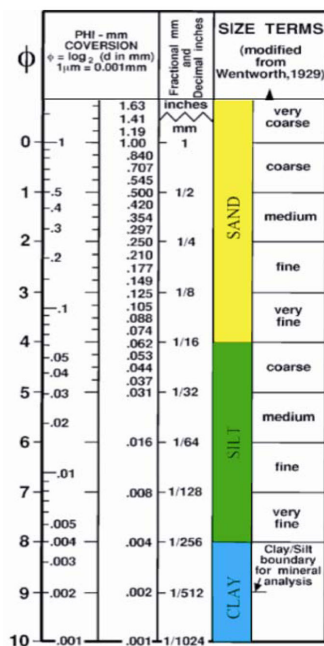
d90 is the coarsest grain size in the sample

T Turbidite

Samples	Turbidite	Tail	Hemipelagic	Base	Structures	Pulses	Sequences
Juan de Fuca 12 PC	9 cm	5 cm	5 cm	not identified	not identified	1	fining upward
Cascadia 25 PC	13 cm	45 cm	1 cm	sharp, erosive	lamination, ripples	3	truncated Bouma
Willapa 14PC at 60 cm	11 cm	7 cm	46 cm	erosive	not identified	2	no sequence
at 42 cm	3 cm	10 cm	not distinguished		lamination	1	fining upward
at 28.5 cm	0.5 cm?	?	not distinguished	?	?	1	no sequence
at 19 cm	0.5 cm?	?	not distinguished	?	?	1	no sequence

Table 1A. Grain size characteristics of Cascadia margin turbidites.

Table 1B. Thickness and features of individual turbidites at Cascadia margin sites.



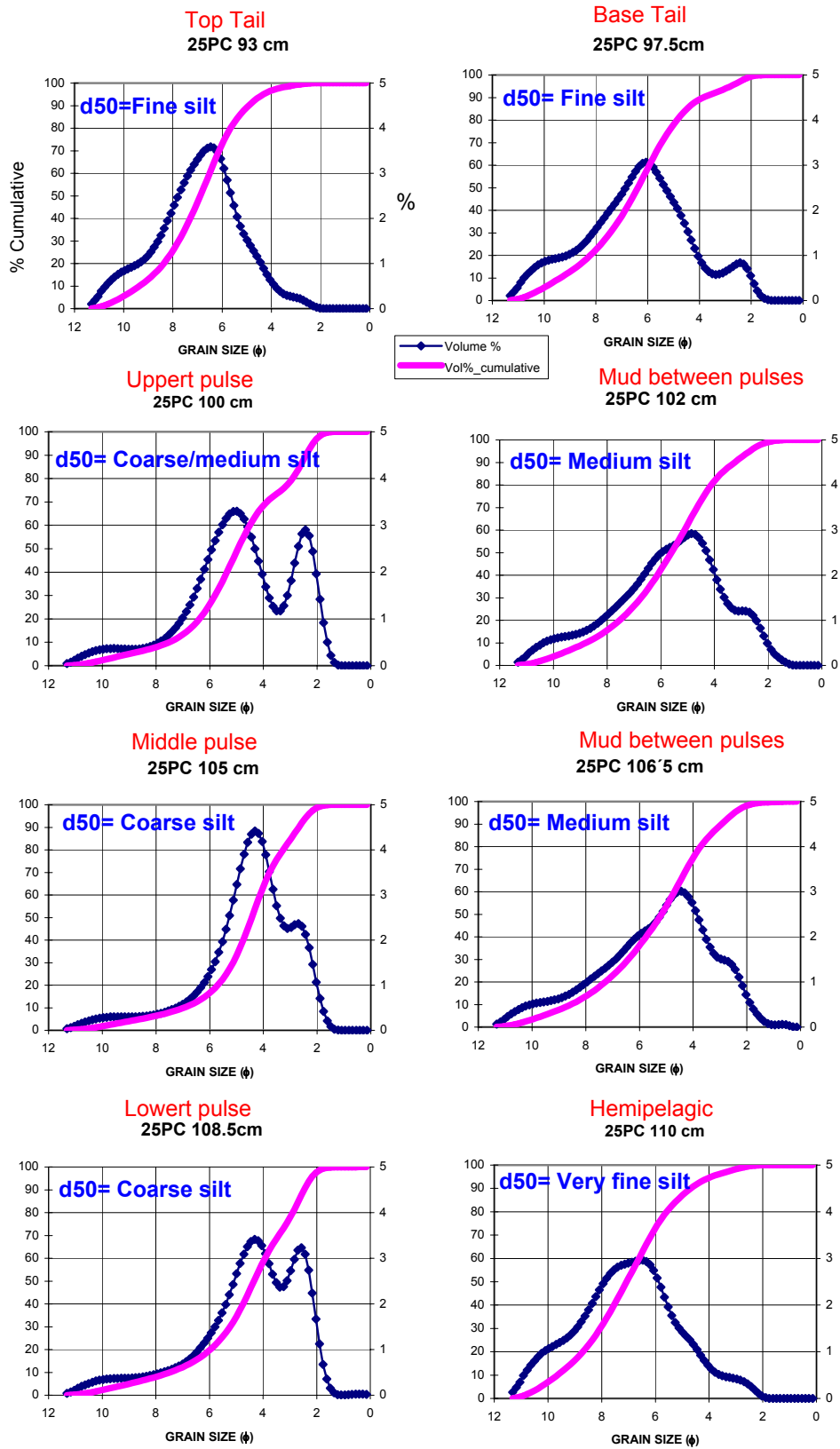


Figure 5. Grain size distribution curves of turbidites from 25PC of Cascadia Channel.

between hemipelagic sediment, turbidite bases and tails because in the base of slope location, hemipelagic sediment is coarser grained than on the abyssal basin floor. Originally, the base of T3 was interpreted to be

at 60 cm because the first prominent and tri-multi-pulse peak of density and magnetic signature agreed with T3 in 12 PC, 25 PC and 14 TC (Fig. 4). Recently, Goldfinger et al. (in press) have revised the interpretation of the turbidite with the base at 60 cm as T6, by correlating physical properties with other cores in Barkley Canyon, Juan de Fuca Channel and Willapa Channel. Because there is no ¹⁴C age below the turbidite at 60 cm in 14PC, the correlation question can not be resolved.

Although the turbidite at 60 cm may not be T3, the grain size analysis of 14PC provides a valid comparison of turbidite pulses with those of T3 in 12PC and 25PC. Looking at the 14PC core and the log signatures it is difficult to distinguish the upper turbidite termination, making it difficult to determine exact turbidite thickness. From 60 cm to 49 cm the sediment is composed of very fine sand rich in shell fragments and forams at the base with some mud intercalation. The density signature shows two peaks while the magnetic log shows two weaker peaks coinciding with this turbidite bed. The base of the turbidite is sharp and scoured. From 49 cm to 14 cm there is mud with some intercalation of 1-2 cm of very fine sand or silt layers at 18 cm, 29cm and 42 cm. The sediment appears mottled in the interval between sand beds. The magnetic signature is generally constant from ~ 50 cm to 0 cm, whereas the density signature shows peaks coinciding with the specific sand layers mentioned above.

In 14PC ten grain size samples have been processed at 60 cm (base of T3/T6?), 58 cm, 55.5 cm, 52 cm, 49.5 cm, 42.5 cm (base of T5?), 41.55 cm, 39.5 cm, 28.5 cm (base of T4?) and 19 cm (base of T3?) (Fig. 3, Table 1A, Appendix 1B). For the first 5 samples the sand content ranges from 29% to 55% and the silt content ranges from 35% to 52%. At 60 cm, the grain size distribution shows a predominant sandy mode that coincides with the sediment interval rich in shell fragments and forams. At 58 cm, 55.5 cm, 52 cm and 49.5 cm the grain size curves show a bi-modal distribution with silt content over 50 % at 58cm, 52cm and 49.5 cm and sand content over 50% at 55.5 cm. The clay content is less than 20% in all the samples (Table 1A, Appendix 1B.). At 60 cm and 55.5 cm the coarsest grain size pulses also coincide with the density log peaks.

The grain size distribution at 42.5 cm, 41.5 cm and 39.5 cm shows a progressive decrease of sand and a progressive increase of silt and clay, with the % of clay always less than 20% (Fig. 4, Table 1A). These three grain size curves are trending clearly to a bi-modal shape with a broader distribution from the deepest to the shallower samples (Appendix 1B). The sandiest sample at 42.5 cm coincides with the density log peak. At 28.5 (T4?) cm and 19 cm (T3?) the distribution curves also display sand modes that are coarser at 28.5 cm (66% sand) and finer at 19 cm (38% sand). Again the sand beds coincide with peaks of the density log signature (Fig. 4). The sample at 19 cm coincides with the Goldfinger et al. (in press) inferred T3 turbidite bed and the grain size of other sand beds at 42.5 cm and 28 cm suggest that the new correlation may be valid, however we need other evidence such as radiocarbon ages to prove that.

Summarizing, at Willapa canyon the turbidite with base at 60 cm (T3/T6?) has a thickness of 11 cm, a muddy tail of 7 cm and hemipelagic sediment below inferred from visual observations and physical properties. Compared with the turbidites at the other Juan de Fuca and Cascadia sites, the T3/T6 turbidite is the coarsest (66% fine sand /coarse silt) and it has the lowest content of clay (5%). Core 14 PC at the Willapa Channel is located in a proximal base of slope area where coarser sediment is expected in turbidites. Also, the presence of shells, forams and erosive base (features that correspond with a typical Ta Bouma sequence) confirm the criteria of proximality for this turbidite. Above the base, the turbidite has heterogeneous silt, sand and mud content without significant sedimentary structures

5.2. Northern California Margin

We have selected individual representative turbidites from two channel systems and their confluence, although many other turbidites have well described by lithology, physical properties, X-ray radiographs and grain size analyses along the northern California margin. As in Cascadia Basin, turbidites have been separated into a coarser grained base, a muddy turbidite tail and hemipelagic sediment below the overlying turbidite (Fig. 3). Detailed grain size analysis has been completed for key turbidites with visually recognizable multiple coarse grained sediment pulses. The goal has been to provide grain size evidence for pulses found in the magnetic and density logs and correlate these with different mineralogic sources shown for the pulses within an individual turbidite. Unlike Cascadia, in the northern California margin we have not followed a specific correlative turbidite because the correlations have yet to be finalized. Nevertheless, we can analyze sediment pulse features of individual turbidites and compare them with the Cascadia margin turbidites.

5.2.1. Noyo Channel turbidite in 49 PC

We have described turbidite T15 that has an age of ~ 3000 Cal. yr B.P (Fig. 6) (Goldfinger et al., 2007). Visually, the turbidite is made up of a 5 cm thick basal part (from 314 cm to 309 cm) of very fine sand with some mud intercalations that is capped by a 12 cm thick muddy tail. No sedimentary structures are evident. There is a 6 cm layer of hemipelagic clay just below the base of this turbidite. The density log signature shows the progressive pattern of decreasing density from the base of the turbidite through the mud turbidite (tail) (Fig. 6). The magnetic susceptibility curve shows some subtle pulses, but in this thin layer, there is not sufficient evidence to determine any possible pulses.

Three grain size samples from the basal sand /silt layer have been processed at 314 cm, 312 cm and 309 cm (Fig. 6, Appendix 2A, Table 2A and B). At 314 cm and 312 cm, the grain size diagrams show a sandy mode whereas at 309 cm the mode is siltier. D50 displays a gradual gradation up the turbidite from very fine sand to coarse silt and then medium silt, which coincides with the density log signature (Table 2A).

5.2.2. Gualala Channel turbidite in 13PC

At this site closely spaced bi-pulsed and uni-pulsed turbidites have been studied. The bi-pulsed turbidite has a sharp base at 157 cm and consists of two sandy/silty laminated pulses up to 152cm. From 152 cm to 150 cm, there is hemipelagic sediment with microfauna of foraminifera and radiolaria in the coarse fraction. The uni-pulsed turbidite consists of a silty pulse from 150 cm to 148 cm, and from 148 cm to 142 cm there is a homogeneous, bioturbated turbidite mud cap with fecal pellets. In both turbidites, typical Tb of the Bouma sequence are evident visually and in the X-ray radiograph, and the grain size pulses correlate with the density and magnetic log peaks (Tables 1A and 1B).

Three grain size samples have been processed in the multi-pulsed turbidite at 157.5 cm, 156 cm and 152 cm, one in the hemipelagic sediment at 150cm and two in the uni-pulsed turbidite at 148 cm and 144 cm (Fig. 6, Appendix 2B, Tables 2A and B). At 157.5 cm, the grain size curve is broad, the percent of silt and clay are high (61% and 31% respectively) and the median shows fine silt grain size. At 156 cm and 152 cm the grain size distribution is alike with sand content of 42% and 37% respectively but with slightly more silt and clay content at 152 cm (46%+16% at 152 cm versus 45%+13% at 156 cm). The coarser grain size is shown by the magnetic log signature with peaks at 156 cm and 152 cm respectively. At 150 cm the

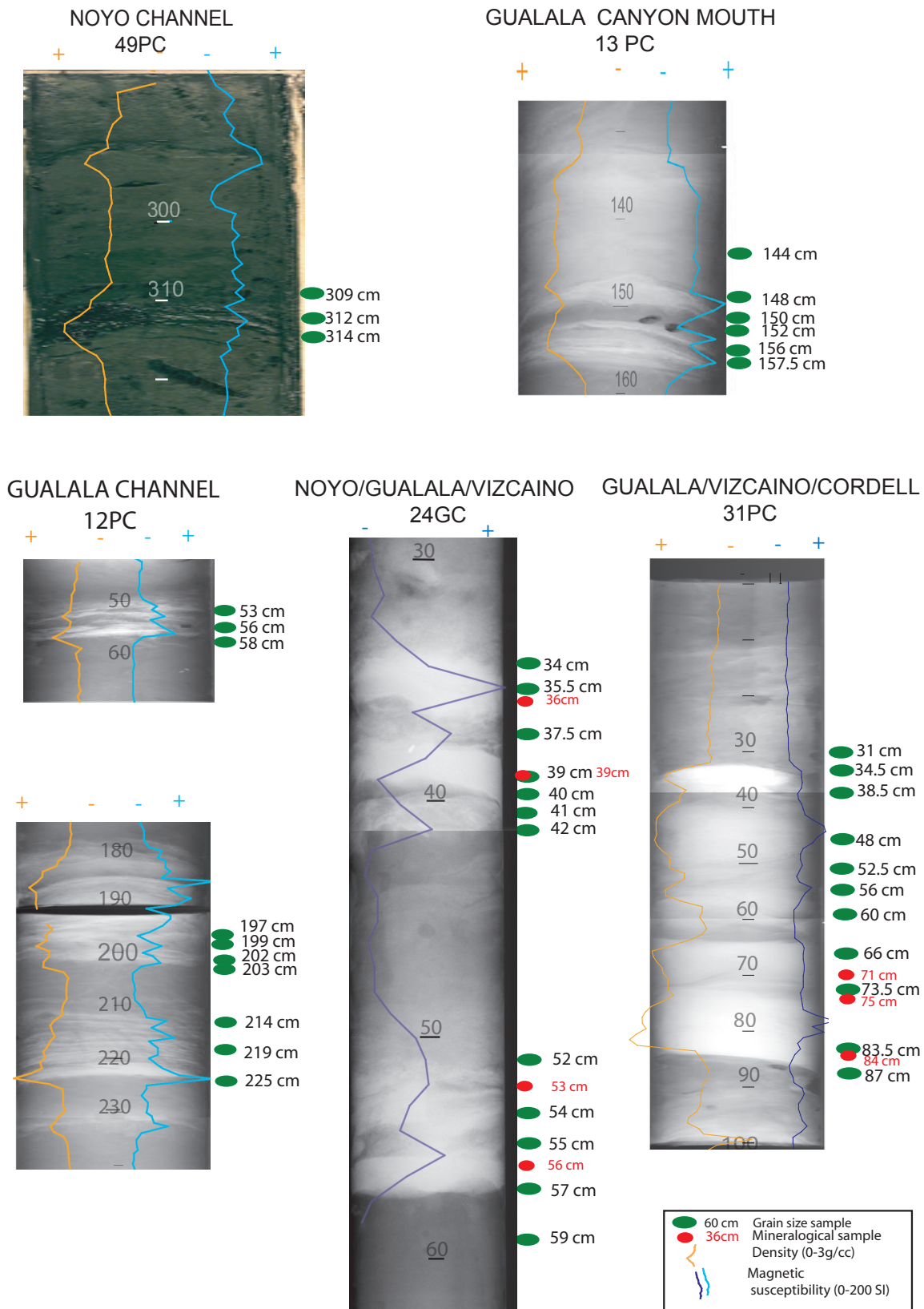


Figure 6. Northern California margin core sections from 49 PC at Noyo Canyon, 13 PC at Gualala Canyon Mouth, 12PC at Gualala Channel, 24GC below Noyo/Gulala/Viscaino confluence channel and 31PC below Viscaino/Cordell channel confluence. Core photo of 49PC, X-ray radiographs of the rest of cores and physical properties (density and magnetic signatures) are represented to show the sedimentological features of individual turbidites. Green ovals are the grain size sample locations and red dots mineralogical sample locations.

TABLE 2.A.

	Sample Depth	d ₅₀ (φ)	d ₉₀ (φ)	% Sand	% Silt	% Clay	Interpretation
Noyo 49 PC	314 cm	3.9	3.2	35	53	12	Tb ?
	312 cm	4.4	3.2	36	49	15	Tb ?
	309 cm	5.1	3.3	20	64	16	Tb or Tc?
Gualala 13PC	157.5 cm	7	4	8	61	31	Hemipelagic
	156 cm	4.3	3.1	42	45	13	Tb or Tc
	152 cm	4.7	3.2	37	46	17	Tb or Tc
	150 cm	7	4.3	6	62	32	Hemipelagic
	148 cm	3.3	3.3	33	55	12	Tb
	144 cm	5.7	2.4	28	53	19	mud, fecal pellets, bi-modal
	225 cm	3.9	3	57	36	7	Tb, less clay, less silt
	219 cm	4.4	3.1	40	46	14	Tb
	214c cm	5.3	3.2	25	58	17	Tb, more clay, more silt
	203 cm	3.8	3	56	33	18	Tb or Tc
Gualala 12 PC	202 cm	5.6	2.9	33	48	10	Bi-modal, Tc
	199 cm	3.9	3	55	35	19	Tb or Tc
	197 cm	4.9	3.1	37	45	11	Bi-modal, Tc
	58 cm	5.9	3.2	23	55	22	sandy /silty lense, high clay content
	56 cm	5.3	3.3	23	60	17	sandy /silty lense
	53 cm	4.4	3.7	33	59	8	sandy /silty lense, low clay content
	59 cm	7.6	4.4	7	52	41	mud with the lowest sand content
	57 cm	1.9	1.2	95	3	2	Ta
	55 cm	5.5	2.1	22	61	17	mud
	54 cm	5.7	1.2	91	8	1	Ta
Noyo/Gualala/Viscaino 24GC	52 cm	4.7	2.5	35	53	12	mud with the highest sand content
	42 cm	7.2	4.4	7	60	33	mud, hemipelagic
	41 cm	4	1.4	51	39	10	Tc or Tb, bi-modal
	40 cm	5.9	1.8	29	46	25	mud
	39 cm	1.9	1.2	96	3	1	Ta
	37.5 cm	5	1.6	32	53	14	mud? High sand content , between pulses
	35.5 cm	2.8	1.2	79	19	2	Tb
	34 cm	5.5	1.5	23	60	17	Tc, mud
	87 cm	7.2	4.4	7	60	33	silty mud
	83.5 cm	1.6	0.5	94	5	1	Ta, high sand %
Viscaino/Cordell 31 PC	73.5 cm	4.1	2.8	45	48	7	mud
	66 cm	4.4	3.5	29	67	4	silty bed
	60 cm	4.6	2.8	34	53	13	Tc?, more and coarser sand
	56 cm	4.9	4	10	85	5	Tc?
	52.5 cm	4.8	3.3	25	65	10	Tc?, more and coarser sand
	48 cm	5.1	4.1	7	87	6	silt, Td?
	38.5 cm	5.2	3.3	22	62	16	silty bed between pulse
	34.5 cm	4.8	3.6	20	73	7	silty bed
	31 cm	7.2	4.4	6	60	34	muf, tail

Table 2A. Grain size analysis of northern California margin turbidites.

TABLE 2.B.

Samples	Turbidite	Tail	Hemipelagic	Base	Structures	Pulses	Sequences
Noyo 49PC	5 cm	9 cm	6 cm	sharp	no identified	1	fining upward
Gualala 13PC							
at 157 cm	6 cm	not distinguished	10 cm?	sharp	lamination	1	fining upward
at 150 cm	2 cm	8 cm?	2 cm	sharp	lamination	1	
12PC							
at 59 cm	8 cm	51 cm?	12cm?		lenses	2 or 3	coarsing upward
at 203 cm	23 cm	40 cm	5 cm	erosional	lamination, ripples, lenses	4	amalgamation, pulses
at 225 cm	13 cm	3-4 cm	2-4cm	erosional	lamination	1	fining upward
24 GC							
at 42 cm	7 cm	22 cm	3 cm	sharp	no identified	3	pulses fining upward, overall coarsing upward
at 58 cm	7 cm	8.5 cm	4.5 cm	sharp	no identified	2	fining upward
31 PC							
at 85 cm	20 cm	?	5 cm?	erosional	lamination	2	fining upward
at 60 cm	28 cm	32 cm	5 cm?	erosional	lamination	3	fining upward

Table 2B. Thickness and features of individual turbidites at northern California margin sites.

broad mode of very fine silt indicates a hemipelagic mud bed similar to the sediment represented by the 157.5 cm sample (Fig. 6, Appendix 2B, Table 2A). In the uni-pulsed turbidite, at 148 cm, the narrow mode over the very fine sand shows a pulse that corresponds with the magnetic and density log peaks, plus the lighter color in the X-ray radiograph (Appendix 2B and Fig. 6). The sand content is slightly less than that at 156 cm and 152 cm. However, the median is coarser ($d_{50} = 3.3 \phi$) with very fine sand. The grain size distribution at 144 cm is broad and bi-modal (Appendix 2B). There is a high content of silt (53%) and sand (28%) but the visual observations suggest fecal pellets instead of sand mineral grains. The magnetic and log signatures display a typical mud pattern without peaks and bays, which supports the visual observation of fecal pellets instead of mineral sand.

5.2.3. Gualala Channel turbidites in 12 PC

Three turbidites are characterized in core 12PC at a location that is downstream from 13PC, as shown in Figs. 2 and 6 and Tables 2A and B.

- Deep turbidite (base at 225 cm):

The deepest turbidite analyzed in Gualala channel has a sharp erosional base at 225 cm. The turbidite consists of four progressively finer sand/silt pulses between 225 cm and 212 cm, with some disruption by burrows (Fig. 6). Gradually, a mottled burrowed mud continues in the upper part of the turbidite from 212 cm to 208 cm depth. The sediment is laminated as shown by the X-ray radiograph (Fig. 6). The coarsest sediment and the thickest lamina are at the base of the turbidite. This is shown by the core observations, a big peak in the magnetic and density signatures and a thicker lighter interval in the X-ray radiograph. Physical properties reveal a fining up sequence of pulses in the magnetic and density signatures. Below the base at 225 cm, there is 2-4 cm of hemipelagic clay.

In this turbidite, three grain size samples at 225 cm, 219 cm and 214 cm were taken on apparent grain size pulses (Fig. 6, Appendix 3, Tables 2A and B). Grain size distribution curves show that the turbidite pulses progressively decrease in sand content (from 50% to 25 %), sand size (from very fine sand to medium silt) and an increase of silt and clay content (> 50% of silt and 17% of clay) (Table 2A).

- Middle turbidite (base at 203 cm):

Below the turbidite base at 203 cm, there is 5 cm of hemipelagic clay, as shown by the weak physical properties log signatures and darker colored sediment in the X-ray radiograph. Visually, the second turbidite analyzed has an erosional sharp flat base at 203 cm and exhibits several distinct very fine sand pulses that end at ~ 185 cm depth; minor sand/silt lenses continue between 185 cm to 180 cm (Fig. 6). Looking at the core and X-ray radiograph, sands up to 185 cm appear laminated and locally exhibit cross-bedding structures. From 185 cm to 180 cm the internal structure is poorly developed. Physical properties display 4 sandy pulses that are difficult to distinguish visually in the X-ray radiograph (Fig. 6). Above 180 cm, the turbidite tail is represented by a mottled mud interval and also shown by the darker X-ray radiograph and reduced values in physical properties (Fig. 6).

Four grain-size analyses have been processed at 203 cm, 202 cm, 199 cm, and 197 cm. Grain size curves at 203 cm and 199 cm are very similar and show a sand content greater than 50% at both depths (Fig. 6, Appendix 3, Table 2A). For both samples, d_{50} is very fine sand (3.8 and 3.9 phi) and d_{90} is fine sand (3 phi), which shows that the coarsest grain size and the median size are similar. Grain size of 202 cm and 197 cm samples are alike and exhibit a silt and sand bi-modal shape, high clay content and representative d_{50} in the medium and coarse silt grain sizes respectively. In summary, grain size at 203 cm and 199 cm represent the first two turbidite coarse-grained pulses that coincide with the two peaks of the magnetic logs. The silty mud between pulses is shown at 202 cm and 197 cm. A third coarse-grained pulse begins at ~ 192 cm and continues until ~ 187 cm. The fourth pulse is shown by a pronounced but thin peak of the magnetic log signature at 185 cm. Summarizing, the middle turbidite with base at 203 is ~ 23 cm thick and has three coarsening up pulses at the bottom and a minor fining up pulse at the top.

- Shallow turbidite (base at 59 cm):

The shallow turbidite has an erosional sharp flat base at 59 cm, but has a gradational upper boundary. The turbidite is composed of progressively finer bioturbated sandy bi-/tri-pulses or lenses from 58 cm to 51 cm as shown by the density and magnetic log signatures and the X-ray radiograph. The basal sandy turbidite is overlain by a muddy mottled interval that continues to the core top. Hemipelagic sediment underlies the turbidite because a coarse fraction sample at 62 cm has a high content of radiolaria and scarce terrigenous material.

There are three grain size samples for this turbidite at 58 cm, 56 cm and 53 cm. At 58 cm the grain size curve shows a single narrow mode over the boundary of silt and sand grain sizes with the highest content of clay (22%) compared with the other samples (Appendix 3, Table 2A). This basal turbidite sand appears to have some underlying hemipelagic sediment mixed into it by bioturbation which explains the anomalous shape of the grain size histogram and the high clay and sand contents simultaneously. At 56 cm and 53 cm the mode is sandy for both samples; however, the content of sand is higher and the content of clay is lower at 53 cm and coincides with the highest peak of the physical properties. The clay content progressively decreases toward the upper part of the sandy and silty pulses at 56 cm and 53 cm. There is an apparent lack of correspondence between the physical properties and the grain size trends, shown by a progressive decrease in the magnetic and density values, which suggests a fining up sequence and contradicts the grain size pattern. The big peak in the magnetic and density log in the lower part of the turbidite at 58 cm may be related to a thicker bed, although the grain size is finer than the upper part of the turbidite (almost fine silt vs coarse silt).

5.2.4. Noyo/Gualala/Viscaino confluence turbidites in 24GC

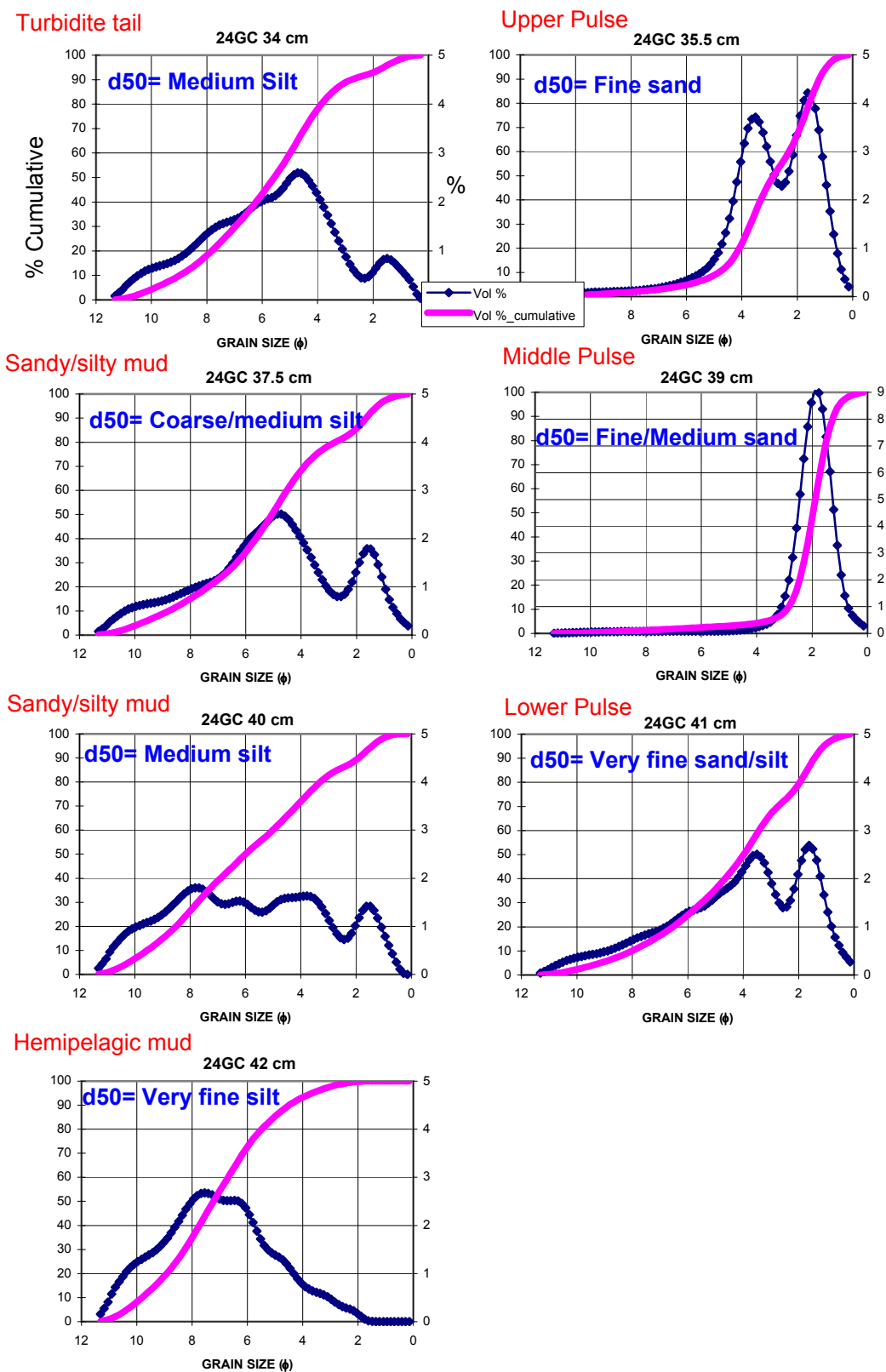


Figure 7. Grain size distribution curves of turbidites from 24GC below Noyo/Gualala/Viscaino Channel Confluence.

Two multi-pulsed turbidites with bases at 42 cm and 58 cm respectively and separated by ~ 3 cm of hemipelagic clay sediment have been characterized independently, however, their interpretation has been

treated jointly (Figs. 6 and 7, Appendix 4, Tables 2A and B).

- Deep turbidite (base at 58cm):

The lower turbidite has the base at 58 cm and it is composed of two pulses with 2 cm and 3.5 cm thickness respectively. These pulses are separated by a 2.5 cm muddier interval. Bases of the pulses are irregular and sharp, but the upper turbidite grades into an 8.5 cm mud turbidite tail. Below the turbidite pulses there is 4.5 cm of hemipelagic clay. The clay is well shown by the dark color of X-radiograph and low values of magnetic susceptibility logs, as well as the visual observations of the core.

Five grain size samples have been analyzed at 59 cm, 57 cm, 55 cm, 54 cm and 52 cm (Fig. 6, Tables 2A and B, Appendix 4). At 59 cm in the hemipelagic mud, below the lower pulse and turbidite base, the broad shape of the grain size mode is dominated by silt and clay (more than 90%). At 57 cm and 54 cm the grain size samples were taken from the sandy/ silty pulses. More than 90 % sand is found in both samples but more than one grain size is represented by the d50 and d90 at 54 cm (5.7 and 1.2 phi respectively). However, similar modes of d50 and d90 suggest just one representative grain size of medium sand at 57 cm (Table 2A). There is a good correspondence between the grain size of pulses and the high peaks of the magnetic and density signatures. A muddier interval at 55 cm has heterogeneous grain size as is shown by the broad mode and irregular grain size curve; a silt matrix predominates compared with the rest of the sizes. The mud tail at 52 cm contains a high sand content (35%). Mud intervals between pulses progressively decrease in sand and silt content from the deepest to the shallowest.

As stated in the Previous Results section, mineralogic analysis has been done for this turbidite at 53 and 56 cm. Tributary canyons have specific mineral content and feed downstream turbidite channels. These mineral assemblages of the tributary canyon sources can be correlated with the coarse grained pulses that form the turbidites. The homogeneous medium sand pulse at 57 cm contains Viscaïno Channel sand and the heterogenous grain size sand pulse at 54 cm contains Gualala mixed minerals (Figs. 3B and 6) (Goldfinger et al., 2007).

- Shallow turbidite (base at 42cm):

Visually, the upper turbidite with a base at 42 cm is composed of three sandy and silty fining upward coarser-grained pulses that have sharp bottoms with each pulse gradually becoming thicker from the base to the top of the turbidite (~1-3 cm thick). Each sequence is truncated by the overlying pulse. The last pulse has a gradational top above 35 cm. Pulses are separated by 0.5 cm to 1 cm of muddy sediment, but there is no hemipelagic sediment between the sandier pulses. From 35 cm to 13 cm there is a bioturbated turbidite mud interval. The sandy pulses are also shown also by the three peaks of the magnetic log signature and the light intervals of the X-radiograph. Internal structures are not observed in the pulses.

Seven grain size samples have been processed at 42 cm, 41 cm, 40 cm, 39 cm, 37.5 cm, 35.5 cm and 34 cm (Figs. 6 and 7, Tables 2A and B). The grain size analysis at 41 cm, 39 cm and 35.5 cm correspond with the sandy/silty pulses. At 41 cm and 35.5 cm the grain size distribution is clearly bi-modal in the silt to sand sizes with more than the 50% and 79 % sand respectively (Fig. 7, Table 2A). However, at 39 cm the grain size curve has a narrow mode with almost 100% medium sand content as shown in the table 2A. There is good correspondence of the coarser grain size with the peaks of the magnetic signatures.

At 42 cm, below the base of the lower pulse, the grain size curve shows typical muddy hemipelagic sediment composed of more than the 90 % silt and clay. Samples taken at 40 cm and 37.5 cm also correspond with the inter-pulse muddier interval. At 40 cm the grain size curve is very broad and represents a heterogeneous grain size distribution (d50 =5.9 phi and d90 = 1.8 phi), but there is a predominance of

mud (~ 70%) (Table 2A). At 37.5 cm the grain size is bi-modal with sand and silt grain sizes, but contains a majority of silt and clay (67%). At 34 cm the grain size curve is a typical muddy interval containing a little sand and corresponding to the turbidite tail.

Mineralogical analyses have been done for the sandy and silty pulses at 36 and 39 cm (Figs. 3A and 6) (Goldfinger et al., 2007). For the lower pulse at 41 cm, the bi-modal grain size curve is associated with the mineral provenance of the Arena/Gualala canyons. The ~ 100% medium sand pulse at 39 cm corresponds to the provenance of the Viscaino Channel. The upper pulse at 35 cm contains the Gualala mixed mineral provenance.

5.2.5. Gualala/Viscaino /Cordell confluence turbidite at 31PC

- Turbidites with bases at 85 cm and 60 cm:

There are two closely spaced turbidites selected from this site. The two turbidites start at 85 cm of depth and extend until the core top. There is a lower bi-pulsed turbidite of sand/silt from 85 cm to 65 cm, a muddy interval from 65 cm to 60 cm and a tri-pulsed turbidite of sand/silt from 60 cm to 32 cm. Above 32 cm, there is a bioturbated turbidite mud tail. The turbidites are laminated and the bases are sharp (Fig. 6, Tables 2A and B).

Eleven grain size samples at 87 cm, 83.5 cm, 73.5 cm, 66 cm, 60 cm, 56 cm, 52.5 cm, 48 cm, 38.5 cm, 34.5 cm, and 31 cm were taken for analyses (31PC) (Fig. 6, Tables 2A and B, Appendix 5). At 87 cm in the hemipelagic sediment below the turbidite, the wide mode of the grain size curve shows predominantly very fine silt ($d_{50} = 7.2 \text{ phi}$). At 83.5 cm, the grain size distribution has a mode of fine to medium sand, and the turbidite is almost 100 % sand (Table 2A). This sample coincides with the first pulse at the base of the deeper turbidite. At 73.5cm and 66 cm, the grain size distributions of the upper pulse of the deeper turbidite are very equal with modes of coarse silt ($d_{50} = 4.1$ and 4.4 phi respectively). At 73.5 cm the sediment is ~ half of silt/sand and sample at 66 cm shows an increase of the silt content with respect to the previous samples.

At 56 cm, the lower pulse of the shallower turbidite has a coarse silt mode (85%) (Table 2A, Appendix 5). At 52.5 cm, the lower part of the second pulse of the shallower turbidite exhibits a narrow mode with d_{50} of coarse silt and very fine sand (Appendix 5 and table 2A). The second pulse is also represented by a sample at 48 cm where the silt content is predominant (87%) with d_{50} of medium silt (Appendix 5, Table 2A). The third pulse of the upper turbidite is represented by the samples at 38.5 cm and 34.5 cm that are dominantly silt (> 50%). with more than 20% sand (Table 2A). The turbidite mud tail at 31 cm has higher silt /clay, lower sand contents and the curve mode has a broad shape.

Mineralogic analysis has been done on the coarser-grained turbidite pulses of 31PC. At 84 cm there is a bi-modal population of coarser grains with a Viscaino source (no heavy minerals), whereas the fine-grained fraction contains heavy/mafic minerals indicative of the Gualala source. This mineralogical sample coincides with the higher sand content and larger grain size. This pattern is similar to that shown in an analogous turbidite of the 24CG core (Figs. 3B and 6). At 75 and 71 cm, mineral samples show a Gualala provenance rich in heavy minerals that coincides with the base of the upper pulse of the deeper turbidite at 31PC. The same trend is also exhibited in the lower bi-pulsed analogous turbidite of the 24GC core (Figs. 3B and 6).

6. DISCUSSION

6.1. Features of turbidites in Cascadia Margin

The sedimentologic features of Holocene turbidites in the active tectonic continental margin of Cascadia support their seismic origin, and supplement additional correlative information from physical properties and radiocarbon ages. We can infer the seismic triggering of turbidites, and also we can compare the sedimentologic variations of the same turbidite from proximal to distal locations in channels. We can base this comparison on the well correlated turbidite T3 from the more proximal Juan de Fuca Channel and the distal Cascadia Channel site below the confluence of the proximal channel tributaries (Figs. 1 and 4, Tables 1A and B).

Turbidites triggered by the same earthquake vary depending on where they have been deposited. Turbidites deposited in a canyon head or proximal channel have different characteristics than the turbidites deposited below a channel confluence. For example, T3 in Cascadia Channel compared to T3 in Juan de Fuca Channel, has the main turbidite body and turbidite tail that are thicker, the turbidite is multi-pulsed with well-defined internal sedimentary structures, the grain size is coarser (up to fine sand) in some turbidite intervals and a wider range of silts sizes are found (Tables 1A and .B). These differences represent an evolution of the behavior of the turbidity current with the travel distance. In Cascadia Channel, the thinner coarse-grained base of the turbidite bed is expected, because the turbidity current would be weaker after traveling several hundred kilometers from the Juan de Fuca tributary channel (Fig. 1). In Cascadia Channel, however, the main turbidite body and tail are thicker than the same correlative turbidite found in the more proximal Juan de Fuca Channel. More turbidite pulses and a thicker turbidite are logical in Cascadia Channel because multiple tributary canyons and channels feed several sediment pulses and more sediment into the Cascadia Channel site below the confluences of the tributary channels.

A good example for the development of turbidite pulses is shown in turbidites deposited in the Trinidad Canyon turbidite system (Fig. 1) (Nelson et al., 2000; Goldfinger et al., in press). The atypical structural setting of the Trinidad Canyon has resulted in slope instability and erosion of a wide (50 km) amphitheater-shaped middle to upper canyon that has extensively gullied multiple canyon heads (Wolf and Hamer, 1999). The lower Trinidad Canyon below canyon confluences, however, funnels downstream into a narrow canyon of a few kilometers width that crosses an unusually steep lower continental slope and feeds into a plunge pool and downstream sediment wave field (Nelson et al., 2000). This morphology contrasts with the other Cascadia margin canyons which are narrow (10 - 20 km) and incised across the slope. The turbidites in the Trinidad system typically have two or rarely 3 distinct 1-3 cm thick, cleaner sand or coarse silt pulses that are separated by several centimeters of muddy silt. Nelson et al., (2000) interpreted that the widely-spaced multiple tributary canyon heads and apparent earthquake triggering contributed to these unusual multi-pulsed turbidites in a proximal location. Travel distances to a pool or wave depositional site from the different tributary canyon heads are different and triggering times vary as the earthquake waves travel 50 km along the subduction zone (Nelson et al., 2000; Goldfinger et al., in press). Thus, several turbidite pulses arrive at each depositional site caused by the combination of different travel distances and sequential earthquake triggering from each canyon head source.

The simpler canyon head setting of Juan de Fuca and Willapa Channels contrasts with that of the Trinidad system. The absence of many tributary canyon heads, and the simple morphology as a single

channel without confluences of tributary channels result in the turbidites that are generally uni-pulsed (Tables 1A and 1B). On the other hand, in Cascadia Channel far downstream from the confluences of Juan de Fuca, Willapa and other channels the T3 turbidite is multi-pulsed. The sediment comes from different tributary channels that have been shaken by the same great earthquake and arrives at the distal Cascadia Channel site at different times, depending on the distance from the source to the deposition site. The arrival of sediment pulses within a short time span explains the lack of hemipelagic sediment between coarse-grained pulses in the individual turbidite (Fig. 4). Also, the multiple tributary channel sources explain why the T3 turbidite in Cascadia Channel is thicker than in the more proximal Juan de Fuca and Willapa sites, because there are amalgamated pulses that increase the overall turbidite thickness.

The classic literature of turbidites explains the amalgamation of turbidite beds as the result of the erosion of a following turbidity current. Most of the turbidity currents are the result of surge-type generation, where the turbidite beds are characterized by a sequence of sedimentary structures that are identified by breaks in textural gradation (Lowe, 1982). Bedding-plane structures in turbidites can be attributed to the erosion caused by the head of the turbidity current, whereas the vertical sequence of sedimentary structures can be explained a rapid waning deposition from the head, the body and the tail of the current as it passes over a specific location with varying flow regimes (Middelton and Hampton, 1976). Sequential turbidity currents may erode to the previous turbidite deposits resulting in an amalgamated turbidite with one or several beds truncated by the erosion of different turbidity currents that follow years to hundred of years later. Synchronous multiple turbidity currents from different tributary canyons that are triggered by an earthquake travel through the confluences of the same channel and arrive at different times in the same site. These turbidity currents may erode the previous sediment pulse or stacks as pulses and also generate amalgamated turbidite beds.

Although Cascadia Channel has no mineralogical analysis for T3, there is another important evidence of multiple upstream sources for the sediment. We find anomalous coarser sediment grain sizes downstream in Cascadia Channel compared with the typical grain size found upstream in Juan de Fuca Channel, one of its tributaries (Table 1A). These coarser grain sizes in Cascadia Channel come from the more proximal Willapa Canyon and Channel, where the sediment is coarser grained and the turbidites are thicker compared to Juan de Fuca Channel. Willapa Channel is the southernmost and closest tributary to Cascadia Channel. During the Holocene, the Washington canyon heads largely receive sediment from the Columbia River rather than their Pleistocene river sources in Washington (Sternberg, 1986). The coarsest Columbia sediment is deposited on the Washington shelf closest to Willapa Canyon head (Wolf et al., 1999, Sternberg, 1986), which explains the greatest input of coarse sediment into the Willapa Canyon/Channel. The Willapa canyon head and base of slope are closer to the 25PC Cascadia Channel site than is Juan de Fuca Channel. The base of slope crossing of the Juan de Fuca Channel is about 200 km northward from the base of slope crossing of Willapa Channel (Fig. 1). The coarse sediment of the Juan de Fuca Channel travels a further distance, losing more of its coarsest load, and needs more time to reach the 25PC site than the coarser sediment of the Willapa Channel. For this reason, the coarse sediment from Willapa Channel creates the coarsest basal pulse of turbidites in Cascadia Channel (Table 1A).

6.2. Features of turbidites in the Northern California Margin

The northern California margin turbidites also are interpreted to be triggered by earthquakes based mainly on correlations of physical properties signatures and radiocarbon ages. Goldfinger et al. (2007)

affirm that the physical properties are the fingerprints of each turbidite and thus the same turbidite can be correlated in other channel systems separated by hundred kilometers along the margin. Similar to Cascadia Basin turbidites, the physical property characteristics result from the earthquake shaking signatures and the morphology of the turbidite canyons and downstream confluences (Figs. 3 and 4). The sedimentologic characteristics and grain size patterns also are characteristic of turbidites that are triggered by earthquakes.

The simple canyon morphology and proximal channel location of 49PC in Noyo Channel result in a gradually fining upward uni-pulsed turbidite (Figs. 2 and 6). In contrast, the turbidites of Gualala Canyon mouth exhibit different characteristics because of proximity to the sediment source and the several canyon tributaries that join at the base of slope to form the Gualala Channel (Fig. 2). As a result of the proximal setting, one turbidite is bi-pulsed with little turbidite tail, another turbidite is single pulsed with an extensive tail containing fecal pellets, and the hemipelagic sediment between turbidites contains a high quantity of terrigenous material (Table 2A).

Compared with the 13PC turbidites at the canyon mouth, the 12PC turbidites 20 km downstream in the main Gualala Channel are multi-pulsed, thicker, more bioturbated and exhibit pulses that fine-upward or coarsen upward (Fig. 6, Table 2A). The variable characteristics of the turbidite pulses may be caused by the close proximity of the multiple canyon heads, the different times of arrival at the site and variable slope stability in the canyon head sources. At 12 PC in the main channel, we would expect thinner turbidites than in 13 PC since it is a more distal location and for this reason the turbidity current would arrive later and weaker. Our observations show the opposite. The thicker multi-pulsed turbidite in 12PC may be the result of a bigger earthquake compared to the turbidite at 13PC, if the beds are not correlative. If this is correct, turbidites can be an alternative tool to measure the strength of the earthquakes by comparing their sedimentologic features from proximal to distal sites in the same turbidite channel-system. However, based on physical properties, Goldfinger et al. (2007) correlate the turbidite with base at 157 cm of 13PC with the turbidite with base at 203 cm of 12PC. If this correlation is correct the thinner and less multi-pulsed turbidites in the canyon mouth may result from sediment bypassing which is common in canyon mouth settings because of erosive turbidity currents that result in of cut and fill processes (Goldfinger et al., in press).

Downstream from the confluence between Gualala, Noyo and Viscaïno channels, the grain-size analyses of turbidites at 24GC, again confirm physical properties data that these are individual turbidites with multiple fining upward sequences. The lack of hemipelagic sediment intervals between pulses indicates that the pulses were deposited during a short interval of time (Figs. 2, 3B and 6) Only the last coarse-grained pulse has a tail, indicating final waning of a turbidity current. We interpret that these pulses are triggered by a single earthquake event because synchronous triggering in multiple tributary canyons results in the arrival of several coarse-grained pulses. Each pulse has a distinct mineralogy from different tributary canyons and channels. For example, Gualala and Viscaïno sands are recorded in separate pulses of individual turbidites, with the Viscaïno pulses arriving first. The Viscaïno sands are coarser and more mature (without mafic minerals) that have been weathered, eroded, and transported by littoral drift northward along the coastline (Fig. 4B). The Viscaïno canyon head intersects the littoral drift along the shoreline and collects the coarser sand that later feeds the turbidites. Viscaïno turbidity currents with coarser sand, and possibly greater volume because of the active littoral drift source, apparently have a greater velocity. Viscaïno currents arrive first to deposit the lower/middle pulses of turbidites below the Noyo/Gualala/Viscaïno confluence, even though the Gualala sands travel a shorter distance to this site (Figs. 4B and 6, Table 2A).

Downstream from 24GC, the turbidites at the 31PC site have the same origin as the individual turbidites

at 24GC because they contain the same type of multi-pulsed turbidites, fining upward sequences, no hemipelagic sediment between pulses, and the pulses result from different canyon head mineral sources (Figs. 2 and 4B, Table 2B). These sedimentologic trends appear to be typical below channel confluences. The provenance input of 31PC is less distinct than 24GC, suggesting further mixing mineralogy downstream (Fig. 4B). Core 31PC, which is actually below a total of four confluences, has an input from a total of six channels, while core 24GC samples three channels. The good correlation between these cores suggests that input mixing at each confluence has little effect on the stratigraphy of the turbidites, even though the number of tributary channels increases at each confluence (Goldfinger et al., 2008). We infer that synchronous triggering in multiple canyon heads is the best explanation for the turbidite characteristics that are observed. Non-synchronous triggering should produce an additive turbidite record that increases in complexity below each confluence. The mixing and stacking of the mineral provenance components further suggests synchronous arrival below the channel confluences. Our results help substantiate the earthquake origin for turbidites that has been postulated by Goldfinger et al. (2007; 2008). A similar use of mineralogic provenance to fingerprint source channels and test for earthquake origin has been used in the Sea of Japan by Shiki et al. (2000).

6.3. Comparison between features of turbidites at Cascadia and northern California margins and implications for other active and passive margins

Although Cascadia and northern California margins have different tectonic settings, both active margins contain comparable turbidites because they are triggered by great earthquakes. Both the T3 turbidite in 12PC of Juan de Fuca Channel in Cascadia and the 49PC turbidite of Noyo Channel on the California margin are located in proximal channels. Turbidite examples in both channels are uni-pulsed, exhibit a single fining upward sequence and do not contain well-developed internal sedimentary structures (Figs. 4 and 6, Tables 1B and 2B). Slight differences between these proximal turbidites appear to result from muddier turbidity currents in the Noyo Channel that deposits a thicker tail or from the more energetic earthquakes that affect the Juan de Fuca site and deposit a thicker turbidite base. Turbidites in proximal channel of Cascadia and northern California margins contain both uni-pulsed and bi-pulsed turbidites

Although we have just shown that some proximal channel turbidites are uni-pulsed, others are multi-pulsed, (Goldfinger et al., 2003a, 2003b; Goldfinger et al., 2007; 2008). For example, in Figure 3 turbidites T8, T9 and T11 of 12PC from the Cascadia margin exhibit two to three pulses whereas the T10 again is uni-pulsed. The presence of both uni-pulse and multi-pulsed turbidites, in proximal channels above confluences, provides important information about the origin of pulses. Multi-pulsed turbidites definitely result below confluences; however there are multi-pulsed proximal turbidites that may result from the shaking signature of an unusually strong earthquake, aftershocks of the same earthquake, or the deposits of tributary canyons that join before the proximal channel sites (Fig. 1). For example, above the confluence, turbidites of 12 PC in the Gualala Channel are multi-pulsed probably because of the proximity of the multiple canyon heads and the variable times of arrival at the proximal sites.

Cascadia margin provides the clearest explanation for uni and multi-pulsed turbidites. Turbidites T3 and T10 of Juan de Fuca Channel and T1/T2? to T2/5? of Willapa Channel are uni-pulsed but correlate downstream below confluences with multi-pulsed turbidites in Cascadia Channel because there is a synchronous triggering in multiple canyon sources and addition of pulses downstream from confluences (Figs. 3 and 4, Table 1A and B). Turbidites T8, T9, and T 11 in Juan de Fuca Channel and T6 in Willapa

Channel are multi-pulsed and suggest that the earthquake and/or aftershock signatures cause multiple pulses. Generally, in Cascadia margin T1 to T5 and T10 are thinner turbidites and thus proximal turbidites from smaller earthquakes may not develop multiple pulses. In contrast, for the strongest earthquakes, proximal channels above confluences may show earthquake signatures and be multi-pulsed

Below confluences, the turbidite from 25 PC in Cascadia Channel can be compared with turbidites of 24GC and 31PC below the Viscaïno, Noyo and Gualala confluences. At all of these locations, multi-pulsed turbidites are encountered that exhibit erosive bases, lamination or ripples in some pulses and with several fining upward grain size sequences. The 24GC and 31PC pulses compared to 25PC pulses are sandier and coarser, thicker from the base to the top of the turbidite and the internal structures are less distinguishable. However at the three sites all turbidites are thick with an extensive turbidite tail (Tables 1A and 2A).

Although we do not have mineralogical analysis for turbidite pulses in Cascadia Channel below the confluence of tributary channels, we can show coarser pulses derived from the Willapa Channel tributary source and we can demonstrate considerable evidence to indicate synchronous triggering (Figs. 1 and 4) (Tables 1A and 2A). There are the 13 post MA turbidites above and below the Cascadia Channel confluence (Adams, 1990; Nelson et al., 2000; Goldfinger et al., 2003a; 2003b; 2008). We find that each of the 13 correlative turbidites have the same high-resolution AMS radiocarbon ages even in different locations of Cascadia Channel and its tributary channels separated by hundreds of kilometers (Fig. 1) (Goldfinger et al., 2003a; 2003b; 2008; in press). In addition, we can verify ages of the 13 correlative turbidites by the analysis of hemipelagic sediment and sedimentation rates (Gutiérrez et al., in press), and by the correlation of physical property signatures for each correlative turbidite (Fig. 4) (Goldfinger et al., 2003a, 2003b; 2008).

Nakajima and Kanai (2000) as well as Shiki et al. (2000) studied seismo-turbidites from the Japan Sea plus Lake Biwa, and Gorsline et al., (2000) analyzed turbidites from the Santa Monica and Alfonso basins, California. Nakajima and Kanai (2000) observed that turbidites triggered by earthquakes exhibit different characteristics than those described by Bouma (1962) and attributed to non-seismic mechanisms. In active tectonic margins with strong earthquakes, Nakajima, Shiki and Gorsline found that turbidites had wide areal extent, presented multi-pulsed beds, irregular sedimentary structures, grain size breaks/fluctuations, abrupt changes in composition within the bed, variable composition among beds and greater depositional volume than turbidites triggered by other mechanisms. Our studies confirm these observations in seismo-turbidites that have detailed age and physical properties correlations along the margin and throughout channels. In addition, we can show proximal to distal variations in seismo-turbidites and can explain the cause of multiple pulses with different mineralogies.

In comparison to active tectonic margins, turbidites in passive margins are more likely to be generated during low stands of sea level and by non-seismic mechanisms such as, storms, floods or sediment failures resulting from overloaded and underconsolidated slope sediment (Twichell et al., 2000; Tripsanas et al., 2004; 2006). The typical muddy and unstable slopes of deltaic margins off large rivers result in turbidite characteristics and systems that may be different from those in active margins. Turbidites appear to have simple fining upward grain size rather than be mainly multi-pulsed such as they are off the active tectonic margins of western North America. In Mississippi Fan and Bryant Canyon in the northern Gulf of Mexico, simple fining upward turbidites are most common (Nelson et al., 1992, in press; Twichell et al., 2000). In Bryant Canyon mini-basins, Tripsanas et al. (2006) found muddy turbidites in the overbank deposits with the complete mud turbidite sequence of Stow and Shanmugam (1980). Although there are suggestions of some general differences in sedimentologic characteristics that distinguish turbidities triggered by

earthquakes compared to those triggered more commonly by other mechanisms in passive margin settings, additional studies are necessary to verify these preliminary suggestions.

7. CONCLUSIONS

Our research leads to the following conclusions:

1. Turbidites along the proximal Juan de Fuca and Willapa channels of Cascadia margin exhibit uni-pulsed (simple fining upward grain size gradation) and multi-pulsed (multiple coarse-grained pulses within an individual turbidite).

2. The absence of many tributary canyon heads and the simple morphology as a single channel without confluences of tributary channels result in the turbidites that are generally uni-pulsed in proximal basin-floor channels.

3. In Cascadia Basin, the same correlative turbidite has different characteristics depending on its proximal to distal location in the turbidite system, because multiple turbidite pulses, especially the coarser grained from Willapa, and sediment thickness are added downstream below the confluence of the tributary Juan de Fuca and Willapa channels that have had synchronous earthquake triggering in their tributary canyons.

4. Similar to Cascadia margin, synchronous earthquake triggering of turbidites along the active tectonic margin of northern California results in uni-pulsed or multi-pulsed turbidites in proximal channels but with a greater trend to be multi-pulsed because there are multiple tributary canyons feeding base-of-slope proximal channels.

5. Because of proximity and greater number of sediment sources, compared to Cascadia, below the confluence of the Noyo, Gualala and Viscaïno Channels seismo-turbidites are sandier, thicker, and display random internal structures in the pulses, but also, like Cascadia, are multi-pulsed without hemipelagic sediment intervals between turbidite pulses,

6. Below tributary channel confluences, synchronous earthquake triggering of California margin turbidites is shown by the different mineralogy of each turbidite pulse that can be correlated with the different mineral source for each tributary canyon.

7. The grain size in each turbidite pulse also corroborates the provenance of sediment from several confluences; for example the pulse with Viscaïno sediment is homogeneous medium sand and the pulse with Gualala sediment is heterogeneous medium silt to medium sand.

8. Along active tectonic margins, seismo turbidites are multi-pulsed for two reasons: confluences of tributary canyons and channels, and earthquake magnitude. In proximal locations, weak earthquakes appear to result in uni-pulsed turbidites whereas strong earthquakes or the morphology of proximal channels with several tributaries cause multi-pulsed turbidites.

9. The active tectonic margins of Cascadia and northern California show that synchronous earthquake triggering in tributary canyons is another explanation for the amalgamation of turbidites below canyon and channel confluences.

10. Seismo-turbidites triggered in active tectonic margins are characterized by multi-pulsed turbidites whereas preliminary evidence suggests that turbidites from passive margins typically are characterized by simple fining upward turbidites; considerable future research is needed to verify these preliminary differences in active and passive margin turbidite characteristics and also to separate 1) which features of multi-pulsed seismo-turbidites relate to earthquake shaking signatures and 2) which

result from synchronous triggering of turbidites in tributary canyons and resultant multiple sediment inputs to an individual turbidite in a downstream channel.

ACKNOWLEDGEMENTS

We are specially grateful the crews of the Scripps Institute of Oceanography ships R.V. Melville and R.V. Roger Revelle and the members of the 1999 and 2002 Scientific Parties: Mike Winkler, Pete Kalk, Antonio Camarero, Clara Morri, Gita Dunhill, Luis Ramos, Alex Raab, Nick Pias Jr., Mark Pourmanoutscheri, David Van Rooij, Lawrence Amy, Churn-Chi “Charles” Liu, Chris Moser, Devin Etheridge, Heidi Stenner, Chris Popham, Claire McKee, Duncan MacMillan, Chris Crosby, Susanne Schmid, Eulalia Gracia, Suzanne Lovelady, Chris Romsos, Jason Chaytor, Vincent Rinterknecht, Rondi Robison, David Casas, Francois Charlet, Britta Hinrichsen, Jeremiah Oxford, Miquel Marin, Marta Mas, Sergio Montes, Raquel Villalonga, Alexis Vizcaino, Santiago Jimenez, Mayte Pedrosa, Silvia Perez, Jorge Perez, Andreu Turra, David Lamas, Himar Falcon, and Andres Barranco. Our sincere gratefulness to the Active Tectonics Group at Oregon State and James H. Power from the U. S. Environmental Protection Agency at Newport, Oregon, to provide the use of the Laser Diffraction Particle Size Analyzer for grain size analysis. We gratefully acknowledge funding by the US National Science Foundation (Awards: 0107093 and 0001074) and U.S. Geological Survey for this research (Awards: GRANT00017981, GRANT00018360, 04HQGR0063, 03HQGR0008, 03HQGR0006, 02HQGR0034, 02HQGR0043) and the Ministerio de Educación y Ciencia (Award CGL2006-27096-E/BTE) and Consejo Superior de Investigaciones Científicas (CSIC)-Spain (Award: PI 2006 3 01 021).

REFERENCES

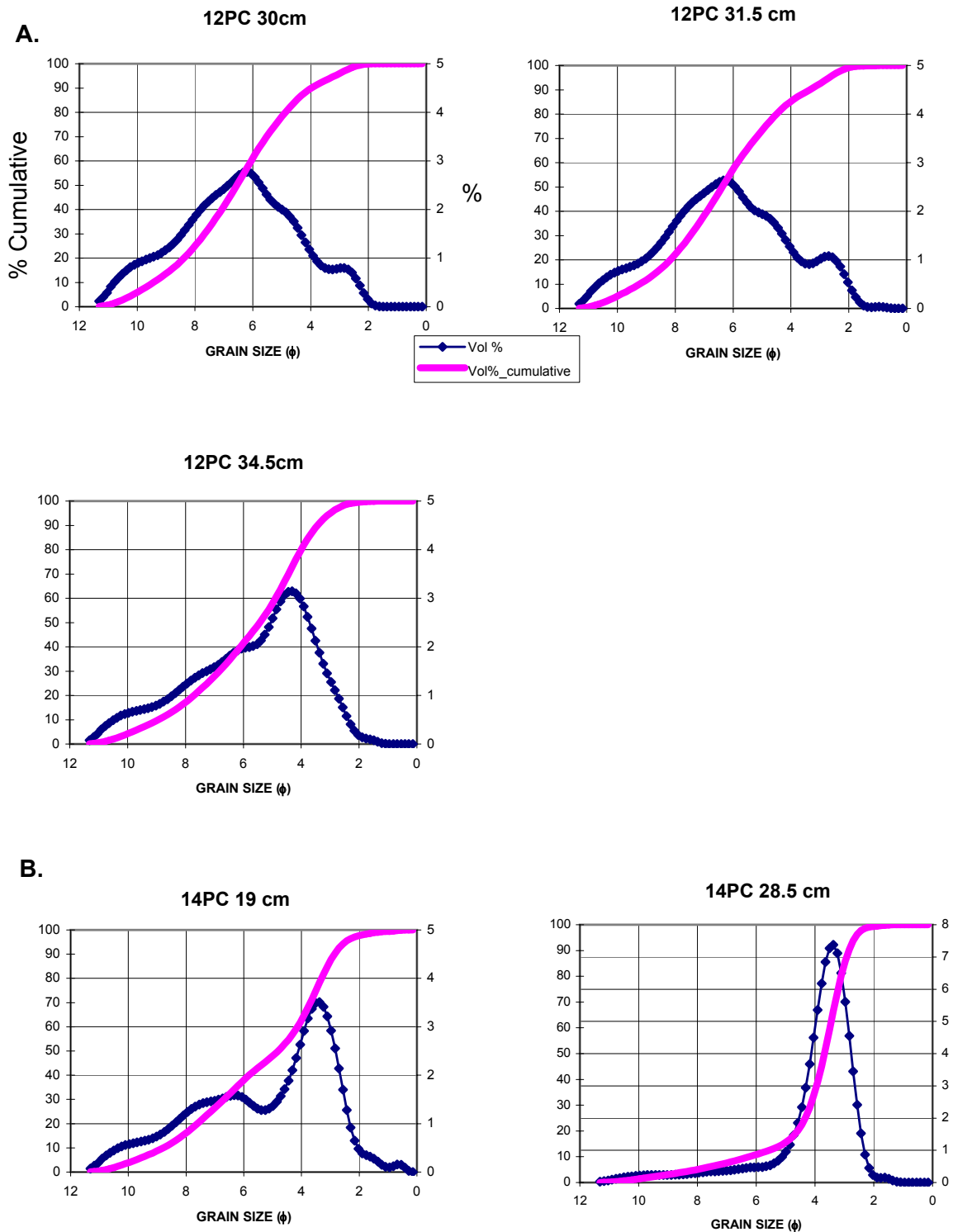
- Adams, J., 1990, Paleoseismicity of the Cascadia Subduction Zone: evidence from turbidites off the Oregon-Washington margin: *Tectonics*, v. 9, p 569-583.
- Atwater, B.F., 1987, Evidence for great Holocene earthquakes along the outer coast of Washington State: *Science*, v. 236, p. 942-944.
- Atwater, B.F., and Hemphill-Haley, E., 1997, Recurrence intervals for great earthquakes of the past 3500 years at northeastern Willapa Bay, Washington: U.S. Geological Survey Professional Paper, 1576, 108 p.
- Blott, S.J., and Pye, K., 2006, Particle size distribution analysis of sand-sized particles by laser diffraction: an experimental investigation of instrument sensitivity and the effects of particle shape: *Sedimentology*, v. 53, p. 671-685.
- Bouma, A. H., 1962, *Sedimentology of some Flysch Deposits*, Elsevier, Amsterdam, 168 p.
- d’Alessio, M. A., I. A. Johansen, R. Bürgmann, D. A. Schmidt, and M. H. Murray 2005, Slicing up the San Francisco Bay Area: block kinematics and fault slip rates from GPS-derived surface velocities, *J. Geophys. Res.* 110, B06403, doi: 10.1029/2004JB003496
- Duncan, J.R., Fowler, G.A., and Kulm, L.D., 1970, Planktonic Foraminiferan-Radiolarian ratios and Holocene-Late Pleistocene deep-sea stratigraphy off Oregon: *Geological Society of America Bulletin*, v. 81, p. 561-566.

- Goldfinger, C., Morey, A., Erhardt, M., Nelson, C.H., Gutiérrez-Pastor, J., Enkin, R., and Dallimore, A. 2006, Cascadia Great Earthquake Recurrence: Rupture Lengths, Correlations and Constrained OxCal Analysis of Event Ages, proceedings of the USGS Tsunami Sources Workshop, Diggles, J., Geist, E., and Lee, H., eds. CD-ROM, April 21 and 22, 2006.
- Goldfinger, C., Morey, A., Nelson, C.H., Gutierrez-Pastor, J., Jonson, J.E., Karabanov, E., Chaytor, J., and the Shipboard Scientific Party, 2007, Rupture Lengths and Temporal History of Significant Earthquakes on the Offshore and North coast Segments of the Northern San Andreas, *Earth and Planetary Science Letters*, v. 254, p. 9–27, doi:10.1016/j.epsl.2006.11.01.
- Goldfinger, C., Grijalva, K., Bürgmann, R., Morey, A. E., Johnson, J. E., Nelson, C. H., Gutiérrez-Pastor, J., Ericsson, A., Karabanov, E., Chaytor, J. D., Patton, J., and Gràcia, E., 2008, Late Holocene Rupture of the Northern San Andreas Fault and Possible Stress Linkage to the Cascadia Subduction Zone, *Earth Bulletin of the Seismological Society of America*, Vol. 98, No. 2, p. 861–889, doi: 10.1785/0120060411
- Goldfinger, C., Nelson, C.H., and Johnson, J., 2003a, Holocene Earthquake Records From the Cascadia Subduction Zone and Northern San Andreas Fault Based on Precise Dating of Offshore Turbidites, *Annual Reviews of Geophysics*: v. 31, p. 555-577.
- Goldfinger, C., Nelson, C.H., and Johnson, J.E., 2003b, Deep-Water Turbidites as Holocene Earthquake Proxies: The Cascadia Subduction Zone and Northern San Andreas Fault Systems: *Annali Geofisica*: v. 46, p. 1169-1194.
- Goldfinger, C., Nelson, C. H., Johnson, J. E., Morey, A. E., Gutiérrez-Pastor, J., Karabanov, E., Eriksson, A., Patton, J. Chaytor, J. D., Patton, J., Dallimore A., Gràcia, E., and the Shipboard Scientific Party, in press, Turbidite Event History: Methods and Implications for Holocene Paleoseismicity of the Cascadia Subduction Zone, *USGS Professional Paper*.
- Gutierrez-Pastor J., Nelson, C.H., Goldfinger, C., Johnson, J. E., Escutia, C., Eriksson, A., Morey, A. E., and the Shipboard Scientific Party, in press, Earthquake Control of Holocene Turbidite Frequency confirmed by Hemipelagic Sedimentation Chronology on the Cascadia and Northern California Active Continental Margins: in B. Kneller, W. McCaffrey and O. J. Martinsen eds., *External Controls on Deepwater Depositional System*, v. 92, *SEPM Special publication*.
- Gorsline, D.S., De Diego, T., and Nava-Sanchez, E.H., 2000, Seismically triggered turbidites in small margin basins: Alfonso Basin, Western Gulf of California and Santa Monica Basin, California Borderland: *Sedimentary Geology*, v. 135, p. 21-35.
- Griggs, G.B., 1969, Cascadia Channel: The anatomy of a deep sea channel: Unpublished Ph.D. Dissertation, Oregon State University, Corvallis, Oregon, 183 p.
- Kelsey, H. M., Witter, R. C., and Hemphill-Haley, E., 2002, Plate-boundary earthquakes and tsunamis of the past 5500 yr, Sixes River estuary, southern Oregon: *Geological Society of America Bulletin*, v. 114, no. 3, p. 298-314.
- Kelson, K., Strieg, A., Koehler, R., and Kang, K., 2006, Timing of Late Holocene Paleoeearthquakes on the Northern San Andreas Fault at the Fort Ross Orchard Site, Sonoma County, California: *Bulletin of the Seismological Society of America*: v.96, no.3, p. 1012-1028. Knudsen, K.L., Witter, R.C., Garrison-

- Laney, C.E., Baldwin, J.N., and Carver, G.A., 2002, Past Earthquake-Induced Rapid Subsidence along the Northern San Andreas Fault: A New Paleoseismological Method for Investigating Strike-Slip Faults: *Bulletin of the Seismological Society of America*, v. 92, n. 7, p. 2612-2636.
- Lowe, D.R., 1982, Sediment gravity flows: II. Depositional models with special reference to the deposits of high-density turbidity current : *Jour. Sed. Petrology*, v. 52, p. 279-297.
- Middleton, G.V., and Hampton, M.A., 1976, Subaqueous sediment transport and deposition by sediment gravity flows, in Stanley, D. G., and Swift, D. J., eds., *Marine Sediment Transport and Environmental Management*: New York, John Wiley, p. 197-217.
- Nakajima, T., and Kanai, Y., 2000, Sedimentary features of seismoturbidites triggered by the 1983 and older historical earthquakes in the eastern margin of the Japan Sea: *Sedimentary Geology*, v.135, p. 1-19.
- Nelson, C.H., 1968, *Marine Geology of Astoria Deep-Sea Fan*: Unpublished Ph.D. Dissertation Oregon State University, Corvallis, 289 p.
- Nelson, C.H., 1976, Late Pleistocene and Holocene depositional trends, processes, and history of Astoria Deep-Sea Fan, northeast Pacific: *Marine Geology*, v. 20, p. 129-173.
- Nelson, C. H., Escutia, C., Goldfinger, C., Karabanov, E. and Gutiérrez-Pastor, J., in press, External Controls on Modern Turbidite Systems: Three Case Studies, in press, in eds: B. Kneller, W. McCaffrey and O. J. Martinsen: *External Controls on Deep-Water Depositional Systems*, v. 92, SEPM, Special Publication.
- Nelson, C.H., Goldfinger, C., Johnson, J.E., and Dunhill, G., 2000, Variation of Modern Turbidite Systems Along the Subduction Zone Margin of Cascadia Basin and Implications for Turbidite Reservoir Beds, in Weimer, P.W., Nelson, C. H. et al., eds., *Deep-water Reservoirs of the World*, Gulf Coast Section Society of Economic Paleontologists and Mineralogists Foundation 20 Annual Research Conference, p.714-738
- Nelson, C.H., Karabanov, E.B., and Colman, S.M., 1995, Late Quaternary Lake Baikal turbidite systems, Russia: in Pickering, K.T., Lucchi, F.R., Smith, R., Hiscott, R.N., Kenyon, N. (eds.): *An Atlas of Deep-Water Environments*, Chapman and Hall, London, p 29-33.
- Nelson, C.H., Kulm, L. D., Carlson, P. R., and Duncan, J. R., 1968, Mazama ash in the northeastern Pacific: *Science*, v. 161, p. 47-49.
- Nelson, C.H., Twichell, D. C., Schwab, W.C., Lee H.J and Kenyon N. H., 1992, Upper Pleistocene turbidite sand beds and chaotic silt beds in the channelized, distal, outer-fan lobes of the Mississippi Fan: *Geology*, v. 20, p. 693-696.
- Niemi, T.M. and Hall, N.T., 1992, Late Holocene slip rate and recurrence of great earthquakes on the San Andreas Fault in northern California: *Geology*, v. 20, p. 195-198.
- Prentice, C.S., Merritts, D.J., Beutner, E.C., Bodin, P., Schill, A., and Muller, J.R., 1999, Northern San Andreas fault near Shelter Cove, California: *Geological Soc. of America Bulletin*, v. 111, p. 512-523.
- Satake, K., Shimazaki, K., Tsuji, Y., and Ueda, K., 1996, Time and size of a giant earthquake in Cascadia inferred from Japanese tsunami records of January, 1700: *Nature* v. 379, p. 246-249.
- Segall, P., 2002, Integrating geologic and geodetic estimates of slip rate on the San Andreas fault system, *Int. Geol. Rev.* v. 44, no. 1, p. 62-82.
- Shiki, T., Kumon, F., Inouchi, Y., Kontani, Y., Sakamoto, T., Tateishi, M., Matsubara, H., and Fukuyama,

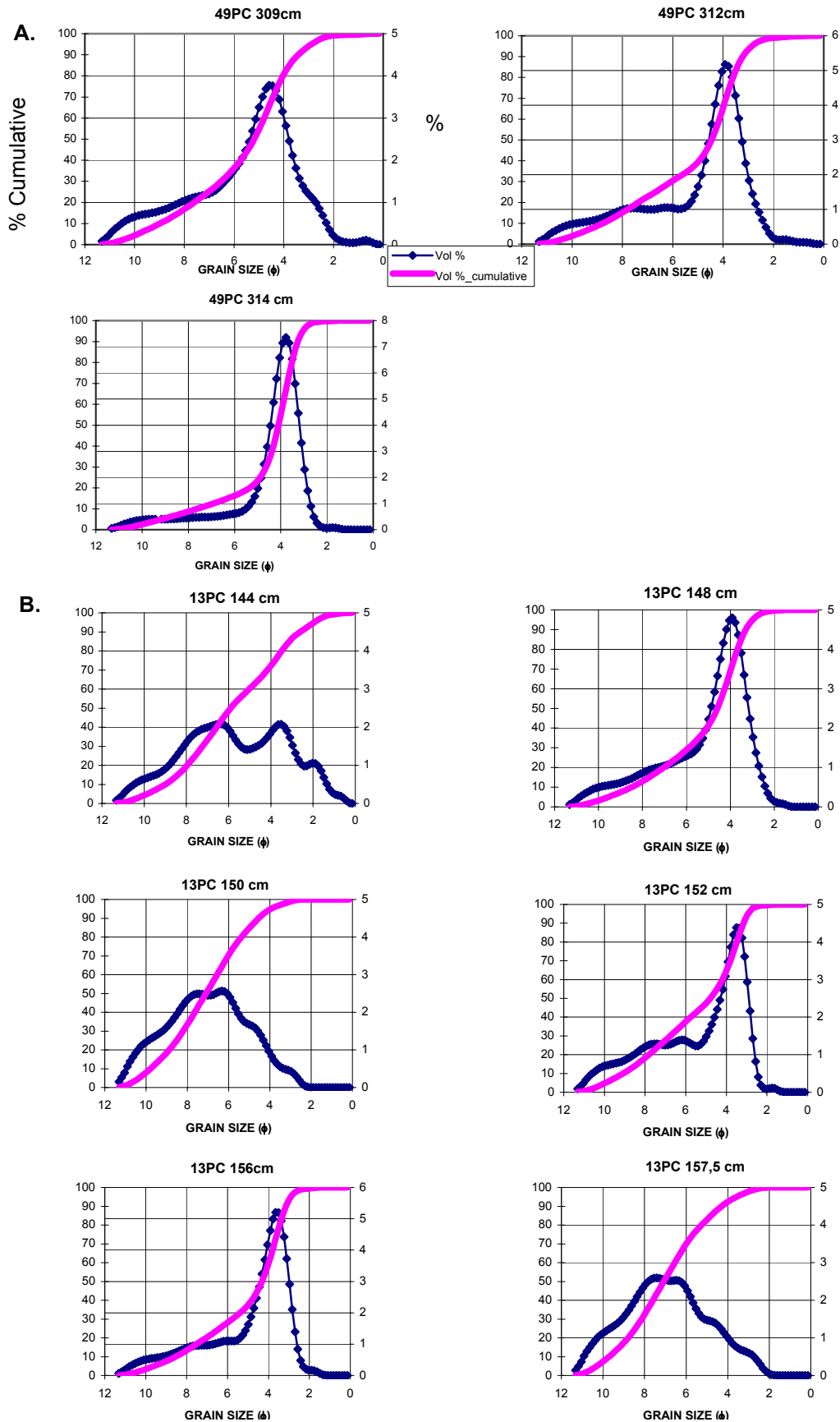
- K., 2000, Sedimentary features of the seismo-turbidites, Lake Biwa, Japan: *Sedimentary Geology*, v. 135, p. 37-50.
- Sternberg, R.W., 1986, Transport and accumulation of river-derived sediment on the Washington continental shelf, USA, *Jour. of Geol. Soc. London*, v. 143, p. 945-956.
- Stow, D.A.V. and Shanmugam, G., 1980, Sequence of structures in fine-grained turbidites: comparison of recent deep sea and ancient flysh sediments, *Sedimentary Geology*, v. 25, p. 23-42.
- Tripsanas, E.K., Bryant, W.R., Slowey, N.C., and Kim, J.W., 2006, Marine Isotope Stage 6 Canyon and Spillover Deposits of the Bryant and Eastern Canyon Systems, Northwest Gulf of Mexico: Importance of Fine-Grained Turbidites on a Delta-Fed Prograding Slope, *Journal of Sedimentary Research*, v. 76; no. 8; p. 1012-1034.
- Twichell, D.C., Nelson, C.H., Damuth, J.E., Olson, H. C., Dunhill, G., 2000, Bryant Canyon Turbidite System Pathway on The Louisiana Continental Slope, Northern Gulf of Mexico, *Gulf Coast Association of Geological Societies Transactions*, , v. L.
- Wolf, S.W. and Hamer, M., 1999, Turbidite pathways in Cascadia Basin and Tufts abyssal plain; Part A, Astoria Channel, Blanco Valley, and Gorda Basin: U.S.G.S. Open File Report OF 99-0157.
- Zdanowicz, C.M., Zielinski, G.A., and Germani, M.S., 1999, Mount Mazama eruption: calendrical age verified and atmospheric impact assessed: *Geology*, v. 27, p. 621-624.
- Zhang, H., Niemi, T., and Fumal, T., 2006, A 3000-year Record of Earthquakes on the Northern San Andreas Fault at the Vedanta Marsh Site, Olema: *California Seismological Research Letters*, v. 77 no. 2, p. 248.

APPENDIX 1. A) GRAIN SIZE DISTRIBUTION CURVES FROM 12 PC OF GUALALA CHANNEL.
 B) GRAIN SIZE DISTRIBUTION CURVES AT 14 PC OF WILLAPA CHANNEL.

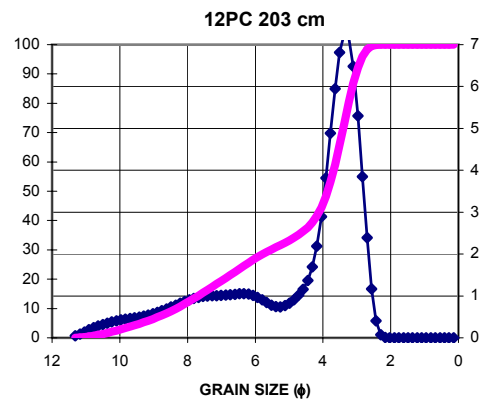
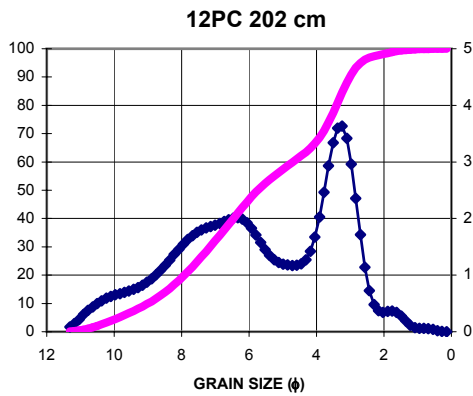
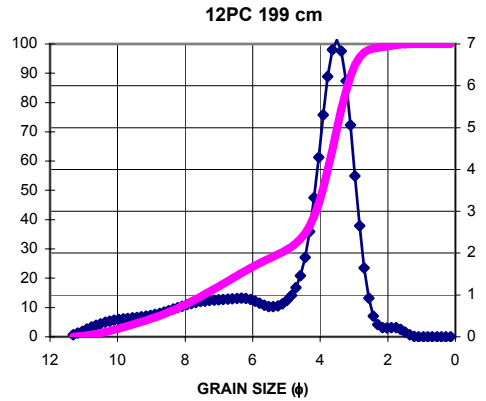
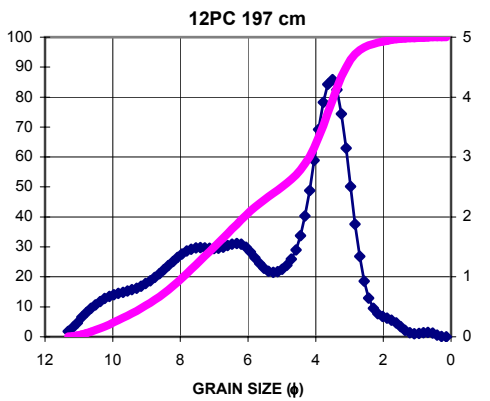
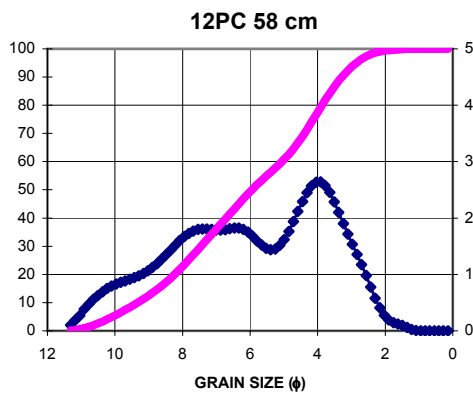
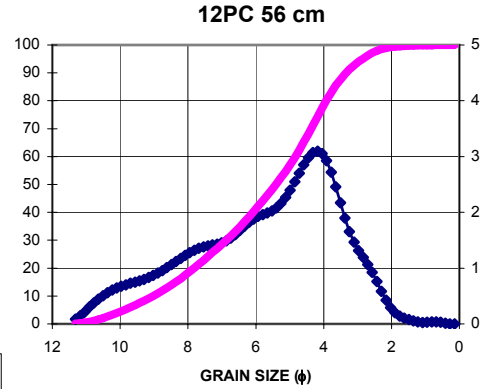
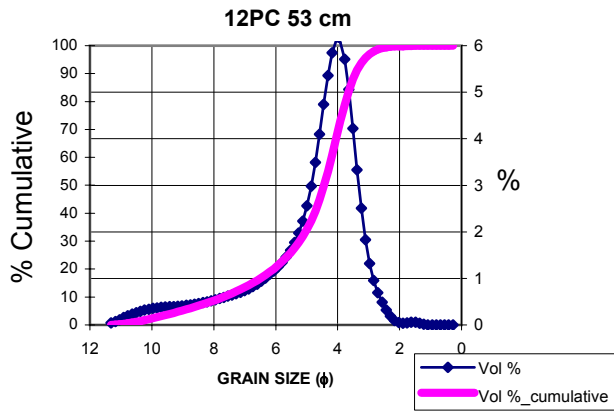


APPENDIX 2. A: GRAIN SIZE DISTRIBUTION CURVES AT 49 PC OF NOYO CANYON.

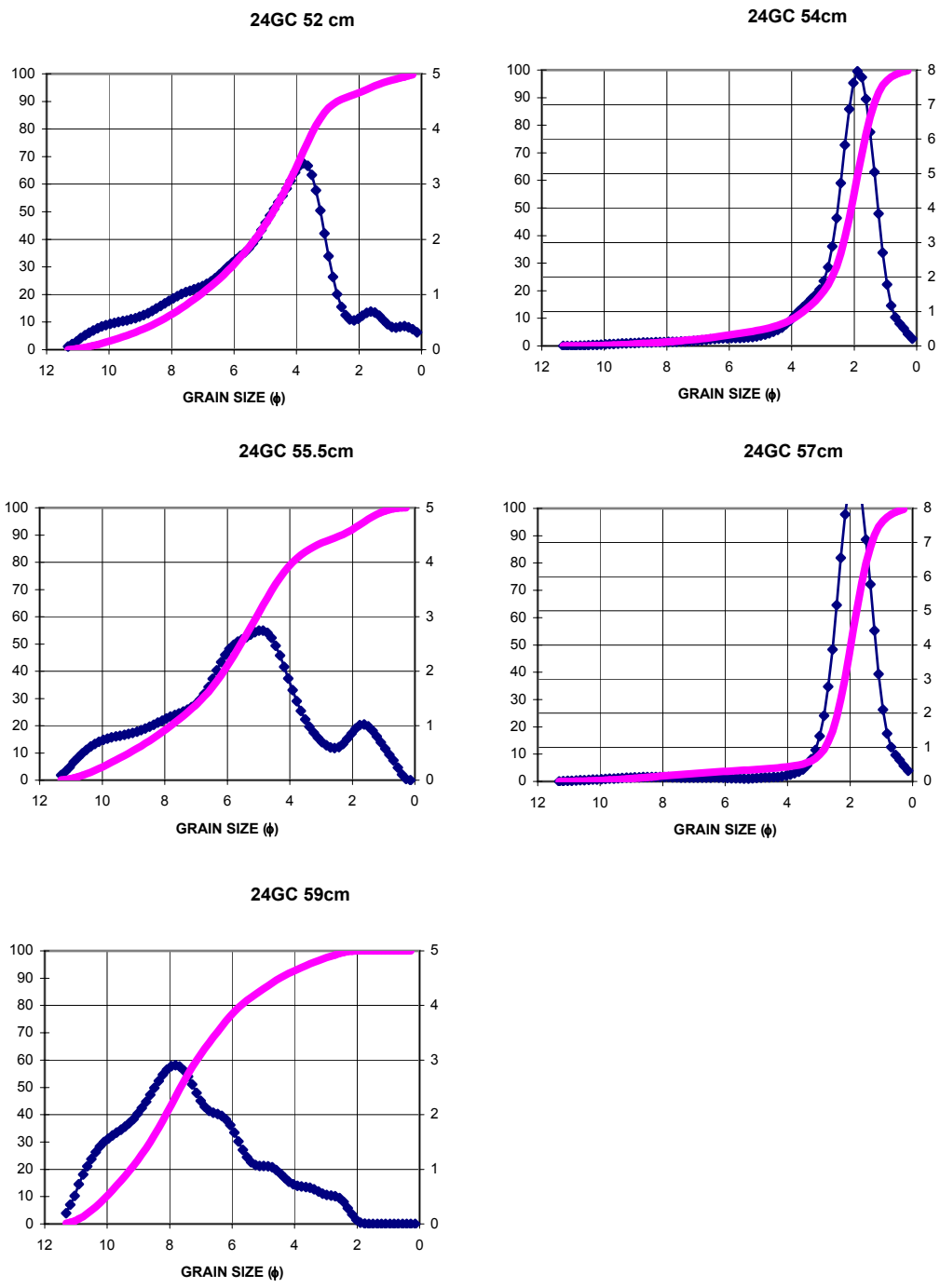
B: GRAIN SIZE DISTRIBUTION CURVES AT 13 PC OF GUALALA CANYON.



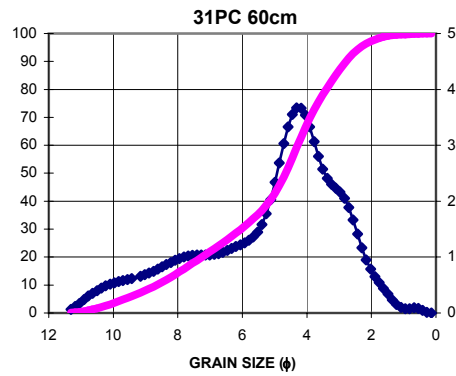
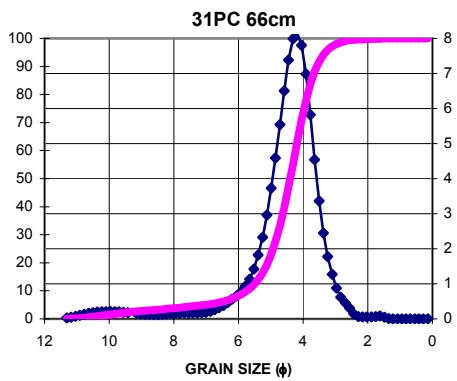
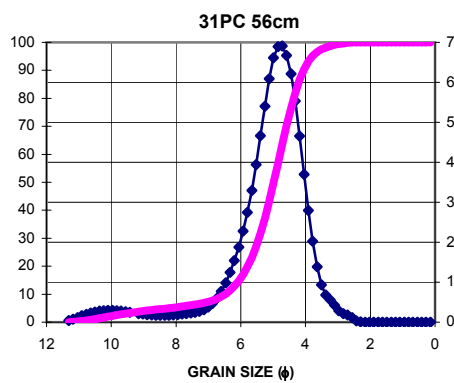
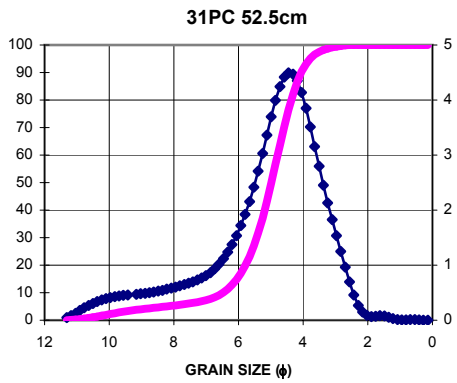
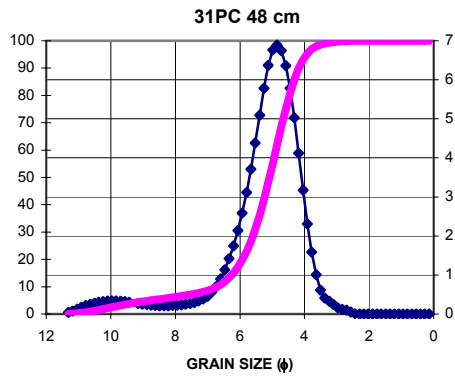
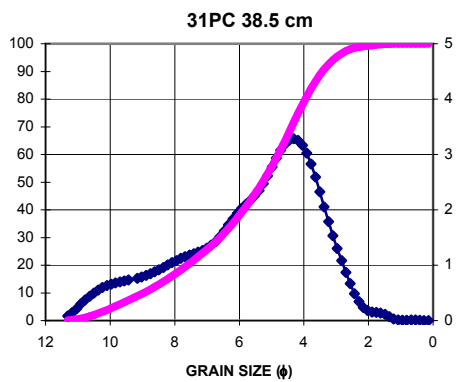
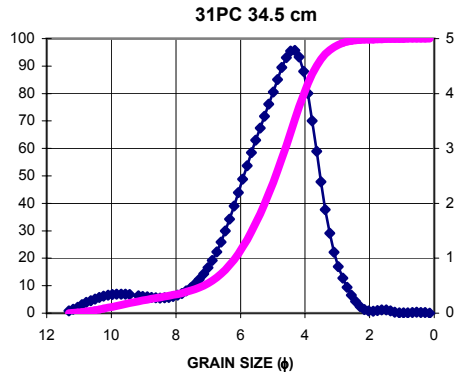
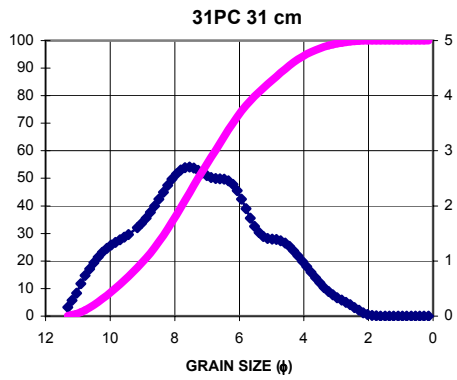
APPENDIX 3. GRAIN SIZE DISTRIBUTION CURVES AT 12 PC OF GUALALA CHANNEL.



APPENDIX 4. GRAIN SIZE DISTRIBUTION CURVES AT 24 GC DEEPEST TURBIDITE OF NOYO/GUALALA/VISCAINO CHANNEL CONFLUENCE.



**APPENDIX 5. GRAIN SIZE DISTRIBUTION CURVES AT 31 PC OF GUALALA/VISCAINO/
CORDELL CHANNEL CONFLUENCE.**





CAPÍTULO V

CONCLUSIONES

CONCLUSIONES

Muchos estudios previos han correlacionado el registro turbidítico a lo largo de los dos márgenes de Cascadia y California utilizando edades de ^{14}C , estratigrafía por medio de eventos bien datados, técnicas de datación relativa en las confluencias de canales y correlación directa a través de las propiedades físicas del sedimento. Uno de los temas de la investigación llevada a cabo en esta tesis doctoral es definir y comparar las edades y los intervalos de recurrencia entre turbiditas Holocenas de los márgenes de subducción de Cascadia y transformante del norte de California mediante dos métodos: 1) datación absoluta (método de ^{14}C) y 2) datación relativa, mediante la medida del tiempo entre el depósito de turbiditas correlativas calculado a partir del grosor de sedimento hemipelágico subyacente a cada turbidita, dividido por la tasa de sedimentación (método H). El método H es de gran importancia para el desarrollo de una historia paleosísmica precisa debido a que: 1) el sedimento hemipelagico se deposita a una tasa constante en las profundidades oceánicas convirtiéndose en una herramienta independiente para medir el intervalo de tiempo entre turbiditas; 2) los datos de sedimento hemipelagico están disponibles bajo cada turbidita en múltiples testigos de sedimento, si lo comparamos con los registros de edades de ^{14}C , en la mayoría de los casos, incompletos; 3) los cálculos del grosor de sedimento/ tasa de sedimentación suministran los tiempos de recurrencia entre turbiditas y estiman edades para ser comparadas con las de ^{14}C ; 4) la evaluación del grosor de sedimento hemipelagico en múltiples testigos de sondeo de un mismo lugar puede servir para evaluar la erosión y corregir las edades de ^{14}C que se perfilan más antiguas debido a los efectos de la erosión; 5) los datos de sedimento hemipelágico pueden ser usados para calcular edades en eventos que no pueden ser datados por otros métodos y 6) los datos de sedimento hemipelágico pueden ser usados para acotar las distribuciones de edades estimadas por ^{14}C para: a) estimar los mínimos intervalos de recurrencia que es el objetivo más importante en el análisis de riesgos sísmicos y b) refinar y evaluar la fiabilidad de las edades de ^{14}C .

En el norte de la zona de subducción de Cascadia hemos estimado que para los últimos ~ 7200 años, grandes terremotos tuvieron lugar cada ~ 575 años de promedio y cada ~ 520 años a comienzos del Holoceno (entre ~ 7200-9800 años) y que para los últimos ~ 5000 años, los mínimos tiempos de recurrencia son ~ 300 años y los máximos ~ 1200 años. En el norte del margen de California hemos estimado que para los últimos ~ 2600 años: a) la frecuencia de los terremotos en el canal de Noyo es ~ 200 años; b) los mínimos intervalos de recurrencia son ~ 176 años, basándonos en el método H y c) los máximos tiempos de recurrencia son ~ 300 años estimados a partir del método H.

Otro tema de la investigación más relevante de esta tesis doctoral ha estado enfocada en el análisis de las características de seísmo-turbiditas a través de la integración de los datos de observaciones litológicas del sedimento, granulometría, radiografías de rayos-x y análisis mineralógico. En la cuenca de Cascadia, una turbidita bien correlacionada tiene diferentes características sedimentológicas dependiendo de su localización, más proximal o más distal, en el sistema turbidítico. La ausencia de un elevado número de cabeceras de cañón de tributarios y la morfología simple de un canal proximal único sin confluencias de canales tributarios da lugar a turbiditas, que son generalmente de un solo pulso, como por ejemplo en el canal de Juan de Fuca.; sin embargo, en el canal de Cascadia, bajo la confluencia del canal de Juan de Fuca junto con otros tributarios, la misma turbidita correlativa es más espesa, con tamaño de grano mayor y con múltiples pulsos. Estas características son debidas a la entrada simultánea de corrientes de turbidez procedentes de diferentes tributarios y que han sido desencadenadas sincrónicamente por un mismo terremoto de elevada magnitud. En el norte de California, en el canal proximal de Noyo y en la cabecera del cañón de

Gualala, las turbiditas son uni-pulsadas, al igual que en el canal de Juan de Fuca. Sin embargo, en el canal proximal de Gualala y bajo las confluencias de tributarios del mismo sistema, las turbiditas son multi-pulsadas, igualmente causadas por un terremoto sincrónico que sacude la totalidad de cañones/canales tributarios que se unen bajo la base del talud para formar un canal producto de la confluencia de canales. En el margen norte de California, esta sincronía causada por un mismo terremoto queda puesta de manifiesto por la diferente mineralogía de cada pulso turbidítico pudiendo ser correlacionados con diferentes áreas fuentes para cada cañón tributario. Por tanto, las seismo-turbiditas individuales bajo las confluencias de canales en los márgenes de Cascadia y California son multi-pulsadas, con más contenido de arena o lodo y más gruesas. Estas características comunes sugieren que la amalgamación en múltiples pulsos para la misma turbidita individual debe de ser típico en márgenes tectónicamente activos. Para corroborar estas características como asociables a este tipo de márgenes, más turbiditas necesitan ser estudiadas y comparadas de otros márgenes activos, y también, pasivos, para definir así las diferencias fundamentales entre turbiditas generadas por terremotos y las producidas por cualquier otro mecanismo.

CONCLUSIONS

Extensive previous studies have correlated the seismo-turbidite record on the Cascadia and northern California active tectonic continental margins by utilizing ^{14}C ages, stratigraphy and marker beds, relative dating tests at channel confluences and direct correlation of physical properties. One topic of my research defines and compares Holocene ages and recurrence time intervals or frequency between turbidites with two methods: 1) absolute dating (^{14}C method) and 2) the time interval between two turbidites, that is calculated using hemipelagic sediment thickness divided by sedimentation rate (H method). The H method is important for developing the most accurate paleoseismic history along a margin because: 1) deep-sea sedimentation provides an independent time yardstick derived from a constant rate of hemipelagic sediment deposited between turbidites; 2) hemipelagic data is available for every turbidite event from multiple cores at each location studied, compared to a single incomplete set of radiocarbon ages; 3) hemipelagic thickness/sedimentation rate provides a set of turbidite recurrence times and calculated ages to compare with similar ^{14}C data sets; 4) the evaluation of hemipelagic sediment thickness in multiple cores at the same site can be utilized to evaluate erosion effects and correct radiocarbon ages where the dates are anomalously old because of erosion, 5) hemipelagic data can be used to calculate ages for events that cannot be dated by other methods and 6) hemipelagic data may be used to constrain radiocarbon age distributions, particularly for a) to estimate minimum recurrence times that are most important for hazards analysis, and b) to refine and test the reliability of radiocarbon ages where the calibration curves result in broad probability density functions.

In the northern Cascadia Subduction Zone we estimate that for the past ~ 7200 Cal. yr B.P., whole plate earthquakes take place every ~ 575 yr on average and every ~ 520 yr in the early Holocene (between ~ 7200 - 9800 yr) and for the past ~ 5000 yr, minimum recurrence times are ~ 300 yr and the maximum recurrence times are ~ 1200 yr. From the northern California margin we estimate that for the past ~ 2600 yr: a) frequency of earthquakes in Noyo Channel is ~ 200 yr, b) the minimum recurrence times are ~ 176 yr based on the H analysis and c) the maximum recurrence times are ~ 300 yr based on the H method.

The second topic focus on the sedimentological characteristics of these correlative seismo-turbidites through the integration of lithologic observations, grain size measurements, x-ray radiography and mineralogic analysis. In Cascadia Basin, a correlative turbidite has different sedimentological characteristics depending on its proximal to distal location in the turbidite system. The absence of many tributary canyon heads and the simple morphology as a single proximal channel without confluences of tributary channels result in turbidites that are generally uni-pulsed, as for example in the Juan de Fuca Channel; however, downstream in Cascadia Channel below tributary channel confluences of Juan de Fuca and other channels, the same correlative turbidite is thicker, coarser grained, and multi-pulsed, because of the multiple inputs of turbidity currents that are synchronously triggered by great earthquakes in the tributary canyons. In the northern California margin in proximal Noyo Channel and the Gualala Canyon mouth, turbidites are mainly uni-pulsed, similar to proximal Juan de Fuca Channel. However, in the main proximal Gualala Channel and downstream below tributary channel confluences turbidites are multi-pulsed, again because of synchronous earthquake triggering in several canyon tributaries that join at the base of slope, or tributary channels that feed into downstream channel confluences. Synchronous earthquake triggering of the California margin turbidites below confluences also is shown by the different mineralogy of each turbidite pulse that can be correlated with the different mineral source for each tributary canyon. Thus, individual seismo-turbidites below channel confluences in both Cascadia and California margins are multi-pulsed, sandier, thicker,

and suggest that amalgamation from multiple pulses in individual turbidites may be characteristic of active tectonic margins. These characteristics of seismo-turbidites need to be investigated in other active tectonic margins and compared with turbidites in passive margins to help define possible fundamental differences of turbidites in these different continental margin settings.



CAPÍTULO VI

PERSPECTIVAS FUTURAS

PERSPECTIVAS FUTURAS

En esta tesis doctoral se ha abordado el estudio de secuencias turbidíticas Holocenas en márgenes activos en los que el mecanismo principal desencadenante de corrientes de turbidez son terremotos de elevada magnitud ($\geq 8Mw$). Cabe esperar, por tanto, que las características sedimentológicas, las propiedades físicas e intervalos de recurrencia de las turbiditas aquí analizadas refleje patrones asociables a un margen como el de subducción de Cascadia o como el transformante del norte de la falla de San Andrés, California.

Durante las campañas oceanográficas de 1999 y 2002 en las costas de Oregon y California, y en los testigos de sedimento de ambos márgenes, se recuperaron turbiditas Pleistocenas siendo unas, producto de los temblores sísmicos y otras, producto de mecanismos sedimentológicos en relación a regímenes de bajada de nivel del mar. En el margen de Cascadia muchas de estas turbiditas han sido datadas por ^{14}C y pueden ser correlacionadas canal a canal a lo largo del margen, sugiriendo un mecanismo desencadenante sincrónico, pero otras, sin embargo, aparecen en medio de la secuencia estratigráfica sin una clara correlación. Trabajos previos han abordado, de forma preliminar, las características sedimentológicas de estas turbiditas Pleistocenas (Duncan et al., 1970; Nelson, 1976). Un análisis más detallado de las mismas con el objetivo de distinguir turbiditas generadas por terremotos de las generadas por otros mecanismos en regímenes de bajo nivel del mar de márgenes activos, podría utilizar los métodos de trabajo para el estudio de las turbiditas Holocenas empleados en esta tesis y aplicarlos a los sedimentos Pleistocenos. Los análisis de la sincronía de los diferentes niveles de turbiditas (tratados en los Capítulos II y III) y sedimentológico detallado (expuesto en el Capítulo IV) permitirá un análisis comparativo en el espacio (a lo largo de un mismo sistema cañón/canal turbidítico) y en el tiempo (a lo largo de la secuencia Holoceno-Pleistoceno) y así, también, servirá para afinar las correlaciones entre turbiditas. La importancia de este estudio radica en el potencial del registro turbidítico para ampliar nuestra capacidad de evaluación del riesgo sísmico en áreas tectónicamente activas en tiempos previos a los 10.000 años.

Como ya ha sido discutido en esta tesis, en los márgenes activos de estudio las turbiditas se caracterizan por presentar múltiples pulsos de diferente mineralogía asociada a los diferentes canales/cañones tributarios que conforman el sistema turbidítico atribuyéndose su origen a terremotos. Por el contrario, en márgenes pasivos las turbiditas han sido estudiadas por previos autores presentando secuencias típicas granodecrecientes sin pulsos con diferentes granulometrías en una misma turbidita (Nelson et al., 1992; Tripsanas et al, 2006; Twichel et al., in press). Por tanto, la caracterización de las turbiditas de un margen pasivo (para compararlas con las de nuestro estudio) es otra de las líneas futuras de investigación. Por ejemplo, en la Cuenca de Brazos Trinity del Golfo de Méjico se han registrado turbiditas, la mayoría, asociadas a periodos claros de bajo nivel de mar, pero otras sin embargo parecen ir asociadas a los intervalos relativos de subida dentro del régimen general de bajada. Esta Cuenca esta siendo estudiada con profundidad como consecuencia de la recuperación de los testigos de sondeo en la Expedición 308 de IODP en el Golfo de Méjico y es uno de los principales objetivos de la doctoranda para investigaciones post-doctorales. Por tanto, el desafío próximo consistiría en caracterizar las turbiditas en la cuenca Brazos Trinity con las mismas herramientas usadas en los márgenes de Cascadia y norte de California (datación por ^{14}C , granulometría, radiografías de rayos-X, propiedades físicas, mineralogía y paleontología) (trabajo que está actualmente en proceso), para poder compararlas y establecer modelos deposicionales asociados a diferentes tipos de márgenes y tipos de mecanismos desencadenantes tanto en regímenes de subida de nivel del mar como de bajada. Dado que las secuencias turbidíticas hoy día se consideran como uno de los mejores indicadores de reservorios de hidrocarburos, estos modelos sedimentarios, a su vez, se pueden

utilizar con el propósito de identificarlos.

También, en márgenes pasivos se puede aplicar igualmente el método de corrección de edades de ^{14}C basado en la correcta medida del sedimento hemipelágico entre turbiditas para evaluar no solo el grado de erosión de las corrientes de turbidez si no también para mejorar la fiabilidad de las dataciones que se traduce en la estimación de los intervalos de recurrencia entre turbiditas y por tanto, en el grado de inestabilidad de taludes y/o deslizamientos de márgenes pasivos.

REFERENCIAS

- Duncan, J.R., Fowler, G.A., and Kulm, L.D., 1970, Planktonic Foraminiferan-Radiolarian ratios and Holocene-Late Pleistocene deep-sea stratigraphy off Oregon: Geological Society of America Bulletin, v. 81, p. 561-566.
- Nelson, C.H., 1976, Late Pleistocene and Holocene depositional trends, processes, and history of Astoria Deep-Sea Fan, northeast Pacific: Marine Geology, v. 20, p. 129-173.
- Nelson, C.H., Twichell, D. C., Schwab, W.C., Lee H.J and Kenyon N. H., 1992, Upper Pleistocene turbidite sand beds and chaotic silt beds in the channelized, distal, outer-fan lobes of the Mississippi Fan: Geology, v. 20, p. 693-696.
- Tripsanas, E.K., Bryant, W.R., Slowey, N.C., and Kim, J.W., 2006, Marine Isotope Stage 6 Canyon and Spillover Deposits of the Bryant and Eastern Canyon Systems, Northwest Gulf of Mexico: Importance of Fine-Grained Turbidites on a Delta-Fed Prograding Slope, Journal of Sedimentary Research, v. 76; no. 8; p. 1012-1034.
- Twichel, L.D., Nelson, C. H., Kenyon, N., Schwab, W., in press, The influence of external processes on the latest Pleistocene and Holocene evolution of the Mississippi Fan, in eds: B. Kneller, W. McCaffrey and O. J. Martinsen: Geological Society/SEPM, Special Publication, External Controls on Deep-Water Depositional Systems, 36 p.

ANEXO 1

Late Holocene Rupture of the Northern San Andreas Fault and Possible Stress Linkage to the Cascadia Subduction Zone

by Chris Goldfinger, Kelly Grijalva, Roland Bürgmann, Ann E. Morey, Joel E. Johnson, C. Hans Nelson, Julia Gutiérrez-Pastor, Andrew Ericsson,^{*} Eugene Karabanov,[†] Jason D. Chaytor,[‡] Jason Patton, and Eulàlia Gràcia

Abstract We relate the late Holocene northern San Andreas fault (NSAF) paleoseismic history developed using marine sediment cores along the northern California continental margin to a similar dataset of cores collected along the Cascadia margin, including channels from Barclay Canyon off Vancouver Island to just north of Monterey Bay. Stratigraphic correlation and evidence of synchronous triggering imply earthquake origin, and both temporal records are compatible with onshore paleoseismic data. In order to make comparisons between the temporal earthquake records from the NSAF and Cascadia, we refine correlations of southern Cascadia great earthquakes, including the land paleoseismic record.

Along the NSAF during the last ~2800 yr, 15 turbidites, including one likely from the great 1906 earthquake, establish an average repeat time of ~200 yr, similar to the onshore value of ~240 yr. The combined land and marine paleoseismic record from the southern Cascadia subduction zone includes a similar number of events during the same period. While the average recurrence interval for full-margin Cascadia events is ~520 yr, the southern Cascadia margin has a repeat time of ~220 yr, similar to that of the NSAF. Thirteen of the 15 NSAF events were preceded by Cascadia events by ~0–80 yr, averaging 25–45 yr (as compared to ~80–400 yr by which Cascadia events follow the NSAF).

Based on the temporal association, we model the coseismic and cumulative post-seismic deformation from great Cascadia megathrust events and compute related stress changes along the NSAF in order to test the possibility that Cascadia earthquakes triggered the penultimate, and perhaps other, NSAF events. The Coulomb failure stress (CFS) resulting from viscous deformation related to a Cascadia earthquake over ~60 yr does not contribute significantly to the total CFS on the NSAF. However, the coseismic deformation increases CFS on the northern San Andreas fault (NSAF) by up to about 9 bars offshore of Point Delgada, most likely enough to trigger that fault to fail in north-to-south propagating ruptures.

Online Material: Relative timing of NSAF and Cascadia events and estimated Cascadia slip models.

Introduction

The development of long paleoseismic records along major fault systems allows correlation of records along

strike and can establish spatial histories of rupture length. Combined with age data, long-correlated records can also address clustering, the applicability of slip-predicable or time-predicable models, and the nature of long-term stress interactions (e.g., Stein *et al.*, 1992; Ward and Goes, 1993; Weldon *et al.*, 2004). We have been using the marine turbidite record as a proxy for earthquake recurrence in both the Cascadia Subduction Zone, and on the northern San Andreas fault (NSAF) (Goldfinger *et al.*, 2003a, 2007). In comparison

^{*}Present address: Continental Energy Corporation, Indonesia, Jl. Kenanga #62, Cilandak Jakarta, 12560, Indonesia.

[†]Present address: Chevron Energy Technology Company, Earth Science Technology Department, 1500 Louisiana St., Houston, Texas 77002.

[‡]Present address: Department of Geology and Geophysics, Woods Hole Oceanographic Institution, MS#24, Woods Hole, Massachusetts 02543.

to land paleoseismic records, turbidite paleoseismology and other off-fault techniques must demonstrate that the events recorded are earthquake triggered, or provide a method to separate earthquakes from other signals in a mixed record. Marine records are commonly longer and more continuous than land records, and provided they are in settings isolated from the effects of sea level change, can actually be more precise in the early to mid Holocene due to the abundance of datable microfossils. In recent years, turbidite paleoseismology has been attempted in Cascadia (Adams, 1990; Nelson *et al.*, 2000; Goldfinger *et al.*, 2003a,b), Puget Sound (Karlin *et al.*, 2004), Japan (Inouchi *et al.*, 1996; Nakajima and Kanai, 2000; Shiki *et al.*, 2000), the Mediterranean (Kastens, 1984), the Dead Sea (Niemi and Ben-Avraham, 1994), northern California (Field, 1984; Garfield *et al.*, 1994), the southwest Iberian Margin (Garcia-Orellana *et al.*, 2006), Marmara Sea (Polonia *et al.*, 2004), and the Arctic Ocean (Grantz *et al.*, 1996) and is a technique that is evolving as a precise tool for seismotectonics.

In 1999, we collected 44 piston cores of 6–8-m length (Fig. 1) and 44 companion trigger cores of 2-m length and seven box cores (50 × 50 × 50 cm) in basin and channel systems throughout Cascadia basin to investigate the paleoseismic history of the Cascadia margin (Goldfinger *et al.*, 2003a). In 1999–2002, we collected 74 piston, gravity, and jumbo Kasten cores from channel/canyon systems draining the northern California margin adjacent to the onshore and nearshore NSAF (Goldfinger *et al.*, 2007; Fig. 2). During both cruises, we mapped channel systems with SeaBeam 2000 and Simrad EM-120 multibeam sonars, collecting both high-resolution bathymetry and backscatter data essential for analysis of channel morphology, sedimentation patterns, and core siting. These data were processed and merged with existing single and multibeam data to develop regional bathymetric datasets.

During these cruises, we sampled all major and many minor channel systems extending from Barclay Canyon off Vancouver Island to the Mendocino Triple Junction (MTJ) in 1999, and from Cape Mendocino to just north of Monterey Bay in 2002 (Figs. 1 and 2). In some cases, sampling both down and across channels was done and particular attention was paid to channel confluences, as these areas afford opportunities to test for synchronous triggering of turbidity currents.

These cores have yielded turbidite records that are in good agreement with the shorter land record of Holocene Cascadia and NSAF earthquakes (Goldfinger *et al.*, 2003a, b, 2007). While Cascadia has an extensive land paleoseismic record from numerous sites, a similar land paleoseismic record for the NSAF system has proven more difficult to establish, despite the intense scientific study of the NSAF stemming from the great seismic hazards to the San Francisco Bay Area. This is particularly true for the segments of the NSAF near and north of San Francisco that ruptured during the great 1906 earthquake.

In this article, we present results from the offshore turbidite event record along the NSAF extending to ~3000 yr B.P., with correlation evidence of the youngest events along strike that augments evidence presented in Goldfinger *et al.* (2007). We present new data from southern Cascadia, where a series of small correlatable marine turbidites and land evidence together suggest limited southern Oregon ruptures in addition to margin-wide ruptures. We then compare the NSAF temporal record to that of the combined land/marine Cascadia temporal record to explore a possible temporal and stress relationship between these two great plate boundary faults.

Geological Setting and Background

NSAF Seismotectonic Setting

The San Andreas fault (SAF) is probably the most intensively studied transform system in the world. Extending along the west coast of North America, from the Gulf of California to Cape Mendocino, the SAF is the largest component of a complex and wide plate boundary that extends eastward to encompass numerous other strike-slip fault strands and interactions with the Basin and Range extensional province. The Mendocino triple junction (MTJ) lies at the termination of the NSAF and has migrated northward since about 25–28 Ma (Dickinson and Snyder, 1979). As the triple junction moves, the former subduction forearc transitions to right-lateral transform motion, and the SAF continues to lengthen.

West of the Sierra Nevada block, three main fault systems accommodate ~75% of the Pacific–North America plate motion, distributed over an ~100-km-wide zone (Frey-mueller *et al.*, 1999; Argus and Gordon, 2001; d'Alessio *et al.*, 2005). Much of the remainder is carried by the eastern California shear zone (Sauber, *et al.*, 1994; Segall and Castillo, 1999). The NSAF accommodates about 25 mm/yr of the ~40 mm/yr distributed across western California. Most of the remainder is taken up on the parallel Hayward–Rodgers Creek system, and the slightly divergent Calaveras–Concord–Green Valley fault system farther to the east. The Hayward and Calaveras systems become the Maacama and Bartlett Springs faults, respectively, in northernmost California. South of San Francisco, the transform system includes the offshore San Gregorio fault, which joins the NSAF at Olema, just north of San Francisco. Between San Francisco and Cape Mendocino, the SAF is a relatively simple system with most strain localized on the primary strand. Several uncertain faults exist offshore, but the age and activity of these faults is unknown (Jennings, 1995). Seismicity offshore is virtually nil, with the exception of the MTJ region. Since the 1906 rupture, the main San Andreas has been nearly aseismic, with only a few small events near Point Arena (Zoback *et al.*, 1999). Seismicity has been greater on the Maacama and Bartlett Springs faults to the east (Castillo and Ellsworth, 1993).

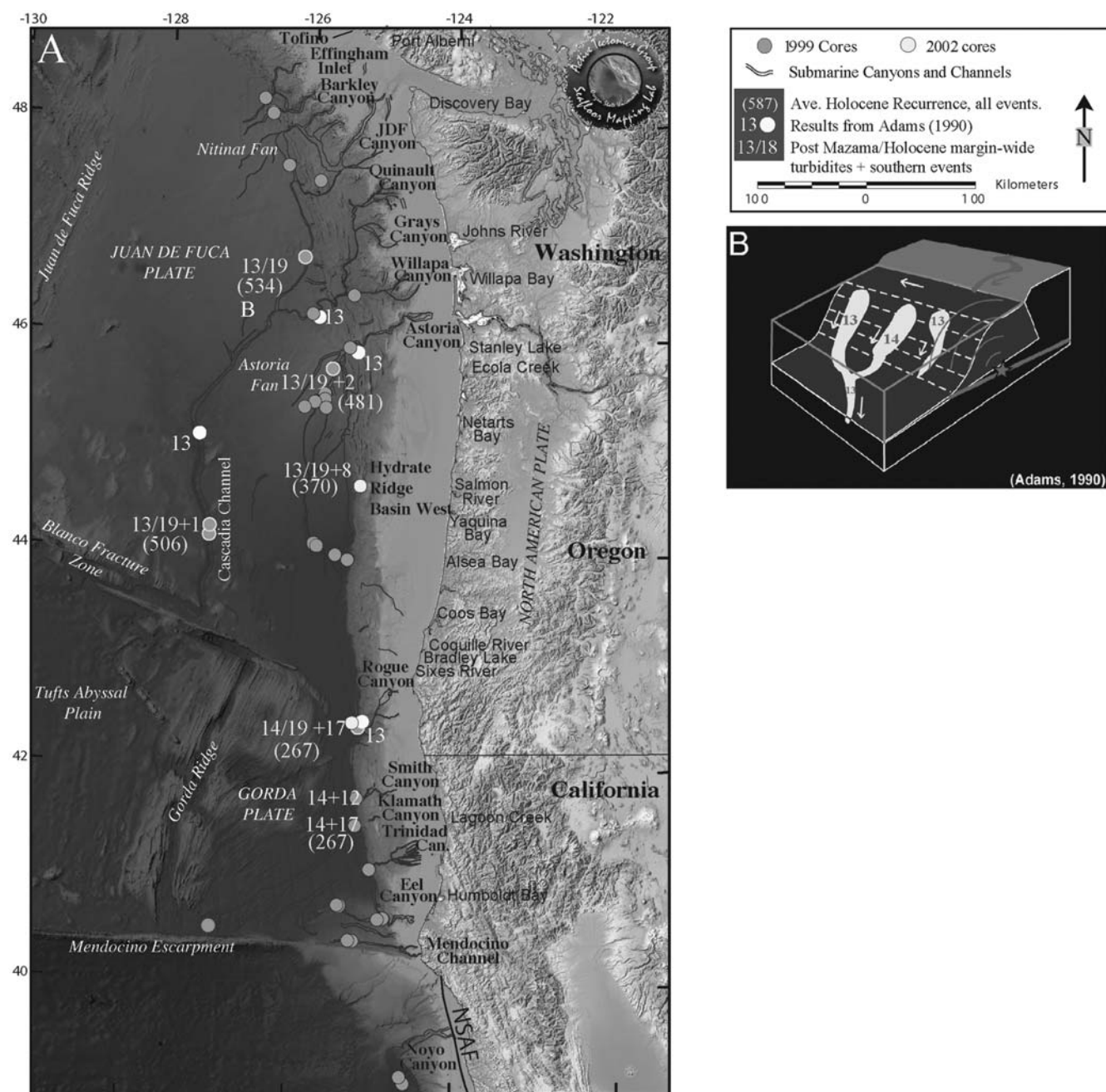


Figure 1. (a) Cascadia margin turbidite canyons, channels, and 1999–2002 core locations. The major canyon systems are outlined. Number of post-Mazama/Holocene correlative turbidites, with southern turbidites denoted with a +, are shown. Average Holocene recurrence times for all events are shown in parentheses. Mazama ash was not present in Barkley Canyon cores or in the cores south of Rogue Canyon. Primary core sites shown with light rim; other cores are gray. (b) Synchronicity test at a channel confluence as applied where Washington channels merge into the Cascadia Deep Sea Channel. The number of events downstream should be the sum of events in the tributaries, unless the turbidity currents were triggered simultaneously by an earthquake (Adams, 1990). This site is at B on the JDF plate.

The 1906 M_w 7.9 earthquake rupture extended from the epicenter near San Francisco north to Shelter Cove near Point Delgada and south to near San Juan Bautista, suggesting a minimum rupture length of ~ 470 km (Fig. 2). The 1906 event clearly ruptured the surface along the San Francisco peninsula to as far north as Point Arena (Lawson, 1908). Some debate exists regarding the full length of the 1906 rup-

ture (McLaughlin *et al.*, 1983), though most investigators now believe the rupture extended to Point Delgada (Song *et al.*, 2008).

Offshore, numerous canyon/channel systems containing Holocene turbidites drain the northern California margin. From the north beginning at Cape Mendocino, to the south at Monterey Bay, the canyons and channels are Gorda,

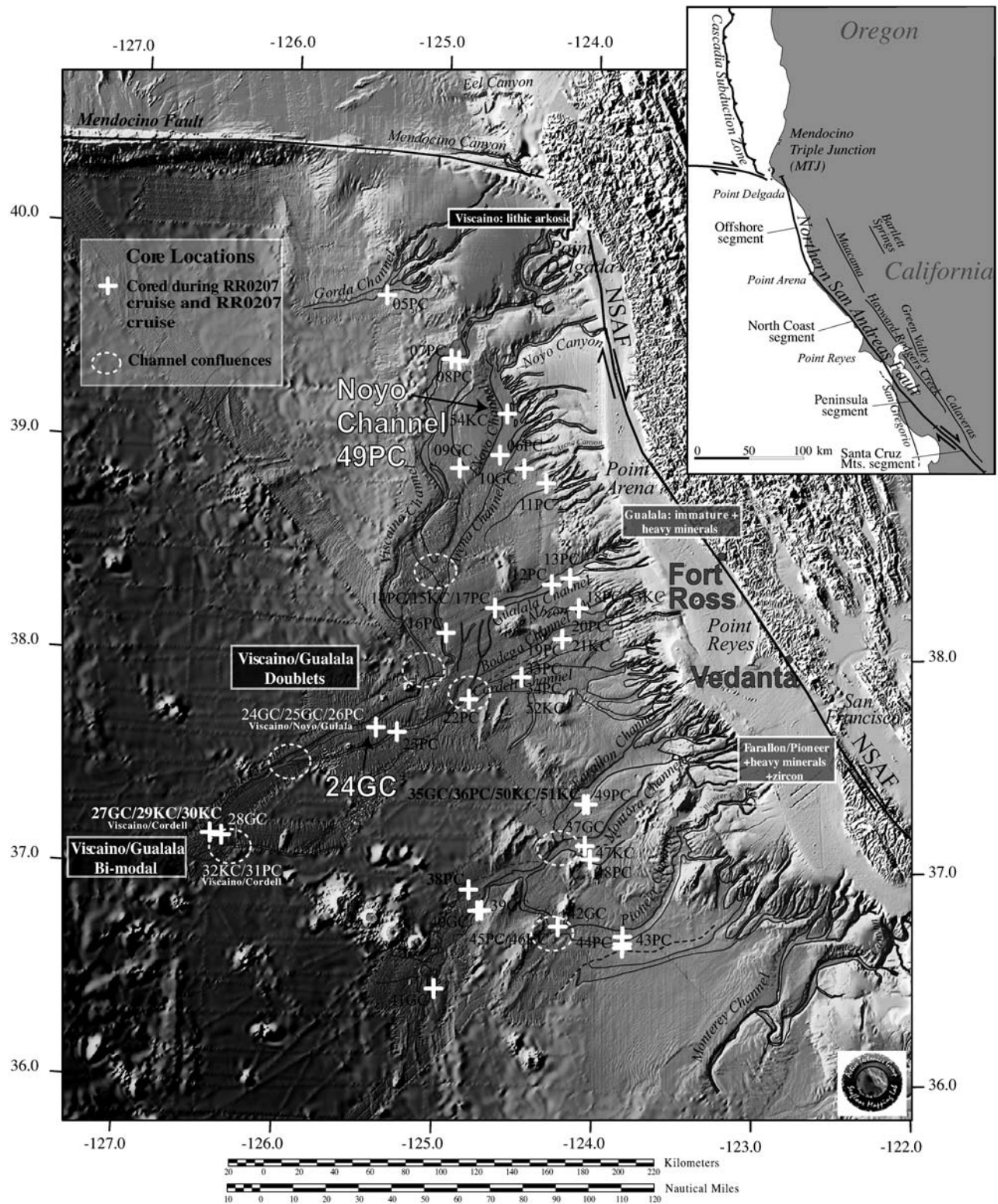


Figure 2. Core locations from 1999 and 2002 cruises on Research Vessel (R/V) Melville and R/V Roger Revelle along NSAF system. Bathymetric and topographic data compiled by Oregon State University (OSU) from archive and newly collected marine survey data during these cruises with NASA Shuttle Radar Topography Mission (SRTM) land data. Channel systems mapped from the new bathymetric grid and sidescan data. Core numbers are referred to in the text: piston core, PC; gravity core, GC; kasten core, KC; and box core, BC. Noyo Cores (including 49PC from Melville 1999 cruise) and 24GC, discussed in text, are also shown. Offshore provenance from heavy mineral analyses is indicated in boxed text. At the confluence upstream of core 24GC, Viscaino and Gualala mineralogies mix and result in stacked pulses, reflecting source mineralogies. Onshore paleoseismic sites Vedanta and Fort Ross are shown onshore.

Viscaino, Noyo, Arena, Gualala, Albion, Bodega Cordell, Farallon, Montara, Pioneer, and Monterey (Fig. 2). Some of these turbidite channels have downstream confluence pathways; for example, Noyo, Viscaino, and Gualala channels join together to form a single channel traveling hundreds of kilometers offshore. The Bodega, Cordell, and Viscaino turbidite systems behave in the same way along the southern half of the northern California margin meeting in another confluence (Goldfinger *et al.*, 2007). Confluences are important because they offer opportunities to test synchronous triggering of turbidity currents (Fig. 1b; Adams, 1990; Goldfinger *et al.*, 2003a, 2007).

Noyo Channel is found south of Cape Mendocino and extends seaward with a length of more than 200 km from the mouth of the canyon to the end of the pathway. The NSAF crosses the Noyo canyon head in ~150-m-water depth on the outer shelf, clearly offsetting the upper canyon head, which has also been captured by and bends 90° to follow the fault (Fig. 2). This makes Noyo canyon particularly sensitive to seismic activity on the NSAF. The Noyo turbidite record is therefore more robust than other channels that increase in distance from the fault southward to ~60 km south of Point Arena (Fig. 2).

Northern San Andreas Onshore Paleoseismicity

The NSAF system has been divided into segments based on its historical record of earthquake behavior. All four northern segments (north of the creeping section at San Juan Bautista, Santa Cruz Mountain, peninsula, north coast, and offshore; Working Group on California Earthquake Probabilities, 2003) ruptured in the 1906 M_w 7.9 earthquake, extending from San Juan Bautista north to the MTJ (Lawson, 1908; Brown, 1995; Thatcher *et al.*, 1997; Prentice *et al.*, 1999; Song *et al.*, 2008).

The onshore paleoseismology of the NSAF has been investigated at Olema, 45-km north of San Francisco; at Dogtown, close to the Olema site; at Bodega Bay, Bolinas Lagoon, Point Arena, and Fort Ross; and at several sites on the San Francisco peninsula and in the Santa Cruz mountains. At the Vedanta site (Fig. 2) near Olema, Niemi and Hall (1992) found a maximum late Holocene slip rate of 24 ± 3 mm/yr, in fair agreement with geodetic data (Segall, 2002; d'Alessio *et al.*, 2005). They estimate that if the 4–5-m slip event recorded in 1906 is characteristic, the recurrence time for such events would be 221 ± 40 yr. The average slip per event at Point Arena similarly implies a recurrence time of 200–400 yr (Prentice, 1989). Recently, 10 new ages from the Vedanta site (Zhang *et al.*, 2006) and sites near Fort Ross (Kelson *et al.*, 2006) (Fig. 2) suggest a recurrence interval of ~200 yr and timing of the penultimate event on the north coast and offshore segments at ~A.D. 1700–1750. Knudsen *et al.* (2002) document probable coseismic relative sea level changes within structural basins along the NSAF in Bodega harbor and Bolinas lagoon, 90 and 27-km north of San Fran-

cisco, respectively. These data suggest two events prior to 1906, one ~400 and another 700–750 yr B.P.

Cascadia Seismotectonic Setting

The Cascadia subduction zone is formed by the subduction of the oceanic Juan de Fuca and Gorda plates beneath the North American plate off the coast of northern California, Oregon, Washington, and Vancouver Island (Fig. 1). The Juan de Fuca–North America convergence rate decreases from 50 mm/yr at southern Vancouver Island to 36 mm/yr at the MTJ (poles of McCaffrey *et al.*, 2007). Juan de Fuca–North American convergence is oblique, with obliquity increasing southward along the margin. The submarine forearc widens from 60 km off southern Oregon to 150 km off the northern Olympic Peninsula of Washington, where the thick Pleistocene Astoria and Nitinat fans are presently being accreted to the margin (Fig. 1). The active accretionary thrust faults of the lower slope are characterized by mostly seaward-vergent thrusts on the Oregon margin from 42° to 44°55' N and north of 48°08' N off Vancouver Island, and by landward-vergent thrusts between 44°55' N and 48°08' N on the northern Oregon and Washington margins (Goldfinger *et al.*, 1997).

The earthquake potential of Cascadia has been the subject of major paradigm changes in recent years. First thought to be aseismic due to the lack of historic seismicity, great thickness of subducted sediments, and low uplift rates of marine terraces (Ando and Balazs, 1979), Cascadia is now thought capable of producing large subduction earthquakes on the basis of paleoseismic evidence (e.g., Atwater, 1987; Satake *et al.*, 1996; Atwater and Hemphill-Haley, 1997), geodetic evidence of elastic strain accumulation (e.g., Dragert *et al.*, 1994; McCaffrey *et al.*, 2000) and comparisons with other subduction zones (e.g., Heaton and Kanamori, 1984; Atwater, 1987). Despite the presence of abundant paleoseismologic evidence for rapid coastal subsidence and tsunamis, the plate boundary remains the quietest of all subduction zones, with only one major interplate thrust event ever recorded instrumentally (Oppenheimer *et al.*, 1993). Cascadia represents an end member of the world's subduction zones not only in seismic activity (Acharya, 1992) but also as the hottest subduction thrust because of its young subducting lithosphere and thick blanket of insulating sediments (McCaffrey, 1997).

Cascadia Paleoseismicity

The past occurrence of great earthquakes in Cascadia is now well established; thus, attention has turned to magnitude, recurrence intervals, and segmentation of the margin. Segmented and whole-margin ruptures should leave distinctly different stratigraphic records in both the coastal marshes and the offshore turbidite channel systems.

The most extensive paleoseismic record on land is found in subsided marshes and tsunami deposits of thin marine sand layers with diatoms that overlie marshes or are in-

terbedded within estuarine or lake muds (Atwater and Hemphill-Haley, 1997; Kelsey *et al.*, 2005; Nelson *et al.*, 2006; site localities shown in Fig. 1). The tsunami deposits are found several kilometers inland from the coast, up river estuaries, or in low-lying freshwater lakes near sea level but above the reach of storm surges. A 3500-yr record of such tsunami events and buried soils due to coseismic land subsidence is found in Willapa Bay, Washington (Atwater and Hemphill-Haley, 1997). In the coastal paleoseismic record, the average recurrence time of great earthquakes along the northern Cascadia subduction zone for the past 3500 yr (526 yr) (Atwater and Hemphill-Haley, 1997) agrees quite closely with the offshore average of 470 yr for the same period (one offshore event was not reported at Willapa Bay) and the 524-yr average over the 10,000-yr turbidite paleoseismic record (revised slightly from Goldfinger *et al.*, 2003a). Along the southern margin, an ~4600-yr record with 14 disturbance events likely from Cascadia subduction earthquakes has been carefully documented in Bradley Lake, on the southern Oregon coast (Kelsey *et al.*, 2005), along with a 5500-yr record at the Sixes River (Kelsey *et al.*, 2002). The Bradley lake record is the most complete land record on the southern margin and yields a shorter recurrence interval of 340 yr along that part of the southern margin. A compilation of southern Cascadia sites reported in Nelson *et al.* (2006) includes Bradley Lake and concludes that Cascadia has segmented ruptures along the southern margin in addition to full-margin ruptures.

Offshore, Cascadia Basin comprises the deep ocean floor over the Juan de Fuca and Gorda Plates, and extends from Vancouver Island, Canada, to the Mendocino Escarpment in northern California (Fig. 1). The Cascadia Basin contains a wide variety of Quaternary turbidite systems with an extensive Holocene history of turbidite deposition (i.e., Griggs and Kulm, 1970; Nelson, 1976). Recent work has documented the linkages between these turbidites and great earthquakes along the Cascadia subduction zone (Adams, 1990; Nelson *et al.*, 2000; Goldfinger *et al.*, 2003a,b).

The Holocene stratigraphy of submarine channels along the Cascadia margin includes Mazama Ash (MA), from the eruption of Mt. Mazama, forming Crater Lake, Oregon (Nelson *et al.*, 1968). The calendar age of the eruption of Mt. Mazama has recently been reevaluated with an age of 7627 ± 150 calendar years B.P. determined from the Greenland Ice Sheet Project (GISP) 2 ice core (Zdanowicz *et al.*, 1999). The Mt. Mazama eruption airfall was distributed northeastward from southern Oregon mainly over the Columbia drainage and some of the coastal rivers. It is also found in the Puget lowland, British Columbia (Hallett *et al.*, 1997), and in inlets on the west coast of Vancouver Island (Dallimore *et al.*, 2005). From these rivers, MA was transported to temporary depocenters in canyon heads of the Cascadia continental margin, such as Mt. St. Helens ash was transported following the 1980 eruption (Nelson *et al.*, 1988). Subsequent turbidity currents transported the ash into Cascadia Basin canyon and channel floor depocenters.

Using the MA marker bed, ^{14}C ages, and stratigraphic correlation, the offshore turbidite record has been demonstrated to be largely, if not entirely, composed of synchronous turbidites, 19 of which are margin wide and others that span shorter segments (Goldfinger, Morey, Erhardt, *et al.*, 2006). The synchronicity of the 10,000-yr turbidite event record along the northern half of the Cascadia subduction zone is best explained by paleoseismic triggering of great earthquakes with a mean recurrence interval for long ruptures of 496–524 yr, depending on the locality. Further refinement of the Cascadia record along the southern margin is discussed in the subsequent section.

Turbidite Methodology and Analytical Methods

Turbidite Methodology and Application to Cascadia and the San Andreas

Identifying Earthquake-Triggered Turbidites. An association between earthquakes and turbidity currents has long been known (Heezen and Ewing, 1952); however, other triggers for turbidity currents exist, including (1) storm or tsunami-wave loading, (2) sediment loading, and (3) storm (hyperpycnal) discharges, as well as less common occurrences such as bolide impacts and major subaerial or submarine landsliding. In some cases, seismic turbidites can be distinguished sedimentologically from storm, tsunami, and other deposits (Inouchi *et al.*, 1996; Nakajima and Kanai, 2000; Shiki *et al.*, 2000), although sedimentological distinction between triggering mechanisms may be somewhat site specific. We use synchronous triggering manifested as a spatial and temporal pattern of event correlations along both the Cascadia and NSAF margins to determine earthquake origin. Synchronicity of event records in separated canyons, over a wide region, is difficult to attribute to nonearthquake sources, which are most often limited spatially and temporally to single canyons. Possible exceptions could include storm or tsunami-wave loading and hyperpycnal flow, which can also occur over large areas and short time scales. These possibilities and the tests used to distinguish Cascadia and NSAF earthquake-generated turbidites from other triggering mechanisms have been presented in Goldfinger *et al.* (2003a, b, 2007) and Nelson *et al.* (2000).

Tests of Synchronous Triggering and Correlative Deposition of Turbidites. A key test of synchronous triggering has become known as the confluence test (Fig. 1b). In Cascadia Basin channels, Adams (1990) observed that most cores contained 13 turbidites overlying the MA (which was included in the thirteenth). Cores from Juan de Fuca Canyon, Willapa, Grays, and Quinault Canyons also contain 13 turbidites and include the MA. The correlative turbidites in Cascadia channel lie downstream of the confluence of those channels. If these events had been independently triggered, with more than a few hours separation in time the channels below, the confluence should contain 26 turbidites, not 13 as observed. This simple observation demonstrates synchronous trigger-

ing of turbidity currents in tributaries whose headwaters are separated by 50–150 km (Fig. 1b). In our Cascadia work, we find that all of the northern Cascadia events that traverse the Willapa–Juan de Fuca Channel confluence pass this test, a total of 19 events including the 6 that lie below the MA. These events pass this test with more precision than simply the number of events upstream and downstream. The events are all composed of 1-to-3 coarse sand pulses with characteristic grain-size distribution, and this structure or event fingerprint is also preserved above and below the confluences, a phenomenon further discussed next.

We also applied a confluence test to the NSAF turbidite data as they pass through six confluences, and we modify the test to include the mineralogic fingerprinting of the input channels during an ~6000-yr period. We broadly distinguish three heavy mineral provenances in the NSAF cores, well linked to the onshore source geology (Figs. 2 and 3). Using these three heavy mineral suites allows us to distinguish the various dominant tributary canyon sources of the stratigraphic

phy within turbidites, both up- and downstream from confluences. With this mineralogic test for synchronous or asynchronous arrival of individual coarse fraction pulses, we can correlate the stacking of these pulses and associated provenance components to establish or refute synchronous triggering. Further details of confluence tests applied to NSAF margin cores are presented in Goldfinger *et al.* (2007).

Analytical Methods

Stratigraphic Correlation and Event Fingerprinting. While at sea, all cores were scanned using a GEOTEK Multi-Sensor Core Logger (MSCL), collecting *P*-wave velocity, gamma-ray density, and relatively coarse magnetic susceptibility data using a loop sensor from the unsplit cores. Cores were then split to collect high-resolution line-scan imagery. Subsequently, high-resolution magnetic susceptibility data were collected from each core using a point probe (Bartington MS2E high-resolution surface sensor) at 1-cm intervals and imaged with *X* radiography (Figs. 3–6). For the upper-

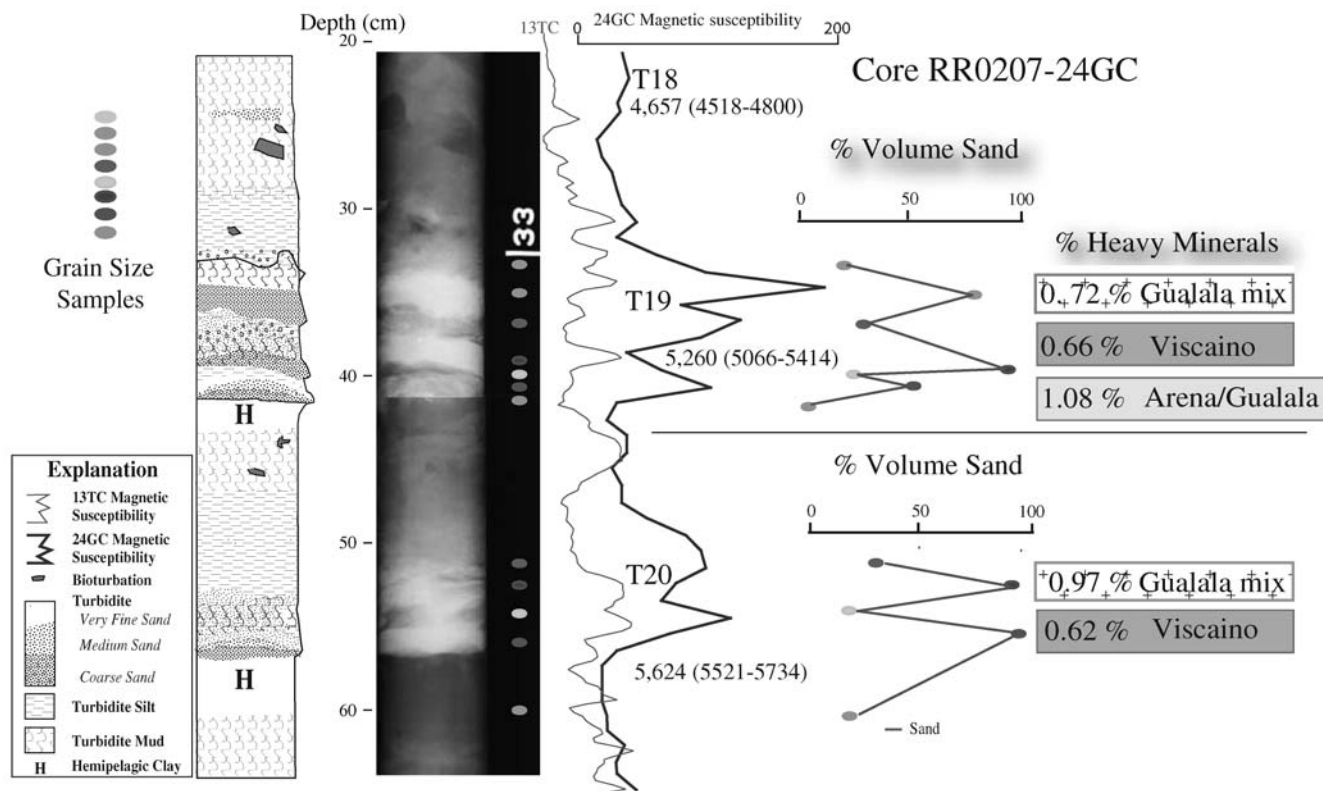


Figure 3. Example grain size analysis, magnetic susceptibility/density signatures and *x*-radiography in turbidites T19 and T20 in core 24GC below the Gualala–Noyo–Viscaino channel confluence (base of T18 is also shown; see Fig. 2 for location). Light tones in the *x*-radiograph represent dense sand/silt intervals; darker gray tones represent clay/mud. Oval dots are grain size samples. Heavy trace is the magnetic susceptibility signature. Right plot is percent sand (obtained with Coulter laser counter method). The good correspondence between grain size, density, and magnetic susceptibility for the lithologies in both Cascadia and NSAF cores is established with selected analyses, and permits use of density and magnetics as mass/grain size proxies that show much greater resolution than possible with grain size analysis. These typical turbidites are composed of 1-3 fining-upward sequences, each truncated by the overlying pulse. No hemipelagic exists between pulses, indicating the three pulses were deposited in a short time interval. Only the last pulse has a fine tail, indicating final waning of the turbidity current. We interpret these signatures as resulting from a single multipulse turbidity current. Number of coarse pulses commonly remains constant in multiple channel systems for a given event. Source provenance affinity for each sand pulse is shown to the right, and keyed to source regions in Figure 2.

most ~1 m, cores along the base of the continental slope along the NSAF were further sampled using point magnetics at a 3 mm spacing to compensate for a low latest Holocene sedimentation rate in those cores. Selected grain-size analyses for both regions were performed with a Coulter laser counter.

Cores were scanned using a GEOSCAN line-scan system using a 3×1024 -pixel charge-coupled device at 1-mm resolution. Color reflectance data (red, green, blue [RGB] traces) were extracted from the high-resolution imagery by averaging a 100-pixel swath across the core for each data point, and these were compiled down the core. Color reflectance is a common high-resolution physical property, which is useful when the stratigraphy has enough color contrast to be diagnostic of stratigraphic detail (Nederbragt *et al.*, 2006; Rogerson *et al.*, 2006). Unlike the other physical property measurements, color reflectance is highly influenced by the surface condition of the split core. Irregularities due to core splitting, smoothing of the core surface, water content, and other factors can influence the color data. Interpretation of the color data thus must be done when directly overlain on the color core imagery so as to remove such artifacts from consideration. Extraction of the RGB data from the imagery was done to best avoid these artifacts. While color reflectance has been commonly used to estimate chemical content, particularly of CaCO_3 (i.e., Lyle *et al.*, 2002), and hyperspectral imagery can extend this capability, we here use color reflectance for detecting the light–dark pattern resulting from alternating fine-grained mud turbidites (dark) and interbedded hemipelagic intervals (light).

Turbidite correlation is done using primarily magnetic susceptibility and density, much as e-logs are correlated in the oil industry (McCubbin, 1982; Lovlie and van Veen, 1995). Physical property correlations of this type are also common practice with academic and ocean drilling program/integrated ocean drilling program (ODP/IODP) cores (e.g., Fukuma, 1998) and have recently come into use for paleoseismology (i.e., Schnellman *et al.*, 2002; Abdelayem *et al.*, 2004; Goldfinger, Nelson, Johnson, Arsenault, *et al.*, 2004; Hagstrum *et al.*, 2004; Iwaki *et al.*, 2004; Karlin *et al.*, 2004; St-Onge *et al.*, 2004; Goldfinger *et al.*, 2007).

In addition to local site correlation, we have found that it is possible to correlate unique physical property signatures of individual turbidites from different sites within individual channels. This suggests that the processes controlling deposition of the turbidite maintain consistency for some considerable distance within a channel. We have also found it possible to correlate event signatures not only down individual channels and past confluences, but between channel systems separated by considerable distance, some of which never meet. These turbidite fingerprints form the basis of long-distance correlations and are beginning to be recognized and used for regional correlation (e.g., Lake Baikal, Lees *et al.*, 1998; off Morocco, Wynn *et al.*, 2002; Cascadia, Goldfinger, Nelson, Johnson, and Morey, 2003; the Laptev Sea: Russian Arctic, Rivera *et al.*, 2006; and elsewhere). Re-

cently, the event signatures of Cascadia turbidites have been linked to coastal fjord records on Vancouver Island (Dallimore *et al.*, 2005; Goldfinger, Morey, Erhardt, *et al.*, 2006).

Figure 3 shows a single representative turbidite in core 24GC, located below two channel confluences, that illustrates the multiple fining-upward sequences (Bouma A–C) that compose each turbidite. Typically, these sequences have only one fine tail (Bouma D) associated with waning of the turbidity current. The signatures we are correlating are comprised of these stacked coarse pulses. This figure shows in detail that the magnetic susceptibility, density, and grain size trends within each event are closely correlated. This is straightforward but important because we can, in most cases, use the high-resolution density and magnetic data as grain size proxies, at least for lithologies along the Cascadia and NSAF systems (Goldfinger, Nelson, Johnson, and Morey, 2003; Morey *et al.*, 2003; Wynn and Masson, 2003). Further details of the use of magnetics and density as grain size proxies are given in Goldfinger *et al.* (2007).

On close inspection of physical property logs, we sometimes see a remarkable similarity between correlative turbidites that are separated by as much as 500 km (Cascadia) and 280 km (NSAF). Figure 4 shows several typical examples of correlative events over a distance of 470 km along the Cascadia margin. We see a general correspondence of relative turbidite thickness downcore that is reflected in separate channels, as well as correlable details such as the number of coarse sandy pulses (density and magnetic peaks).

For example, Cascadia turbidite events T2, T10, and T12 are small events in all cores, whereas T11 and T16 are very large events in all cores, and many other events follow similar size patterns across both Cascadia and the NSAF margins. Vertical sequences of turbidite size and number of pulses are commonly preserved between remote sites, and were used to aid in the correlation framework. We observe similar patterns along the NSAF margin, where size trends and individual characteristics persist over large distances. Goldfinger *et al.* (2007) also show the evolution of a single event down channel over a distance of 74 km, showing the gradual merging of two sand pulses into a bimodal grain distribution. Stratigraphic correlation has the potential to establish links of individual events between core sites, independent of radiocarbon ages. Possible explanations for the correlation signatures are discussed in the following sections.

Radiocarbon Analysis. To date the turbidites, we extract Planktic foraminifers from the hemipelagic sediment below each turbidite. We do this because the boundary between the top of the turbidite tail and the hemipelagic sediment is difficult to identify, and bioturbation is concentrated at this boundary, possibly because the organic material brought down in the turbidite tail results in a benthic bloom (Smith *et al.*, 1993). Sensitivity tests for species-specific biases are presented in Goldfinger *et al.* (2007), as are the methods used to evaluate basal erosion. The close match and lack of consistent bias in ages between land and marine events observed

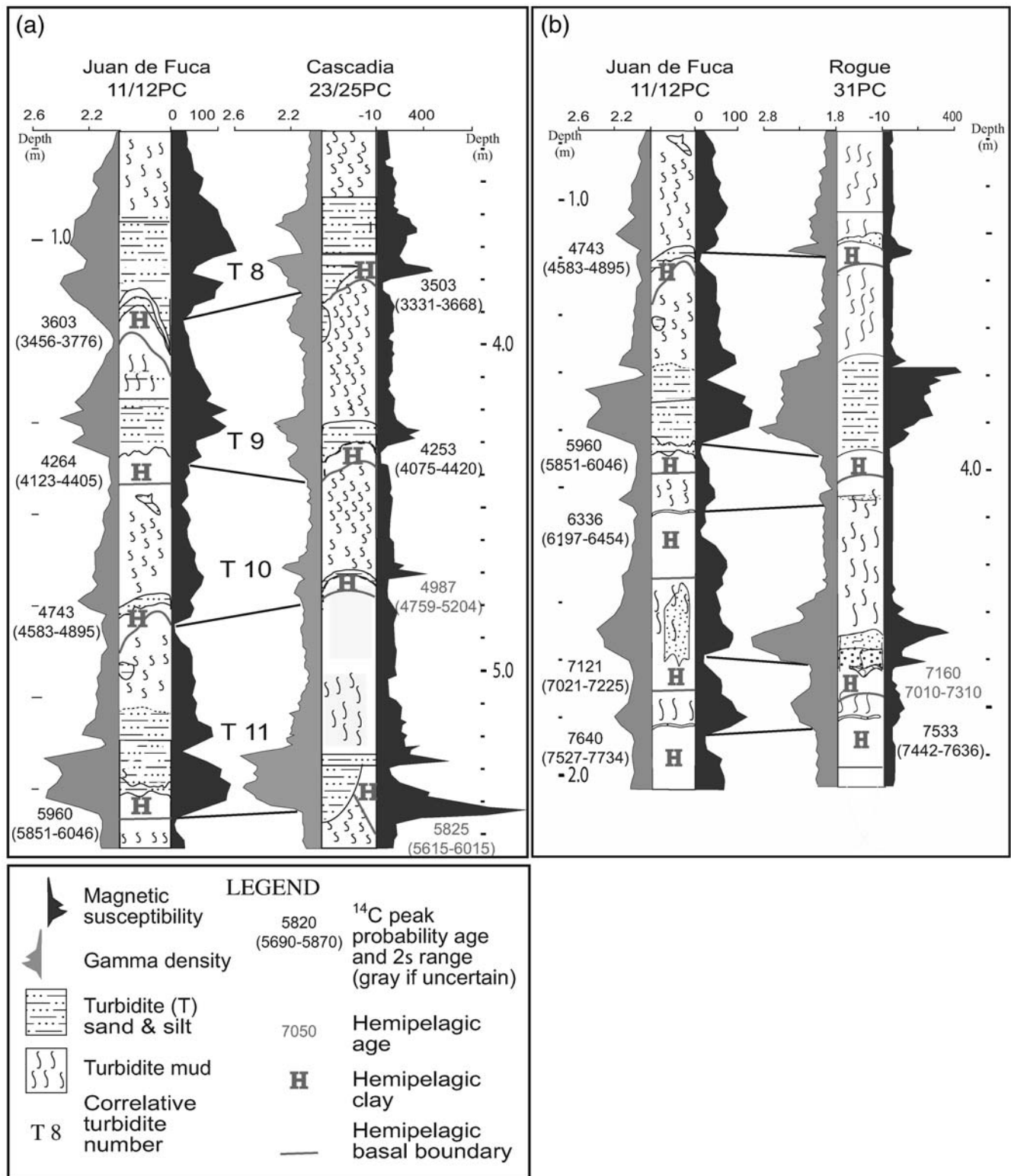


Figure 4. Correlation details from two representative pairs of cores on the Cascadia margin. (a) Events 8–11 in cores from Juan de Fuca Channel (left) and Cascadia Channel (right). Left traces are raw gamma density; right traces are magnetic susceptibility. Lithologic logs are also shown. The vertical scale is core depth in meters. Note correspondence of size, spacing, number of peaks, trends between events, and shape of physical property traces between these cores. (b) Events 10–14 in Juan de Fuca Channel (left) and Rogue Channel (right). In (a) cores are part of the same channel system; distance is 475 km. In (b) cores are in channels that do not meet; distance is 500 km. These are representative of full-margin events that are included in the southern margin correlation of Figure 6. Full correlation details presented in Goldfinger, Morey, Erhardt, *et al.* (2006a) and C. Goldfinger *et al.*, unpublished manuscript, 2007).

in both Cascadia and on the NSAF also suggests that neither bioturbation (Wheatcroft, 1992; Thomson *et al.*, 1995) nor basal erosion significantly bias ^{14}C ages derived from Planktic foraminifers in most cases. In several cases for Trinidad, Smith, and Klamath Channels, we dated benthic forams where Planktic foraminifers were not abundant enough to obtain a result. These ages were calibrated using the additional reservoir difference between benthic and planktic samples established locally for those cores in the 0–3000-yr time range. This method is similar to that used to establish the modern reservoir value (e.g., Hughen *et al.*, 2004).

Using a moving window average sedimentation rate, we corrected the original AMS ages for the radiocarbon sample thickness by subtracting the time corresponding to the thickness of the sample interval. Hemipelagic thickness was then converted to time for input into OxCal calibration software using the Marine04 database (Ramsey, 1995; Ramsey, 2001; Reimer *et al.*, 2004). A sedimentation-rate regression analysis was employed to flag erosion at a given interval and to provide a check for consistency downcore, as sudden hemipelagic sedimentation-rate changes in the marine environment are relatively rare (see the electronic edition of *BSSA*). Outliers in this analysis are most likely caused by basal erosion because ages appear to be older, with less sediment thickness between events than expected. To evaluate flagged outliers, we tested them for basal erosion by comparing the hemipelagic thickness of that interval among several closely spaced cores. In a few cases, multiple cores revealed that these anomalous intervals were the result of basal erosion on the core from which the sample was taken, based on a thinner hemipelagic section in only that core. If the dated interval was found to wholly or partially come from an interval suspected of erosion, and other dating options were exhausted, we calculated a corrected age based on the full hemipelagic thickness represented in the nearby cores. This correction applies to four samples in this study; the calculations and criteria are given in Table 2 in the electronic edition of *BSSA*. If more than one sample was used for the anomalous age, the correction was weighted by the proportion of the sample weights. See Gutierrez-Pastor *et al.* (2007) for a full discussion of these methods. To verify this type of correction, or to calculate the age of an undated turbidite, we can additionally calculate the age of the turbidite based on a dated turbidite below or above (or both if possible) the suspect/missing turbidite. The reference age above or below must be well dated at the suspect site and at other nearby sites to provide a stable reference. We can then calculate the age of the suspect event by adding the hemipelagic time to or subtracting it from the reference age to establish a calculated age for the event. This can also be done with OxCal, though the Bayesian calculation actually provides weaker constraints than those of the analytical solution using the full hemipelagic time constraint. We have included ages corrected by these methods where the erosion correction and the calculated age methods produce similar results (significant overlap at the 1-sigma level). These are indicated as

such in the tables and figures, with calculations given in Table 2 of the electronic edition of *BSSA*.

Goldfinger *et al.* (2007) illustrate use of OxCal to take advantage of multiple ages (if within analytical error of one another), including constraints imposed by the time represented by hemipelagic sediment between events. In one case (the penultimate NSAF event) we used the establishment of the first San Francisco mission in 1769 to restrict the age. Where age data are missing, sedimentation rates alone can be used to model event ages, which we have done for several events in our time series due to scarcity of foraminifers in those intervals. Figure 1 in the electronic edition of *BSSA* shows the analyses for the A.D. 1906 and the penultimate NSAF events, as well as the A.D. 1700 Cascadia event using OxCal with hemipelagic sedimentation and historical constraints. Using these well-known events, and time constraints provided by the hemipelagic sediment deposited in the interseismic period, OxCal returns the calendar age of the A.D. 1906 NSAF and A.D. 1700 Cascadia earthquakes to within a few years. The penultimate event is similarly constrained to a narrower time window than obtained by simple calibration. Further details of the OxCal analysis and the reservoir corrections applied are given in Goldfinger *et al.* (2007). Also of importance here is the significance of the probability peaks in the probability density functions (PDFs). Multiple peaks and broad distributions in the PDFs are generated largely from the slope of the atmospheric radiocarbon curves, and without other data, can only be treated statistically. For marine data in this study, we have both hemipelagic intervals that represent the time elapsed between turbidites, and sedimentation-rate curves that serve to further constrain the time of emplacement. The hemipelagic intervals represent time during which earthquakes are precluded and restrict the time intervals in which earthquakes could have occurred. Similarly, sedimentation rates derived from multiple cores at a site can be used to show that most events occur near the probability peaks, eliminating much of the probability tail and additional peaks in the case of multiples. Our data show that marine sedimentation rates vary little, and can be used in this setting to support the use of probability peaks as shown by Goslar *et al.* (2005). We show the NSAF PDFs and rate curve fit in Figure 2 in the electronic edition of *BSSA*. This method presently cannot be used in Cascadia because no individual site has a record with all or nearly all events dated.

Heavy Mineral Analysis. Broad provenance bins were determined from standard heavy-mineral analysis techniques. We sieved samples of coarse material from the sand fraction of selected turbidites, and separated the heavy minerals with tetrabromoethane (specific gravity is 2.9), separating light and heavy fractions. We then made grain mounts of the heavy mineral fraction with piccolyte (refractive index is 1.52) and point counted at least 300 grains, 200 being true heavy minerals.

Results: Southern Cascadia and Northern San Andreas Turbidite Record

Southern Cascadia Event Correlation

Stratigraphic Correlation. The ^{14}C age framework and stratigraphic correlation of Cascadia margin turbidites, supported by extensive onshore paleoseismic work, allow a relatively complete Holocene assessment of rupture lengths and timing of Cascadia events. A full documentation of the combined onshore/offshore analysis is presented in C. Goldfinger *et al.* (unpublished manuscript, 2007). In this article (© and in the electronic edition of *BSSA*), we present a subset of the Cascadia data and analyses focusing on the southern Cascadia margin during the past ~3000 yr in order to make comparisons between the southern Cascadia and NSAF time series.

The southern Cascadia margin has a paleoseismic record both onshore and offshore that differs from the record of the northern margin. Kelsey *et al.* (2005) and Nelson *et al.* (2006) present evidence for segmentation of the southern Cascadia margin. Our offshore record from southern Cascadia also suggests segmentation not initially recognized in Goldfinger *et al.* (2003a,b) and similar to that proposed by

Kelsey *et al.* (2005) and Nelson *et al.* (2006). We now recognize 19 paleoseismic turbidites correlated along the northern 2/3 of the Cascadia margin, one more than reported previously because one event was discovered to be a closely spaced couplet. All 19 events were originally correlated to Rogue Canyon. We now find that most of these events can be correlated southward to Klamath, Smith, and Trinidad Canyons (younger than 4000 yr) off northern California as well. We find evidence of additional events along the southern margin, some of which appear to extend north to Central Oregon, and others that extend approximately to the Rogue site only, involving northern California and southern Oregon. These events are smaller muddy turbidites that can be observed as magnetic and density signatures between the larger margin-wide events. These small events are also noted in the original core logs as darker intervals within what was initially logged as hemipelagic sediment between major turbidites. The origin of the darker intervals was initially unknown; however, we now interpret these darker intervals as fine-grained mud turbidites on the basis of stratigraphic correlation between sites, and more detailed lithologic examination. An example, event T2a, is shown in Figure 5 (we retain the original 18 event numbers to maintain consistency with

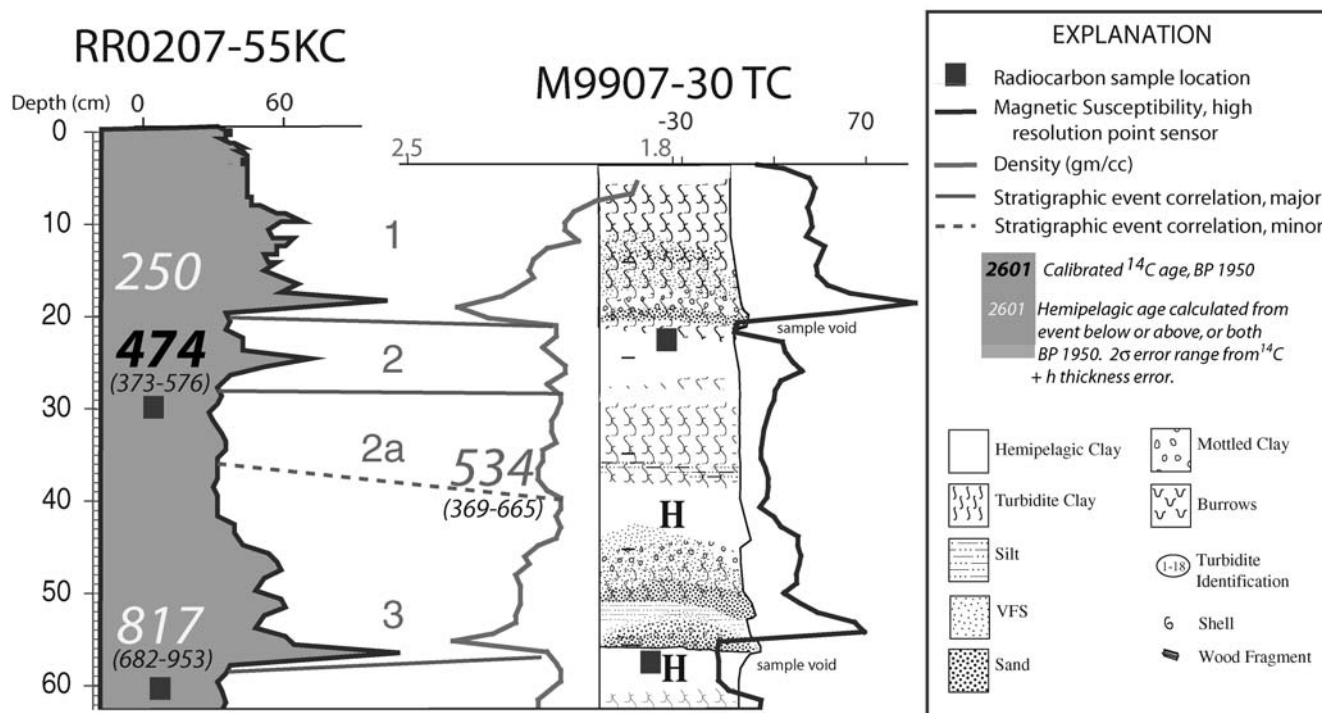


Figure 5. Grain size distribution for small southern event T2a. This event is representative of the smallest of the southern Oregon events correlated in this study. Detailed magnetic susceptibility and Gamma density records reveal a minor event between T2 and T3, which was originally logged as darker clay thought to be hemipelagic material. Closer inspection revealed this silt stringers and turbidite mud at this interval and also for T3a, T4a, T5a, T5b, and T6a. Similarity of small event grain size patterns between cores (magnetic susceptibility and density proxies), consistent appearance at the same intervals in multiple cores, and the observed silt/turbidite mud stringers supports interpretation of them as small mud/silt turbidites. Lithologic detail is composited from cores 55KC, 30TC, and 31TC. The vertical scale is core depth in centimeters. Ages calculated from adjacent ^{14}C ages shown with errors propagated from the radiocarbon age and the estimated error range for hemipelagic thickness. T1 (A.D. 1700 is 250 B.P. 1950) age assumed, not dated in this core. Regional correlation including this event is shown in Figure 6.

earlier publications, and insert smaller southern Cascadia events as a–c designations between margin-wide events in this study). Some of these weak events are not presently datable by ¹⁴C methods, and for these events we have calculated their ages based on hemipelagic intervals above or below well-dated larger events as described previously.

Figure 6 shows stratigraphic correlation and ¹⁴C ages for the Cascadia margin for the period 0–3000 yr B.P. Stratigraphic correlation of events is particularly good for the northern margin, with no events uncorrelated (i.e., appear in only one or two systems). For the northern margin, all events pass a strict synchronicity test, as they are found both above and below the confluence of Willapa and Juan de Fuca

Channels with no change in number of events above (or below) the Mazama ash datum. This synchronicity test is critical to the establishment of synchronous triggering, and thus to the establishment of earthquake origin. Further discussion of Cascadia and NSAF synchronicity tests can be found in Adams (1990), Goldfinger *et al.* (2003a,b), and C. Goldfinger *et al.* (unpublished manuscript, 2007). Stratigraphic correlation as shown in Figure 6 illustrates the recognizable fingerprints for individual events, which also can be observed on both sides of the Willapa–Juan de Fuca (JDF) confluence. This indicates that not only are individual turbidity currents merging to form one at the channel confluence, but that the fingerprints of individual events are preserved, im-

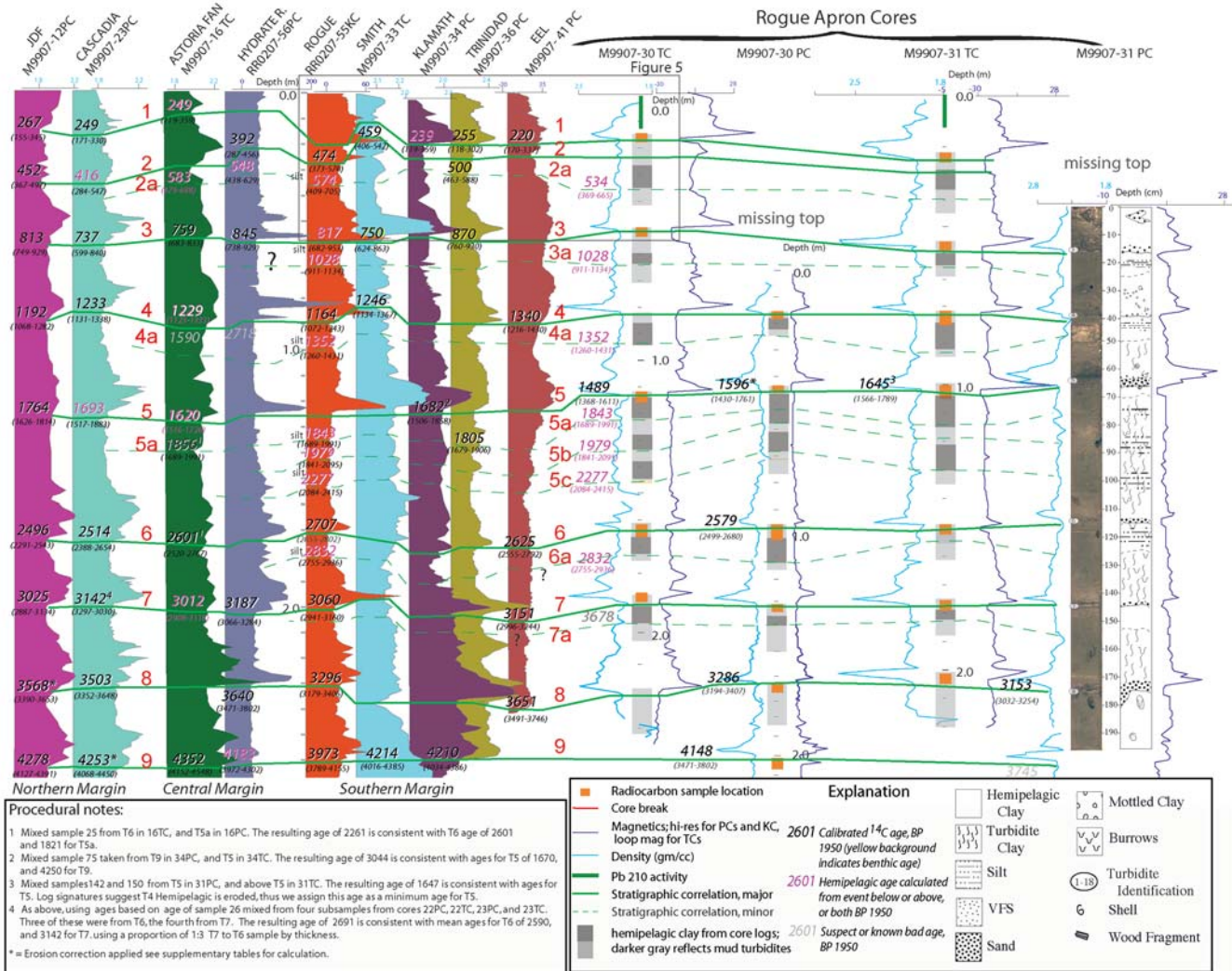


Figure 6. Correlation plot of marine turbidite core records and ¹⁴C ages along the Cascadia margin from the JDF Channel to Eel Channel for the most recent ~4200 yr. Stratigraphic correlation allows resolution of some of the ambiguities pointed out by Nelson *et al.* (2006) for Southern Cascadia events. Event ages are shown using probability peaks from OxCal calibrations and combines where multiple ages at a site are available. See Figure 9 for PDFs for these ages. Events and sites linked by stratigraphic correlations are shown by connecting lines. Full-margin events correlated using stratigraphy and ¹⁴C are shown thicker; local southern Cascadia events are thinner and dashed. The vertical scales for all cores are hung on the vertical scale of the Rogue cores, which are shown in expanded detail at the right. Relatively sparse dating of southernmost cores reflects low abundance of forams and thin hemipelagic intervals. Margin-wide event correlation represented by Juan de Fuca and Cascadia channel cores shown at left. Ages modified after Goldfinger *et al.* (2003a,b), Johnson (2004), and Gutierrez-Pastor *et al.* (2007) using additional data and analyses. Data in Figure 5 outlined by gray box.

plying that they were similar above and below the confluence. This further constrains the timing and increases the significance of the stratigraphic correlations in that the structure of the multipulse turbidity current that deposited the multipulse turbidite must have been similar in separate channels above the confluence, and must have survived the merging at the confluence.

Cascadia Time-Stratigraphic Event Correlation. Figure 7 shows a space-time diagram for the Cascadia margin for the past ~3000 yr, including the land and marine data used in this study as well as land data not included in the tabular age calculations. [Ⓔ] These data are also found in Tables 1–3 in the electronic edition of *BSSA*. This figure shows the time series of major Cascadia margin events interpreted as earthquakes recorded both onshore and offshore. The onshore events have been subjected to rigorous tests of earthquake origin that typically comprise rapid subsidence and sudden burial of marsh surfaces with tsunami sand. Details of the tests applied to individual sites are contained in the original literature. We favor the most recent work in which these tests and sampling methods are more robust than in the earlier works, and favor sites that have multiple well-constrained ages for each event, and ages that use seeds and needles over those that use peat-plant material. Event records vary somewhat in their preservation of events and in natural variability that comes from segmented margin ruptures. For events interpreted to be full-margin events based on the joint land/marine data, we use the best ages from sites along the margin to constrain event ages. For southern Cascadia events, we follow Kelsey *et al.* (2005) and Nelson *et al.* (2006) in attempting to clarify segmented ruptures through addition of the marine turbidite record.

The total number of events in the 3000-yr time range of this study, whether onshore or offshore, is similar, with a few differences noted here. The correspondence between offshore and onshore events in time is also striking. We suggest that the smaller events recorded offshore are in some cases the same events recorded onshore, though we cannot with certainty demonstrate this link. Some of the smallest events offshore likewise are represented by a spotty or absent record onshore. While this reduces our confidence in these events, it is also consistent with smaller earthquakes leaving a more discontinuous geologic record. We also note that the smaller turbidites offshore correspond reasonably well to the local southern Oregon events where they have been dated. In some cases, these turbidites cannot be dated directly, but have hemipelagic ages similar to onshore earthquakes, and lie in time ranges constrained by bracketing turbidite ages that also have corresponding onshore earthquakes. These earthquakes have limited rupture length in both onshore and offshore records, suggesting a first-order compatibility between offshore turbidite size, shaking intensity or duration (controlling turbidite volume), and rupture length. The offshore rupture limits reflected in the Figure 6 correlation are derived

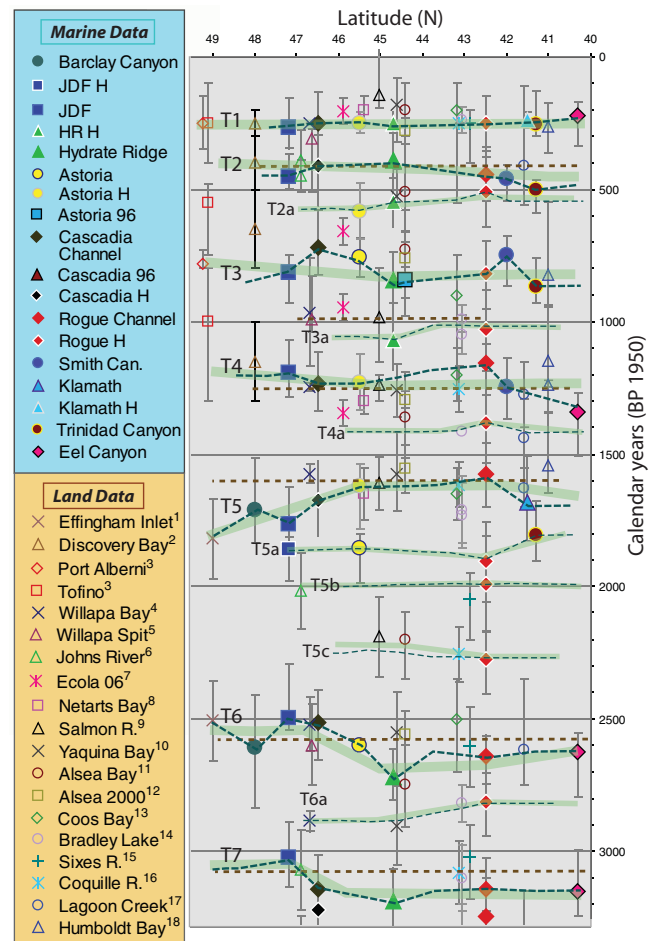


Figure 7. Space-time diagram for the Cascadia margin showing land and marine data for the past ~3300 yr. Filled symbols are marine turbidite data; open symbols are land paleoseismic data. Blue dashed lines show stratigraphic correlation of the turbidite data. Smaller southern Cascadia events are shown with thinner dashed lines. Site localities shown by symbology; locations shown on Figure 1. Marine symbols surrounded by white border are ages calculated from events above, below, or both using hemipelagic thickness and sedimentation rates. Green bars are best-fitting marine age trends for Cascadia earthquakes. Marine trends show space and time variant trends in some locations and time ranges due to reservoir age variability, further discussed in text. Best-fitting combined land/marine trends shown in brown dashed lines where reservoir effect is apparent. [Ⓔ] Land data and numbered sources and marine data are in Tables 1 and 2 of the electronic edition of *BSSA*, respectively.

from our interpretation of the combined land/marine data shown in Figure 7.

Offshore, the turbidite record gives a positive stratigraphic method of determining rupture length, limited by the uncertainty in triggering distance between canyons (estimated to be less than 90 km for full-margin events, and almost certainly less for smaller events, Goldfinger *et al.*, 2007) and uncertainties in correlation. ¹⁴C ages for offshore events also provide constraints on rupture lengths. Onshore, the constraints are weaker because individual events cannot be correlated directly. The links between onshore events are thus mostly based on ¹⁴C with some additional constraints

from the stratigraphic sequences at the land sites. In no cases do we find land events extending beyond the latitude limits of the marine record. In most cases, latitude limits are similar, but in a few cases, such as T2, the marine correlatives extend to greater latitude limits. Several of the smaller events in the marine record apparently have no land equivalents (T2a and T6a). These are the smallest of the marine events, with narrow latitude limits; thus, we suggest that the marine record is likely more sensitive to these small events. Limited rupture lengths and presumably magnitudes for these events may lack sufficient stress drop to generate significant tsunami or land subsidence, though they apparently do generate small correlatable marine turbidites. Alternatively, these small offshore events may not correlate as we infer, and would then be uncorrelated local events of no significance in the marine earthquake record. Although the correlation evidence and limited ^{14}C ages for these events make them less robust than the larger events, their appearance at the same intervals in numerous cores from isolated environments in Cascadia basin channels and slope basin cores makes such a coincidence unlikely.

Cascadia Rupture Modes. From the combined land/marine stratigraphic and radiocarbon data, we infer that in contrast to the northern margin, the southern Cascadia margin records a total of 38 probable earthquakes (10,000-yr record, Goldfinger, Morey, and Nelson, 2006) that are correlated between multiple sites, and thus define a mean recurrence interval for the southern Cascadia margin of ~ 260 yr in the Holocene,

and a recurrence interval of 215 yr during the ~ 3000 -yr period considered in this study. The combined stratigraphic correlations, hemipelagic analysis, and ^{14}C framework represented in the correlation figures, the space-time diagram, and the supplementary tables can be summarized in Figure 8, which shows groupings of rupture lengths supported by the combined onshore and offshore records. We show the most recent 3000-yr period relevant to this article. For this 3000-yr interval, and considering the uncertainties in the southern rupture limit, we consider four rupture lengths as shown in Figure 8, which include the event numbers as shown in Figures 6 and 7 corresponding to the four modes. Overall, the Holocene record suggests that the Cascadia margin effectively has five rupture modes (refined from the four shown in Goldfinger, Morey, Erhardt, *et al.* [2006]): 19 full- or nearly full-length ruptures (50%), 2 ruptures comprising the central and southern half of the margin (5%), and 17 smaller southern margin ruptures that have three general groupings of rupture length (45%) during the Holocene. The southern limits of each rupture are not as well constrained as the northern limits; thus, rupture mode D could include other events, or may be the same as mode C. Interestingly, the northern limits of the shorter southern ruptures appear to terminate at three major structural uplifts known as Nehalem, Heceta, and Coquille Banks. Brudzinski and Allen (2007) have recently suggested that episodic tremor and slip (ETS) events down-dip on the subduction interface may also terminate at these same latitudes (Fig. 8). Two other boundaries suggested by

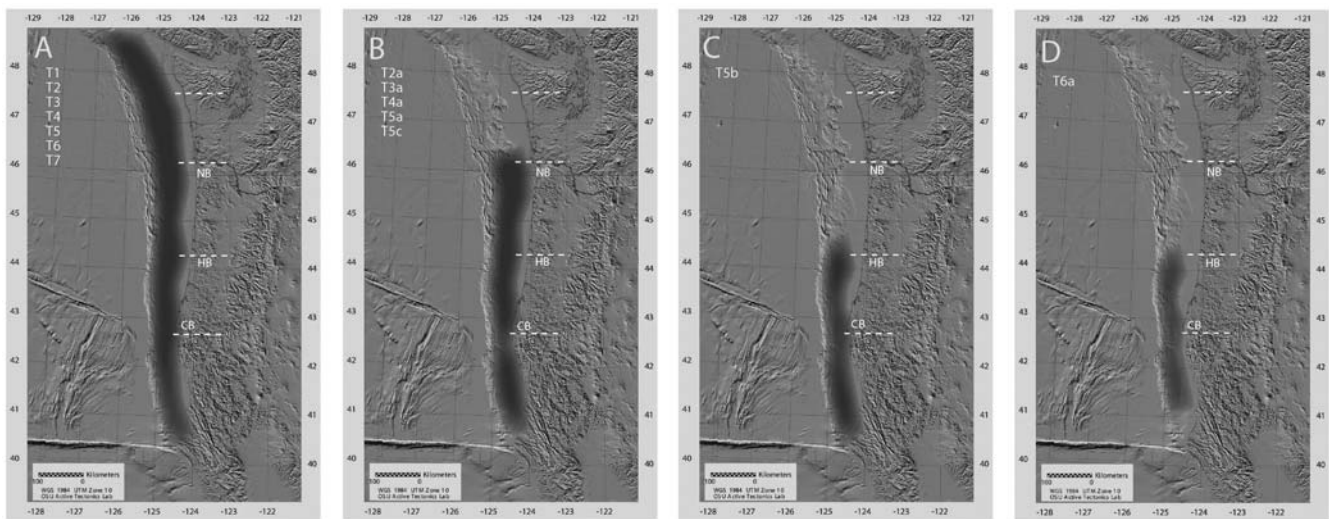
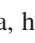
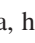


Figure 8. Late Holocene rupture lengths of Cascadia great earthquakes for the ~ 3000 -yr period discussed in this article. Four panels showing preliminary rupture modes identified using turbidite correlation. (a) Full rupture, represented at all sites by seven events. (b) Mid-southern rupture, represented at all sites as far south as 40.7°N by five events. (c) Southern rupture from central Oregon southward to at least 41°N , represented by one event. (d) Southern Oregon/northern California events, represented by one event. (e) Slightly varying southern limits from turbidite data shown the same here are given in Table 4 of the electronic edition of *BSSA*. Rupture terminations appear to occur at three forearc structural uplifts: Nehalem Bank (NB), Heceta Bank (HB), and Coquille Bank (CB). Approximate updip and downdip limits from Clarke and Carver (1992), Goldfinger *et al.* (1992, 1996), Oleskevich *et al.* (1999), and Goldfinger (2007). Paleoseismic segmentation shown corresponds well to the latitudinal boundaries of episodic tremor and slip (ETS) events proposed for the downdip subduction interface (Brudzinski *et al.*, 2007). These boundaries are shown by white dashed lines. A northern segment proposed from ETS data does not appear to have a paleoseismic equivalent.

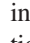
ETS recurrence periods for Washington seem not to correlate with paleoseismic evidence presented here.

NSAF Event Correlation

We have added color data analysis to the correlation of events along the length of the NSAF margin presented in Goldfinger *et al.* (2007). Color analysis is of greater resolution than the magnetic or density traces, with scan lines of 1 mm; however, these data are subject to surface irregularities on the surface of the split core. Nevertheless, for many intervals, the detailed color traces offer additional correlation ties and strengthen the stratigraphic framework. The correlation is made within a ^{14}C -age framework, with some vertical stretching of cores required due to varying sedimentation rates.

Goldfinger *et al.* (2007) show a regional correlation of NSAF turbidite stratigraphy spanning the Holocene. Here we focus on the upper ~2800 yr of record, making use of high-resolution magnetic susceptibility data (3-mm spacing, point sensor) and color reflectivity data. Our Noyo Canyon cores, 49PC and companion Kasten core 54KC, are particularly important because unlike all the other channel systems, Noyo Canyon is actually cut and offset by the NSAF. Most likely for this reason, the turbidite record there is expanded in thickness, making investigation of the details of each event much clearer in those cores. Cores to the south have much reduced sedimentation rates, even though they are closer to the Russian River source, the largest river along the north coast section of the NSAF. Possible reasons for this are discussed in Goldfinger *et al.* (2007). By comparison to the robust Noyo record, most of the events along the NSAF in other channels are subdued, and indeed the upper 10 events shown in these figures are very fine silt turbidites not visible to the naked eye. Their unique signatures in the physical property data, however, allow good correlation between sites.  We have collapsed a much larger set of core records onto the representative correlation diagrams shown in Figure 3 in the electronic edition of *BSSA*. A key stratigraphic datum in this correlation is T11, which is a robust event correlated and visible as a sandy turbidite in all cores, dated at 2574 (2397–2681) yr B.P. in Noyo Channel, and 2256 (2080–2401) yr B.P. in Gualala Channel. We suspected that the original ^{14}C age for this event (~2600 yr B.P.) was too old (possible basal erosion) and have used constraints from hemipelagic sedimentation rates surrounding this interval to estimate the ~2100-yr B.P. age in  Figure 3 of the electronic edition of *BSSA* (Goldfinger *et al.*, 2007).

As in Cascadia, correlation of individual events based on the grain size distribution represented by the magnetic and density data are possible both along strike and down channel. Robust event signatures that can be recognized both within single channels, between multiple channel systems, and above and below confluences support the inference that they in fact represent the same source events, independent of other methods. We observe that the correlated events retain

their essential character, typically made up of a stack of coarse pulses, for considerable distances along the margin. The signatures are observed to evolve downstream where coarse pulses merge with distance from the margin. The event signatures also evolve to some extent along strike in some cases, although in other cases stratigraphic sections at opposite ends of the fault system match as well as close neighbors. These properties can be observed through close inspection of Figures 3–6,  Figure 3 of the electronic edition of *BSSA*, and Goldfinger *et al.* (2007).

NSAF Confluences and Mineralogy. At the site of core 24GC, below several confluences of Viscaino, Noyo, and Gualala Channels (confluences shown in Fig. 2), we find that multiple coarse pulses reveal the heavy mineral assemblage from individual canyon sources, stacked vertically in order of arrival at the core site. The turbidites at this site also have no hemipelagic sediment between the sand pulses, indicating little time passage between the deposition of the pulses (see the timing discussion later in this article). The alternative, removal by erosion, is possible, but would have to occur at each turbidite base at every correlative site. Further downstream, we observe bimodal heavy mineral coarse fractions, with mineralogical peaks representing the separate provenance components (Goldfinger, Nelson, and Johnson, 2004). We observe no significant changes in the stratigraphy between upstream and downstream sites, despite input from multiple sources at the confluences. Further downstream at the site of core 31PC, we find that individual turbidites have the same stacking of coarse pulses, but the provenance input is less distinct, suggesting further mixing downstream. This can also be observed directly in the downstream evolution of each turbidite. Goldfinger *et al.* (2007, fig. 3) show a typical example of a two-pulse turbidite as the two pulses begin to merge along the 74-km distance between the proximal and distal cores. This evolution is expected as the turbidity current wanes and originally separated internal structures become less distinct downstream. Goldfinger *et al.* (2007) show stratigraphic correlation details for a series of cores upstream, near, and downstream of the confluences of Viscaino, Noyo, Gualala, Albion, and Cordell Channels. The data span the time period from ~3500 to ~10,000 yr B.P. because the upper section is poorly preserved in some of the downstream cores. The downstream cores have, as yet, only a few dated turbidites, in part due to the low foraminifer abundance at water depths in excess of 3500 m at these sites. The section ages are bounded by several late Pleistocene ages, and the age of 4676 (4525–4810) yr B.P. for T18 in core 26PC, which we use to constrain the upper part of the correlation.

While additional ^{14}C ages are still needed, we can test for synchronicity by carefully matching events between upstream cores at Noyo and Gualala Channels and correlative events in the downstream cores in this time range. We matched the stratigraphy and checked for presence/absence of hemipelagic sediment between events (or an erosive event

that removed it), as well as the multiple cues used in physical property based stratigraphic correlation. We observe that upstream (49PC) and downstream cores (e.g., 25GC) both contain 22 events in this time range. Differences between the two are minor, and appear mostly attributable to local basal erosion. Included in the confluence analysis of Goldfinger *et al.* (2007) is a correlation with core 31PC, which is actually below a total of four confluences, with input from a total of six channels, while cores 24GC, 25GC, and 26PC each sample three channels. The good correlation between these cores suggests that input mixing at each confluence has little effect on the stratigraphy of the turbidites, even though the number of sources increases at each confluence. We infer that synchronous triggering is the only viable explanation for this, and are unable to suggest an alternative. Nonsynchronous triggering should produce an amalgamated record that increases in complexity below each confluence, with only partial correlations, if any, for the synchronous events. The mixing and stacking of the provenance components further suggests synchronous arrival at the confluence.

We observe that while the overall stratigraphy of the turbidite sequence is maintained through confluences, the internal complexity and stratigraphic thickness of some events actually increases for distal cores, just the opposite behavior expected for distal sites where thinning and homogenization of turbidites would be expected. We attribute this to the reinvigoration and addition of new material injected at each confluence, and potentially to the slight mistiming of coarse pulses expected due to variable travel times for channel tributaries.

From these results, we infer that the events and sites included in this analysis pass a strict test of synchronicity, and are most likely of earthquake origin. Further analysis of the remaining confluence sites is in progress. A similar use of mineralogic provenance to fingerprint source channels and test for earthquake origin has been used in the Sea of Japan by Shiki *et al.* (2000).

NSAF Radiocarbon Time Series and Comparison to Onshore Paleoseismic Sites. In terms of event ages and their distribution in time, the youngest 15 NSAF events have a mean repeat time of ~ 200 yr, with a standard deviation of 60 yr. Using peak probability density function (PDF) values for event ages, the minimum interval value is ~ 95 yr between T7a and T7 and T12a and T12, and the maximum value is ~ 270 yr between T5 and T6 and T10–T11 (we refer to the third event as T3–4 because it is a doublet that may yet prove to be two events). We find these values reasonably consistent with previous paleoseismic data onshore. The ages shown in Figure 9 include 11 ages reported by Zhang *et al.* (2006) from the Vedanta Marsh site, two ages reported by Knudsen *et al.* (2002) at Bodega Bay and Bolinas Lagoon, and five ages reported by Kelson *et al.* (2006) from sites at Fort Ross. The PDF curves for ages in Figure 9 are color shaded to represent the time interval constraint from the hemipelagic sediment between events. The center (dark) part

of the PDF represents the unconstrained part of the PDF, and the two outward lightening shades represent 100% and 75% of the full hemipelagic constraint as used in OxCal. These constraints cannot strictly trim the distributions because they are not completely independent constraints (the sedimentation rates depend on the ^{14}C ages); however, the position of these constraints is part of the OxCal output when the ages and hemipelagic constraints are input in stratigraphic order.

These results indicate that the penultimate event probably occurred between A.D. 1700–1750 north of San Francisco. The mean age for this event from all sources is indistinguishable from A.D. 1700. The age correspondence between NSAF land and marine data is good for the last ~ 2300 yr when comparing Noyo Canyon marine ages to Vedanta Bolinas and Fort Ross land ages. For a given time interval when individual land records overlap with the marine record, we see approximately the same total number of events (± 1) onshore and offshore, suggesting either a coincidence or that land and marine sites are recording the same events. Further support for a linkage between the turbidite series presented here and onshore earthquakes, is the good correspondence between land and turbidite recurrence intervals, which are 200 and 240 yr for marine and land ages, respectively. Individually, most ages except Noyo T3–4 (a doublet) and T7a have significant overlap of age ranges (Fig. 9). Tom Fumal (T. Fumal, personal comm., 2007) reports that an additional event has been found in a new trench at Vedanta, which may correspond to the second event in our T3–4 couplet. Our event T3–4 was not reported at Fort Ross, and our event T9 was apparently not observed at Vedanta. Our current stratigraphic correlation and age series, taken together, suggest that the previous 11 events may be correlated from Noyo Canyon to at least to the latitude of Vedanta, just north of San Francisco. Our initial along-strike correlations imply rupture lengths for many (or most) events of > 250 km. Other events may well have occurred, but without being recorded (or yet discovered) either offshore or onshore.

Temporal Association of Southern Cascadia and NSAF Earthquake Series

Cascadia-NSAF Temporal Comparison

The average recurrence interval for the southern Cascadia margin in the last ~ 3000 yr (ignoring the slightly different southern rupture limits) is 223 yr ($(3154 \text{ (average age of T7)} - 250)/13 = 223$ yr). The similarity between the mean NSAF recurrence time and the southern Cascadia recurrence (~ 200 offshore, 230 onshore versus ~ 223 yr, respectively) and the relatively close correspondence between the A.D. 1700 Cascadia event and the penultimate NSAF event, at A.D. ~ 1700 –1760, prompted us to examine both the temporal connection between the two fault systems and the potential stress interactions between them. In Figure 9, we plot the NSAF time series over the past ~ 3000 yr with Cascadia events shown using both peak probability and PDF functions for offshore turbidite ages and onshore paleoseismic data.

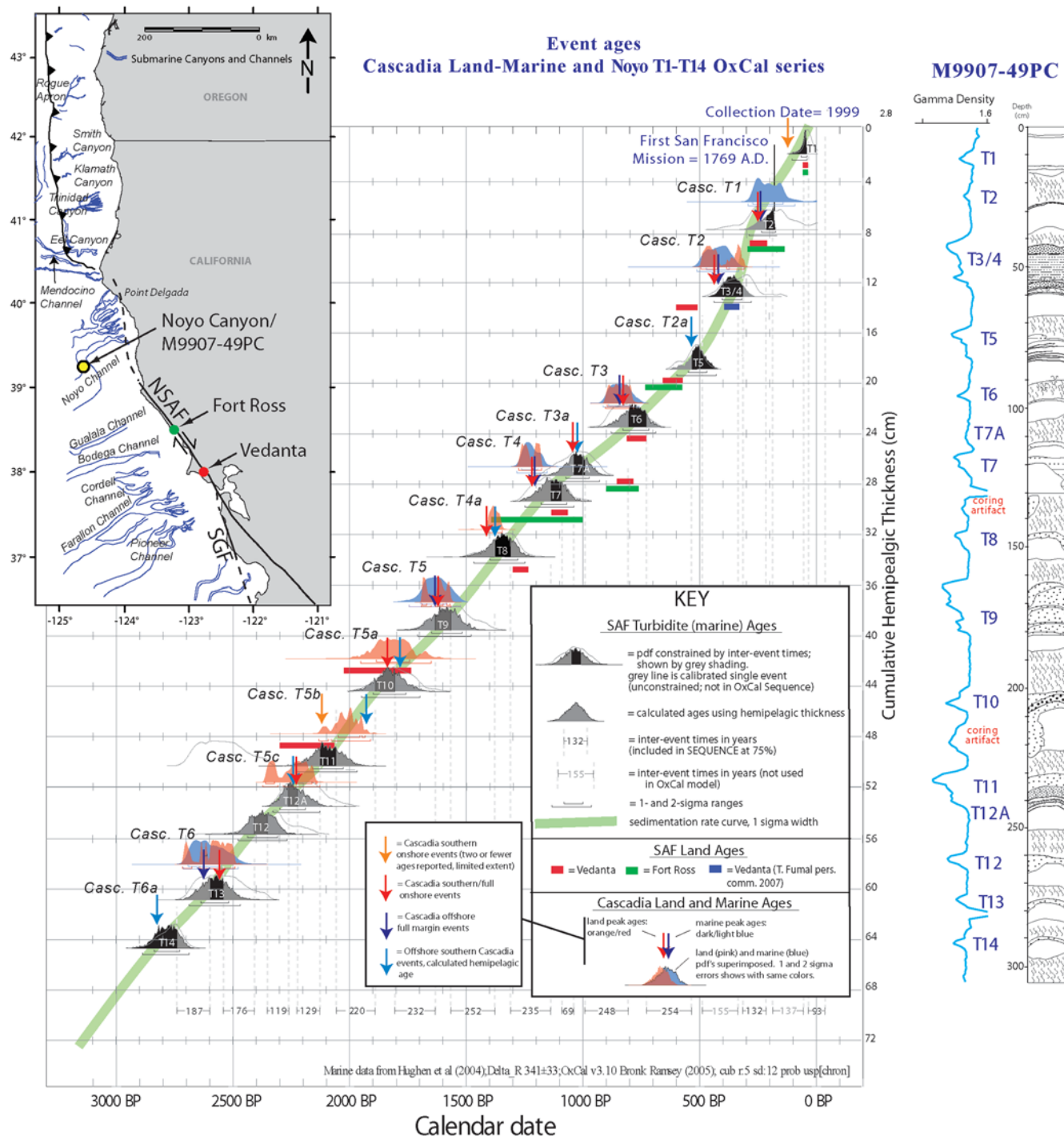


Figure 9. OxCal age model for the youngest 15 events in the NSAF offshore system, onshore NSAF ages, and comparison to Cascadia event ages. Cascadia OxCal PDFs are shown in blue. Land ages from OxCal combines are shown in red. Cascadia mean event ages are also shown with blue arrows for well-dated turbidite events, light blue arrows for hemipelagic age estimates, and red arrows for onshore paleoseismic events. See text for discussion and tables for data used and criteria, and discussion of temporal relationships. Intervent times based on hemipelagic sediment thickness (represented by gray segments of NSAF PDFs) were used to constrain original NSAF ^{14}C calendar-age distributions (gray traces) using the SEQUENCE option in OxCal. Intervent times were estimated by converting hemipelagic sediment thickness between each pair of events to time using the sedimentation rate. Events dated more than once were combined in OxCal prior to calibration if results were in agreement; if not in agreement, the younger radiocarbon age was used in the final model. Five ages are calculated from sedimentation rates where not enough forams were present for ^{14}C dating. The resulting probability distributions (filled gray) are mostly in good agreement with land ages from Fort Ross except for T3–4 and T7a (green lines; Kelson *et al.*, 2006), Vedanta (red lines; Zhang *et al.*, 2006), Bolinas Lagoon and Bodega Bay (purple lines; Knudsen *et al.*, 2002), and Point Arena (light blue lines; Prentice *et al.*, 2000). Additional Vedanta event is also shown (T. Fumal, personal comm., 2007). See inset for geographic locations. The vertical scale is cumulative hemipelagic sediment thickness. © See the electronic edition of BSSA for OxCal input data and further detail of sedimentation-rate curve.

For Cascadia marine events that have multiple ages for the same event, we first exclude outliers, then combine the well-correlated ages using the Bayesian method in OxCal. The statistical merging of the PDFs for these events yields a narrower PDF for a single event dated independently with multiple samples. For land ages, we use the combined land-marine dataset to determine the best ages to use for this study based on their reported error ranges, the fit of the reported age to the larger dataset, and the fit of the age within the data reported by the original authors for land data. In most cases we have adopted the rationale used by the original authors to report their preferred ages for each event. In some cases we have further culled multiple ages to remove outliers. ⑤ The ages selected for use in this study and original references are given in Table 1 of the electronic edition of *BSSA*. Since the full original data were not always published, we have obtained the lab data from original authors and recalibrated the ages used in OxCal, yielding a more consistent representation of single and combined ages. In two cases, there are land ages reported for which there are only one or two reported ages and no observed turbidite evidence. These are shown with separate symbology in Figure 9. These could either be spurious bad ages in the land record, or a real event of limited spatial extent not observed in the marine record.

In addition to the close correspondence between the Cascadia A.D. 1700 earthquake, and the penultimate NSAF event ~1700–1760 and recurrence intervals noted previously, we also see an apparent coincidence of Cascadia events and NSAF events occurring at approximately the same time for 12 and possibly 14 of 15 NSAF earthquakes (Fig. 9; Goldfinger *et al.*, 2007). During the 0–3000-yr period, the combined onshore/offshore paleoseismic record for Cascadia includes 12 events, and 2 possible additional events. The thirteenth event is recorded by significant subsidence in Eel River Basin in the early 1800s, though it is not observed elsewhere and not known in the offshore paleoseismic record, which is only poorly known at Eel Channel at present (Carver and Plafker, 1999; Carver, 2000). The fourteenth event is one that includes three reported land ages (two of high quality) in the range 2100–2255 yr B.P. in central and southern Oregon, and a small turbidite event. This event, T5c, is undated offshore, but we include a calculated age based on the hemipelagic sediment accumulated above well-dated T6 (Fig. 6).

To a first order, the recurrence intervals for southern NSAF and Cascadia (200 versus 220) are quite similar, and clearly distinct from northern Cascadia (496–526 yr; Goldfinger, Morey, Erhardt, *et al.*, 2006; C. Goldfinger *et al.*, unpublished manuscript, 2007). If we include the uncertain 1800s event described previously, the average repeat time for southern Cascadia would be 212 yr over the last 3000 yr. For the 15 NSAF events, we observe that with the exception of NSAF event T12 (and the weaker associations of T12 and T1), the remaining NSAF earthquakes each have a corresponding Cascadia event in temporal proximity. The relationship can be seen graphically in Figure 9. The question arises then: Is this similarity in time series coincidental?

While considerable uncertainty exists in comparing ^{14}C ages, the marine record brings significant advantages in terms of constraining event ages. First, we have focused on several key cores from both systems in which the majority of the events are dated, and thus are constrained to be in stratigraphic order (also true for land sites). The remaining event ages come from cores that have been stratigraphically correlated. This constraint is significant and reduces the possibility of miscorrelation that plagues onshore paleoseismology, though of course is subject to errors of interpretation. In Figure 9 we summarize the two time series and the relationship between them. For all NSAF events, we have used the relaxed hemipelagic constraint (75% of the calculated time interval) in the OxCal calculations. In the figure, we show this graphically by shading the portions of the PDF that fall within these time intervals, and thus are less likely to contain the time of the event. The PDFs themselves reflect the relaxed constraint, but statistically do not terminate abruptly at these boundaries. Full constraints using hemipelagic data for the Cascadia margin are not used in this study, and await completion of the reservoir model discussed in a subsequent section of this article.

We can examine the temporal relationship (if any) between the NSAF and southern Cascadia by several methods: the relationship of mean ages, peak probability ages, and probability distributions. We have calculated the means from the midpoint in the 2-sigma ranges for Cascadia events in several groupings: the mean for offshore correlated events, the mean for onshore events thought to correlate, and the combined means. These, along with the probability peak ages are given in Tables 1 and 2, which include comparisons to the NSAF data. ⑤ The ages used and sources are given in Tables 1–3 in the electronic edition of *BSSA*. We use ages calculated from marine sedimentation rates for only a few cases where the event was not datable or the number of ^{14}C ages for a given event was low. Several of the smaller local southern-Cascadia-inferred events could not be dated with ^{14}C , and for these events we calculate the age based on well-constrained bracketing events above and below, using hemipelagic thickness and the local sedimentation rate.

Comparing raw means for 12 events for which we can make a comparison, the Cascadia turbidite events differ from NSAF events by an average 36 yr (S.D. 28 yr), with 12 means preceding NSAF and three virtually identical. The time interval by which NSAF events preceded Cascadia is 150 yr, larger by a factor of ~4 (Table 1; ⑤ Fig. 4 in the electronic edition of *BSSA*). For events interpreted to be the same events onshore (excepting Cascadia T2a and T6a, which may not be observed), 9 of 12 Cascadia peak ages precede NSAF events, with three ages nearly identical, yielding an average delta of 37 yr (S.D. 42 yr). The alternate hypothesis of NSAF precedence yields a mean delta of 202 yr, greater by a factor of ~5 (Table 2). Comparing peak and midpoint PDF ages from marine-correlated ages combined with OxCal where possible yields a slight narrowing of the delta to 37 and 26 yr, respectively, or 159–170 yr for NSAF preceding Cascadia, larger by

Table 1
Comparison of Marine NSAF Ages with Marine OxCal Combined Ages and Peak Single Ages from Cascadia Marine Data

NSAF Event No.	NSAF Mean Peak Age	Cascadia Event No.	Mean Peak Turbidite Age	Marine OxCal Combine		Marine OxCal Peaks		Marine OxCal Mid		Marine Peak Means		
				Peak	Mid	Predate Delta	Postdate Delta	Predate Delta	Postdate Delta	Predate Delta	Postdate Delta	
1	44											
2	230	1	246	250	205	-20.0	115	25.0	160	-15.5	119	
3-4	365	2	425	410	388	-45.0	100	-23.0	122	-59.6	85	
5	510	2a	512							-2.4	263	
6	775	3	800	815	830	-40.0	215	-55.0	200	-25.4	230	
7a	1030	3a	1030*							-0.1	105	
7	1135	4	1214	1240	1232	-105.0	100	-97.0	108	-79.4	126	
8	1340	4a	1384							-43.9	206	
9	1590	5	1682	1535	1557	55.0	295	33.0	273	-91.9	148	
10	1830	5a	1856*							-25.5	239	
11	2095	5b	?									
12a	2250	5c	2277*							-27.0	103	
12	2380											
13	2570	6	2601	2640	2610	-70.0	130	-40.0	160	-30.6	169	
14	2770	6a	2812							-42.5		
		7	3130	3210	3210							
						Mean delta	-37.5	159.2	-26.2	170.5	-37.0	149
						S.D.	53.9	79.2	49.3	59.8	28.3	62

*Calculated age. Delta is defined as the time difference (years) between NSAF and Cascadia earthquakes.

Table 2
Comparison of Cascadia Land Ages, Combined Cascadia Land-Marine and Cascadia OxCal Combines with NSAF Marine Event Ages

Onshore Mean Cascadia Age	Cascadia Event No.	Land Mean		OxCal Peak Land			Combined Land-Marine Mean	Predate Delta	Postdate Delta	With Prototype Reservoir Model Turbidite Age	With Prototype Reservoir Model Peak Means	
		Predate Delta	Postdate Delta	Age	Predate Delta	Postdate Delta					Predate Delta	Postdate Delta
120		-76.0	110									
250	1	-20.0	115				247.8	-17.8	117.2	246	-15.5	119
448	2	-83.0	62	335	30.0	175.0	436.3	-71.3	73.7	425	-59.6	85
No record?	2a									530	-20.3	245
846	3	-70.8	184	690	85.0	340.0	823.1	-48.1	206.9	787	-11.9	243
1050	3a	-20.0	85				1040.1	-10.1	94.9	1030	-0.1	105
1217	4	-81.7	123	1200	-65.0	140.0	1215.5	-80.5	124.5	1198	-63.1	142
1428	4a	-87.5	163	1385	-45.0	205.0	1405.7	-65.7	184.3	1384	-43.9	206
1622	5	-31.7	208	1685	-95.0	145.0	1651.8	-61.8	178.2	1585	5.1	245
1808	5a	22.0	287	1820	10.0	275.0	1831.8	-1.8	263.2	1856	-25.5	239
2120	5b	-25.0	130	2000	95.0	250.0	2120.0	-25.0	130.0	1842		
2228	5c	22.5	343	2220	30.0		2252.2	-2.2		2277	-27.0	
2560	6	10.0	210	2580	-10.0	190.0	2580.3	-10.3	189.7	2501	69.4	269
No record?	6a									2712	57.5	
3021.25	7									3050		
	Mean delta	-36.8	202	Mean delta	4.4	215.0	Mean delta	-39.4	156.3	0	-11.2	190.0
	S.D.	41.9	83	S.D.	64.6	69.0	S.D.	30.0	60.6		40.7	69.4

a factor >4 (Table 1, 2-sigma ranges given in Table 3). Land OxCal peaks differ from the NSAF by an average of 4 yr (but S.D. is large at 65) and 215 yr for predate and postdate, respectively. Combined land/marine Cascadia mean ages differ from NSAF events by an average of 39 yr, with 11 preceding and 5 events nearly identical in age (Table 2). The mean postevent delta is 156 yr, larger by a factor of ~ 4 . The preceding deltas calculated by five methods are all statistically indistinguishable from one another considering the associated error budgets, as are the postdate deltas.

Comparison of the PDFs for Cascadia and NSAF events in Figure 9 shows that the PDFs of most events from both regions have overlap at the 95% level; however, the time between events represented by hemipelagic sediment, and shown in the figure, reduces considerably the probability that earthquakes occurred in the low probability portions of the PDF. Regionally, most events for each system are also precluded from overlap by virtue of being in stratigraphic order in a single core, or well correlated between cores for the marine data. The detailed comparison of ^{14}C ages is of course fraught with multiple uncertainties, and should be considered with caution.

One additional uncertainty is the reservoir correction applied to marine ages to obtain calendar ages (Stuiver and Braziunas, 1993). This value, representing the age of the seawater populated by microfossils we use to date the turbidites, is a published spatially varying value specific to west-coast sites. The published value is derived usually from paired shell/wood dates that establish the age of the water in which some shelled animals lived with stratigraphically correlated terrestrial material. The published values are almost exclusively from the twentieth century, though it is known that these values change through time (i.e., Kovanen and Easterbrook, 2002). We have observed probable time and space variant mismatches between land and marine ages for the

same earthquake events, for earlier periods of time, and have attempted to map the variability using the numerous ages from the land and marine earthquake record as part of an ongoing separate investigation. This mapping is included in Table 2 of the electronic edition of *BSSA* and shown graphically in Figure 7. If we apply this prototype reservoir model to our marine ages, we find that in addition to tighter groupings of land-marine ages, which would be expected, the mean delta between the NSAF and preceding Cascadia earthquakes is reduced to 11 yr. For Cascadia, following the NSAF, the delta is 190 yr, larger by a factor of >17 . Application of this prototype reservoir age mapping is not included in Figure 9; however, its application appears promising and is included in Table 2 for comparison.

The age series in total suggest a temporal relationship between Cascadia and NSAF events that does not appear to be random and strongly favors Cascadia earthquakes preceding the NSAF. The alternate relationship that Cascadia events consistently postdate NSAF events is possible as well, though the average time separation would be greater by a factor of 4–6. We also note that the Cascadia ages for offshore events may change somewhat as a result of better definition of the marine reservoir correction in the future, and this may help close the gap for some time and latitude ranges for which the modern correction appears to be inadequate.

Dynamic Links between the Cascadia Megathrust and the NSAF

Coseismic and Postseismic Deformation from Cascadia Earthquakes

In order to quantify the influence of Cascadia earthquakes on the NSAF, we model the coseismic and postseismic deformation from the Cascadia earthquake. First we verify the geometry of the NSAF system, which has only

Table 3

Summary of Error Ranges for OxCal Marine-Combined Data

NSAF Event Number	NSAF 2-sigma Ranges	CASC OxCal 2-sigma Ranges	Cascadia Event Number	Turbidite Age	Cascadia Marine 2-sigma Ranges
T1	39.5–104.5				
T2	169.5–289.5	101–287	1	246	155.3–328.3
T3/4	279.5–439.5	298–460	2	425	325.5–503.1
T5	429.5–599.5		2a	512	
T6	689.5–879.5	742–907	3	800	684.3–916.3
T7A	929.5–1119.5		3a	1030	
T7	1039.5–1249.5	1162–1287	4	1214	1113.4–1328.4
T8	1249.5–1469.5		4a	1384	
T9	1479.5–1709.5	1527–1731	5	1682	1542.8–1783
T10	1699.5–1949.5		5a	1856	
T11	1969.5–2229.5		5b	?	
T12A	2129.5–2329.5		5c	2277	
T12	2269.5–2479.5				
T13	2469.5–2689.5	2480–2706	6	2601	2497.5–2756.7
T14	2689.5–2889.5		6a	2812	
		3090–3321	7	3130	3027.2–3263.4

been poorly mapped previously. Offshore, the NSAF traverses the continental shelf between Point Arena and Point Delgada and was mapped using early seismic reflection profiles (Curry and Nason, 1967). In 2004, we collected multi-beam bathymetric data and several 3.5-kHz profiles across the offshore NSAF. We used these data and a newly released dataset of migrated industry multichannel reflection profiles to verify that the NSAF indeed traverses the shelf and comes ashore again at Point Delgada (Fig. 10) and verify the original mapping of Curry and Nason. We also observe some additional compressional deformation, particularly within the northeast part of the Viscaïno block, but are unable to evaluate this deformation in terms of recency and rates, and thus we do not consider it in the subsequent modeling.

We model the elastic coseismic deformation, deformation from deep afterslip, and 60 yr of postseismic deformation resulting from viscoelastic relaxation of elastic stress changes due to the earthquake in the mantle. We initially assume that the entire subduction zone slipped in a megathrust event such as the A.D. 1700 earthquake (Satake *et al.*, 1996; Goldfinger *et al.*, 2003a; Satake *et al.*, 2003) and also model a smaller southern-margin earthquake.

The first-order slip model involves 14 m of slip on each of the 16 planes spanning the 1050-km-long megathrust rupture and 7 m of slip on the 8 deep afterslip planes. The elastic coseismic and postseismic deformation is calculated in a layered spherical geometry using the method of Pollitz (1996). The geometry of the megathrust rupture is based on the plate-interface model of Flueck *et al.* (1997), and the elastic structure of the Earth is based on the seismically determined global Earth model, Preliminary Reference Earth Model (PREM; Dziewonski and Anderson, 1981). The modeled earthquake has a magnitude of M_w 9.1 based on the fault geometry, slip values and Earth model. Viscoelastic deformation is calculated on a spherical Earth using the method of Pollitz (1992). We use the preferred spherically layered Earth model presented by Pollitz *et al.* (2006) for a study of postseismic deformation following the 2004 and 2005 Sumatra megathrust events, which employs a biviscous (Burgers body) viscoelastic rheology in the asthenosphere (Pollitz *et al.*, 2006). In this model, the asthenosphere has an initial short-term viscosity of 5×10^{17} Pa s that dominates the deformation during the first few years and a long-term viscosity of 1×10^{19} Pa. This model matches both the spatial pattern and temporal evolution of the first year of postseismic Global Positioning System (GPS) measurements in Southeast Asia. The modeled postseismic surface velocities after several decades of transient deformation are also of similar magnitude as those currently measured along the rupture zones of the great 1960 Chile (Hu *et al.*, 2004) and 1964 Alaska (Zweck *et al.*, 2002) earthquakes.

Figure 11a,b,c shows the far-reaching surface displacement fields (only displacements < 0.3 m are shown) from the coseismic and postseismic deformation models. The horizontal coseismic displacements near the updip end of the rupture approximate the 14 m of modeled slip and decrease

to about 2 cm in the San Francisco Bay Area (Fig. 11a; ⑤ Fig. 5 in the electronic edition of *BSSA*). Coseismic displacements exceeding 0.1 m extend for up to 500 km to the east and west of the rupture. The vertical displacements from our coseismic model are to a first-order compatible with the subsidence observed and estimated from coastal marsh studies for the 1700 earthquake (compiled in Leonard *et al.*, 2004). Detailed matching of subsidence data is made problematic however by the complexities of the onshore accretionary wedge in southern Cascadia, the unknown slip distribution of the 1700 earthquake, the multiple subsidence methodologies used, and the weak constraints imposed by these methodologies. The horizontal surface displacements resulting from deep afterslip peak at about 2.5 m and are between 2–3 cm in the Bay Area (Fig. 11c; ⑤ Fig. 6 in the electronic edition of *BSSA*). The cumulative motions from mantle relaxation in the first 60 yr of postseismic relaxation exceed 0.1 m to distances greater than 1000 km. The horizontal viscoelastic displacements at the surface peak at about 1.65 m and are between 0.15–0.25 m in the Bay Area (Fig. 11b; ⑤ Fig. 7 in the electronic edition of *BSSA*). However, except for the segment offshore from Point Delgada, the NSAF is located in a low-strain lobe for both the coseismic and postseismic deformation.

Stress Changes from Cascadia Earthquakes along the NSAF

We evaluate the stress changes along the NSAF associated with coseismic and postseismic deformation from Cascadia megathrust events in order to test the possibility that Cascadia earthquakes triggered subsequent NSAF events. We model the Coulomb failure stress (CFS), which takes into consideration both shear- and normal-stress changes across the NSAF. Previous studies have shown that CFS increases of 1–3 bars are generally sufficient to trigger seismicity (e.g., Stein and Lisowski, 1983; Toda *et al.*, 1998; Rydelek and Sacks, 1999; Freed, 2005). We use a CFS function given by $CFS = \Delta\tau + \mu' \Delta\sigma_n$, which defines CFS as a sum of the change in shear stress τ and the change in normal-stress σ_n , multiplied by an effective coefficient of friction μ . Positive CFS enhances loading on the right-lateral NSAF. CFS is modeled on 48 NSAF receiver-fault segments at 10 km depth, based on the geometry of the 1906 earthquake rupture (Thatcher *et al.*, 1997), assuming $\mu' = 0.4$. CFS values are also computed for a ~ 100 -km-wide zone along the NSAF, assuming the same receiver-fault geometry.

Deformation and stress changes from megathrust earthquakes are large and far reaching (e.g., Banerjee *et al.*, 2005; Nalbant *et al.*, 2005). Significant postseismic deformation transients due to viscous relaxation in the mantle further expand the reach of fault interactions and are likely to persist for many decades (e.g., Pollitz *et al.*, 1998, 2006). The magnitude of CFS change on a nearby fault depends on the relative position, its orientation, and distance to the earthquake source. Thus, stress changes along the NSAF due to a Cas-

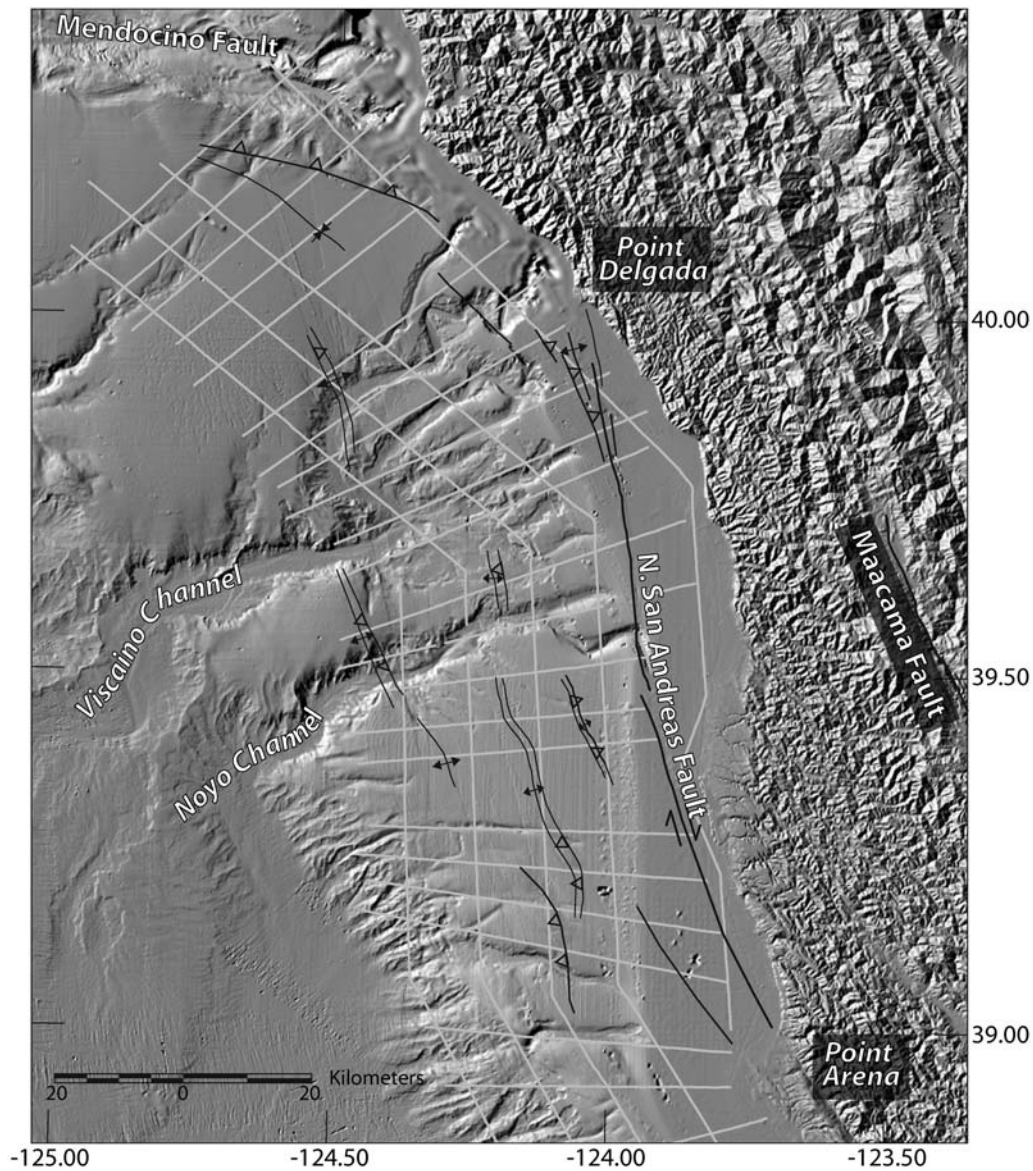


Figure 10. Shaded relief image and structure map of the offshore NSAF region. NSAF trace was mapped using multibeam bathymetry from Point Arena to Point Delgada, and recently released industry multichannel seismic reflection profiles (tracklines shown in gray). Re-mapping main offshore trace shows original mapping by Curray and Nason (1967) to be correct, and main trace comes ashore again at Point Delgada. NSAF offsets and captures the head of Noyo Canyon at the N in the San Andreas fault. Additional details of the fault trace show modest stepovers and additional deformation of the northeast Viscaino block.

cadia megathrust rupture and subsequent relaxation vary significantly along the fault due to both changes in distance and strike of the fault, ranging from N55W to N1W. Overall, we find that coseismic CFS changes are large and likely to enhance subsequent rupture only on the northernmost segment of the NSAF (Fig. 12a). CFS changes along the remainder of the fault are modest, as the NSAF lies in a nodal lobe of coseismic deformation. Postseismic viscous relaxation appears to reduce CFS along much of the NSAF and can therefore not be considered as a significant triggering mechanism in this case. Future work will evaluate if consideration of three-dimensional heterogeneity of Earth rheology significantly changes this conclusion.

The coseismic deformation increased CFS at 10 km depth by a maximum of about 9 bars in the section of the fault near Point Delgada (Fig. 12a). The CFS resulting from the viscous deformation peaks at about 2.5 bars; however, this peak is in the northernmost region of the fault where there is a large negative coseismic CFS (Fig. 12c). Postseismic afterslip both increases and reduces CFS along the NSAF, but its negative peak reduces the extent of the largest positive coseismic CFS by half (Fig. 12b).

We also compare our uniform-slip full-margin earthquake model with coseismic and postseismic CFS changes resulting from a southern Cascadia earthquake approximating the smaller southern events from the paleoseismic record. We

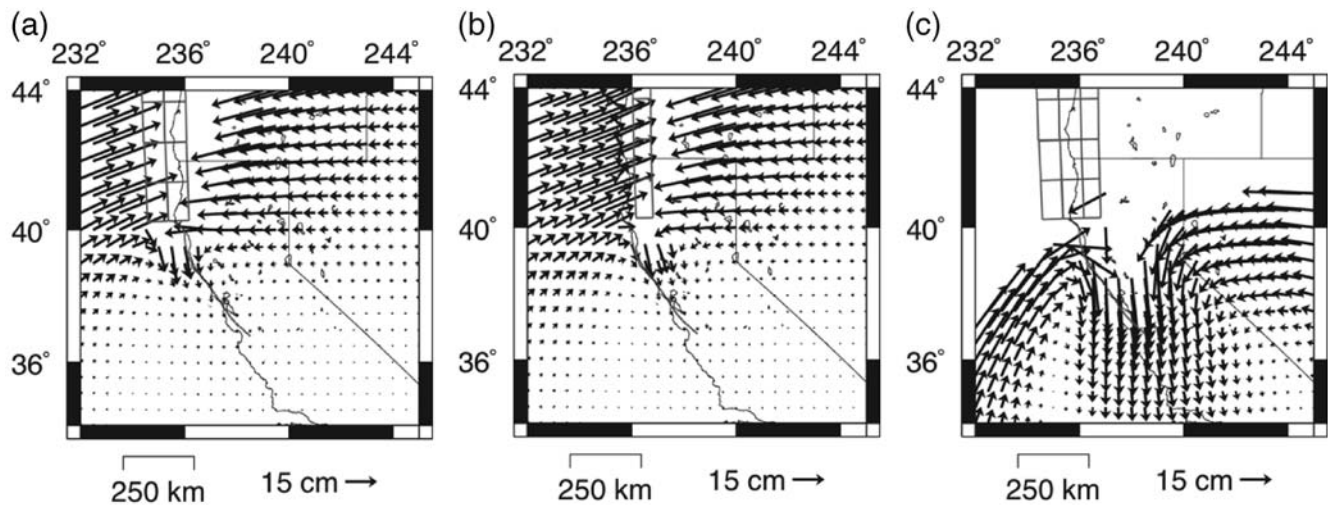


Figure 11. Comparison of the far-field coseismic and postseismic deformation for displacements less than 30 cm at the surface (absent grid points have displacements greater than 30 cm). © See the electronic edition of *BSSA* for total displacement fields. (a) Coseismic deformation from Cascade megathrust. (b) Displacement from afterslip on the Cascade megathrust. (c) Cumulative viscoelastic displacement after 60 yr from Cascade megathrust and afterslip.

apply 8 m of slip on the six southernmost Cascade fault planes (380 km strike length) and from a heterogeneous full-margin earthquake that includes less slip on the southern fault planes (Pollitz *et al.*, 2008). Total CFS on the NSAF from both the southern Cascadia earthquake and the heterogeneous full-margin earthquake peaks in the same northern location as from the homogenous full-margin model; however, the CFS peaks are reduced by about a factor of 2. Based on these results, it appears that the most likely nucleation point of a triggered NSAF event, from whichever of the three Cascadia source models, would be near Point Delgada. The coseismic CFS alone would be large enough to trigger an earthquake, while the postseismic contributions from the viscous relaxation and afterslip do not significantly increase the total CFS on the NSAF. This result suggests a directivity to many past NSAF ruptures that is opposite to that of the south–north rupture in 1906, one of the few events that was not preceded by a Cascadia earthquake.

In addition to subduction earthquakes, we also examine the possible contribution from significant triggered slip on the Mendocino transform fault (MTF), the Little Salmon fault (LSF), or the Mad River fault (MRF). A triggered earthquake on the MTF might be expected shortly following a Cascadia earthquake because CFS on the western segment, at 10-km depth, is always positive and peaks at over 40 bars, while CFS changes on the eastern segment fluctuate greatly between about -1000 and 1000 bars. The MRF is not likely to be triggered by the Cascadia subduction zone, as CFS at 10-km depth is always negative with a negative peak of more than -60 bars. A Cascadia megathrust earthquake may trigger an LSF earthquake, as the CFS increases by up to ~ 100 bars, and is at least 10 bars for more than 10 km on the offshore part of the thrust fault. Our first-order slip models for the LSF and MTF consist of 2 m of uniform slip based

on their characteristic earthquake magnitudes (Clarke and Carver, 1992; McCrory, 1996; Petersen *et al.*, 1996). The combined coseismic and postseismic CFS from 2 m of slip on the LSF peaks at 0.1 bars and would not significantly increase CFS on the NSAF (Fig. 12e). The CFS change on the NSAF from the MTF is highly dependent on the strike and location of the MTF rupture; the 270° striking western segment would only increase CFS on the NSAF by a maximum of 0.4 bars, whereas slip on the 285° striking eastern MTF segment would increase CFS on the offshore NSAF by as much as 30 bars (Fig. 12e). However, the CFS increase from the eastern MTF is located in the northernmost section of the NSAF, where there is a comparably larger decrease in CFS resulting from the combined coseismic and postseismic deformation from the Cascadia earthquake. Therefore, although the eastern MTF on its own could significantly increase CFS on the immediately adjoining, northernmost portion of the NSAF, it would not significantly extend the region of positive CFS when combined with the Cascadia megathrust earthquake.

We also tested the reverse triggering scenario and modeled CFS on the Cascadia receiver planes from an NSAF-type earthquake using a distributed slip model for the 1906 earthquake (Thatcher *et al.*, 1997). The maximum positive coseismic CFS on the southern tip of the margin is about 20 bars at depths between 12–16 km (Fig. 12f). At these depths, CFS increases of at least 1 bar extend north for about 30–40 km. The CFS resulting from viscoelastic relaxation is mostly negative on the southern Cascade receiver planes. This may be sufficient to trigger an earthquake on southern Cascadia or on the smaller upper plate thrust faults, such as the MRF and the LSF, although the 1906 event failed to do so. The paleoseismic record, however, strongly favors the former case, with Cascadia events preceding the NSAF by ~ 50 yr, whereas

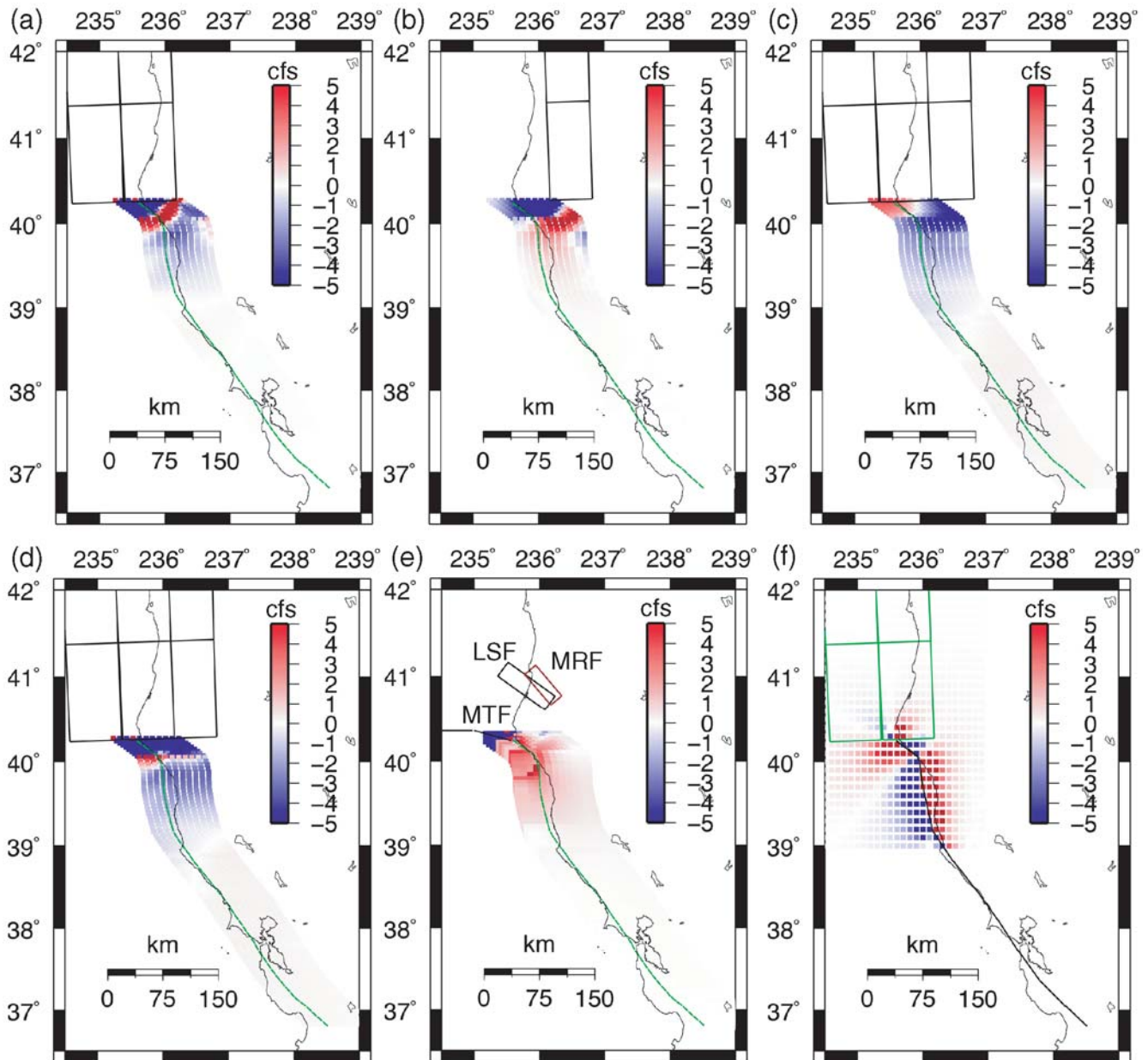


Figure 12. Comparison of CFS changes (bars) at 10-km depth on the NSAF from (a) coseismic deformation, (b) afterslip, (c) 60 yr of viscoelastic relaxation, (d) combined coseismic, afterslip, and viscoelastic relaxation, and (e) coseismic deformation and viscoelastic relaxation from MTF and LSF. Fault segments in black are source faults; green segments signify receiver faults. (f) CFS change on the Cascadia receiver faults from an NSAF earthquake.

Cascadia earthquakes follow NSAF events on average by 150 yr.

Could the temporal relationship between Cascadia and the NSAF be due to some of the turbidite events actually being the same source events, recorded on both sides of the triple junction? Indeed, it is possible that the thin mud turbidites could have been triggered in southern Oregon canyons by the NSAF and bear no relationship to Cascadia events. We consider this possibility less likely than Cascadia triggering, as the required triggering distances from the northern tip of the NSAF to Rogue (220 km), Klamath

(180 km), and Trinidad (130 km) Canyon heads are 50%–240% greater than the 90-km distance from southern Cascadia to Noyo Canyon. Since Cascadia events did not trigger Noyo turbidity currents (see previous explanation and Goldfinger *et al.*, 2007), we consider NSAF triggering of Rogue, Smith, Klamath, or Trinidad Canyon turbidity currents unlikely. Triggering in the poorly known Eel Canyon may be possible, though the uppermost turbidite there has an age of ~233 yr (2σ 188–350), consistent with the A.D. 1700 Cascadia earthquake and suggesting no 1906 triggering occurred there. We note that the smaller undated events appear to be

more robust southward from Smith to Klamath to Trinidad canyons, which could support NSAF triggering. However, this equally well could be due to southward increases in submarine drainage areas or river discharge and sediment supply for these systems. In any case, only two of the thin mud turbidites that are not reported at both Cascadia land and marine sites are part of the post 3000-yr correlation shown in Figures 6 and 7. All other events are correlated too far north in Cascadia, and likely coincide with tsunami and subsidence deposits on land, precluding any connection to the NSAF. Similarly, the NSAF events are correlated southward for over 250 km both stratigraphically and more indirectly by their temporal relationship to land event ages from the Fort Ross, Vedanta, and Bolinas sites, making any direct triggering by Cascadia earthquakes unlikely.

Conclusions

We have tested the turbidite record along the Cascadia and NSAF continental margins for synchronous triggering of turbidity currents as a method for determining the origin of these deposits, whether from earthquake or other sources. We have used ^{14}C ages, relative dating tests at channel confluences, and direct correlation of physical properties to determine whether turbidites deposited in separate channel systems are correlative, that is, whether they were triggered by a common event. The NSAF late Holocene turbidite record examined thus far has passed these tests, and can be correlated with multiple proxies along multiple canyon systems from the MTJ to offshore San Francisco. Correlations of the youngest 10 events are improved by addition of color reflectance data to the geophysical proxies used for stratigraphic correlation.

Preliminary comparisons of our event ages with existing and in-progress work at onshore sites show good correspondence, further circumstantial evidence that the offshore record is primarily earthquake generated. During the last ~2100 yr, we observe 11 most likely correlative turbidites, including one likely generated by the 1906 earthquake, that can be traced between Noyo Canyon, near the MTJ, and Cordell Channel near Point Reyes. Using combined constraints from physical property correlation, radiocarbon ages, and interevent sedimentation, we conclude that it is likely that at least 8 of 11 NSAF events recorded both onshore and offshore in the past 2100 yr have rupture lengths of at least 250 km and extend from the MTJ region to near the latitude of San Francisco.

Onshore and offshore paleoseismic records from the Cascadia subduction zone suggest that margin-wide and segmented southern Cascadia earthquakes precede NSAF events by ~0–80 yr, averaging 25–45 yr for 13 of 15 probable earthquakes or 87% of NSAF events in the past 3000 yr, with two additional Cascadia events too poorly constrained for comparison. On the other hand, NSAF events precede Cascadia

earthquakes on average by ~150–200 yr, most likely too long for a stress change effect.

Modeling of the static coseismic and both viscoelastic and afterslip-induced postseismic stress changes suggests that coseismic stress changes from Cascadia earthquakes are more than sufficient to trigger NSAF events, if they nucleate along the northernmost section of the NSAF near Point Delgada.

Acknowledgments

We thank the officers and crew of the Scripps vessels R/V Melville and R/V Revelle and the members of the 1999 and 2002 scientific parties. We thank David Schwartz, Mary Lou Zoback, Tom Fumal, Tina Niemi, Fred Pollitz, Alan Nelson, Rob Witter, Harvey Kelsey, and many others for insightful discussions on the NSAF and Cascadia faults; Alan Nelson, Tom Fumal, and Rob Witter for sharing unpublished data; and Harvey Kelsey and anonymous reviewers for thoughtful reviews that resulted in numerous improvements to the paper. We gratefully acknowledge funding by the U.S. National Science Foundation, Earth Sciences Division and by the U.S. Geological Survey National Earthquake Hazards Reduction Program. The authors acknowledge WesternGeco and the U.S. Geological Survey (USGS) for providing the seismic reflection data for the purpose of this research. Neither the data provider nor the USGS warrant the use of these data, nor make any claims or guarantees as to the accuracy of the data identification, acquisition parameters, processing methods, navigation, or database entries.

References

- Abdelayem, A. L., K. Ikehara, and T. Yamazaki (2004). Flow path of the 1993 Hokkaido-Nansei-Oki earthquake seismoturbidite, southern margin of the Japan Sea north basin, inferred from anisotropy of magnetic susceptibility, *Geophys. J. Int.* **157**, 15–24.
- Acharya, H. (1992). Comparison of seismicity parameters in different subduction zones and its implications for the Cascadia subduction zone, *J. Geophys. Res.* **97**, 8831–8842.
- Adams, J. (1990). Paleoseismicity of the Cascadia subduction zone: evidence from turbidites off the Oregon-Washington margin, *Tectonics* **9**, 569–583.
- Ando, M., and E. I. Balazs (1979). Geodetic evidence for aseismic subduction of the Juan de Fuca plate, *J. Geophys. Res.* **84**, 3023–3027.
- Argus, D., and R. Gordon (2001). Present tectonic motion across the Coast Ranges and San Andreas fault system in central California, *Geol. Soc. Am. Bull.* **113**, 1580–1592.
- Atwater, B. F. (1987). Evidence for great Holocene earthquakes along the outer coast of Washington State, *Science* **236**, 942–944.
- Atwater, B. F., and E. Hemphill-Haley (1997). Recurrence intervals for great earthquakes of the past 3500 years at northeastern Willapa Bay, Washington, *U.S. Geol. Surv. Profess. Pap.* **1576**, 108 pp.
- Banerjee, P., F. Pollitz, and R. Bürgmann (2005). The size and duration of the Sumatra-Andaman earthquake from far-field static offsets, *Science* **308**, 1769–1772.
- Brown, R. D. (1995). 1906 Surface Faulting on the San Andreas fault near Point Delgada, California, *Bull. Seismol. Soc. Am.* **85**, no. 1, 100–110.
- Brudzinski, M. R., and R. A. Allen (2007). Segmentation in episodic tremor and slip all along Cascadia, *Geology* **35**, 907–910.
- Carver, G. A. (2000). Paleoseismic geology of the southern part of the Cascadia subduction zone Penrose conference: great Cascadia earthquake tricentennial (program summary and abstracts), Oregon Department of Geology and Mineral Industries, Seaside, Oregon, 38–39.
- Carver, G. A., and G. Plafker (1999). Cascadia subduction zone segmentation in the Mendocino triple junction region, *Seism. Res. Lett.* **70**, 245–246.

- Castillo, D. A., and W. L. Ellsworth (1993). Seismotectonics of the San Andreas fault system between Point Arena and Cape Mendocino in northern California: implications for the development and evolution of a young transform, *J. Geophys. Res.* **98**, no. 4, 6543–6560.
- Clarke, S. H., Jr., and G. A. Carver (1992). Late Holocene tectonics and paleoseismicity, southern Cascadia subduction zone, *Science* **255**, 188–191.
- Curry, J. R., and R. D. Nason (1967). San Andreas fault north of Point Arena, California, *Geol. Soc. Am. Bull.* **78**, 413–418.
- d'Alessio, M. A., I. A. Johansen, R. Bürgmann, D. A. Schmidt, and M. H. Murray (2005). Slicing up the San Francisco Bay Area: block kinematics and fault slip rates from GPS-derived surface velocities, *J. Geophys. Res.* **110**, B06403, doi 10.1029/2004JB003496.
- Dallimore, A., R. E. Thomson, and M. A. Bertram (2005). Modern to late Holocene deposition in an anoxic fjord on the west coast of Canada: implications for regional oceanography, climate and paleoseismic history, *Mar. Geol.* **219**, no. 1, 47–60.
- Dickinson, W. R., and W. S. Snyder (1979). The geometry of the triple junctions related to San Andreas transform, *J. Geophys. Res.* **84**, 561–572.
- Dragert, H., R. D. Hyndman, G. C. Rogers, and K. Wang (1994). Current deformation and the width of the seismogenic zone of the northern Cascadia subduction thrust, *J. Geophys. Res.* **99**, 653–668.
- Dziewonski, A. M., and D. L. Anderson (1981). Preliminary reference Earth model, *Phys. Earth Planet. Interiors* **25**, 297.
- Field, M. E. (1984). The submarine landslide of 1980 off northern California, *U. S. Geol. Surv. Circ.* **928**, 65–72.
- Flueck, P., R. D. Hyndman, and K. Wang (1997). Three-dimensional dislocation model for great earthquakes of the Cascadia subduction zone, *J. Geophys. Res. B: Solid Earth Planets* **102**, 20,539–20,550.
- Freed, A. M. (2005). Earthquake triggering by static, dynamic, and postseismic stress transfer, *Ann. Rev. Earth Planet. Sci.* **33**, 335–368.
- Freymueller, J. T., M. H. Murray, P. Segall, and D. Castillo (1999). Kinematics of the Pacific–North American plate boundary zone, northern California, *J. Geophys. Res.* **104**, 7419–7441.
- Fukuma, K. (1998). Origin and applications of whole-core magnetic susceptibility of sediments and volcanic rocks from Leg 152, *Proc. Ocean Drill. Prog.: Sci. Res.* **152**, 271–280.
- García-Orellana, J., E. Gràcia, A. Vízcaíno, P. Masqué, C. Olid, F. Martínez Ruiz, E. Piñero, J. A. Sanchez-Cabeza, and J. J. Dañobeitia (2006). Identifying instrumental and historical earthquake records in the SW Iberian margin using ^{210}Pb turbidite chronology, *Geophys. Res. Lett.* **33**, L24601, doi 10.1029/2006GL028417.
- Garfield, N., T. A. Rago, K. J. Schnebele, and C. A. Collins (1994). Evidence of a turbidity current in Monterey Submarine Canyon associated with the 1989 Loma Prieta earthquake, *Cont. Shelf Res.* **14**, no. 6, 673–686.
- Goldfinger, C. (2007). DOGAMI Final Project Report 07-02, Paleoseismic slip history and geologic constraints on splay faulting and interplate coupling along the Cascadia subduction zone, Oregon State University, Corvallis, Oregon, 13 pp.
- Goldfinger, C., L. D. Kulm, R. S. Yeats, C. Hummon, G. J. Huftile, A. R. Niem, C. G. Fox, and L. C. McNeill (1996). Oblique strike-slip faulting of the Cascadia submarine forearc: the Daisy Bank fault zone off central Oregon, in *Subduction Top to Bottom*, G. E. Bebout, D. Scholl, S. Kirby and J. P. Platt (Editors), American Geophysical Monograph **96**, 65–74.
- Goldfinger, C., L. D. Kulm, R. S. Yeats, L. C. McNeill, and C. Hummon (1997). Oblique strike-slip faulting of the central Cascadia submarine forearc, *J. Geophys. Res.* **102**, 8217–8243.
- Goldfinger, C., M. E. Mackay, G. F. Moore, L. D. Kulm, R. S. Yeats, and B. Appelgate (1992). Transverse structural trends along the Oregon convergent margin: implications for Cascadia earthquake potential and crustal rotations, *Geology* **20**, 141–144.
- Goldfinger, C., A. Morey, M. Erhardt, C. H. Nelson, J. Gutierrez-Pastor, R. Enkin, and A. Dallimore (2006). Cascadia great earthquake recurrence: rupture lengths, correlations and constrained OxCal analysis of event ages, in *Proc. U.S. Geol. Soc. Tsunami Sources Workshop*, 21–22 April 2006, M. Diggles, E. Geist and W. Lee (Editors), (available on CD-ROM).
- Goldfinger, C., A. Morey, and C. H. Nelson (2006). Deep-water turbidites as Holocene earthquake proxies along the northern San Andreas fault system, *Seism. Res. Lett.* **77**, no. 2, 195–196.
- Goldfinger, C., A. E. Morey, C. H. Nelson, J. Gutierrez-Pastor, J. E. Johnson, E. Karabanov, J. Chaytor, and A. Ericsson (2007). Rupture lengths and temporal history of significant earthquakes on the offshore and north coast segments of the northern San Andreas fault based on turbidite stratigraphy, *Earth Planet. Sci. Lett.* **254**, 9–27.
- Goldfinger, C., C. H. Nelson, and J. Johnson (2003a). Holocene earthquake records from the Cascadia subduction zone and northern San Andreas fault based on precise dating of offshore turbidites, *Ann. Rev. Geophys.* **31**, 555–577.
- Goldfinger, C., C. H. Nelson, and J. E. Johnson (2003b). Deep-water turbidites as Holocene earthquake proxies: the Cascadia subduction zone and northern San Andreas fault systems, *Ann. Geofis.* **46**, 1169–1194.
- Goldfinger, C., C. H. Nelson, J. E. Johnson, and A. Morey (2003). Physical property correlations and radiocarbon ages illuminate Cascadia earthquake recurrence patterns (Abstract S42A-0144), *EOS Trans. AGU* **84**, no. 46 (Fall Meet. Suppl.), S42A-0144.
- Goldfinger, C., C. H. Nelson, and J. E. Johnson (2004). Deep-water turbidites as Holocene earthquake proxies, *U.S. Geol. Soc. Northern San Andreas Fault System, San Andreas Fault Workshop*, Menlo Park, California.
- Goldfinger, C., C. H. Nelson, J. E. Johnson, M. A. Arsenault, A. Eriksson, E. Karabanov, and J. Chaytor (2004). Physical property correlations from Cascadia great earthquakes: what are they telling us about the triggering events? (Abstract OS21E-01), *EOS* **85**, no. 47 (Fall Meet. Suppl.), OS21E-01.
- Goslar, T., W. O. van der Knaap, S. Hicks, M. Andric, J. Czernik, E. Goslar, S. Räsänen, and H. Hyötylä (2005). Radiocarbon dating of modern peat profiles: pre and postbomb ^{14}C variations in the construction of age-depth models, *Radiocarbon* **47**, 115–134.
- Grantz, A., R. L. Phillips, M. W. Mullen, S. W. Starratt, G. A. Jones, S. S. Naidu, and B. P. Finney (1996). Character, paleoenvironment, rate of accumulation, and evidence for seismic triggering of Holocene turbidites, Canada abyssal plain, Arctic Ocean, *Mar. Geol.* **133**, 51–73.
- Griggs, G. B., and L. D. Kulm (1970). Sedimentation in Cascadia deep-sea channel, *Geol. Soc. Am. Bull.* **81**, 1361–1384.
- Gutierrez-Pastor, J., H. C. Hans Nelson, C. Goldfinger, C. Escutia, and A. Morey (2007). Earthquake control and frequency of generation on the Cascadia and San Andreas active continental margins, SEPM Spec. Pap. on Turbidites, in press.
- Hagstrum, J. T., B. F. Atwater, and B. L. Sherrod (2004). Paleomagnetic correlation of late Holocene earthquakes among estuaries in Washington and Oregon, *Geochem. Geophys. Geosys.* **5**, Q10001, doi 10.1029/2004GC000736.
- Hallett, D. J., L. V. Hills, and J. J. Clague (1997). New accelerator mass spectrometry radiocarbon ages for the Mazama tephra layer from Kootenay National Park, British Columbia, Canada, *Can. J. Earth Sci.* **34**, 1202–1209.
- Heaton, T. H., and H. Kanamori (1984). Seismic potential associated with subduction in the northwestern United States, *Bull. Seismol. Soc. Am.* **74**, 993–941.
- Heezen, B. C., and M. Ewing (1952). Turbidity currents and submarine slumps, and the 1929 Grand Banks earthquake, *Am. J. Sci.* **250**, 849–873.
- Hu, Y., K. Wang, J. He, J. Klotz, and G. Khazaradze (2004). Three-dimensional viscoelastic finite element model for postseismic deformation of the great 1960 Chile earthquake, *J. Geophys. Res.* **109**, B12403, doi 10.1029/2004JB003163.
- Hughen, K., S. Lehman, J. Southon, J. Overpeck, O. Marchal, C. Herring, and J. Turnbull (2004). ^{14}C activity and global carbon cycle changes over the past 50,000 years, *Science* **303**, 202–207.

- Inouchi, Y., Y. Kinugasa, F. Kumon, S. Nakano, S. Yasumatsu, and T. Shiki (1996). Turbidites as records of intense palaeoearthquakes in Lake Biwa, Japan, *Sed. Geol.* **104**, 117–125.
- Iwaki, H., A. Hayashida, N. Kitada, H. Ito, S. Suwa, and K. Takemura (2004). Stratigraphic correlation of samples from the Osaka Bay off Kobe based on magnetic properties and its implication for tectonic activity of the Osaka-Wan fault for the last 6300 years (Abstract GP41C-0053), *EOS* **84**, (Fall Meet. Suppl.) GP41C-0053.
- Jennings, C. W. (1995). New fault map of California and adjacent areas, *Calif. Geol.* **48**, no. 2, 31–42.
- Johnson, J. (2004). Deformation, fluid venting, and slope failure at an active margin gas hydrate province, Hydrate Ridge, Cascadia accretionary wedge, *Ph.D. Thesis*, Oregon State University, Corvallis, 145 pp.
- Karlin, R. E., M. Holmes, S. E. B. Abella, and R. Sylwester (2004). Holocene landslides and a 3500-year record of Pacific Northwest earthquakes from sediments in Lake Washington, *Geol. Soc. Am. Bull.* **116**, no. 1–2, 94–108.
- Kastens, K. A. (1984). Earthquakes as a triggering mechanism for debris flows and turbidites on the Calabrian Ridge, *Mar. Geol.* **55**, 13–33.
- Kelsey, H. M., A. R. Nelson, E. Hemphill-Haley, and R. C. Witter (2005). Tsunami history of an Oregon coastal lake reveals a 4600 yr record of great earthquakes on the Cascadia subduction zone, *Geol. Soc. Am. Bull.* **117**, 1009–1032.
- Kelsey, H. M., R. C. Witter, and E. Hemphill-Haley (2002). Plate-boundary earthquakes and tsunamis of the past 5500 yr, Sixes River estuary, southern Oregon, *Geol. Soc. Am. Bull.* **114**, 298–314.
- Kelson, K., A. Strieg, R. Koehler, and K. Kang (2006). Timing of late Holocene paleoearthquakes on the northern San Andreas fault at the Fort Ross Orchard site, Sonoma County, California, *Bull. Seismol. Soc. Am.* **96**, no. 3, 1012–1028.
- Knudsen, K. L., R. C. Witter, C. E. Garrison-Laney, J. N. Baldwin, G. A. Carver, L. B. Grant, and W. R. Lettis (2002). Past earthquake-induced rapid subsidence along the northern San Andreas fault: a paleoseismological method for investigating strike-slip faults, *Bull. Seismol. Soc. Am.* **92**, 2612–2636.
- Kovanen, D. J., and D. J. Easterbrook (2002). Paleodeviations of radiocarbon marine reservoir values for the northeast Pacific, *Geology* **30**, 243–246.
- Lawson, A. C. (1908). *The California Earthquake of April 18, 1906: Report of the State Earthquake Investigation Commission*, Publ. 87, Vol. 1–2, Carnegie Institution of Washington, Washington, D.C., (reprinted 1969).
- Lees, J. A., R. J. Fowler, and P. G. Appleby (1998). Mineral magnetic and physical properties of surficial sediments and onshore samples from the southern basin of Lake Baikal, Siberia, *J. Paleolimnol.* **20**, no. 2, 175–186.
- Leonard, L. J., R. D. Hyndman, and S. Mazzotti (2004). Coseismic subsidence in the 1700 great Cascadia earthquake: coastal estimates versus elastic dislocation models, *Geol. Soc. Am. Bull.* **116**, 655–670.
- Lovlie, R., and P. van Veen (1995). Spec. Pub. 98, Magnetic susceptibility of a 180 m sediment core: reliability of incremental sampling and evidence for a relationship between susceptibility and gamma activity, in *Palaeomagnetic Applications in Hydrocarbon Exploration and Production*, P. Turner and A. Turner (Editors), Geological Society, London, 259–266.
- Lyle, M., A. C. Mix, and N. G. Pisias (2002). Patterns of CaCO₃ deposition in the eastern tropical Pacific Ocean for the last 150 kyr: evidence for a southeast Pacific depositional spike during marine isotope stage (MIS) 2, *Paleoceanography* **17**, no. 2, 1013, doi 10.1029/2000PA000538.
- McCaffrey, R. (1997). Influences of recurrence times and fault zone temperatures on the age-rate dependence of subduction zone seismicity, *J. Geophys. Res.* **102**, 22,839–22,854.
- McCaffrey, R., M. D. Long, C. Goldfinger, P. C. Zwick, J. L. Nabelek, C. K. Johnson, and C. Smith (2000). Rotation and plate locking at the southern Cascadia subduction zone, *Geophys. Res. Lett.* **27**, 3117–3120.
- McCaffrey, R., A. Qamar, R. W. King, R. W. Wells, G. Khazaradze, C. Williams, C. Stevens, J. J. Vollick, and P. C. Zwick (2007). Fault locking, block rotation and crustal deformation in the Pacific Northwest, *Geophys. J. Int.* **169**, 1315–1340.
- McCrorry, P. A. (1996). Evaluations of fault hazards, northern coastal California, *U.S. Geol. Surv. Open-File Rept.* 96-656, 87 pp.
- McCubbin, D. G. (1982). Barrier-Island and Strand-Plain Facies, in *Sandstone Depositional Environment*, P. A. Scholle and D. Spearing (Editors), AAPG, Tulsa, Oklahoma, 247–279.
- McLaughlin, R. J., K. R. LaJoie, D. H. Sorg, S. D. Morrison, and J. A. Wolfe (1983). Tectonic uplift of a middle Wisconsin marine platform near the Mendocino triple junction, California, *Geology* **11**, 35–39.
- Morey, A., C. Goldfinger, C. H. Nelson, J. Chaytor, J. E. Johnson, and A. Ericsson (2003). Turbidite based earthquake record along the northern San Andreas fault (Abstract T41C-02), *EOS* **84**, no. 46 (Fall Meet. Suppl.), T51C-02.
- Nakajima, T., and Y. Kanai (2000). Sedimentary features of seismoturbidites triggered by the 1983 and older historical earthquakes in the eastern margin of the Japan Sea, *Sediment. Geol.* **135**, 1–19.
- Nalbant, S. S., S. Steacy, K. Sieh, D. Natawidjaja, and J. McCloskey (2005). Earthquake risk on the Sunda trench, *Nature* **435**, 756–757.
- Nederbragt, A. J., R. B. Dunbar, A. T. Osborn, A. Palmer, J. W. Thurow, and T. Wagner (2006). Spec. Pub. 267, Sediment colour analysis from digital images and correlation with sediment composition, in *New Techniques in Sediment Core Analysis*, R. G. Rothwell and F. R. Rack (Editors), Geological Society, London, 112–128.
- Nelson, C. H. (1976). Late Pleistocene and Holocene depositional trends, processes and history of Astoria Deep-sea Fan, *Mar. Geol.* **20**, 129–173.
- Nelson, C. H., P. R. Carlson, and C. R. Bacon (1988). The Mount Mazama climatic eruption (~6900 yr BP) and resulting convulsive sedimentation on the Crater Lake caldera floor, continent, and ocean basin, *Geol. Soc. Am. Spec. Pap.* 229, 37–57.
- Nelson, C. H., C. Goldfinger, J. E. Johnson, and G. Dunhill (2000). Variation of modern turbidite systems along the subduction zone margin of Cascadia Basin and implications for turbidite reservoir beds, in *Deep-Water Reservoirs of the World: 20th Annual Res. Conf. Gulf Coast Section Society of Economic Paleontologists and Mineralogists*, P. W. Weimer and C. H. Nelson (Editors), 31 pp.
- Nelson, A. R., H. M. Kelsey, and R. C. Witter (2006). Great earthquakes of variable magnitude at the Cascadia subduction zone, *Quat. Res.* **65**, 354–365.
- Nelson, C. H., L. D. Kulm, P. R. Carlson, and J. R. Duncan (1968). Mazama ash in the northeastern Pacific, *Science* **161**, 47–49.
- Niemi, T. M., and Z. Ben-Avraham (1994). Evidence for Jericho earthquakes from slumped sediments of the Jordan River delta in the Dead Sea, *Geology* **22**, 395–398.
- Niemi, T. M., and N. T. Hall (1992). Late Holocene slip rate and recurrence of great earthquakes on the San Andreas fault in northern California, *Geology* **20**, 195–198.
- Oleskevich, D. A., R. D. Hyndman, and K. Wang (1999). The updip and downdip limits to great subduction earthquakes: thermal and structural models of Cascadia, south Alaska, SW Japan, and Chile, *J. Geophys. Res. B: Solid Earth Planets* **104**, 14,965–14,991.
- Oppenheimer, D., G. Beroza, G. Carver, L. Dengler, J. Eaton, L. Gee, F. Gonzalez, A. Jayko, W. H. Li, M. Lisowski, M. Magee, G. Marshall, M. Murray, R. McPherson, B. Romanowicz, K. Satake, R. Simpson, P. Somerville, R. Stein, and D. Valentine (1993). The Cape Mendocino, California, earthquakes of April 1992: subduction at the triple junction, *Science* **261**, 433–438.
- Petersen, M. D., W. A. Bryant, C. H. Cramer, T. Cao, M. S. Reichle, A. D. Frankel, J. J. Lienkaemper, P. A. McCrorry, and D. P. Schwartz (1996). Probabilistic seismic hazard assessment for the State of California, *Calif. Div. Mines Geol. Open-File Rept.* 96-08 (published jointly as *U.S. Geol. Surv. Open-File Rept.* 96-706).
- Pollitz, F. F. (1992). Postseismic relaxation theory on the spherical earth, *Bull. Seismol. Soc. Am.* **82**, 422–453.

- Pollitz, F. F. (1996). Coseismic deformation from earthquake faulting on a layered spherical earth, *Geophys. J. Int.* **125**, 1–14.
- Pollitz, F., R. Bürgmann, and P. Banerjee (2006). Post-seismic relaxation following the great 2004 Sumatra-Andaman earthquake on a compressible self-gravitating Earth, *Geophys. J. Int.* **167**, 397–420, doi 10.1111/j.1365-246X.2006.03018.x.
- Pollitz, F., R. Bürgmann, and B. Romanowicz (1998). Viscosity of oceanic asthenosphere inferred from remote triggering of earthquakes, *Science* **280**, 1245–1249.
- Pollitz, F. F., P. A. McCrory, J. L. Svarc, and J. Murray (2008). Dislocation models of interseismic deformation in the western United States, *J. Geophys. Res.*, doi 10.1029/2007JB005174, in press.
- Polonia, A., L. Gasperini, A. Amorosi, E. Bonatti, G. Bortoluzzi, N. Cagatay, L. Capotondi, M. H. Cormier, N. Gorur, C. McHugh, and L. Seebber (2004). Holocene slip rate of the North Anatolian fault beneath the Sea of Marmara, *Earth Planet. Sci. Lett.* **227**, 411–426.
- Prentice, C. S. (1989). Earthquake geology of the northern San Andreas fault near Point Arena, California, *Ph.D. Thesis*, California Institute of Technology, Pasadena, California, 252 pp.
- Prentice, C., R. Langridge, and D. Merritts (2000). Paleoseismic and quaternary tectonic studies of the San Andreas fault from Shelter Cove to Fort Ross in *3rd Conference on Tectonic Problems of the San Andreas Fault System*, R. L. Kovach and G. Bokelmann (Editors), Stanford University, Stanford, California.
- Prentice, C. S., D. J. Merritts, and E. C. Beutner (1999). Northern San Andreas fault near Shelter Cove, California, *Geol. Soc. Am. Bull.* **111**, no. 4, 512–523.
- Ramsey, C. B. (1995). Radiocarbon calibration and analysis of stratigraphy: the OxCal program, *Radiocarbon* **37**, no. 2, 425–430.
- Ramsey, C. B. (2001). Development of the radiocarbon program OxCal, *Radiocarbon* **43**, 355–363.
- Reimer, P. J., M. G. L. Baillie, E. Bard, A. Bayliss, J. W. Beck, C. J. H. Bertrand, P. G. Blackwell, C. E. Buck, G. S. Burr, K. B. Cutler, P. E. Damon, R. L. Edwards, R. G. Fairbanks, M. Friedrich, T. P. Guilderson, A. G. Hogg, K. A. Hughen, B. Kromer, F. G. McCormac, S. W. Manning, C. B. Ramsey, R. W. Reimer, S. Remmele, J. R. Southon, M. Stuiver, S. Talamo, F. W. Taylor, J. van der Plicht, and C. E. Weyhenmeyer (2004). IntCal04 Terrestrial radiocarbon age calibration, 26–0 ka BP, *Radiocarbon* **46**, 1029–1058.
- Rivera, J., E. B. Karabanov, D. F. Williams, V. Buchinskyi, and M. Kuzmin (2006). Lena River discharge events in sediments of Laptev Sea, Russian Arctic, *Estuar. Coast. Shelf Sci.* **66**, 185–196.
- Rogerson, M., P. P. E. Weaver, E. J. Rohling, L. J. Lourens, J. W. Murray, and A. Hayes (2006). Colour logging as a tool in high-resolution palaeoceanography, in *New Techniques in Sediment Core Analysis*, R. G. Rothwell and F. R. Rack (Editors), Volume Geol. Soc. Spec. Pub. 267, Geological Society of London, London, U.K., 99–112.
- Rydelek, P. A., and I. S. Sacks (1999). Large earthquake occurrence affected by small stress changes, *Bull. Seismol. Soc. Am.* **89**, 822–828.
- Satake, K., K. Shimazaki, Y. Tsuji, and K. Ueda (1996). Time and size of a giant earthquake in Cascadia inferred from Japanese tsunami records of January, 1700, *Nature* **379**, 246–249.
- Satake, K., K. Wang, and B. F. Atwater (2003). Fault slip and seismic moment of the 1700 Cascadia earthquake inferred from Japanese tsunami descriptions, *J. Geophys. Res. B: Solid Earth Planets* **108**, 2325, doi 10.1019/2003JB002521.
- Sauber, J. W., W. Thatcher, S. C. Solomon, and M. Lisowski (1994). Geodetic slip-rate for the eastern California shear zone and the recurrence time for Mojave Desert earthquakes, *Nature* **367**, 264–266.
- Schnellmann, M., F. S. Anselmetti, D. Giardini, and S. N. Ward (2002). Pre-historic earthquake history revealed by lacustrine slump deposits, *Geology* **30**, no. 12, 1131–1134.
- Segall, P. (2002). Integrating geologic and geodetic estimates of slip rate on the San Andreas fault system, *Int. Geol. Rev.* **44**, no. 1, 62–82.
- Segall, P., and D. Castillo (1999). Kinematics of the Pacific-North American plate boundary zone, northern California, *J. Geophys. Res.* **104**, 7419–7441.
- Shiki, T., F. Kumon, Y. Inouchi, Y. Kontani, T. Sakamoto, M. Tateishi, H. Matsubara, and K. Fukuyama (2000). Sedimentary features of the seismo-turbidites, Lake Biwa, Japan, *Sed. Geol.* **135**, 37–50.
- Smith, C. R., R. H. Pope, D. J. DeMaster, and L. Magaard (1993). Age-dependent mixing of deep-sea sediments, *Geochim. Cosmochim. Acta* **57**, 1473–1488.
- Song, S., G. C. Beroza, and P. Segall (2008). A unified source model for the 1906 San Francisco earthquake, *Bull. Seismol. Soc. Am.* **98**, no. 2, 823–831.
- Stein, R. S., and M. Lisowski (1983). The 1979 Homestead Valley earthquake sequence, California: control of aftershock and postseismic deformation, *J. Geophys. Res.* **88**, 6477–6490.
- Stein, R. S., G. C. P. King, and J. Lin (1992). Change in failure stress on the southern San Andreas fault system caused by the 1992 M 7.4 Landers earthquake, *Science* **258**, 1325–1328.
- St-Onge, G., T. Mulder, D. J. W. Piper, C. Hillaire-Marcel, and J. S. Stoner (2004). Earthquake and flood-induced turbidites in the Saguenay Fjord (Québec): a Holocene paleoseismicity record, *Quat. Sci. Rev.* **23**, 283–294.
- Stuiver, M., and T. F. Braziunas (1993). Modeling atmospheric ¹⁴C influences and ¹⁴C ages of marine samples to 10,000 BC, *Radiocarbon* **35**, 137–189.
- Thatcher, W., G. Marshall, and M. Lisowski (1997). Resolution of fault slip along the 470 km long rupture of the great 1906 San Francisco earthquake, *J. Geophys. Res.* **102**, 5353–5367.
- Thomson, J., G. T. Cook, R. Anderson, A. B. Mackenzie, D. D. Harkness, and I. N. McCave (1995). Radiocarbon age offsets in different-sized carbonate components of deep-sea sediments, *Radiocarbon* **37**, no. 2, 91–103.
- Toda, S., R. S. Stein, P. A. Reasenber, J. H. Dieterich, and A. Yoshida (1998). Stress transferred by the 1995 $M_w = 6.9$ Kobe, Japan, shock: effect on aftershocks and future earthquake probabilities, *J. Geophys. Res. B: Solid Earth Planets* **103**, 24,543–24,565.
- Ward, S. N., and S. D. B. Goes (1993). How regularly do earthquakes recur? A synthetic seismicity model for the San Andreas fault, *Geophys. Res. Lett.* **20**, no. 19, 2131–2134.
- Weldon, R. J., K. M. Scharer, T. E. Fumal, and G. P. Biasi (2004). Wrightwood and the earthquake cycle: what a long recurrence record tells us about how faults work, *Geol. Soc. Am. Today* **14**, no. 9, 4–10.
- Wheatcroft, R. A. (1992). Experimental tests for particle size-dependent bioturbation in the deep ocean, *Limnol. Oceanogr.* **37**, 90–104.
- Working Group on California Earthquake Probabilities (2003). Earthquake probabilities in the San Francisco Bay region: 2003 to 2032, *U.S. Geol. Surv. Open-File Rept. 03-214*, 235 pp.
- Wynn, R. B., and D. G. Masson (2003). Canary Islands landslides and tsunami generation, in *Proc. 1st Int. Symposium on Submarine Mass Movements and their Consequences*, Nice, J. Locat and J. Meinert (Editors), Kluwer, Dordrecht, 325–332.
- Wynn, R. B., P. P. E. Weaver, D. G. Masson, and D. A. V. Stow (2002). Turbidite depositional architecture across three interconnected deep-water basins on the north-west African margin, *Sedimentology* **49**, no. 4, 669–695.
- Zdanowicz, C. M., G. A. Zielinski, and M. S. Germani (1999). Mount Mazama eruption: calendrical age verified and atmospheric impact assessed, *Geology* **27**, 621–624.
- Zhang, H., T. Niemi, and T. Fumal (2006). A 3000-year record of earthquakes on the northern San Andreas fault at the Vedanta Marsh site, Olema, *Calif. Seism. Res. Lett.* **77**, no. 2, 248.
- Zoback, M. L., R. C. Jachens, and J. A. Olson (1999). Abrupt along-strike change in tectonic style: San Andreas fault zone, San Francisco peninsula, *J. Geophys. Res.* **104**, 10719–10742.
- Zweck, C., J. T. Freymueller, and S. C. Cohen (2002). The 1964 great Alaska earthquake: present day and cumulative postseismic deformation in the western Kenai Peninsula, *Phys. Earth. Planet. Interiors* **132**, 5–20.

Oregon State University
College of Oceanic and Atmospheric Sciences
104 Ocean Admin. Bldg.
Corvallis, Oregon 97331
gold@coas.oregonstatet.edu
drewerksson@yahoo.com
jchaytor@whoi.edu
(C.G., A.E.M., A.E., J.D.C., J.P.)

Department of Earth and Planetary Science
307 McCone Hall
Univ. of California, Berkeley
Berkeley, California 94720-4767
burgmann@seismo.berkeley.edu
(K.G., R.B.)

University of New Hampshire
Department of Earth Sciences
56 College Rd.
Durham, New Hampshire 03824-3589
joel.johnson@unh.edu
(J.E.J.)

Instituto Andaluz de Ciencias de la Tierra (IACT), CSIC-Univ. de Granada
Campus de Fuentenueva
s/n 18002 Granada, Spain
odp@ugr.es
(C.H.N., J.G.)

Institute of Geochemistry
Siberian Branch of Russian Academy of Sciences
1A Favorsky St.
Irkutsk 664003, 22 Russia 29208
lenadelta2002@yahoo.com
(E.K.)

Centre Mediterrani d'Investigacions Marines i Ambientals Unitat de
Tecnologia Marina (CSIC)
Passeig Marítim de la Barceloneta, 37-49
08003 Barcelona, Spain
egracia@cmima.csic.es
(E.G.)

Manuscript received 12 March 2007

EXTERNAL CONTROLS ON MODERN CLASTIC TURBIDITE SYSTEMS: THREE CASE STUDIES

C. HANS NELSON AND CARLOTA ESCUTIA

*Instituto Andaluz de Ciencias de la Tierra (Consejo Superior Investigaciones Científicas (CSIC)-
Universidad de Granada (UGR)), Campus de Fuente Nueva s/n 18002 Granada, Spain*

e-mail: odp@ugr.es, cescutia@ugr.es

CHRIS GOLDFINGER

*Oregon State University, College of Oceanic and Atmospheric Sciences,
104 Ocean Admin. Bldg. Corvallis, Oregon 97331, U.S.A.*

e-mail: gold@coas.oregonstate.edu

EUGENE KARABANOV

Chevron Energy Technology Company, 1500 Louisiana St. Houston, Texas 77002, U.S.A.

e-mail: eugk@chevron.com

AND

JULIA GUTIERREZ-PASTOR

*Instituto Andaluz de Ciencias de la Tierra (Consejo Superior Investigaciones Científicas (CSIC)-
Universidad de Granada (UGR)), Campus de Fuente Nueva s/n 18002 Granada, Spain*

e-mail: juliagp@ugr.es

ABSTRACT: Three case studies are used to exemplify the wide variety of controlling factors that combine to influence the development of modern turbidite systems, and how these vary with location and time. For example, Cascadia Basin in the Pacific Ocean off western North America, which is underlain by the Cascadia Subduction Zone, exhibits the dominant tectonic control of earthquake triggering for turbidity currents, the increased sediment supply effects of the Mt. Mazama catastrophic volcanic eruption in 7626 yr B.P., the glacial climatic and sea-level lowstand control on rapid turbidite-system growth rates, and the recent anthropogenic control that reduces sediment supply rates. Lake Baikal in Russia shows how the rift-basin tectonic setting controls the number and type of sediment input points, the amount of sediment supply, and the consequent types of turbidite systems developed along different margins of the Baikal basin. Pleistocene glacial climatic changes, without changes in lake base level, causes increased sediment input and the rapid growth rate of Baikal turbidite systems that is three to five times greater than that during the Holocene interglacial climate. The Ebro turbidite systems in the northwest Mediterranean Sea exhibit control of system types by the Messinian salinity-crisis lowstand, of channel locations by oceanographic current patterns, and of sediment supply increase by glacial climatic changes as well as recent decrease by anthropogenic changes.

Both active-margin and passive-margin settings have some common controls such as climatic and sea-level changes, and develop similar types of turbidite systems such as base-of-slope aprons, submarine fans, and deep-sea/axial channels. Each margin also has specific local controlling factors, for example the volcanic events in Cascadia Basin, glacial climatic without erosional base-level control in Lake Baikal, and the Messinian extreme lowstand in the Mediterranean Sea. Comparison of modern turbidite systems points out new insights on external controls such as importance of: (1) earthquakes for triggering turbidity currents on active margins, (2) equal or greater Pleistocene climatic control compared to lowered base level for sediment supply, (3) direct glacial sediment input that results in doubled proximal channel size, (4) greatly reduced deposition rates in drained compared to ponded turbidite basins, (5) importance of ocean currents on location of turbidite systems and channel development, and (6) anthropogenic effects from river damming during the last century that sometimes reduces present sediment supply to turbidite systems by orders of magnitude.

KEY WORDS:

INTRODUCTION

Modern marine, seismic stratigraphic, and outcrop studies agree that three fundamental controlling factors for turbidite systems are tectonic setting, sediment supply, and interplay of climate and sea level interplay (e.g., Nelson and Nilsen, 1984). Debates have focused on whether tectonic control or control of base-level erosion by lowering sea level, or climatic factors dominate. Modern marine research in active and passive margins shows that the majority of present-day turbidite systems on the sea floor were deposited during Pleistocene time, suggesting a dominant control by the high-frequency climatic/sea-level Pleis-

tocene cycles (Nelson and Nilsen, 1984). Seismic stratigraphic studies have postulated that the different stages of one sea-level cycle (i.e., lowering and rise) control changes in the turbidite systems (e.g., Posamentier and Vail, 1988). From extensive studies of turbidite outcrops, tectonic controls often are indicated as the dominant control for turbidite system development (e.g., Pickering et al., 1989). Examining the interplay between the common external controls on the development of present-day turbidite systems provides analogues that help our understanding of the controls through past geologic time and that help resolve debates about climatic, sea-level, or tectonic controls on turbidite systems. Our three basin examples in this paper do not,

however, offer a review of external controls that is complete enough to relate architectural elements in ancient turbidite systems to specific external controls.

The purpose of this paper is to combine our observations of many years of research on turbidite systems in three present-day basin settings. Each of these active, passive, and deep-rift-lake tectonic settings has various types and scales of modern turbidite systems. The three examples of turbidite systems illustrate common fundamental tectonic, sediment-supply, and climate/sea-level controlling factors that are important in each system. Our studies also show that in addition to the common controls, each system has site-specific controls that are significant. Both common and site-specific controls combine in each system to determine characteristics of the turbidite systems. Cascadia Basin has been selected as an example because: (1) the generation of turbidites is controlled mainly by the tectonic factor of earthquakes during the Holocene, (2) the amount of sediment supply and turbidite system growth rate are controlled by climatic changes, sea-level lowstands, and volcanic eruptions, and (3) anthropogenic changes have controlled sediment supply of the past century. Our Baikal basin is an example, where (1) tectonic control of the rift-basin morphology determines amounts and input points of sediment supply, and turbidite system types (e.g., apron vs. fan), and (2) without significant Pleistocene lake-level changes (Colman, 1998), climatic control can be assessed as an independent factor determining the growth rate of turbidite systems. The Ebro margin provides an example where (1) climate and sea-level lowstand control turbidite system growth rates, except for anthropogenic effects of the last century, and (2) channel development in Pleistocene turbidite systems is controlled by the underlying Messinian subaerial drainage patterns and geostrophic ocean currents.

CASCADIA BASIN TURBIDITE SYSTEMS

Tectonic and Morphologic Control

The unique Holocene tectonic/paleoseismic and volcanic history of Cascadia Basin, in addition to the thorough analysis of glacial and interglacial (Pleistocene/Holocene) turbidite systems, provides an ideal place to define the interplay of tectonic, volcanic, sediment-supply, climate/sea-level, ocean-current, and anthropogenic controls (Fig. 1). Cascadia Basin is underlain by the Juan de Fuca and Gorda Plates. The tectonic control of this convergent margin is generated by the Cascadia Subduction Zone fault, which underlies and determines the morphology of the continental margin of North America from Vancouver Island to the Mendocino Triple Junction (Fig. 1). This active tectonic margin contains a variety of turbidite systems including Nitinat Fan, which drains south into Cascadia Channel, and Astoria Fan, which partially drains laterally into Cascadia Channel. The Nitinat Fan has sediment supplied by multiple erosional canyons, whereas Astoria Fan is fed by the fault-controlled Astoria Canyon, which supplies Columbia River sediment (Fig. 1) (Carlson, 1967; Carlson and Nelson, 1969). Cascadia Channel is a tectonically controlled deep-sea channel that has eroded through the Blanco Fracture Zone and feeds into Tufts fan (Fig. 1) (Griggs and Kulm, 1970; Carter, 1988; Nelson et al. 2000a; Normark and Reid, 2003). To the south of these large turbidite systems, smaller canyons associated with local rivers are found feeding from a narrower shelf. These include the Rogue base-of-slope apron, Trinidad and Eel Canyons, which terminate in plunge pools feeding radiating sediment-wave fields, and channel-levee complexes and lobes

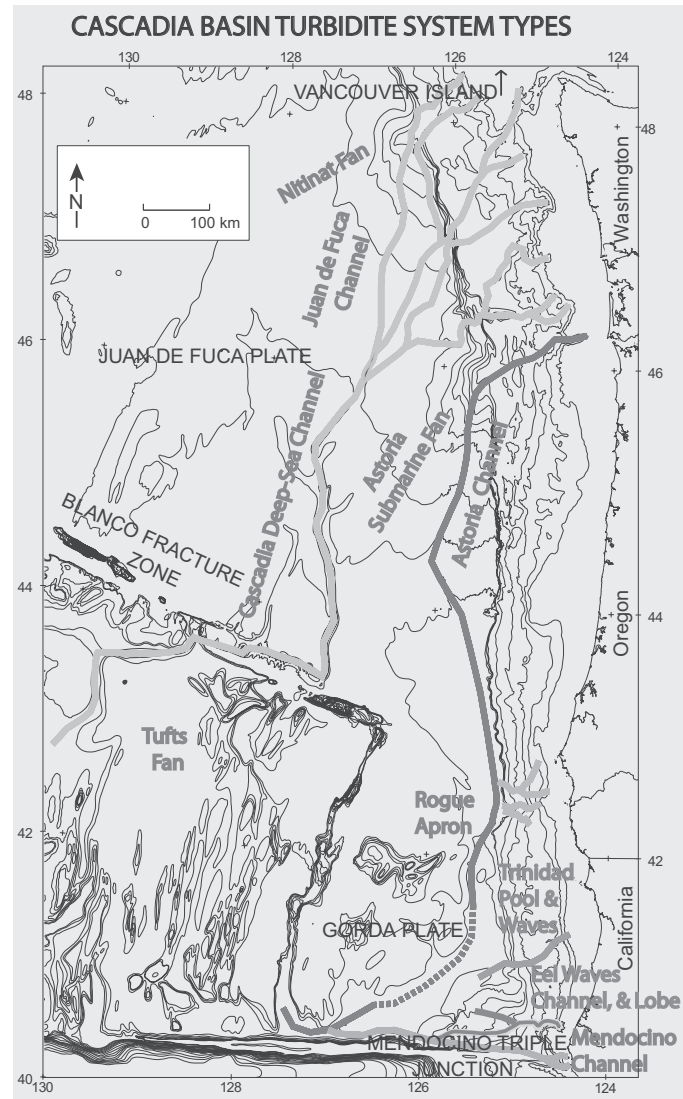


FIG. 1.—Physiographic map showing the plate-tectonic setting and turbidite systems of Cascadia Basin. Northern Cascadia Basin contains the Nitinat Fan, Cascadia Channel, and Astoria Fan turbidite systems, which overlie the Juan de Fuca Plate, which extends from Juan de Fuca Ridge on the west and Blanco Fracture Zone on the south to the Cascadia Subduction Zone at the base of the continental slope off Vancouver Island, Washington and Oregon. Southern Cascadia Basin contains the Rogue Apron, Trinidad, Eel, and Mendocino Channel turbidite systems, which overlie the Gorda Plate which extends from Gorda Ridge on the west and the Mendocino Escarpment on the south (followed by Mendocino Channel at the bottom of the map) to the Cascadia Subduction Zone at the base of the continental slope off southern Oregon and northern California. For definition of the types of turbidite systems, see text. (Modified from Nelson et al., 2000b.)

such as the distal Eel and Mendocino turbidite systems (Figs. 1, 2) (Nelson et al., 1991; Nelson et al., 2000b; Wolf et al., 1999a; Wolf et al., 1999b). In summary, this active tectonic margin is not dominated by one characteristic type of turbidite system, but exhibits many types.

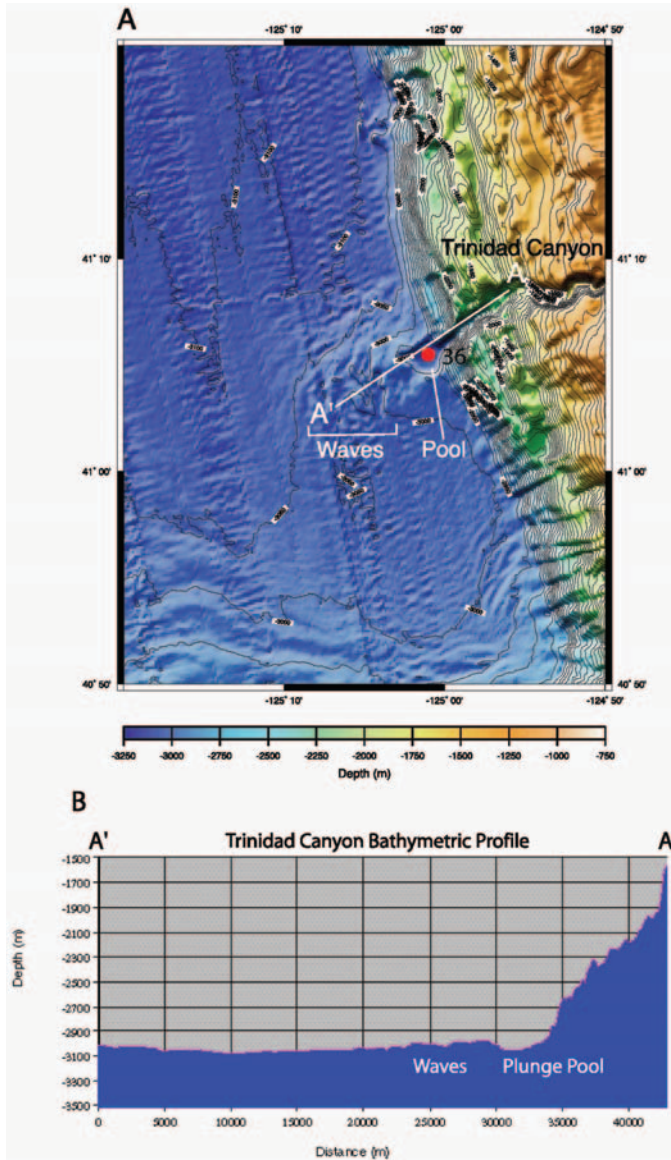


FIG. 2.—A three-dimensional swath bathymetric image looking down on the Trinidad canyon, plunge pool, and radiating sediment wave field at the base-of-slope environment in southern Cascadia Basin. An axial profile downstream across these proximal to distal environments. (From Nelson et al., 2000b.)

Volcanic Control

The catastrophic volcanic eruption of Mount Mazama in the southern Cascade Mountains of Oregon had a significant influence on the Holocene turbidite systems of Cascadia Basin (Fig. 3) (Nelson et al., 1968; Nelson et al., 1988; Nelson et al., 2000b). The Mount Mazama eruption occurred in 7626 yr B.P. and is recorded in the Greenland ice cores as one of the major Quaternary volcanic events (Zdanowicz et al., 1999). The initial plinian eruption of 50 km³ covered about 1 × 10⁶ km² of the Columbia River drainage and was 100 times greater than the Saint Helens eruption (0.5 km³) of 1980 (Fig. 3) (Nelson et al., 1988). The second phase of fiery avalanche deposits filled the Rogue and other river valleys with

volcanic debris for up 75 km from the mountain. Finally, the mountain formed a collapse caldera that contains the famous Crater Lake in the Cascade Mountains of Oregon. As a result, large amounts of volcanic and forest debris washed from the Columbia and Rogue River drainages into the sea and then eventually were resedimented as woody tuffaceous turbidites for hundreds of kilometers along turbidite-system channels (Figs. 3, 4B).

During the Holocene, in contrast to the typical thin sand turbidites, thick (~30–100 cm) tuffaceous turbidites deposited in Cascadia Basin channels after Mount Mazama volcanic glass was transported to canyon depocenters, mixed with Columbia and Rogue Canyon sands when Cascadia Subduction Zone earthquakes triggered turbidity currents, and deposited as tuffaceous turbidites (Figs. 3–5) (Nelson et al., 1968; Nelson et al., 1988; Nelson et al., 2000b). Correlation of the initial marker bed containing ash shows that overbank suspension flows, rich in volcanic glass, deposited thin-bedded turbidites on interchannel areas of the proximal inner and middle Astoria Fan (Figs. 3, 4). Correlative tuffaceous turbidites also reveal that poorly sorted, high-matrix (20%) and wood-rich deposits of the canyon mouth evolved 150 km downstream to well sorted, low-matrix (5%) graded sands with a nearly complete Bouma sequence of vertical sedimentary structures (Fig. 4B) (Nelson and Carlson, 1969; Nelson, 1976).

Climatic, Sea-Level, and Sediment-Supply Controls

In the mid-1960s to 1970s extensive morphologic and coring (several hundred piston cores) studies were conducted on all Cascadia turbidite systems (Carlson, 1967; Nelson, 1968, 1976; Carlson and Nelson, 1969; Griggs, 1969; Griggs and Kulm, 1970; Duncan et al., 1970a; Duncan et al., 1970b). Excellent biostratigraphic, lithologic, compositional, and Mazama ash marker beds permitted definition of the glacial late Pleistocene lowstand (> 12,750 cal. yr. BP) and interglacial Holocene highstand deposits (< 12,750 cal yr BP) (Nelson et al., 1968; Duncan et al., 1970a; Duncan et al., 1970b; Guttierrez-Pastor et al., this volume). Astoria Fan was the first location in which a pattern of thick sand beds (10–50 cm) deposited during glacial sea-level lowstand time (i.e., lowstand fans) was observed (Fig. 4A) (Nelson, 1968, 1976). Pleistocene turbidity currents mainly bypassed to outer-fan lobes where the highest sand:shale ratios are found (Fig. 5). In contrast, during the Holocene interglacial highstand time of warmer climate and significant Pacific Northwest forestation, turbidite deposition was confined to channel floors and, except for tuffaceous turbidites, consisted mainly of thin turbidite sand beds (1–4 cm) and thick mud turbidites (~50 cm) in Cascadia Channel (Figs. 4A, 5) (Griggs and Kulm, 1970; Nelson, 1976, 2000b).

Holocene Paleoseismic Control on Turbidite Deposition

Beginning in the late 1980s, and still continuing, onshore studies from Vancouver Island to northern California have completed thousands of high-resolution AMS ¹⁴C and tree-ring ages to correlate the onshore paleoseismic record of co-seismic drowned trees and marine tsunami sand layers in brackish-water lagoonal muds (Fig. 1) (A.R. Nelson et al., 1995; A.R. Nelson et al., 2004; A.R. Nelson et al., 2006; Atwater and Hempill-Haley, 1997; Kelsey et al., 2002; Kelsey et al., 2005; Witter et al., 2003). The youngest 1700 AD great earthquake of Cascadia has been correlated with a sand deposit in Japan from a 3–5 m set up transoceanic Cascadia-derived tsunami (Satake et al., 1996; Satake et al., 2003).

During the past decade, all of the previous archive cores and sixty new cores have been restudied to determine the Holocene

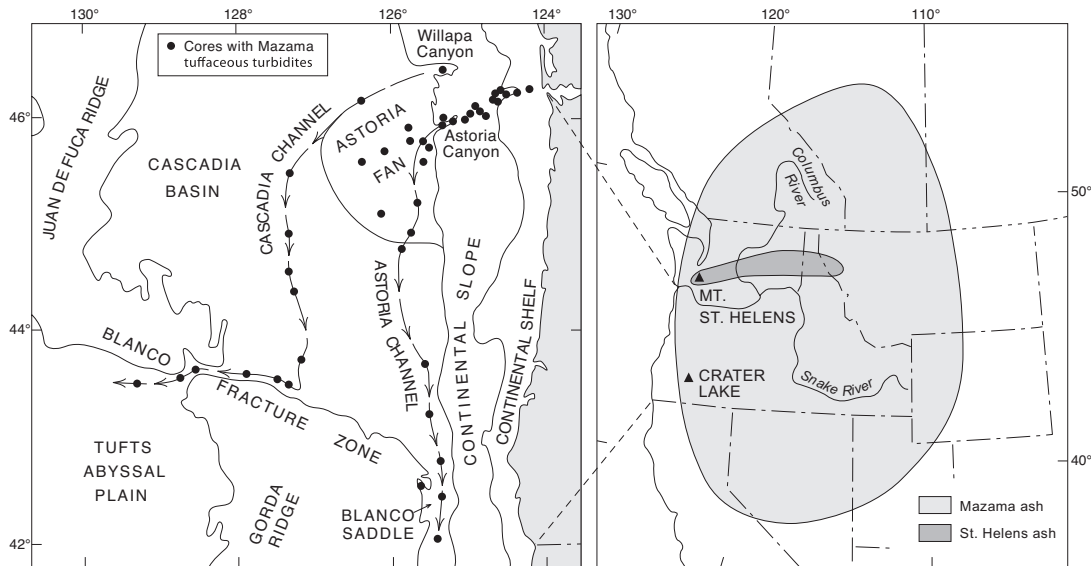


FIG. 3.—Distribution of ash onshore from the Mount Mazama eruption in the Pacific Northwest and of Mazama tuffaceous turbidites offshore in Cascadia Basin. The distribution of ash from the May, 1980, Mount St. Helens eruption to the 0.5 cm isopach (uncompacted), which is approximately the same thickness as the limit of Mazama ash occurrence, is shown for comparison. (Modified from Nelson et al., 1988.)

turbidite paleoseismic history of the Cascadia Subduction Zone fault (Adams, 1990; Nelson et al., 2000b; Goldfinger et al., 2003; Goldfinger et al., in press; Gutierrez Pastor et al., this volume). During this investigation, hundreds of high-resolution AMS ^{14}C ages, hemipelagic sedimentation-rate ages, physical-property signatures (i.e., density, velocity), magnetic susceptibility, color scans, and mineralogic studies of volcanic glass and heavy minerals have been undertaken to correlate all 18 Holocene turbidites that were deposited during the past 10,000 cal. yr BP in major channel systems of the Cascadia Basin.

The oldest turbidite containing Mazama ash has provided an excellent marker bed for paleoseismic research (Fig. 4A, see layer A) (Nelson, 1976; Nelson et al., 1968; Nelson et al., 2000b; Gutierrez Pastor, this volume). The first occurrence of the Mazama turbidite (~7200 cal yr BP) in submarine fan, deep-sea channel, and base-of-slope apron turbidite systems in Cascadia Basin permits us to correlate 13 post-Mazama Holocene turbidites that were synchronously triggered by great earthquakes of the Cascadia Subduction Zone (Adams, 1990; Nelson et al., 2000b). Because multiple tributary canyons upstream had the same 13 post-Mazama turbidites as those downstream below the canyon confluence in Cascadia Channel (i.e., they were not additive), Adams (1990) first suggested that the 13 turbidites had to be synchronously triggered by great earthquakes of Cascadia Subduction Zone.

Our new results indicate that most of the 18 Holocene earthquakes, like the AD 1700 event, ruptured the full Cascadia margin (Nelson et al., 2000b; Goldfinger et al., 2003; Goldfinger et al., in press; Gutierrez Pastor et al., this volume). The stratigraphic correlation of turbidite events, in addition to their age correlation with extensive Cascadia coastal and Japanese transoceanic tsunami deposits suggests that the turbidite record mainly monitors great earthquakes (>8 Ma) similar to the ~300 second Sumatra 26 Dec. 2004 event (Table 1) (Nelson et al., 2005; Atwater et al., 2004; Goldfinger et al., in press).

Two lines of evidence support the hypothesis that the turbidite paleoseismic record mainly monitors great earthquakes in the

Cascadia Subduction Zone, whose ~1000 km ruptures and shaking of the margin generated turbidites from failed walls in multiple canyons along the margin. The Japanese find that >Mw 7.4 earthquakes are required to trigger turbidity currents (Shiki et al., 2000). Similarly, we have monitored turbidite deposition in Mendocino Channel in 1986 and 1999 before and after two Mw 7.2 earthquakes in the Mendocino Canyon head that did not produce turbidite deposits (Nelson et al., 2000b).

Tsunami marine sand deposits provide the second line of evidence that suggests Cascadia turbidites result mainly from great earthquakes. Sumatra earthquakes show that the Mw 8.7 earthquake of 28 March 2005 created only small local tsunamis compared to the earlier Mw 9.2 earthquake in December 2004 that created extensive large tsunamis in Sumatra and large transoceanic tsunamis in Thailand, Sri Lanka, India, and Africa. The Cascadia onshore and transoceanic Japanese tsunami records are comparable to the Sumatra 2004 and 2005 tsunami records because great earthquakes of ~Mw 9 appear to be responsible for the tsunamis with 3-5 m set up and several kilometer runups on the coast (Table 1). The age correlation of the Cascadia onshore tsunami and turbidite paleoseismic records (Satake et al., 1996; Goldfinger et al. 2003; Goldfinger et al., in press; Atwater et al., 2004) (i.e., this is not a correlation of tsunamis generating turbidites), in addition to correspondence of the Sumatra, Cascadia, and Japanese tsunami records (Table 1), imply long fault rupture length and support the hypothesis that mainly great earthquake ruptures of ~1000 km generate the ~550 yr frequency of the Holocene turbidite deposition in the Juan de Fuca Plate region of Cascadia Basin.

To the south, in the Gorda Plate region, the frequency of turbidites progressively increases towards the Mendocino Triple Junction (i.e., 133 years off Trinidad Canyon, 75 years in Eel Channel, and 34 years in Mendocino Channel) as the seismicity progressively increases (Fig 1; Wells et al., 1998; Gutierrez Pastor, this volume). The correlative increase in turbidite frequency and seismicity might suggest that earthquakes are a dominant

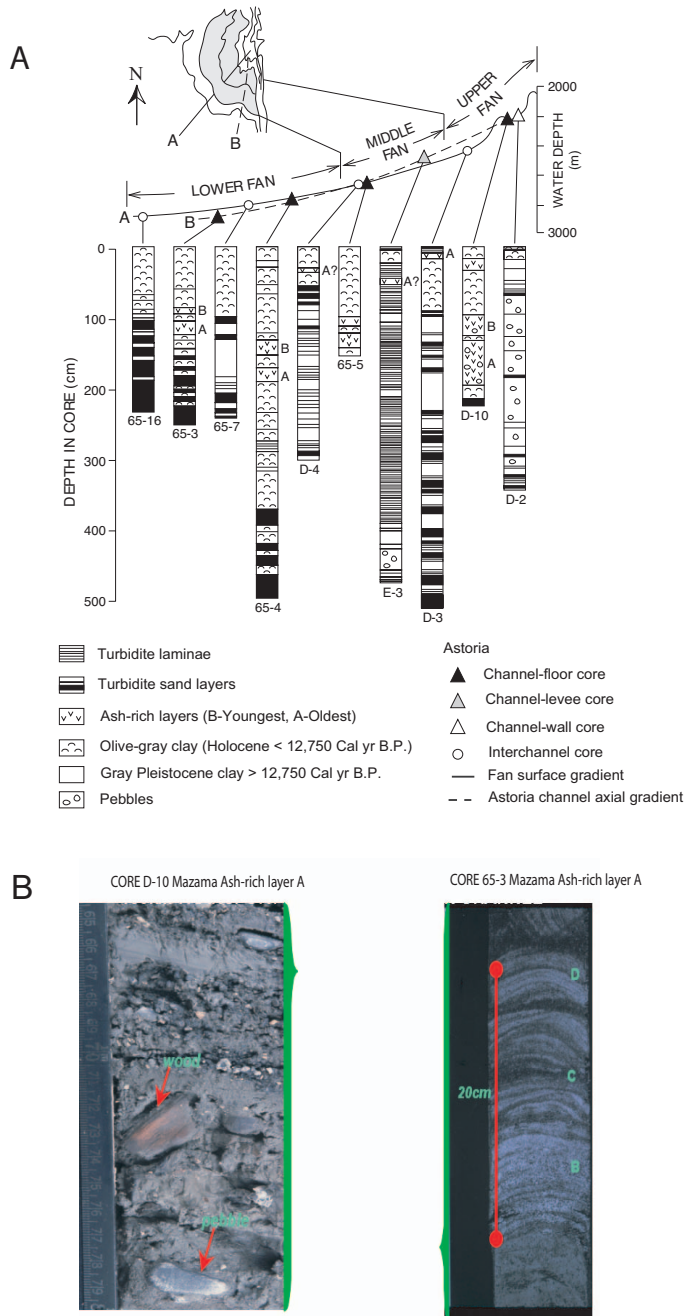


FIG. 4.—Lithology and stratigraphy at representative locations on Astoria Fan. (modified from Nelson, 1976). Changes in correlated Mazama Turbidite 13 during 150 km transport down Astoria Fan Channel. Turbidite 13 of Part B is keyed in Part A, as layer A in proximal channel core D-10 and distal channel core 65-3.

trigger for the turbidity currents during the Holocene. The canyon heads, however, become progressively closer to the shoreline towards the south and intersect the littoral drift at the Mendocino Canyon head (Fig. 1). Although the turbidite and onshore paleoseismic data record the ~ 18 Holocene great earthquakes of the Cascadia Subduction Zone, as they did in the Gorda Plate area in 1700 AD (Nelson et al., 1995; Goldfinger et al., in press), there may be an interplay of local earthquake and storm

triggering of turbidity currents to account for the more frequent turbidites (~ 34 to 133 yr) on the Gorda Plate compared to those on Cascadia Plate (~ 550 yr).

Late Holocene Sea Level, Ocean-Current, and Anthropogenic Controls

The Holocene sediment budget calculations for the Columbia River not only show the typical shift of the sediment depositor to the shelf during the highstand sea level, but also show that the majority of the river sediment is dispersed toward the north by geostrophic ocean currents (Fig. 6); (Table 2). This contrasts with the Pleistocene lowstand sea level, when the majority of the sediment was dispersed toward the south, thick turbidite sand beds were deposited on the outer Astoria Fan, and the Fan deposition is 300 to 2000 m thick (Figs. 4A, 5, 6) (Shipboard Scientific Party, 1973; Nelson et al., 1987). Consequently, the external controls on the Columbia River sediment dispersal system have resulted in rapid Pleistocene lowstand submarine-fan growth in one direction by turbidity currents and Holocene highstand-sea-level deposition on the continental shelf in the opposite direction by geostrophic ocean currents (Fig. 6; Table 2).

During the past century, anthropogenic effects have added a significant new control on the sediment supply to Cascadia Basin. Because the Columbia River system has more dams than any other river in North America, most of the sediment load is now trapped and does not reach the river mouth to feed the turbidite systems. By utilizing the Holocene to Pleistocene stratigraphic datum (Fig. 4A), the pre-dam Holocene sediment load of the Columbia River is calculated to be about 20 million metric tons of sediment per year (Table 2) (Wolf et al., 1999b; Sternberg, 1986). Since the advent of dams, measurements indicate that the present sediment load has been reduced to about 5 million metric tons of sediment a year (Sherwood et al., 1990).

LAKE BAIKAL TURBIDITE SYSTEMS

Setting

Lake Baikal is located in central Siberia in Russia along the active Baikal Rift Zone, which separates the Siberian Platform to the northwest from the Mongolian fold belt to the southeast (Fig. 7) (Hutchinson et al., 1992). The Lake is divided into three half-graben rift segments, the North, Central, and South Basins, all of which bounded by border faults on the western side (Fig. 8) (Hutchinson et al., 1992). The lake is the deepest in the world at 1637 m and is about 600 km in length and 50 to 100 km in width. The lake level, unlike sea level, appears to have had little fluctuation related to the glacial-interglacial periods of the Pleistocene and Holocene times (Colman, 1998) and therefore the turbidite systems have no erosional base-level control. However, extensive Pleistocene ice fields and valley glaciation were developed, mainly in the mountains around the northern edges of the lake (Fig. 7). The climatic changes and glaciations have had a significant impact on grain size and sediment supply to the turbidite systems (Nelson et al., 1995; Back et al., 1998; Back et al., 1999).

Tectonic Control of Turbidite System Type

The tectonic setting controls the drainage systems, number and types of sediment input points to Lake Baikal, volume of sediment supply at input points, and consequent basic types of turbidite systems. The fault-bounded western margin of the lake

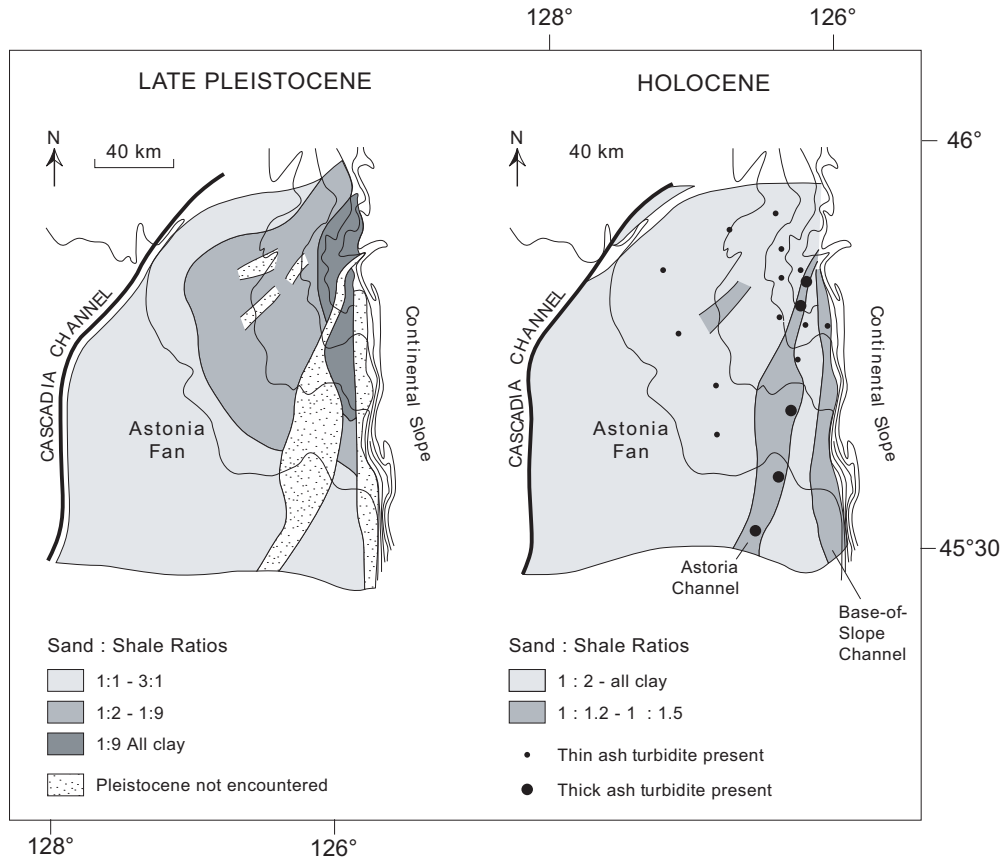


FIG. 5.—Sand:shale ratios for the late Pleistocene (left diagram) and Holocene (right diagram) deposits of Astoria Fan. Ratios are based on total thickness of gravel, sand, and coarse silt turbidite beds compared to total thickness of mud beds found in each piston core taken from Astoria Fan. The sand:shale ratio of Pleistocene deposits of each core was calculated separately from the Holocene deposit of each core. To make a comparison with sand:shale ratios of consolidated rocks in outcrops and drill cores, the unconsolidated mud of Astoria Fan mud beds was compacted to one-third of original thickness for the calculations of sand:shale ratio (Hamilton, 1970). (Figure modified from Nelson, 1976.)

mainly drains to the exterior basins of the Lena and Kirenga Rivers, which carry sediment away from the lake (Figs. 7, 9A) (Back et al., 1999; Nelson et al., 1999). Only the drainage of the border-fault scarp itself supplies restricted amounts of sand and gravel from multiple, short stream input locations to local Gilbert fan deltas on the western side of the lake, which in turn feed local base-of-slope aprons on the lake floor (Figs. 8, 9) (Nelson et al., 1995, 1998; Colman et al., 2003). In contrast, the small interior drainage basins with local rivers on the eastern ramp side feed sublacustrine sand-rich fans. The large Selenga River of central Siberia enters the low topography of the accommodation zone between the South and Central Basins and feeds a large delta (Fig. 8). North- and south-trending canyons from the delta in turn feed large longitudinal mud-rich fans of the South and Central Basins. Similar to Cascadia Basin, most of the general types of turbidite systems (i.e., aprons, fans, and axial channels) are present in this tectonically active setting.

The half-graben morphology of the rift basin establishes the basic control for the amount and type of sediment supply, which in turn determines the different type of turbidite systems in Lake Baikal. Steep border fault slopes (footwall) along half-graben basins provide multiple small sources of gravel/sand to feed nonchannelized, small (< 10 km diameter) sublacustrine base-of-slope sand-rich aprons on the lake floor (Figs. 8, 9)

(Nelson et al., 1995; Nelson et al., 1999; Colman et al., 2003). Shallow slopes of the southeastern ramp margins (hanging wall) of the lake basins, conversely, feed finer-grained sediment, in greater volumes from larger drainage basins into two different types of channelized turbidite sublacustrine fan systems: (1) small (15–20 km) laterally fed sand-rich fans sourced by local rivers, which commonly originated from glaciated valleys (Figs. 7, 9C) and (2) large (> 65 km) axially fed, elongate silt-rich fans sourced by regional exterior drainage of the Selenga River (Figs. 7–9). Lake Baikal thus provides an ideal example to show that the coarser grain size sediment supply of small rivers results in coarser-grained sand turbidites of the “sand-rich fans” and that the finer-grain-size sediment supply of large rivers results in finer-grained silt turbidites of the “mud-rich fans” (Nelson et al., 1995).



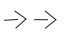


These same relationships related to tectonic control of morphology, sediment supply, and development of turbidite system types also are shown in models of ancient rift-basin turbidite systems (e.g., Prosser, 1993). The similarity of modern and ancient turbidite system types related to rift tectonic settings thus provides a way to predict the expected type of turbidite system architecture in ancient systems. For example, the typical turbidite systems on the border-fault margin of an ancient rift basin are most likely to start as sand-rich aprons.

TABLE 1.—Comparison of tsunami records and earthquake rupture lengths from Cascadia, Japan, and Sumatra subduction zones.

TSUNAMI DEPOSIT CHARACTERISTICS						
SUBDUCTION ZONE	RUPTURE LENGTH (km)	HEIGHT m > MSL	ONSHORE INUNDATION km from shore	TRANS-OCEANIC	LOCAL TSUNAMI	SITES STUDIED
CASCADIA	~1000	> 5.5	> 10upriver			~ 70
1700 AD	~1000	1–5	2	X (Japan)		7
JAPAN	~ 1000	> 5	> 3		X	33
JAPAN	100–200	< 4	< 0.5		X	33
SUMATRA 04	~ 1300	5–22	> 2		X	~ 25
SUMATRA 04	~ 1300	3–12	> 1	X (Sri Lanka)		~ 15
SUMATRA 04	~ 1300	3–11	1.5 +	X (Thailand)		~ 15
SUMATRA 04	~ 1300	5–9	?	X (Africa)		5
SUMATRA 05	~ 330	3–5	< 1	None	X	10

Data Sources: Cascadia see Atwater and Hemphill-Haley, 1997; Kelsey et al., 2002; Nelson, A. R. et al., 2004; 2006; Witter et al., 2003 Cascadia 1700 AD see Satake et al., 1996; 2003 Japan see Nanayamal et al., 2003; Sumatra 04 see <http://earthquake.usgs.gov/eqinthenews/2004/usslav/>; http://neic.usgs.gov/neis/eq_depot/2004/eq_041226/neic_slav_summary.html; <http://walrus.wr.usgs.gov/news/reports-Sumatra> and Sri Lanka; American Civil Engineering Society Field Reports-Thailand; Sumatra 05 see <http://earthquake.usgs.gov/eqinthenews/2005/usweax/>; NOAA Tsunami Bulletin Board



-  Pleistocene lowstand turbidite systems
-  Lowstand sediment-dispersal pattern
-  Lowstand channel
-  Holocene Highstand Prodelta Deposits
-  Highstand sediment dispersal from geostrophic currents

Pleistocene Climatic Control of Turbidite System Growth

Once the basic types of turbidite systems have been established by the tectonic control of basin morphology, Pleistocene glacial climatic and sediment-supply changes have determined the growth rate of all of the turbidite system types in Lake Baikal (Nelson et al., 2000a). The restricted growth rates, low sedimentation rates, and thin-bedded mud and silt turbidites are characteristic of the Holocene interglacial climate (Fig. 10; Table 3). In contrast, rapid growth rates, high sedimentation rates, thick sand turbidites, and oversized fan channels are characteristic of Pleistocene glacial climates (Figs. 10, 11; Table 3) (Nelson et al., 1995; Escutia et al., 2000). As sediment supply decreased during final glacial recession (Back et al., 1998; Back et al., 1999), fan lobes backstepped and thinner and finer-grained turbidites were deposited on the Tompuda Fan (Fig. 12; Table 3) (Nelson et al., 1995).

Sediment always has direct access down the steep border-fault basin walls to the lake-floor turbidite systems during glacial or interglacial times, because of (1) the lack of significant lake-level variations (Colman, 1998) and (2) restricted lakeshore shelf development to trap sediment (Figs. 8, 9) (Nelson et al., 1995; Colman et al., 2003). Consequently in Lake Baikal, only glacial climatic changes have increased sediment supply and grain size. Thus climate alone controls turbidite system growth rates that are comparable to those in marine basins that have climatic and sea-level controls (Figs. 4A, 10; Table 3) (Nelson et al., 1995; Nelson et al., 2000a). The Lake Baikal example isolates Pleistocene climatic

←

FIG. 6.—Sea-level lowstand Pleistocene and highstand Holocene reversal of Columbia River sediment dispersal system. The lowstand dispersal to Astoria Fan is shown by the high sand:shale ratios in Figure 5, and the highstand dispersal to the Washington continental shelf is shown by the Holocene sediment budget of Table 2. (Modified from Nelson and Maldonado, 1990.)

TABLE 2.—Minimum estimated Columbia River sediment discharge per year during the past 5000 years (modified from Wolf et al., 1999b).

GEOGRAPHIC AREA	VOLUME Km ³	DRY BULK (1) DENSITY (metric tons/m ³)	WEIGHT (metric tons/yr)	CORRECTION FACTOR (2)	CORRECTED WEIGHT (TONS/YR)	% COLUMBIA R. BUDGET
WA/OR MID/OUTER SHELF	48.500	1.41	13,677,000	-3.5%	13,198,305	65.87
WASHINGTON SLOPE *	N/A	N/A	N/A	N/A	1,300,000	6.49
WASHINGTON CANYONS *	N/A	N/A	N/A	N/A	1,255,000	6.27
N. CASCADIA BASIN	2.612	0.85	444,040	-3.2%	429,830	2.15
CASCADIA CHANNEL	5.757	0.85	978,690	-3.8%	941,499	4.70
ASTORIA CANYON FLOOR	0.873	0.96	167,529	-2.9%	162,670	0.81
NORTHERN OREGON SLOPE	3.493	0.96	670,656	-2.9%	651,206	3.25
NORTHERN ASTORIA FAN	3.287	0.85	558,879	-3.0%	542,112	2.71
CENTRAL ASTORIA FAN	7.809	0.85	1,327,530	-36.2%	846,964	4.23
SOUTHERN ASTORIA FAN	14.138	0.85	2,403,460	-70.8%	701,810	3.50
TOTAL OFFSHORE COLUMBIA RIVER SEDIMENT PER YEAR **					20,017,110	100.00
* Washington slope and canyons from Sternberg (1986) ** not including inner shelf, shoreline, and estuarine sediments						

(1) Dry bulk density numbers were derived mainly from sediment water content and textural data of Carlson (1967), Griggs (1969), Nelson (1968), and Nittrouer (1978) converted to dry bulk density values with the formulas of Hamilton (1970) and Lamb and Whitman (1969). In addition, cores taken in 1998, on the Washington and Oregon shelf along N–S and E–W transects had measurements of density that were taken by the core sediment logger.

(2) Correction factors account for the autochthonous organic carbon and carbonate carbon contents measured in sediment cores from the different physiographic areal compartments: the shelf sediment factor is from Nittrouer (1978); N. Cascadia Basin and Cascadia channel factors are from Griggs (1969); Astoria Canyon floor and northern Oregon slope factors are from Carlson (1968); Astoria Fan factors are from Nelson (1968). The large central and southern Astoria Fan correction factors are derived from Holocene clay mineralogical analyses of Duncan et al. (1970b) which show that about 33% of clays in the central Astoria Fan and about 68% of clays from the southern Astoria Fan are from non-Columbia River sources.

change as a major factor controlling sediment supply in contrast to the conceptual idea that lowered sea level and erosional base level of drainages mainly control sediment supply and turbidite system growth rate (Posamentier and Vail, 1988).

EBRO TURBIDITE SYSTEMS

Setting and Control of Turbidite Systems by the Extreme Messinian Lowstand

The Ebro turbidite systems are associated with the Ebro River drainage system, which derives sediment from the Pyrenees Mountains and the Ebro Basin of north-central Spain (Fig. 13). The Ebro Delta enters the northwestern Mediterranean Sea and has successively fed a number of Pleistocene submarine canyons and channel-levee complexes along this passive continental margin (Figs. 13, 14) (Nelson and Maldonado, 1988). These channels, which are oldest in the northeast and are progressively younger toward the southwest, have drained into Valencia Valley, a deep-sea channel that bypasses sediment 200 km downstream into the Valencia Fan on the Balearic Abyssal Plain (Fig. 13).

The subaerial drainage system, formed during the Messinian desiccation in the Mediterranean Sea, exerted control on the late

Pleistocene Ebro turbidite systems (Escutia and Maldonado, 1992). For example, the Pleistocene Valencia Valley now follows the pathway of a Messinian subaerial valley (Fig. 15). In the slope, the 20-km-wide and 500-m-deep Messinian Canyon of the Ebro, but not the younger adjacent Pleistocene canyons, rapidly filled with Pliocene deep-water clays when the Mediterranean refilled. This thick, rapidly deposited Pliocene mud in the deeply eroded Messinian Ebro Canyon now is unstable (Figs. 14, 15) (Nelson and Maldonado; Escutia and Maldonado, 1992). The result is a central Ebro margin segment that is underlain by the mud-filled Messinian Canyon, and now is dominated by sediment failures and three wide gullied canyons (Fig. 14). These sediment failures from the gullied canyons prevent the development of turbidite systems along this central segment of the margin because the recurrent deposition of mass-transport deposits destroys incipient turbidite systems on the basin floor below the canyons (Figs. 13, 14) (Nelson and Maldonado, 1988; Nelson et al., 1991).

In contrast, Pleistocene canyons that feed channel-levee complexes develop in adjacent areas of the slope where there is no evidence for underlying Messinian canyons. The channel systems 1 to 4 extend from canyon mouths to the Valencia Valley without developing typical radiating fan morphology or outer-

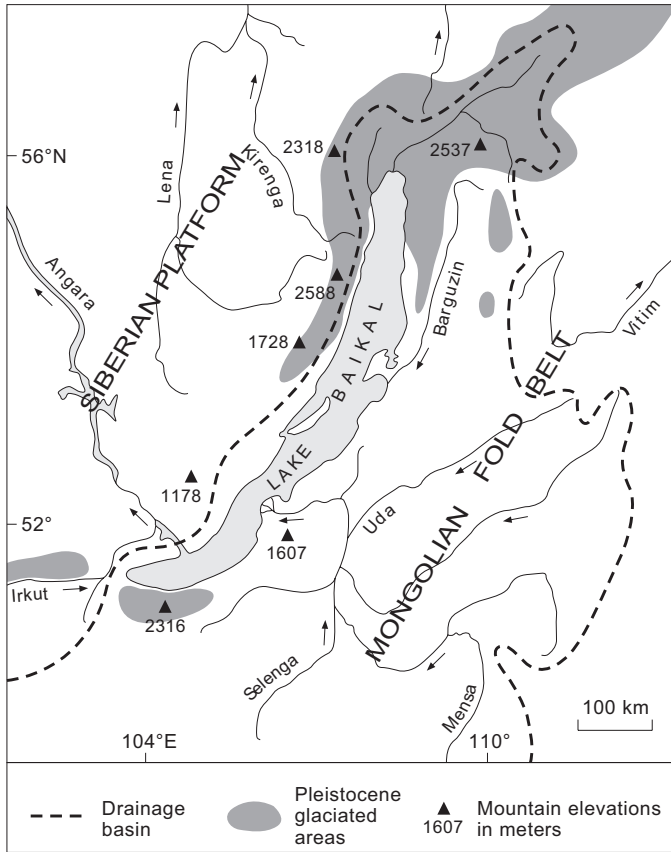


FIG. 7.—Lake Baikal setting in the Baikal rift zone of central Siberia. The entire western edge of the Lake Baikal is bounded by border faults (see Figure 8 for location), and drainage is mainly away from the lake into headwaters of the major Lena and Angara Rivers of Siberia. The eastern ramp margin of Lake Baikal is drained by numerous local rivers, particularly in the heavily glaciated region surrounding northern Lake Baikal. The large Selenga River deposits a delta over the accommodation zone that separates the South and North Basins of Lake Baikal and feeds sediment into mud-rich fans of these basins (see figure 8). (Modified from Back et al., 1999.)

fan-lobe deposits (Figs. 13, 14). The lack of submarine-fan-lobe deposition in this case apparently is caused by the continuous steep drainage gradients along the channels that connect into the Valencia Valley, where the gradient is controlled by the underlying Messinian subaerial valley (Fig. 15) (Escutia and Maldonado, 1992). Typical fan gradients in sand-rich fans change from 1:25 to 1:100 in proximal fans to 1:500 downstream in distal fans (Nelson and Nilsen, 1984). In the Ebro channels, however, the gradients never change significantly along the entire channel length, gradients remain at 1:25 to 1:100, and sediment drains into Valencia Valley without forming outer-fan lobes (Figs. 13, 14) (Nelson and Maldonado, 1988).

PLEISTOCENE CLIMATIC, SEA-LEVEL AND OCEAN-CURRENT CONTROL ON SEDIMENT SUPPLY

The Messinian, Pliocene, Pleistocene, and Holocene seismic reflection surfaces as well as sedimentation rates can be used to estimate the Ebro River sediment supply to highstand deltaic

and lowstand turbidite systems (Figs. 15–17) (Nelson, 1990). The continuous sea-level highstand conditions of the Pliocene, similar to the Holocene highstand, resulted in a low discharge of Ebro River sediment (~ 6.5 million metric tons/yr) and a sediment drape across the margin that was deposited at rates of ~ 24–40 cm/ky (Fig. 16, 17; Table 4) (Nelson, 1990). In contrast, sediment supply increased two-to-three times during the Pleistocene, the margin prograded rapidly seaward for 80 km, and deposition occurred at rates of 101–165 cm/ky on the outer shelf and slope (Fig. 17; Table 4). On the basin floor, however, sedimentation rates in the turbidite channel systems and Valencia Valley remained anomalously low (21–26 cm/ky) compared to typical Pleistocene turbidite system rates (~ 100 cm/ky or more) (Fig. 18). These low rates resulted because turbidity currents drained along Valencia Valley, which follows the relict subaerial Messinian pathways, and then currents bypassed sediment eastward to be broadly dispersed in Valencia Fan (Figs. 13–16) (Nelson and Maldonado, 1990; Escutia and Maldonado, 1992).

Throughout high to low Pleistocene sea levels, geostrophic ocean currents have dispersed sediment to the southwest and there has been a progressive southwestward progradation of Ebro prodeltas, canyons 1 to 4 and turbidite systems (Figs. 13, 14) (Nelson and Maldonado, 1990). During the late Pleistocene rise of sea level, the main depocenters progressively shifted shoreward and sedimentation rates greatly decreased from 175 cm/ky on the upper slope during the early transgression to 106 cm/ky on the outer shelf and then to 63 cm/ky on the mid-shelf during the late transgression as the river sediment discharge dropped to less than half by Holocene time (~ 6.2 million tons/yr) (Fig. 17; Table 4) (Nelson, 1990). Maximum sedimentation rates occur in active depocenters such as the present Holocene delta (370 cm/ky) or the youngest Pleistocene number 1 chan-

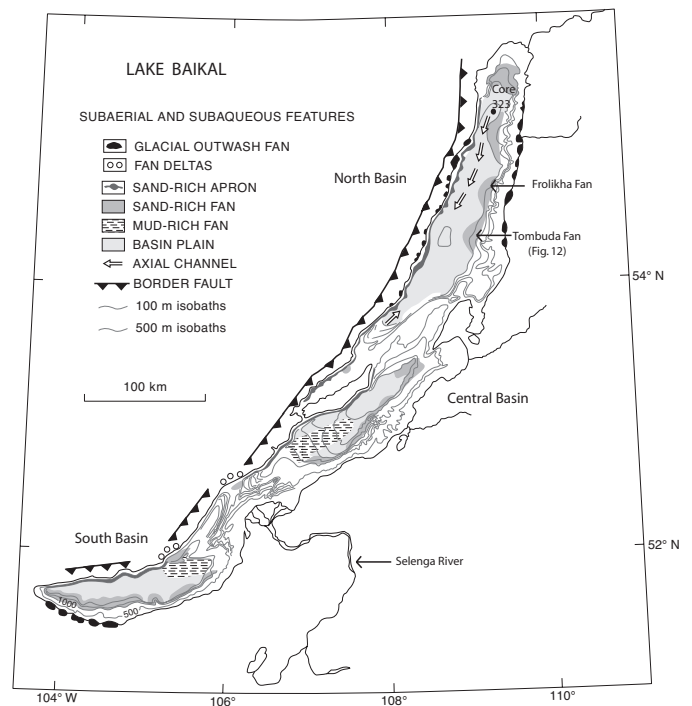


FIG. 8.—Turbidite systems and related features in Lake Baikal, based on seismic profile and core data (Nelson et al., 1995; Colman et al., 2003). (Modified from Nelson et al., 1999.)

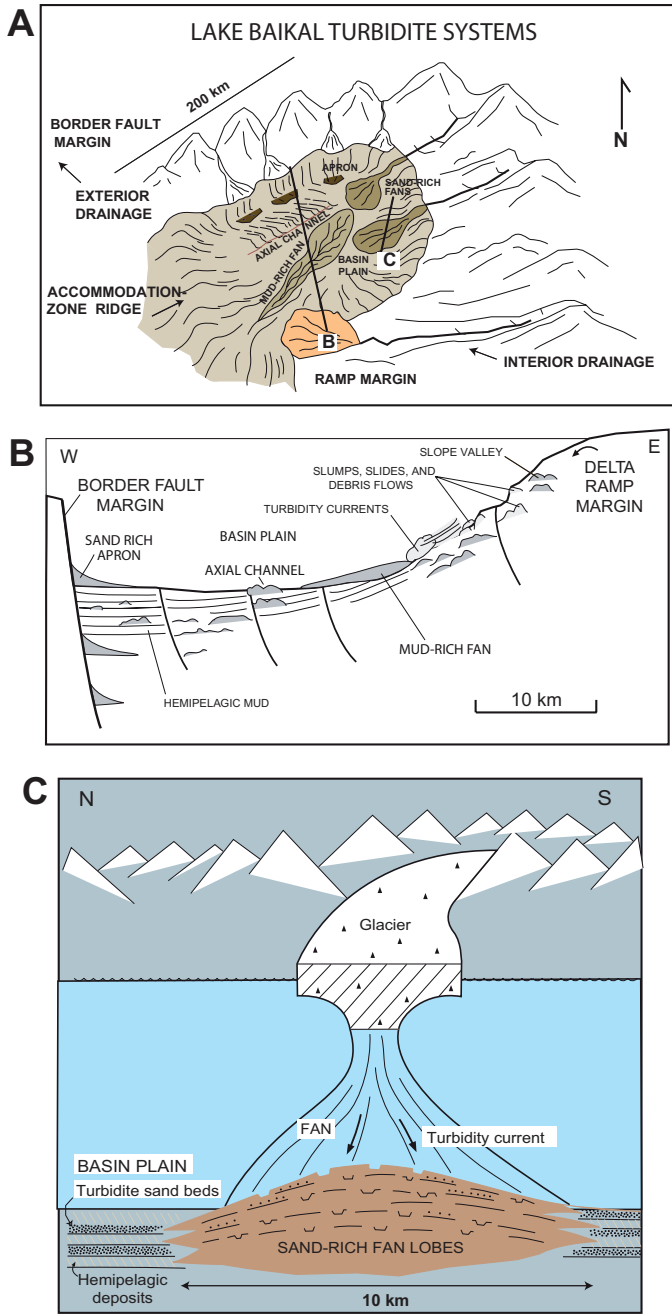


FIG. 9.—**A**) Schematic pattern of turbidite systems in Lake Baikal half-graben basin. **B**) Cross section of basin, from border-fault margin with small-fan-delta supplies of sand-rich sediment, to ramp margin with large river supply of mud-rich sediment (Part B modified from Scholz et al., 1990). **C**) Cross section of basin along the ramp margin with small river or Pleistocene glacial supply of sand-rich sediment. Locations of cross sections B and C are shown in Part A. (Modified from Nelson et al., 1999.)

estation of the Iberian Peninsula also more than doubled the Ebro sediment supply (Table 4). Beginning with Roman civilization 2000 years ago, pollen assemblages changed abruptly from pines of the Pyrenees and oaks of the Ebro Basin to grasses in the Pyrenees (like the Pleistocene) and grapes and grains in the Ebro Basin (Nelson, 1990). This change of vegetation showed that deforestation, whether caused by Pleistocene climatic change or humans, can more than double the Ebro sediment supply.

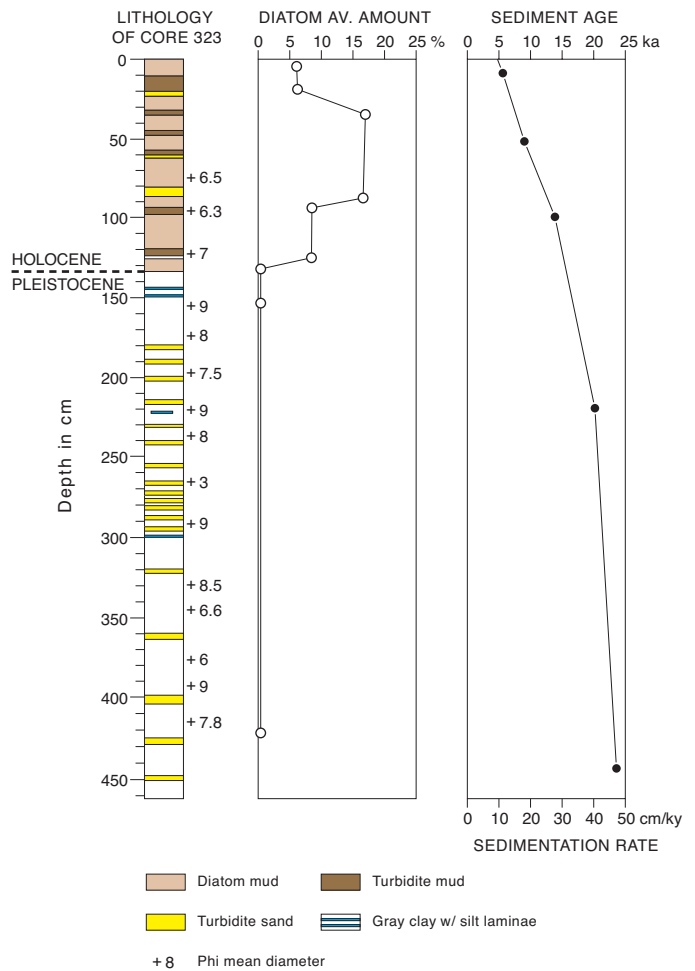


FIG. 10.—Lithology, median grain size (mm) of mainly mud interbeds, diatom abundance estimated from smear slides, and radiocarbon ages for USGS core 323-PCI sampled from the North Basin plain of Lake Baikal (see Figure 8 for location). (Modified from Nelson et al., 1995.)

nel-levee complex (750 cm/ky), where deposition rates are more than an order of magnitude greater than to average Ebro prodeltaic (38 cm/ky) or turbidite system rates (21 cm/ky) during the Pleistocene (Fig. 17) (Alonso and Maldonado; Nelson, 1990).

The sedimentation rates verify the importance of sea-level control on the successive change in location of depocenters, in direction of sediment dispersal and, in part, the amount of sediment supply (Figs. 13, 17; Table 4). Pleistocene climatic change and resultant deforestation alone, however, appear to be mainly responsible for the more than doubled sediment supply during the glacial climates (Table 4) (Nelson, 1990). The importance of climatic change and deforestation for controlling sediment supply is indicated by the observation that human defor-

TABLE 3.—Comparison of Pleistocene and Holocene sand/silt bed content in all basins of Lake Baikal.

	PLEISTOCENE	HOLOCENE
Sediment rate all basins (sm/ka)	75	20
Net sand % all basins	21	7
Net sand % north basin	5x	
Turbidite bed thickness (north basin)	3x	

Anthropogenic Control on Sediment Supply

During the past 2000 years, humans have controlled sediment supply to the Ebro margin system: first, by deforestation that more than doubled river sediment discharge and shelf deposition rates to equal those of Pleistocene time; and second, by construction of river dams that then reduced sediment discharge to less than 1% of normal Holocene discharge (Table 4) (Nelson, 1990; Palanques et al., 1990). Similar anthropogenic reductions in sediment discharge from the Nile, Po, and Rhone Rivers suggest that during the past century there has been a significant loss of river sediment supply for deltaic progradation and turbidite system growth in most of the Mediterranean Sea. As a result, the Ebro Delta now has a net recession of 1 cm/yr for the delta shoreline compared to a net progradation of 4 cm/yr prior to the development of dams (Nelson and Maldonado, 1990).

EXTERNAL CONTROLS OBSERVED IN INDIVIDUAL BASINS

Cascadia Basin

The tectonic setting and resulting drainage basins for sediment supply, continental-margin morphology, and Cascadia Basin floor gradients provide the basic control for the types of turbidite systems that developed in Cascadia Basin (Fig. 1). Similar erosional canyons have cut through the accretionary folds of the continental slope and have fed each Cascadia turbidite system (Fig. 1). The multiple tributary canyons that join to form Cascadia Channel, and the tectonic lineament of the channel, are factors that control the development of this deep-sea channel type of turbidite system (Fig. 1) (Carter, 1988). The tectonic lineament and steep downstream gradients at the base of the Mendocino Escarpment also result in the single channel levee complex that follows the escarpment. Similar to other systems, the narrow margin, which has a lower continental slope steeper than 5 degrees in southern Cascadia Basin, apparently causes the plunge pool and sediment wave turbidite systems at the mouth of the Trinidad and Eel canyons (Fig. 2) (Lee and Talling, 1998). Without the specific tectonic controls of tectonic lineaments or steep continental slopes, the general tectonic control on drainage-basin size, morphology, and amount of sediment supply mainly controls the type of Cascadia Basin turbidite systems. For example, the larger sediment supply causes the downstream channel levee and lobe formation in the Eel compared to the absence of the lobe deposits in the Trinidad and Mendocino turbidite systems (Figs. 1, 2) (Nelson et al., 2000b). Large or coalescing drainages result in a large sediment supply to form the Astoria and Nitnat submarine fans, respectively, whereas the small river

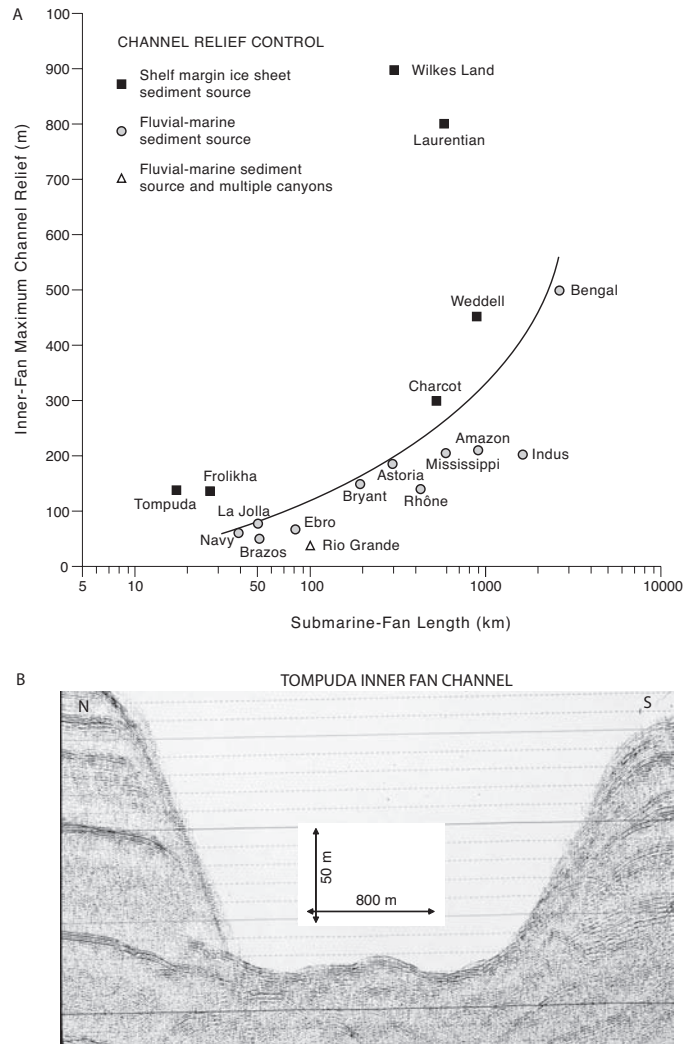


FIG. 11.—**A**) Graph of modern submarine-fan length versus maximum channel relief on the inner fan. The line separates the fans that are sourced by fluvial-marine sediment from fans that are sourced by shelf-margin ice sheets. Inner-fan channel relief in fluvial-marine-sourced fans increases progressively with fan length. Unusually high relief of the inner-fan channel relative to fan length is observed in most shelf-margin ice-sheet-sourced fans (see Part B). (Modified from Escutia et al., 2000.) **B**) Seismic profile (location shown in Figure 12) across the proximal fan valley of Tompuda Fan (location shown in Figure 8). Seismic profile was provided by Marc De Batist, University of Gent, Belgium (Hus et al., in press).

drainage of the Rogue River results in the small Rogue Apron.

Cascadia Basin shows the direct control that earthquake activity can have on timing, periodicity, and cycles of Holocene turbidite deposition. This control undoubtedly has persisted throughout the Pleistocene history of turbidite systems. However, the controls of glacial climatic change and lowered sea levels of the Pleistocene result in strong turbidity currents that erode channels, and the record of earthquake controls cannot be confirmed during glacial times. Consequently during the Quaternary, three main epochs of dominant controls for the development of turbidite systems are evident in Cascadia Basin. During

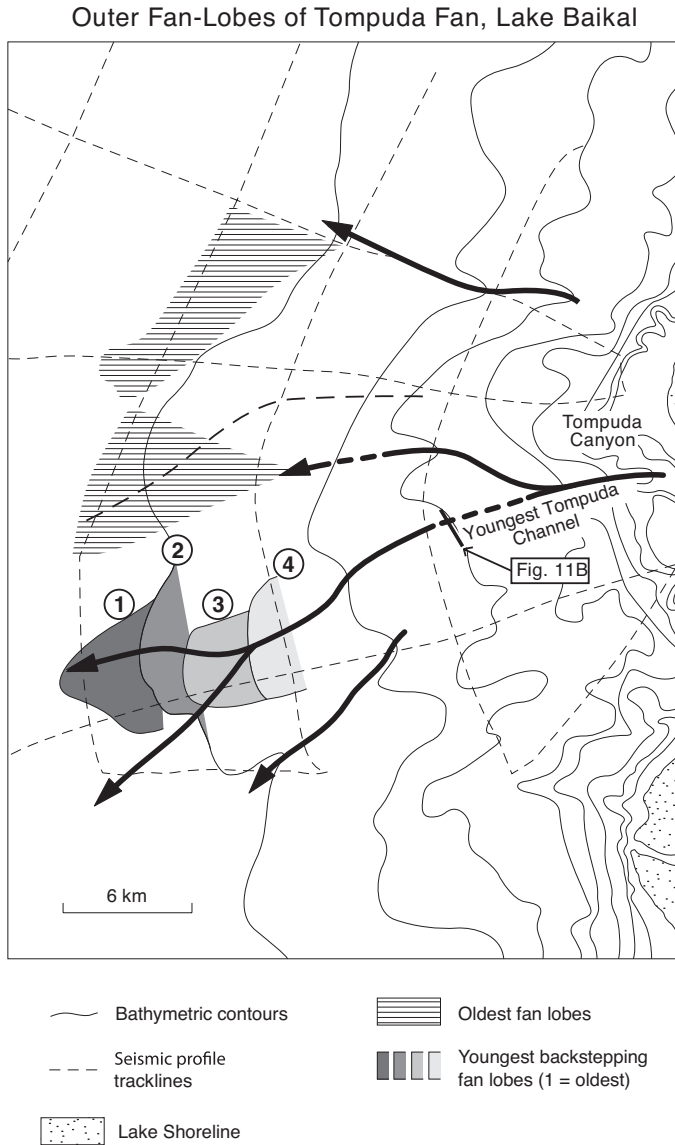


FIG. 12.—A series of backstepping outer-fan lobes related to the youngest fan valley on Tompuda Fan (location shown in Figure 8). Lobes are interpreted from seismic profiles provided by Marc De Batist, University of Gent, Belgium (Hus et al., in press).

the epoch of glacial times of lowered sea level, thick, sandy and possibly more frequent turbidites are widespread throughout the turbidite systems (Figs. 4A, 5 Pleistocene). During the epoch of interglacial times of high sea levels, the reduced sediment supply restricted turbidite deposition mainly to the channel floors, and the triggering of turbidity currents by great earthquakes is evident (Fig. 5 Holocene). During the last century and the present epoch of human civilization, the sediment supply from the Columbia River to Cascadia Basin has been reduced by 75%, and these effects on turbidite systems remain to be seen. Any of these three main epochs of varying dominant controls (i.e., tectonic, climatic/ sea-level, and anthropogenic) on turbidite systems can be interrupted by increased turbidite deposition caused by catastrophic volcanic eruptions such as that of Mt. Mazama during the mid-Holocene (Figs. 3–5).

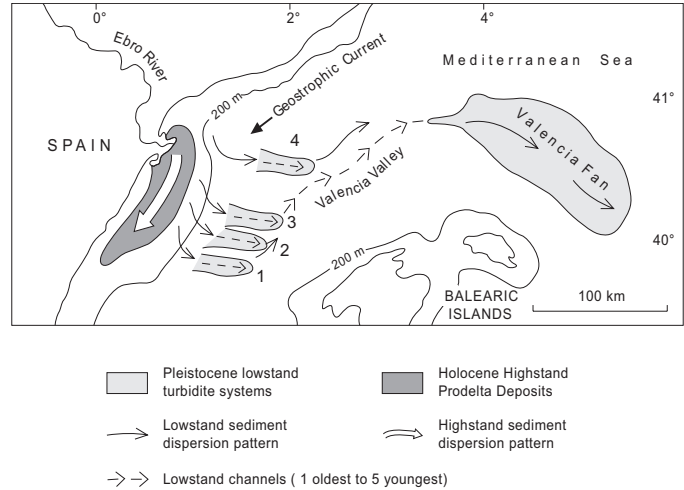


FIG. 13.—Sea-level highstand and lowstand reversal of sediment dispersal pathways in the Ebro system consisting of highstand prodeltaic deposits and lowstand Ebro turbidite channels 1 to 4, Valencia Valley and Valencia Fan. (Modified from Nelson and Maldonado, 1990.)

Lake Baikal

The rift-basin tectonics of Lake Baikal control the organization of river drainages, the basin morphology, the distribution of sediment input points to the Lake, and the amount and grain size of sediment supply. These factors in turn establish the type and location of turbidite systems on the lake floor. For example, the multiple small drainages of the border-fault scarp on the western lake margin result mainly in development of base-of-slope aprons, whereas sand- and mud-rich fans are fed from larger river drainages on the eastern ramp margin of the lake basin (Figs. 8, 9).

The glacial climates and increased glaciation of the drainage basins during the Pleistocene also influenced sediment supply and determined the growth rates of the turbidite systems in Lake Baikal (Fig. 7). During glacial times, thick sandy turbidites were deposited rapidly compared to the interglacial time of the Holocene, when a condensed section of mud and silt turbidites was deposited slowly (Fig. 10; Table 3). Because there were no significant lake level changes between the late Pleistocene glacial and Holocene interglacial times (Colman, 1998), climatic change alone, and not erosional base level, controlled the increased Pleistocene sediment supply and high growth rates of the Lake Baikal turbidite systems (Fig. 10; Table 3). The abnormally large inner-fan channels fed by valley glaciers that reached the canyon heads again substantiates the control of ice-sheet sediment sources on turbidite systems (Fig. 11) (Escutia et al., 2000) as does the backstepping of submarine fan lobes associated with the final recession of the valley glaciers (Fig. 12(Back et al., 1998; Back et al., 1999)).

Ebro Turbidite Systems

Similar to Cascadia turbidite systems, the Pleistocene climatic change, coupled with sea-level lowstands, may be equally important in causing tripled sediment supply to turbidite systems and 80 km of progradation of the Ebro continental margin (Figs.16; Table 4). Both the Ebro and the Cascadia systems also show not only that sea-level change results in a change of the main sediment depocenters from deep-sea turbidite systems to shelf mud

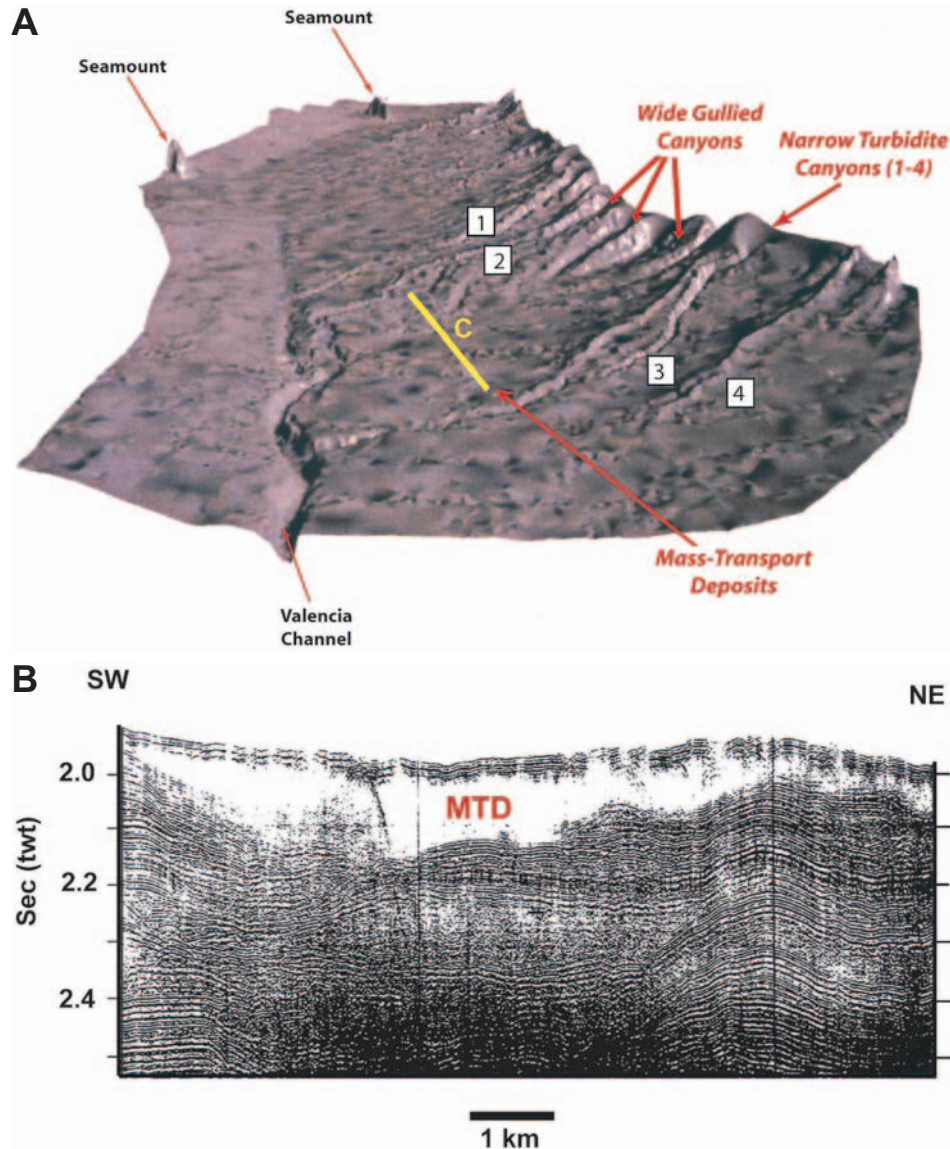


FIG. 14.—**A)** Sidescan mosaic of the Ebro turbidite canyon and channel system viewed from east to west (modified from Canels et al., 2000). **B)** Sparker (3000-J) profile B is a transverse section across the mass-transport deposit apron between turbidite channels 2 and 3 (see location in Part A). Transparent upper section in the profile consists of mass-transport deposits as shown by deep-tow side-scan sonar and echo character (Alonso et al., 1985) as well as multiple cores from the apron (Nelson et al., 1991).

blankets, but also that the sediment dispersal systems change to opposite directions between lowstand to highstand sea-level conditions when geostrophic ocean currents become important (Figs. 6, 13).

An unusual site-specific controlling factor for the Ebro turbidite systems was the Messinian desiccation of the Mediterranean Sea, which resulted in the erosion and enlargement of the subaerial Ebro Canyon and a main basin-floor drainage valley (Fig. 15) (Escutia and Maldonado, 1992). The subaerial canyon was filled by muddy Pliocene transgressive and highstand deposits (Nelson and Maldonado, 1990). These muds became unstable during the Pleistocene, resulting in wide, gullied Pleistocene submarine canyons and mass transport apron deposits below on the basin floor (Fig. 14) (Nelson et al., 1991). The Messinian subaerial valley has controlled the eastward Valencia

Valley pathway on the abyssal sea floor as well; however, the fundamental control on the subaerial Messinian and later Pleistocene Valencia Valley is an original fault lineament from the aborted rift system (Figs. 13, 15, 16) (Escutia and Maldonado, 1992; Nelson and Maldonado, 1990).

During highstands and fluctuations of the Pleistocene sea level, the strong westward geostrophic currents have resulted in the progressive development of submarine canyons from northeast to southwest along the continental slope and the asymmetric progradation of the margin toward the southwest (Figs. 13, 14) (Farran and Maldonado, 1990). Within historical times, the anthropogenic changes of deforestation have equaled the effects of the deforestation from Pleistocene climatic change by increasing sediment supply threefold (Table 4). During the last century, however, river dams have now reduced the sediment supply to

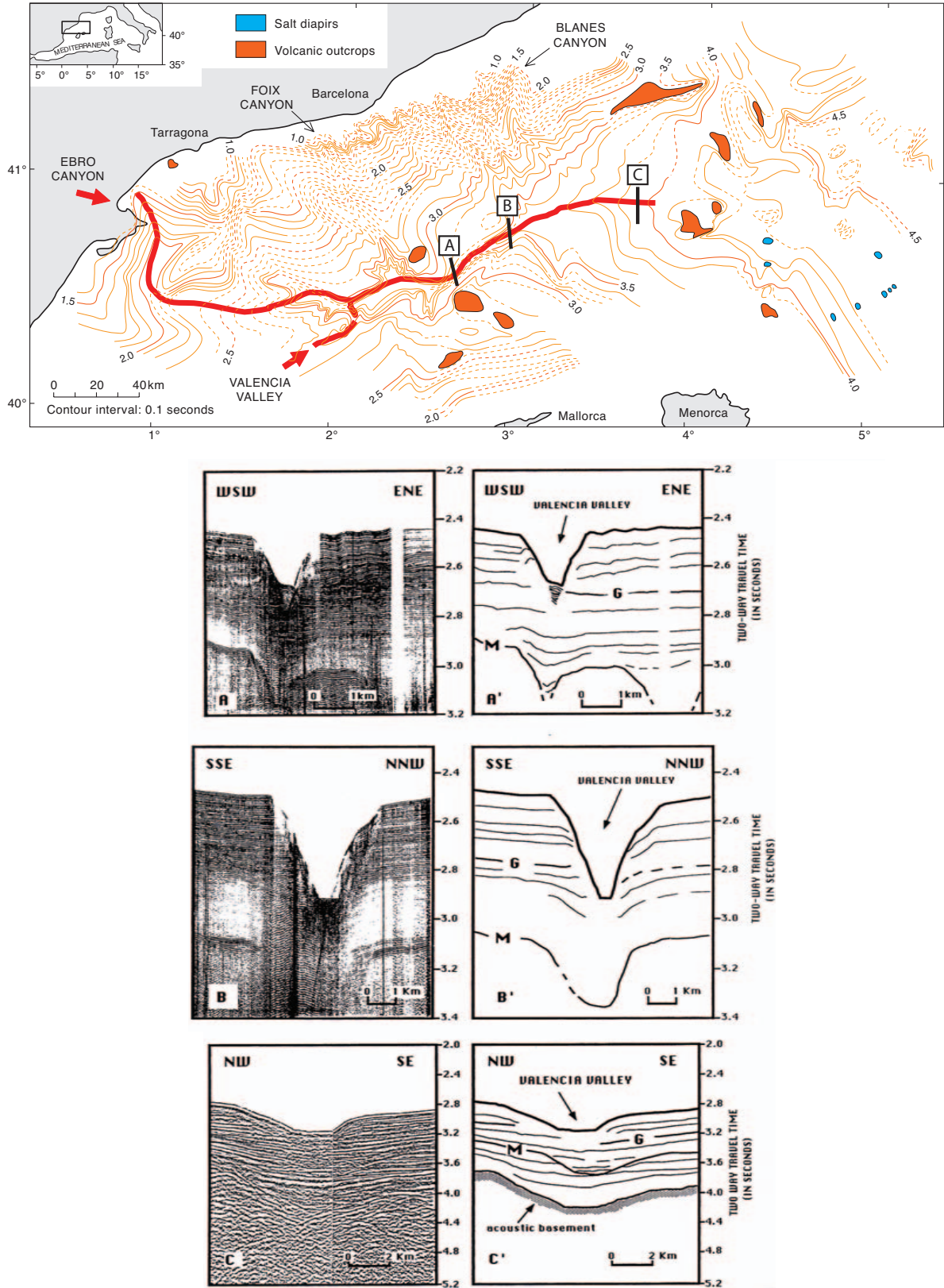


FIG. 15.—Isobath map of the Messinian surface in seconds (contour interval 0.1 s) outlining the Messinian subaerial drainage pathways. Proximal to distal seismic profiles across the Messinian subaerial valley and Pliocene Valencia Valley are shown as uninterpreted (A, B, C) and interpreted (A', B', C') cross sections. The Pleistocene surface deep-sea channel of Valencia Valley overlies and follows the subsurface Messinian subaerial valley (modified from Escutia and Maldonado, 1992).

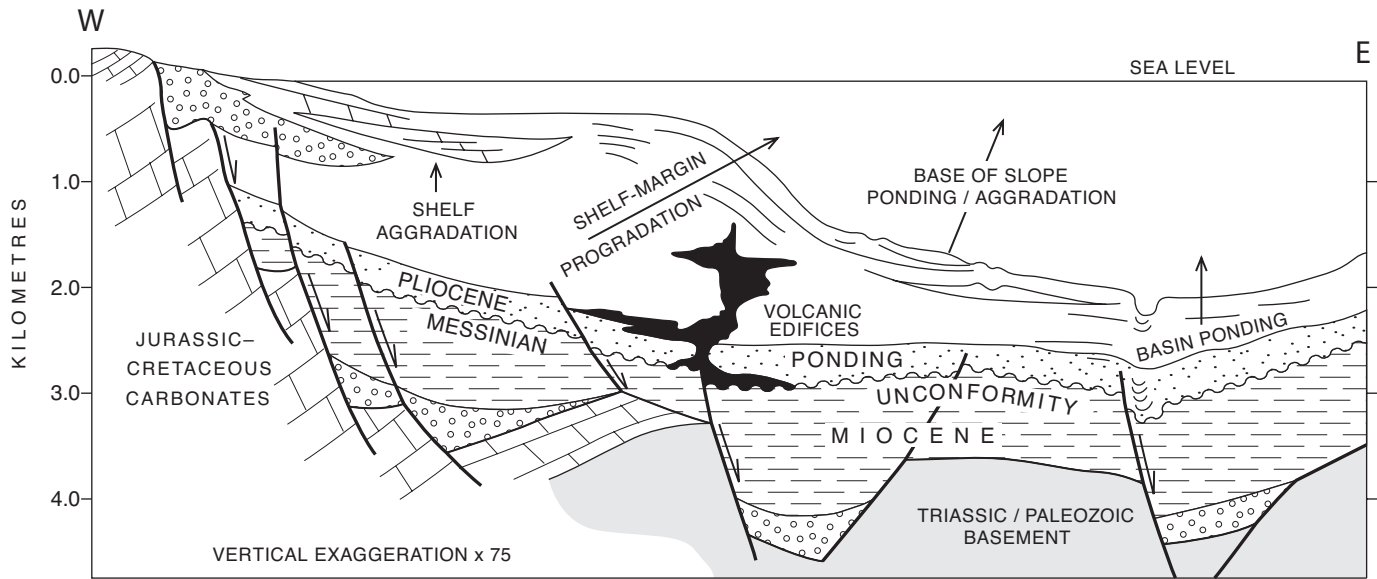


FIG. 16.—Interpreted west-to-east cross section of the tectonic setting and post-Messinian growth patterns of the central Ebro margin based on multichannel seismic profiles. (Modified from Nelson and Maldonado, 1990.)

less than 1% of normal Holocene sediment supply (Table 4) (Palanques et al., 1990).

COMMON EXTERNAL CONTROLS

The tectonic setting provides fundamental control for the morphology of the hinterland drainage basins, turbidite basin morphology and basin-floor gradients, sediment supply, basin sediment input points, turbidite system locations, and turbidite system types. The relations of tectonic setting, drainage basins, sediment-input points, and amount of sediment supply are particularly evident in the Baikal Rift setting (Fig. 9). In the Cascadia and Ebro Basins, the line source of canyons with large sediment supplies and drainage along fault lineaments results in deep-sea channels. On a smaller scale, axial channels develop and drain along faults on the rift-basin floors of Lake Baikal and other modern and ancient rift systems (Fig. 8) (Scholz et al., 1990; Nelson et al., 1995; Nelson et al., 1999; Prosser, 1993).

Tectonic control on basin-floor gradients helps determine present-day, and most likely ancient, turbidite-system depositional rates during sea-level lowstands. The Ebro turbidite systems exhibit the lowest average sedimentation rates (Fig. 18). The low rates result because turbidity currents drain downstream into Valencia Valley. The Valley follows steep river-channel gradients inherited from the underlying Messinian subaerial drainage systems that follow faults from the rifted basement (Figs. 13–18) (Escutia and Maldonado, 1992). In contrast, sedimentation rates are an order of magnitude greater than Ebro rates in turbidite systems that are in ponded basin settings like Navy Fan in a California borderland basin and Mississippi Fan in the Gulf of Mexico (Fig. 18). Apparently, the drainage gradient of the turbidite basin appears to control deposition rates because the amount of sediment supply and size of the turbidite system (i.e., the small Navy or large Mississippi Fans) are not related to deposition rates (Fig. 18).

As expected, we find that the external control of increased sediment supply and the main growth phase of turbidite systems occurs during low stands of sea level (Figs. 4A, 5, 6, 10, 13, 27;

Tables 3, 4). In contrast, significantly reduced sediment supply and development of hemipelagic-clay condensed sections takes place during high stands such as the Pliocene, Pleistocene interglacial times, and the Holocene. A caveat is that if the canyon head feeding a turbidite system extends into the present shoreline and intersects littoral-drift sediment supplies, systems such as Mendocino Channel or Var Fan remain active during sea-level high stands (Fig. 1) (Mulder et al., 1998). Another exception is active tectonic areas, like Cascadia, where although turbidite deposition is generally restricted during high stands, the earthquake triggering of turbidity currents and catastrophic volcanic eruptions result in some thick turbidite deposition in channel floors (Figs. 4A, 5) (Nelson et al., 2000b).

Turbidite deposits, whether from Lake Baikal with a subarctic climate or Ebro system with a Mediterranean climate, both show the importance of Pleistocene glacial climatic control as an independent factor for increasing sediment supply compared to tectonic activity or lowering of sea level. In Lake Baikal, even though this is an extremely active tectonic basin, during glacial climatic epochs, sediment supply, deposition rates, sand percent, and turbidite bed thickness increase three to five times with no change in base level (Table 3). Even in the Mediterranean Ebro system, which did not have as extensive changes in hinterland glaciation as Baikal, sediment supply increases two to three times during deforestation of glacial cycles, just as it has done during deforestation by humans when there have been no changes in base level (Table 4).

The importance of climatic change increasing sediment supply also helps to explain the anomalously high deposition rates in Pleistocene turbidite systems compared with older pre-Pleistocene systems, which may be controlled more by tectonic and sea-level changes rather than climate (Nelson and Nilsen, 1984). However, there is a caveat that high-resolution chronologies are difficult to obtain and thus accurately constrain sedimentation rates in ancient systems. The climatic effect from the high frequency and amplitude of sea-level lowering as well as increased sediment supply help clarify why the majority of present day submarine fans formed during the Pleistocene. Prior to the Pleis-

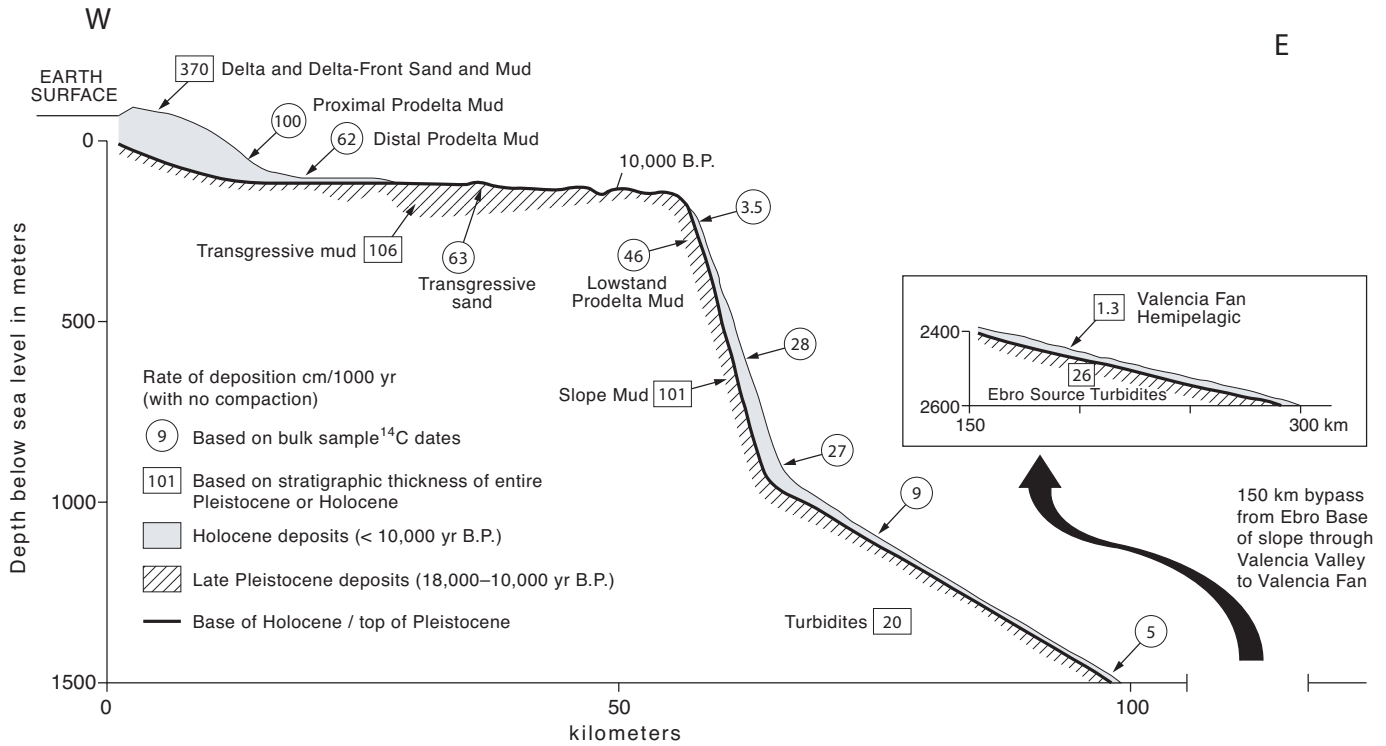


FIG. 17.—Late Pleistocene lowstand, transgressive and Holocene sedimentation rates and main depocenters for the Ebro continental margin. Thickness of deposits is exaggerated and not related to water-depth scale. Sedimentation rates shown for Valencia Fan are two-thirds of total rates to reflect only the Ebro River source contribution. (Modified from Nelson, 1990.)

tocene, the smaller number of fans and lower sedimentation rates may have resulted because of the reduced scale and frequency of sea-level lowering as well as less rapid changes in climate, forestation, and sediment supply. The absence of base-level control in Lake Baikal and the formation of the majority of submarine fans on the present-day sea floor during the extreme Pleistocene climatic changes also suggests that mainly these climatic changes, and not lowered erosional base level in drainage systems, were the main control on the growth of turbidite systems during the Pleistocene.

The Cascadia and Ebro turbidite systems also exhibit the recent anthropogenic control caused by damming of river systems during the past century; this now greatly reduces sediment supply for many systems compared to that earlier in the Holocene (Tables 2, 4). However, prior to the dams on the Ebro River, the anthropogenic effects of deforestation, overgrazing, and desertification had greatly increased sediment supply to the Ebro system (Table 4) (Palanques et al., 1990). These anthropogenic effects causing increased sediment supply still exist for many other rivers that do not have dams, such as the Eel River in Cascadia Basin (Schymiczek and Suchsland, 1987).

The Cascadia, Baikal, and Ebro deepwater basins all provide information about dominant external controls that determine basic types of turbidite systems in both active tectonic and passive-margin settings. Cascadia Basin shows that a large sediment supply, such as the Columbia River, results in large submarine fans (e.g., Astoria Fan), even in a subduction-zone trench setting (Fig. 1) (Shipboard Scientific Party, 1973; Nelson et al., 1987). In contrast, if the sediment supply is small such as the Rogue River, a base-of-slope Rogue Apron without channels is formed (Fig. 1) (Wolf et al., 1999b). Similarly in Lake Baikal, small drainages and a number of small sediment input points on the border-fault

margin control development of base-of-slope aprons, just as the limited sediment supply controls the development of the Rogue Apron (Figs. 7–9). If the sediment supply to canyons is intermediate between that of large submarine fans like Astoria and small aprons, then small sand-rich fans develop like those on the ramp margin of Lake Baikal (Figs. 8, 9).

Both Cascadia and Ebro systems verify that if multiple tributary canyons with a large sediment supply drain into a tectonically controlled channel pathway, an extensive deep-sea channel will drain and bypass sediment to detached abyssal plain fans like Valencia Fan or Tufts fan (Figs. 1, 13, 14, 15, 16) (Carter, 1988; Normark and Reid, 2003). When tectonic lineaments and morphologic setting of the basin results in small turbidity currents draining from one part into another part of the basin, connecting channel-levee systems such as Mendocino Channel and the North Baikal Basin axial channel, develop without fan deposits (Figs. 1, 8, 9, 13, 14).

Both the Cascadia and Ebro marine systems show that another external control of geostrophic ocean currents together with sea-level change can influence location of the lowstand turbidite system and highstand shelf depocenters. During the Pleistocene along the Ebro margin, the southwest geostrophic currents have caused the asymmetric southwest progradation and successive development of submarine canyons and channel systems (1 to 5) (Figs. 13, 14) (Nelson and Maldonado, 1988; Alonso and Maldonado, 1990). Both lowstand shelf-margin deltas and slope canyons, as well as the transgressive and regressive sediment packages of intermediate sea levels, have progressively developed toward the southwest because of the geostrophic currents (Farran and Maldonado, 1990; Nelson and Maldonado, 1990). In both Cascadia and Ebro margins, there are opposite sediment dispersal directions between lowstand turbidite sys-

TABLE 4.—Estimated Ebro river sediment discharge per year from the Pleistocene to Holocene (modified from Nelson, 1990).

	millions of metric tons	
Post-Dam Ebro 1983–1986	0.12 (0.6% pre dam)	
Pre-Dam Ebro 1912–1935	15–21*	
Holocene (highstand) < = 10,000 yr	6.2**	
Pleistocene (high + lowstand) 10,000–1.65 million yr	15*	Note human & glacial effects are equal
Pliocene (highstand) 1.65–4.8 million yr	6.5**	** Note highstands are equal
Data Sources: Ebro:	Pre-Dam and Post-Dam, Palanques, 1990.	
	Ebro : Pliocene to Holocene, Nelson, 1990.	

tems and highstand shelf mud blankets (Figs. 6, 13). During the lowstand, turbidity currents transport sediment eastward or southward in the Ebro and Cascadia systems, respectively, whereas during the high stands geostrophic ocean currents transport sediment westward or northward in the Ebro and Cascadia systems, respectively (Figs. 6, 13).

Although this study focuses on the late Quaternary external controls on turbidite systems on the present-day sea floor, we can observe some significant changes in external controls prior to the Pleistocene glacial and interglacial controls. In Cascadia Basin, no turbidite systems were present prior to the Pleistocene climatic changes (Shipboard Scientific Party, 1973; Nelson et al., 1987). On the Ebro margin, during the continuous sea-level high stand of the Pliocene, only a mud drape without turbidite systems was deposited over the Ebro margin, and the sediment supply from the Ebro River was nearly the same as the Holocene highstand time (Fig. 16; Table 4) (Nelson and Maldonado, 1990). Similar to the Holocene, the warm interglacial climates and high stand of the Pliocene time were the dominant controls while this condensed section was deposited (Figs. 16, 17). In contrast to the Pliocene highstand, during the Messinian, when the tectonic changes severely restricted water circulation from the Atlantic Ocean into the Mediterranean Sea, the result was the near desiccation of the deep Mediterranean sea floor. Consequently during this extreme lowstand, subaerial drainage systems prevailed (Fig. 15) (Escutia and Maldonado, 1992) rather than the deepwater depositional systems of the Pliocene and Quaternary.

Prior to the mid-Quaternary, the Baikal rift tectonic activity, which has continued from the Miocene until the present, has also affected the Lake Baikal depositional systems (Hutchinson et al., 1992). For the past ~ 650,000 years, deepwater deposition dominated by turbidite systems has prevailed, but before that mainly shallow-water deltaic deposits were present (Moore et al., 1997; Colman et al., 2003). The locations of the deltaic systems, prior to the Pleistocene Selenga Delta, changed greatly with time and rift-basin tectonic activity (Agar and Klitgord, 1995; Moore et al., 1997). Thus, in the Cascadia, Baikal, and Ebro systems, when time scales beyond the Quaternary are considered, external tectonic controls are dominant whereas the high-frequency climatic and amplitude sea-level changes are the dominant controls for Pleistocene turbidite systems. This glimpse at longer time scales of the Baikal and Ebro systems indicates that the extensive history of many ancient turbidite systems needs to be probed before a

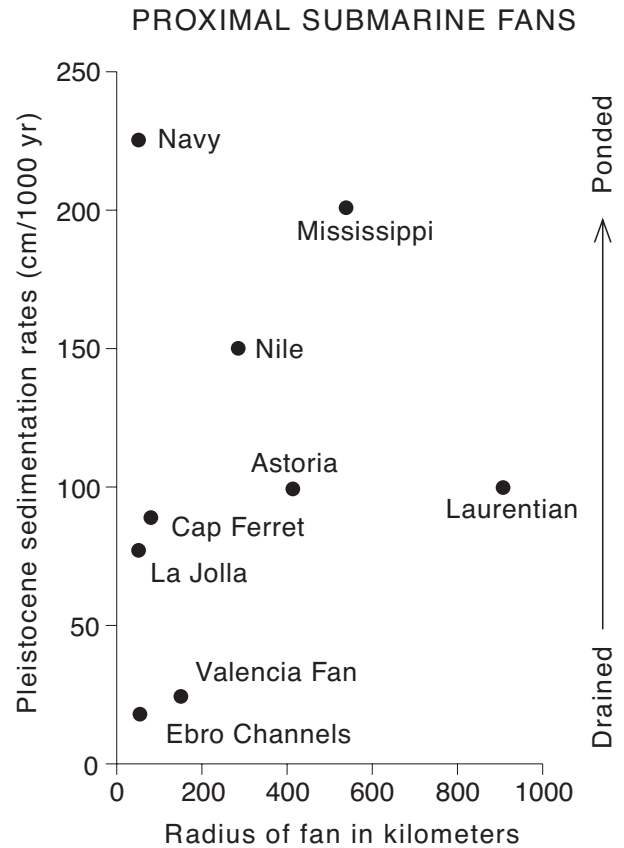


FIG. 18.—Comparison of average sedimentation rates from unconsolidated late Pleistocene deposits located in proximal modern turbidite systems. High sedimentation rates of ~ 200 cm/ky or more are found in ponded basin settings, intermediate rates of ~ 75–150 cm/ky are found in partially drained basin settings, and low rates of less than ~ 25 cm/ka are found in highly drained basin settings. Data sources from Nelson and Nilsen (1984) and Figure 17.

thorough understanding the interplay of tectonic, sediment-supply, and climatic/sea-level controls on turbidite systems can be achieved.

CONCLUSIONS

Both active and passive tectonic margin settings have some common external controls such as the tectonic setting, which determines the morphology of the basin, or the Pleistocene high-frequency climatic cycles and sea-level lowstands that result in rapid growth of turbidite systems. Active- and passive-margin settings also both develop similar types of turbidite systems such as base-of-slope aprons, submarine-fans, and deep-sea/axial channels. Each margin, however, has specific local controlling factors, for example: (1) the volcanic events in Cascadia Basin that cause unusually thick Holocene turbidites on channel floors, (2) climatic without lake-level control of sediment supply in Lake Baikal, and (3) the Messinian extreme lowstand in the Mediterranean Sea, which created unusually steep subaerial drainage gradients followed later by the Pleistocene turbidite-system channels.

The main common external controls that determine the types of turbidite systems are size of the drainage basin, morphology of

the turbidite basin, amount and type of sediment supply, and characteristics of the sediment input points. The tectonic setting affects the area of the drainage basin, sediment supply, and location of sediment input points. If there is a small volume of sediment supply, only small base-of-slope aprons a few kilometers in diameter form, whether there may be one canyon like Rogue Canyon or multiple sediment input points of a line source and many individual aprons like those along the border fault of Lake Baikal. If a small to medium volume of sand-rich sediment is supplied at a canyon mouth, a sand-rich fan tens of kilometers in diameter with channels develops, such as those associated with local rivers of the ramp margin in Lake Baikal. If there is a large volume of muddy to sandy sediment supplied at a canyon or deep-sea channel mouth, mud-rich fans hundreds of kilometers form. If multiple tributary canyons coalesce and drain along a tectonic lineament, large (several km wide) deep-sea channels such as Cascadia Channel or Valencia Valley extend for hundreds of kilometers. Small (ca. 1 km wide) channels that connect parts of turbidite systems form when there is a small volume of sediment supply that drains for tens of kilometers along local tectonic gradients in turbidite basins. These connecting channels are found as axial valleys draining along faults of the basin plains in Lake Baikal, as channels that connect Ebro canyons to Valencia Valley, and as channels that drain from the Eel plunge pool or along the Mendocino Channel escarpment in Cascadia Basin.

At longer time scales, not studied in depth in this paper, we observe that the tectonic control appears to be the dominant external control that determines the fate of turbidite systems. Examples of this are the Messinian alluvial systems in the Ebro seafloor and pre-mid-Pleistocene shallow-water deltaic systems in the Baikal Basin. The interplay of high-frequency climatic and sea-level cycles are the main common external controls that determine the formation and growth rates of the Pleistocene turbidite systems. Turbidite systems were not formed in Cascadia and Ebro marine basins until the presence of glacial climatic cycles. The climatic changes, vegetation changes, and increase in sediment supply appear to be the dominant control on the growth of Lake Baikal turbidite systems and together with sea-level changes resulted in the formation of the Cascadia and Ebro systems. The main effect of Pleistocene sea-level change appears to be allowing sediment access to canyon heads at lowstands and limiting sediment access at highstands. This becomes most important when there are wide shelves and geostrophic ocean currents that transport sediment away from canyon heads. As a result at highstands of sea level, if canyon heads do not intersect shoreline sediment supplies, condensed hemipelagic sediment units are deposited over the turbidite systems, whereas thick turbidite sand beds are deposited during lowstands. An exception to this sea-level and climatic control is found in Cascadia Basin, where earthquake triggering of turbidity currents and catastrophic volcanic eruptions result in turbidite deposits that are limited mainly to channel floors.

The turbidite-system links to the combination of common and specific external controls that determine their development provide the potential to assess: (1) resources such as petroleum reservoirs in turbidite deposits, (2) environmental changes, such as the recent anthropogenic effects on sediment supply and the consequent rapidly eroding Mediterranean deltas, and (3) geologic hazards, such as the paleoseismic history of the Cascadia Subduction Zone.

ACKNOWLEDGMENTS

It is impossible to adequately and individually acknowledge the hundreds of people and thousands of hours they dedicated to

providing the data of this summary paper that covers several decades of research. Numerous ship officers, crew members, scientific technicians, graduate students, and undergraduate students from many countries and universities spent grueling hours at sea and in the laboratory. Similarly, numerous scientific agencies from several countries provided millions of dollars of funding in many grants for the ship time and research work. These include Office of Naval Research, U.S. Geological Survey, National Science Foundation from the United States, Consejo Superior de Investigaciones Ciencias from Spain, and Akademiya Nauk from Russia. We thank Barry Fulton from University of Aberdeen and Silvia Perez from University of Granada for assisting with drafting of the figures. David Hodgson and David J.W. Piper provided helpful reviews of the paper.

REFERENCES

- ADAMS, J., 1990, Paleoseismicity of the Cascadia subduction zone: evidence from turbidites off the Oregon–Washington margin: *Tectonics*, v. 9, p. 569–583.
- AGAR, S.M. AND KLITGORD, K.D., 1995, Rift flank segmentation, basin initiation and propagation: A neotectonic example from the Baikal Rift: *Geological Society of London, Journal*, v. 152, p. 849–860.
- ALONSO, B., KASTENS, K.A., MALDONADO, M., MALINVERNO, A., NELSON, C.H., O'CONNELL, S., PALANQUES, A., AND RYAN, W.B.F., 1985, Morphology of the Ebro Fan Valleys from SeaMARC and Sea Beam profiles: *Geological Marine Letters*, v. 5, p. 141–148.
- ALONSO, B., AND MALDONADO, A., 1990, Late Quaternary patterns of the Ebro turbidite systems (northwestern Mediterranean): Two styles of deep-sea deposition, *in* Nelson, C.H., and Maldonado, A., eds., *Marine Geology of the Ebro Continental Margin, Northwestern Mediterranean Sea: Marine Geology*, v. 95, p. 353–377.
- ATWATER, B.F., GOLDFINGER C., AND NELSON C.H., 2004, Onshore—offshore correlation of geologic evidence for great Cascadia earthquakes—permissive agreement between Washington estuaries and Cascadia Deep-Sea Channel (abstract): *Eos, Transactions, v. AGU, v. 85, no. 47, Fall Meeting Supplement, Abstract T12B-01*.
- ATWATER, B.F., AND HEMPHILL-HALEY, E., 1997, Recurrence intervals for great earthquakes of the past 3500 years at northeastern Willapa Bay, Washington: U.S. Geological Survey, Professional Paper 1576, 108 p.
- BACK, S., DE BATIST, M., KIRILLOV, P., STRECKER, M.R., AND VANHOUWAERT, P., 1998, The Frolikha fan: a large Pleistocene glacial-lacustrine outwash fan in northern Lake Baikal: *Journal of Sedimentary Research*, v. 68, p. 841–849.
- BACK, S., DE BATIST, M., STRECKER, M.R., AND VANHOUWAERT, P., 1999, Quaternary depositional systems in northern Lake Baikal: *Journal of Geology*, v. 107, p. 1–12.
- CARLSON, P.R., 1967, Marine geology of Astoria Submarine Canyon: Unpublished Ph.D. Dissertation, Oregon State University, Corvallis, Oregon, 259 p.
- CARLSON, P.R., AND NELSON, C.H., 1969, Sediments and sedimentary structures of Astoria Canyon–Fan system: *Journal of Sedimentary Petrology*, v. 39, p. 1269–1282.
- CARTER, R.M., 1988, The nature and evolution of deep-sea channel systems: *Basin Research*, v. 1, p. 41–54.
- COLMAN, S.M., 1998, Water level changes in Lake Baikal, Siberia: tectonism versus climate: *Geology*, v. 26, p. 531–534.
- COLMAN, S.M., KARABANOV, E.B., AND NELSON C.H., 2003, Quaternary sedimentation and subsidence history of Lake Baikal, Siberia, based on seismic stratigraphy and coring: *Journal of Sedimentary Research*, v. 73, p. 941–956.
- DUNCAN, J.R., FOWLER, G.A., AND KULM, L.D., 1970a, Planktonic foraminiferal–radiolarian ratios and Holocene–Late Pleistocene deep-sea stratigraphy off Oregon: *Geological Society of America, Bulletin*, v. 81, p. 561–566.

- DUNCAN, J.R., KULM, L.D., AND GRIGGS, G.B., 1970b, Clay mineral composition of late Pleistocene and Holocene sediments of Cascadia Basin, northeastern Pacific Ocean: *Journal of Geology*, v. 78, p. 213–221.
- ESCUTIA, C., EITREIM, S.L., COOPER, A.K., AND NELSON, C.H., 2000, Morphology and acoustic character of the Antarctic Wilkes Land turbidite systems: ice-sheet-sourced versus river-sourced fans: *Journal of Sedimentary Research*, v. 70, p. 84–93.
- ESCUTIA, C., AND MALDONADO, A., 1992, Paleogeographic implications of the Messinian surface in the Valencia trough, NW Mediterranean Sea: *Tectonophysics*, v. 203, p. 263–284.
- GOLDFINGER, C., GRIJALVA, K., BURGMANN, K., MOREY, A., JOHNSON, J.E., NELSON, C.H., GUTIÉRREZ-PASTOR, J., KARABANOV, E., PATTON, J., AND GRACIA, E., in press, Late Holocene rupture of the northern San Andreas Fault and possible stress linkage to the Cascadia Subduction Zone: *Seismological Society of America, Bulletin*, 55 p.
- GOLDFINGER, C., NELSON, C.H., AND JOHNSON, J.E., 2003, Deep-water turbidites as Holocene earthquake proxies: the Cascadia Subduction Zone and northern San Andreas Fault systems: *Annals of Geophysics*, v. 46, p. 1169–1194.
- GRIGGS, G.B., 1969, Cascadia Channel: The anatomy of a deep sea channel: Unpublished Ph.D. Dissertation, Oregon State University, Corvallis, Oregon, 183 p.
- GRIGGS, G.B., AND KULM, L.D., 1970, Sedimentation in Cascadia Deep-Sea Channel: *Geological Society of America, Bulletin*, v. 81, p. 1361–1384.
- GUTIÉRREZ-PASTOR, J., NELSON, C.H., GOLDFINGER, C., JOHNSON, J.E., ESCUTIA, C., ERIKSSON, A., MOREY, A., AND THE SHIPBOARD SCIENTIFIC PARTY, in press, Earthquake control of Holocene turbidite frequency confirmed by hemipelagic sedimentation chronology on the Cascadia and northern California active continental margins, in Kneller, B., McCaffrey, W., and Martinsen, O.J., eds., *Geological Society of London/SEPM, Special Publication, External Controls on Deep-Water Depositional Systems*, 30 p.
- HAMILTON, E.L., 1970, Sound velocity and related properties of marine sediments, north Pacific: *Journal of Geophysical Research*, v. 75, p. 4423–4446.
- HUS, R., POORT, J., CHARLET, F., NAUDTS, L., KHLYSTOV, O., KLERKX, J., AND DE BATIST, M., in press, Lake Baikal, in Bally, A.W., and Roberts, D.G., eds., *Phanerozoic Geology Regional Geology of the World: Amsterdam, Elsevier*, 5 p.
- HUTCHINSON, D.R., GOLMSHTOK, A.J., ZONENSHAIN, L.P., MOORE, T.C., SCHOLZ, C.A., AND KLITGORD, K., 1992, Depositional and tectonic framework of the rift basins of Lake Baikal from multichannel seismic data: *Geology*, v. 20, p. 589–592.
- KELSEY, H.M., NELSON, A.R., HEMPHILL-HALEY, E., AND WITTER, R.C., 2005, Tsunami history of an Oregon coastal lake reveals a 4600 yr record of great earthquakes on the Cascadia subduction zone in Southern Oregon: *Geological Society of America, Bulletin*, v. 117, p. 1009–1032.
- KELSEY, H.M., WITTER, R.C., AND HEMPHILL-HALEY, E., 2002, Plate-boundary earthquakes and tsunamis of the past 5500 yr, Sixes River estuary, southern Oregon: *Geological Society of America, Bulletin*, v. 114, p. 298–314.
- LAMBE, T.W., AND WHITMAN, R.V., 1969, *Soil Mechanics*: New York, John Wiley & Sons, 553 p.
- LEE, S.E. AND TALLING, P.J., 1998, Origin of submarine plunge pools at the base of the continental slope (abstract): University of Leeds, England, Conference, Particulate Gravity Currents, Program and Abstract Volume, p. 36.
- MOORE, T.C., KLITGORD, K.D., GOLMSTIK, A.J., AND WEVER, E., 1997, Sedimentation and subsidence patterns in the Central and North Basins of Lake Baikal from seismic stratigraphy: *Geological Society of America, Bulletin*, v. 109, p. 746–766.
- MULDER, T., SAVOYE, B., SYVITSKI, J.P.M., AND PIPER, D.J.W., 1998, The Var Submarine Sedimentary System: understanding Holocene sediment delivery processes and their importance to the geological record, in Stoker, M.S., Evans, D., and Cramp, A., eds., *Geological Processes on Continental Margins: Sedimentation, Mass Wasting and Stability*: Geological Society of London, Special Publication 129, p. 145–166.
- NANAYAMAL, F., SATAKE, K., FURUKAWA, R., SHIMOKAWA, K., ATWATER, B.F., SHIGENO, K., AND YAMAKI, S., 2003, Unusually large earthquakes inferred from tsunami deposits along the Kuril trench: *Nature*, v. 424, p. 660–663.
- NELSON, A.R., ASQUITH, A.C., AND GRANT, W.C., 2004, Great earthquakes and tsunamis of the past 2000 years at the Salmon River Estuary, central Oregon coast, USA: *Seismological Society of America, Bulletin*, v. 94, p. 1276–1292.
- NELSON, A.R., ATWATER, B.F., BROBOWSKI, P.T., BRADLEY, L.A., CLAGUE, J.J., CARVER, G.A., DARIENZO, M.E., GRANT, W.C., KRUEGER, H.W., SPARKS, R., STAFFORD, T.W., AND STUIVER, M., 1995, Radiocarbon evidence for extensive plate-boundary rupture about 300 years ago at the Cascadia subduction zone: *Nature*, v. 378, p. 371–374.
- NELSON, A.R., KELSEY, H.M., AND WITTER, R.C., 2006, Great earthquakes of variable magnitude at the Cascadia subduction zone: *Quaternary Research*, v. 65, p. 354–365.
- NELSON, C.H., 1968, Marine geology of Astoria deep-sea fan: Unpublished Ph.D. Dissertation, Oregon State University, Corvallis, Oregon, 287 p.
- NELSON, C.H., 1976, Late Pleistocene and Holocene depositional trends, processes and history of Astoria deep-sea fan, northeast Pacific: *Marine Geology*, v. 20, p. 129–173.
- NELSON, C.H., 1983, Modern Submarine fans and debris aprons: an update of the first half century, in Boardman, S.J., ed., *Revolution in the Earth Sciences: Advances in the Past Half Century*: Dubuque, Iowa, Kendall Hunt, p. 148–166.
- NELSON, C.H., 1990, Estimated Post-Messinian sediment supply and deposition rates of the Spanish Ebro margin, in Nelson, C.H., and Maldonado, A., eds., *Marine Geology of the Ebro Continental Margin, Northwestern Mediterranean Sea: Marine Geology Special Issue*, v. 95, p. 395–418.
- NELSON, C.H., CARLSON, P.R., AND BACON, C.R., 1988, The Mt. Mazama climactic eruption (7626 B.P.) and resulting convulsive sedimentation on the continent, ocean basin, and Crater Lake caldera floor, in Clifton, H.E., ed., *Sedimentologic Consequences of Convulsive Geological Events*: Geological Society of America, Special Paper 229, p. 37–56.
- NELSON, C.H., ESCUTIA, C., KARABANOV, E.B., AND COLMAN, S.M., 2000a, Tectonic and sediment supply control of deep rift lake turbidite systems, Lake Baikal, Russia, Reply: *Geology*, v. 28, p. 190–191.
- NELSON, C.H., GOLDFINGER, C., GUTIÉRREZ-PASTOR, J., AND JOHNSON, J., 2005, Holocene turbidite paleoseismic record of great earthquakes on the Cascadia Subduction Zone: confirmation by onshore records and the Sumatra 2004 Great earthquake (abstract): European Geophysical Union Meeting 05, Vienna, A07269.
- NELSON, C.H., GOLDFINGER, C., JOHNSON, J.E., AND DUNHILL, G., 2000b, Variation of modern turbidite systems along the subduction zone margin of Cascadia Basin and implications for turbidite reservoir beds, in Weimer, P.W., Nelson, C.H., et al., eds., *Deep-Water Reservoirs of the World: Gulf Coast Section, SEPM, Annual Research Conference, CD ROM*, p. 714–738.
- NELSON, C.H., HAMPTON, M.A., KARL, H.A., AND BARBER, J.H., JR., 1987, Astoria Fan, a trench-filling elongate deep-sea fan, in Schumiczek, H., and Suchsland, R., eds., *Tectonics, Sedimentation and Evolution of the Eel River and Associated Coastal Basins of Northern California*: Bakersfield, California, San Joaquin Geological Society, Miscellaneous Publication 37, p. 113–120.
- NELSON, C.H., KARABANOV, E.B., AND COLMAN, S.M., 1995, Late Quaternary Lake Baikal turbidite systems, Russia, in Pickering, K.T., Ricci Lucchi, F.R., Smith, R., Hiscott, R.N., and Kenyon, N., eds., *An Atlas of Deep-Water Environments*: London, Chapman & Hall, London, p. 29–33.
- NELSON, C.H., KARABANOV, E.B., COLMAN, S.M., AND ESCUTIA, C., 1999, Tectonic and sediment supply control of deep rift lake turbidite systems, Lake Baikal, Russia: *Geology*, v. 27, p. 163–166.

- NELSON, C.H., KULM, L.D., CARLSON, P.R., AND DUNCAN, J.R., 1968, Mazama ash in the northeastern Pacific: *Science*, v. 161, p. 47–49.
- NELSON, C.H., AND MALDONADO, A., 1988, Factors controlling depositional patterns of Ebro turbidite systems, Mediterranean Sea: *American Association of Petroleum Geologists, Bulletin*, v. 72, p. 698–716.
- NELSON, C.H., AND MALDONADO, A., 1990, Factors controlling Late Cenozoic Ebro margin growth from the Ebro delta to the western Mediterranean deep sea, *in* Nelson, C.H., and Maldonado, A., eds., *The Ebro continental Margin, Northwestern Mediterranean Sea: Marine Geology, Special Issue*, v. 95, p. 419–440.
- NELSON, C.H., MALDONADO, A., BARBER, J.H., JR., AND ALONSO, B., 1991, Modern sand-rich and mud-rich siliciclastic aprons, alternative base-of-slope turbidite systems to submarine fans, *in* Weimer, P., and Link, M.H., eds., *Seismic Facies and Sedimentary Processes of Modern and Ancient Submarine Fans*: New York, Springer-Verlag, p. 171–190.
- NELSON, C.H., AND NILSEN, T.H., 1984, Modern and ancient deep-sea fan sedimentation: *SEPM, Short Course 14*, 403 p.
- NITTROUER, C.A., 1978, The process of detrital sediment accumulation in a continental shelf environment: an examination of the Washington shelf: Unpublished Ph.D. Dissertation, 279 p. University of Washington, Seattle, 243 p.
- NORMARK, W.R., AND REID, J.A., 2003, Extensive deposits on the Pacific Plate from late Pleistocene North American glacial lake outbursts: *Journal of Geology*, v. 11, p. 617–637.
- PALANQUES, A., PLANA, F., AND MALDONADO, A., 1990, Recent influence of man on the Ebro margin sedimentation system, northwestern Mediterranean Sea, *in* Nelson, C.H., and Maldonado, A., eds., *The Ebro continental Margin, Northwestern Mediterranean Sea: Marine Geology, Special Issue*, v. 95, p. 247–264.
- PICKERING, K.T., HISCOTT, R.N., AND HEIN, F.J., 1989, *Deep Marine Environments; Clastic Sedimentation and Tectonics*: London, Unwin Hyman Ltd., 352 p.
- POSAMENTIER, H.W., AND VAIL, P.R., 1988, Eustatic controls on clastic deposition II—Sequence and systems tract models, *in* Wilgus, C.K., and others, eds., *Sea Level Changes: An Integrated Approach*: *SEPM, Special Publication 42*, p. 125–154.
- PROSSER, S., 1993, Rift-related linked depositional systems and their seismic expression, *in* William, G.D., and Dobb, A., eds., *Tectonic and Seismic Sequence Stratigraphy*: *Geological Society of London, Special Publication 71*, p. 35–66.
- SATAKE, K., SHIMAZAKI, K., TSUJI, Y., AND UEDA, K., 1996, Time and size of a giant earthquake in Cascadia inferred from Japanese tsunami records of January, 1700: *Nature*, v. 379, p. 246–249.
- SATAKE, K., WANG, K., AND ATWATER, B.F., 2003, Fault slip and seismic moment of Cascadia 1700 earthquake inferred from Japanese tsunami descriptions: *Journal of Geophysical Research*, v. 108, ESE 7-1 to 10.
- SCHOLZ, C.A., ROSENDAHL, B.R., AND SCOTT, D.L., 1990, Development of coarse-grained facies in lacustrine rift basins: examples from East Africa: *Geology*, v. 18, p. 140–144.
- SCHYMICZEK, H., AND SUCHSLAND, R., 1987, *Tectonics, Sedimentation and Evolution of the Eel River and Associated Coastal Basins of Northern California*: Bakersfield, California, San Joaquin Geological Society, *Miscellaneous Publication 37*, 330 p.
- SHERWOOD, C.R., JAY, D.A., HARVEY, R.B., HAMILTON, P., AND SIMENSTAD, C.A., 1990, Historical changes in the Columbia River estuary: *Progress in Oceanography*, v. 25, p. 299–352.
- SHIKI, T., KUMON, F., INOUCHI, Y., KONTANI, Y., SAKAMOTO, T., TATEISHI, M., MATSUBARA, H., AND K. FUKUYAMA, K., 2000, Sedimentary features of the seismo-turbidites, Lake Biwa, Japan: *Sedimentary Geology*, v. ___, p. 137–150.
- SHIPBOARD SCIENTIFIC PARTY, 1973, Site 174, *in* Kulm, L.D., Von Huene, R.E., et al., eds., *Initial Reports of the Deep Sea Drilling Project*, v. 18: Washington, D.C., Government Printing Office, p. 97–167.
- STERNBERG, R.W., 1986, Transport and accumulation of river-derived sediment on the Washington continental shelf, USA: *Geological Society London, Journal*, v. 143, p. 945–956.
- WELLS, R.E., WEAVER, C.S., AND BLAKELY, R.J., 1998, Fore-arc migration in Cascadia and its neotectonic significance: *Geology*, v. 26, p. 759–762.
- WITTER, R.C., KELSEY H.M., AND HEMPHILL-HALEY, E., 2003, Great Cascadia earthquakes and tsunamis of the past 6700 years, Coquille River estuary, southern coastal Oregon: *Geological Society of America, Bulletin*, v. 115, p. 1289–1306.
- WOLF, S.C., NELSON, C.H., AND HAMER, M.R., 1999a, Turbidite pathways on Cascadia Basin and Tufts Abyssal Plain. Pt. A Astoria Channel to Mendocino Channel: U.S. Geological Survey, Open-File Repr 99-157, 7 sheets, scale 1:250,000.
- WOLF, S.C., NELSON, C.H., HAMER, M.R., DUNHILL, G., AND PHILLIPS, R.L., 1999b, The Washington and Oregon mid-shelf silt deposit and its relation to the late Holocene Columbia River sediment budget: U.S. Geological Survey, Open-File Report 99-173, 1 map and text.
- ZDANOWICZ, C.M., ZIELINSKI, G.A., AND GERMANI, M.S., 1999, Mount Mazama eruption: calendrical age verified and atmospheric impact assessed: *Geology*, v. 27, p. 621–624.

Goldfinger, Nelson et al., Cascadia Turbidites

(Abstract de Professional Paper, USGS, in press, 100 p.)

Turbidite Event History: Methods and Implications for Holocene Paleoseismicity of the Cascadia Subduction Zone

Chris Goldfinger*, C. Hans Nelson† Joel E. Johnson*‡Ann E. Morey*, **Julia Gutiérrez-Pastor**†, Eugene Karabanov**, Andrew T. Eriksson*^o, Eulàlia Gràcia****, Gita Dunhill††, Jason Patton*, Randy Enkin***, Audrey Dallimore***, Tracy Vallier§, and the Shipboard Scientific Parties

*Oregon State University, College of Oceanic and Atmospheric Sciences
104 Ocean Admin. Bldg., Corvallis OR 97331, USA. gold@coas.oregonstatet.edu

†Instituto Andaluz de Ciencias de la Tierra (IACT) CSIC-Univ. de Granada
Campus de Fuentenueva s/n 18002 Granada, Spain hansnelsonugr@hotmail.com, juliagp@ugr.es

** Institute of Geochemistry, Siberian Branch of Russian Academy of Sciences, Irkutsk, 64033, Russia, and Chevron, Energy Technology Company, Earth Science Technology Department, 1500 Louisiana St., Houston, TX, 77002, USA.

*** Geological Survey of Canada-Pacific, Natural Resources Canada
9860 West Saanich Road, Sidney, B.C., V8L 4B2, Canada

**** Centre Mediterrani d'Investigacions Marines i Ambientals Unitat de Tecnologia Marina – CSIC
Passeig Marítim de la Barceloneta, 37-49 08003 Barcelona, Spain egracia@cmima.csic.es

††Department of Earth & Environmental Sciences
California State University, East Bay, 25800 Carlos Bee Blvd., Hayward, CA 94542-3088
gita.dunhill@csueastbay.edu

§ formerly US Geological Survey, 345 Middlefield Road MS 999 [Menlo Park](http://MenloPark), CA 94025, now retired

‡ Present address: University of New Hampshire, Department of Earth Sciences 56 College Rd. Durham, NH 03824-3589

^o Present address: Continental Energy Corporation, Jl. Kenanga 62, Cilandak, Jakarta, Se latan, 12560, Indonesia. ateriksson@continentalenergy.com

Abstract

Turbidite systems located on the continental margin of Cascadia Basin from Vancouver Island, Canada to Cape Mendocino California, USA have been examined with swath bathymetry, newly collected and archive piston, gravity, kasten, and box cores and AMS radiocarbon ages. The purpose is to test the applicability of the Holocene turbidite record as a paleoseismic record for the Cascadia Subduction Zone. Turbidite Systems of the Cascadia Basin are an ideal place to develop a turbidite paleoseismologic method and record because: (A) a single subduction zone fault underlies the Cascadia submarine canyon systems, (B) multiple tributary canyons and a variety of turbidite systems and sedimentary sources exist to use in tests of synchronous turbidite triggering; (C) the Cascadia trench is completely sediment filled, allowing channel systems to trend seaward across the abyssal plain rather than merging in the trench, (D) the continental shelf is wide, favoring disconnection of Holocene river systems from their largely Pleistocene canyons, and (E) excellent stratigraphic datums, including the Mazama ash (MA) and a distinguishable Holocene/Pleistocene boundary (H/P) are present for correlation of events and anchoring the temporal framework in turbidite systems within the northern two thirds of the basin.

Multiple tributary channels with 50-150 km spacing and a wide variety of turbidite systems with different sedimentary sources contain 13 post-MA turbidites in Cascadia Channel, Juan de Fuca Channel off Washington, Hydrate Ridge slope basin, and Astoria Fan off northern and central Oregon. All of these events are also recorded on Rogue Apron of Southern Oregon, with the addition of smaller local events recorded as silt or mud turbidites. Similarly, 19 Holocene turbidites are found along the northern and central margin, and are recorded in southern cores with 16 interspersed smaller events.

We use ^{14}C ages, relative dating tests at channel confluences, and stratigraphic correlation of turbidites to determine whether turbidites deposited in separate channel systems are correlative, that is they were triggered by a common event. These tests can, in most cases, separate earthquake triggered turbidity currents from other possible sources. The Holocene turbidite record along the Cascadia margin passes several tests for synchronous triggering, and correlates well with the shorter onshore paleoseismic record. The synchronicity of a 10,000 year turbidite event record for 500 km along the northern half of the Cascadia Subduction Zone is best explained by paleoseismic triggering by great earthquakes. Similarly, we find a synchronous record in southern Cascadia, including correlated additional events along the southern margin. We examine the applicability of other regional triggers such as storm waves and tele-tsunami specifically for the Cascadia margin.

The average age of the oldest Holocene turbidite event is 9830 \pm 180 cal BP and the youngest was deposited in AD 1700, (250 cal. BP) thus the northern events define a Holocene great earthquake recurrence of \sim 530 years. The recurrence times and averages are also supported by the thickness of hemipelagic sediment deposited between turbidite beds. The southern Oregon and northern California margins represent at least three segments that include all of the northern ruptures, as well as \sim 18 thinner turbidites of restricted latitude range that are correlated between multiple sites. At least two Northern California sites, Trinidad and Eel Canyons, probably also record numerous small sedimentologically or storm triggered turbidites, particularly during the early Holocene when a close connection existed between these canyons and associated river systems.

The combined stratigraphic correlations, hemipelagic analysis, and ^{14}C framework suggest that the Cascadia margin effectively has three rupture modes: 19 full or nearly full-length ruptures; 2 ruptures comprising the southern 50-70% of the margin, and 18 smaller southern margin ruptures during the Holocene. The shorter rupture extents and thinner turbidites of the southern margin correspond reasonably well with spatial extents interpreted from the onshore paleoseismic record, supporting margin segmentation of southern Cascadia. The total of 38 events define a Holocene recurrence for the southern Cascadia margin of \sim 260 years. Probabilities for segmented ruptures range from 7-9% in 50 years for full margin ruptures, to \sim 30% in 50 years for a southern segment rupture.

The long earthquake record established in Cascadia allows tests of recurrence models rarely possible elsewhere. Correlatable turbidite mass along the Cascadia margin reveals a consistent record of turbidite mass per event along the margin for many of the Cascadia turbidites. We infer that larger turbidites likely represent larger earthquakes, and therefore the correlation with following time intervals suggests that Cascadia full margin ruptures may follow a time-predictable model. The long paleoseismic record also indicates a repeating pattern of clustered earthquakes that includes three Holocene cycles of 5 earthquakes followed by an unusually long interval.

We suggest that the pattern of long time intervals and longer rupture for the northern and central margin may be a function of high sediment supply on the incoming plate smoothing asperities and potential barriers. The smaller southern Cascadia segments correspond to thinner sediment supply and potentially greater interaction between lower plate and upper plate heterogeneities.

The Cascadia Basin turbidite record establishes new paleoseismic techniques utilizing marine turbidite event stratigraphy during sea level highstands. These techniques can be applied in other specific settings worldwide where an extensive fault traverses a continental margin with several active turbidite systems.

ANEXO 2

HOLOCENE EARTHQUAKE RECORDS FROM THE CASCADIA SUBDUCTION ZONE AND NORTHERN SAN ANDREAS FAULT BASED ON PRECISE DATING OF OFFSHORE TURBIDITES

Chris Goldfinger

College of Oceanic and Atmospheric Sciences, Oregon State University, Corvallis, Oregon 97331; email: gold@coas.oregonstate.edu

C. Hans Nelson¹

Department of Oceanography, Texas A & M University, College Station, Texas 77843; email: hans@ocean.tamu.edu

Joel E. Johnson

College of Oceanic and Atmospheric Sciences, Oregon State University, Corvallis, Oregon 97331; email: jjohnson@coas.oregonstate.edu

The Shipboard Scientific Party

Key Words paleoseismology, submarine, recurrence patterns, submarine landslides, turbid flows

■ **Abstract** We present preliminary evidence for a ~10,000-year earthquake record from two major fault systems based on sediment cores collected along the continental margins of western North America. New stratigraphic evidence from Cascadia demonstrates that 13 earthquakes ruptured the entire margin from Vancouver Island to at least the California border since the eruption of the Mazama ash 7700 years ago. The 13 events above this prominent stratigraphic marker have an average repeat time of 600 years, and the youngest event ~300 years ago coincides with the coastal record. We also extend the record of past earthquakes to the base of the Holocene (at least 9800 years ago), during which 18 events correlate along the same region. The sequence of Holocene events in Cascadia appears to contain a repeating pattern of events, a tantalizing first look at what may be the long-term behavior of a major fault system.

The northern California margin cores show a cyclic record of turbidite beds that may represent Holocene earthquakes on the northern segment of the San Andreas Fault. Preliminary results are in reasonably good agreement with onshore paleoseismic data that indicate an age for the penultimate event in the mid-1600s at several sites and the most likely age for the third event of ~AD 1300.

¹Now at Institute Andaluz de Ciencias de la Tierra, CSIC, Universidad de Granada, Campus de Fuente Nueva s/n, Granada, 18002.

Deep-water turbidites as Holocene earthquake proxies: the Cascadia subduction zone and Northern San Andreas Fault systems

Chris Goldfinger⁽¹⁾, C. Hans Nelson⁽²⁾ (*), Joel E. Johnson⁽¹⁾ and the Shipboard Scientific Party

⁽¹⁾ College of Oceanic and Atmospheric Sciences, Oregon State University, Corvallis, Oregon, U.S.A.

⁽²⁾ Department of Oceanography, Texas A & M University, College Station, Texas, U.S.A.

Abstract

New stratigraphic evidence from the Cascadia margin demonstrates that 13 earthquakes ruptured the margin from Vancouver Island to at least the California border following the catastrophic eruption of Mount Mazama. These 13 events have occurred with an average repeat time of ~ 600 years since the first post-Mazama event ~ 7500 years ago. The youngest event ~ 300 years ago probably coincides with widespread evidence of coastal subsidence and tsunami inundation in buried marshes along the Cascadia coast. We can extend the Holocene record to at least 9850 years, during which 18 events correlate along the same region. The pattern of repeat times is consistent with the pattern observed at most (but not all) localities onshore, strengthening the contention that both were produced by plate-wide earthquakes. We also observe that the sequence of Holocene events in Cascadia may contain a repeating pattern, a tantalizing look at what may be the long-term behavior of a major fault system. Over the last ~ 7500 years, the pattern appears to have repeated at least three times, with the most recent A.D. 1700 event being the third of three events following a long interval of 845 years between events T4 and T5. This long interval is one that is also recognized in many of the coastal records, and may serve as an anchor point between the offshore and onshore records. Similar stratigraphic records are found in two piston cores and one box core from Noyo Channel, adjacent to the Northern San Andreas Fault, which show a cyclic record of turbidite beds, with thirty-one turbidite beds above a Holocene/Pleistocene faunal «datum». Thus far, we have determined ages for 20 events including the uppermost 5 events from these cores. The uppermost event returns a «modern» age, which we interpret is likely the 1906 San Andreas earthquake. The penultimate event returns an intercept age of A.D. 1664 (2 σ range 1505-1822). The third event and fourth event are lumped together, as there is no hemipelagic sediment between them. The age of this event is A.D. 1524 (1445-1664), though we are not certain whether this event represents one event or two. The fifth event age is A.D. 1204 (1057-1319), and the sixth event age is A.D. 1049 (981-1188). These results are in relatively good agreement with the onshore work to date, which indicates an age for the penultimate event in the mid-1600's, the most likely age for the third event of ~ 1500-1600, and a fourth event ~ 1300. We presently do not have the spatial sampling needed to test for synchronicity of events along the Northern San Andreas, and thus cannot determine with confidence that the observed turbidite record is earthquake generated. However, the good agreement in number of events between the onshore and offshore records suggests that, as in Cascadia, turbidite triggers other than earthquakes appear not to have added significantly to the turbidite record along the northernmost San Andreas margin during the last ~ 2000 years.

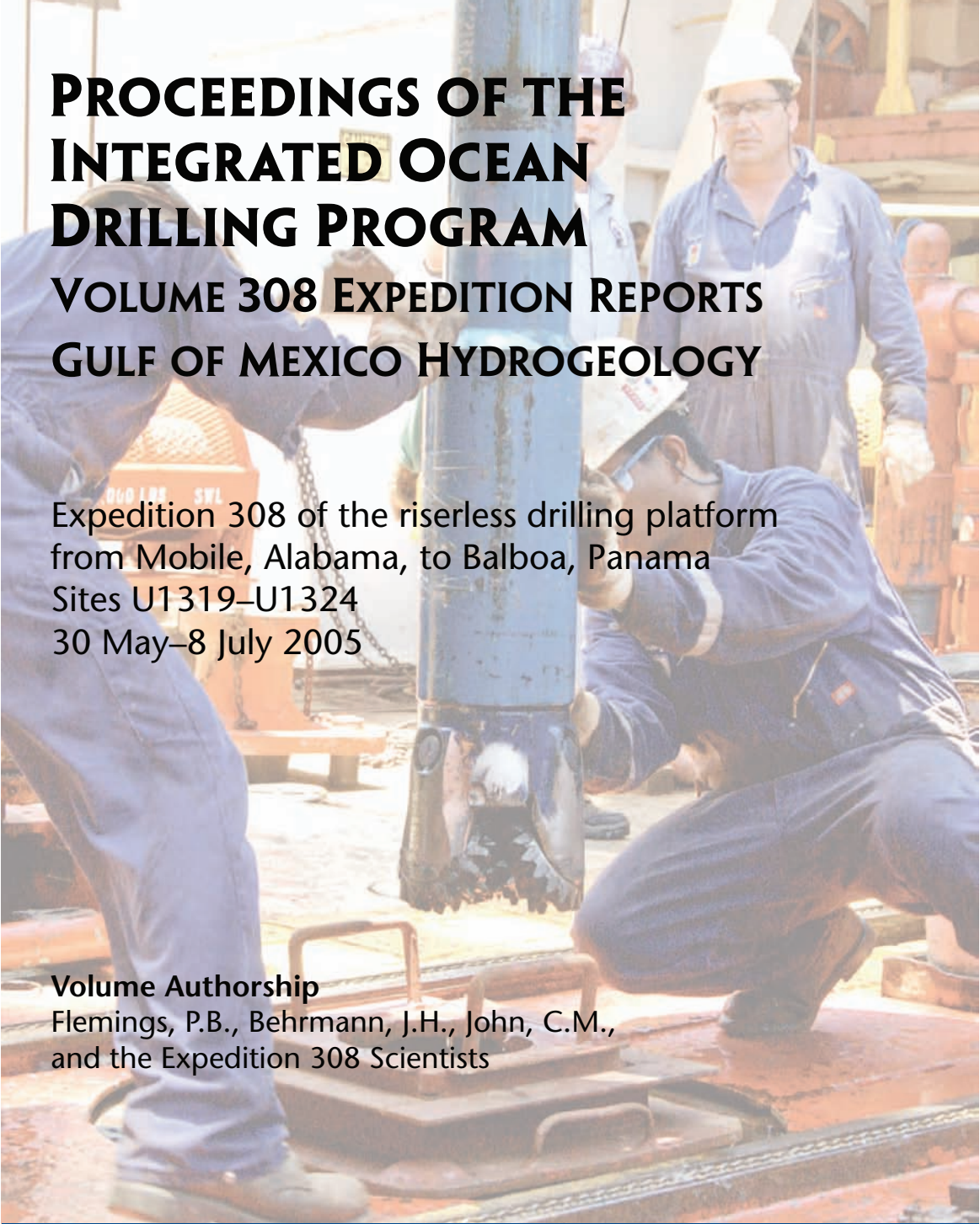
Key words *paleoseismology – earthquake – submarine – recurrence patterns – submarine landslides – turbid flows*

Mailing address: Dr. Chris Goldfinger, College of Oceanic and Atmospheric Sciences, Oregon State University, Marine Geology Active Tectonics Group, Ocean Admin. Bldg. 104, Corvallis, Oregon 97331, U.S.A.; e-mail: gold@coas.oregonstate.edu

(*) *Now at:* Instituto Andaluz de Ciencias de la Tierra, CSIC, Universidad de Granada, Campus de Fuente Nueva s/n, Granada 18071, Spain.

1. Introduction

The study of plate boundary fault systems has been revolutionized by two relatively recent sub-disciplines: paleoseismology and crustal motion as measured by the Global Positioning System. GPS technology now makes it possible to measure crustal strain accumulation at plate boundaries with a high degree of certainty in



PROCEEDINGS OF THE INTEGRATED OCEAN DRILLING PROGRAM VOLUME 308 EXPEDITION REPORTS GULF OF MEXICO HYDROGEOLOGY

Expedition 308 of the riserless drilling platform
from Mobile, Alabama, to Balboa, Panama
Sites U1319–U1324
30 May–8 July 2005

Volume Authorship

Flemings, P.B., Behrmann, J.H., John, C.M.,
and the Expedition 308 Scientists

Published by
Integrated Ocean Drilling Program Management International, Inc.,
for the Integrated Ocean Drilling Program

Prepared by
U.S. Implementing Organization Science Services, Texas A&M University

Expedition 308 science party*

Expedition 308 scientists

Peter B. Flemings

Co-Chief Scientist

Department of Geosciences
Pennsylvania State University
307 Deike Building
University Park PA 16802-2714
USA

flemings@geosc.psu.edu

Jan H. Behrmann

Co-Chief Scientist

Albert-Ludwigs-Universität Freiburg
Geologisches Institut
Albertstrasse 23B
79104 Freiburg
Germany

jan.behrmann@geologie.uni-freiburg.de

Cédric M. John

Expedition Project Manager/Staff Scientist

Department of Earth Sciences
University of California, Santa Cruz
1156 High Street
Santa Cruz CA 95064
USA

Present address (5 January 2005):
Integrated Ocean Drilling Program
Texas A&M University
1000 Discovery Drive
College Station TX 77845-9547
USA

john@iodp.tamu.edu

Gerardo J. Iturrino

Logging Staff Scientist

Borehole Research Group
Lamont-Doherty Earth Observatory of Columbia
University
PO Box 1000, 61 Route 9W
Palisades NY 10964
USA

iturrino@ldeo.columbia.edu

Yasutaka Aizawa

Physical Properties Specialist

Department of Geology and Mineralogy
Kyoto University
Kitashirakawa-Oiwakecho
Sakyo-ku, Kyoto 606-8502
Japan

inaho0go@kueps.kyoto-u.ac.jp

Nguyen Thi Thanh Binh

Physical Properties Specialist

Department of Geosystem Engineering
University of Tokyo
Faculty of Engineering Building 4
7-3-1 Hongo
Bunkyo-ku, Tokyo 113-8656
Japan

TT47152@mail.ecc.u-tokyo.ac.jp

Neil De Silva

Geophysicist

389 Ambleside Drive
London ON N6G 4Y2
Canada

ndesilva@rogers.com

Brandon Dugan

Logging Scientist

Department of Earth Science
Rice University
6100 Main Street, MS-126
Houston TX 77005
USA

dugan@rice.edu

Tommy M. Edeskär

Physical Properties Specialist

Department of Civil, Mining and Environmental
Engineering
Luleå University of Technology
Division of Geotechnical Engineering
97187 Luleå
Sweden

tommy.edeskar@ltu.se

*Addresses at time of expedition, except where updated by the participants.



Christine Franke

Paleomagnetist

Department of Geosciences
Universität Bremen
PO Box 330440
28334 Bremen
Germany
cfranke@uni-bremen.de

Aurélien Gay

Physical Properties Specialist

Challenger Division for Seafloor Processes
Southampton Oceanography Centre
Room 786/12 SOC
Empress Dock
Southampton SO14 3ZH
United Kingdom
ayg@soc.soton.ac.uk

William Patrick Gilhooly III

Inorganic Geochemist

Department of Environmental Sciences
University of Virginia
291 McCormick Road
111 Clark Hall
Charlottesville VA 22904-4123
USA
wpg6n@virginia.edu

Julia Gutierrez-Pastor

Sedimentologist

Instituto Andaluz de Ciencias de la Tierra
Universidad de Granada
Campus de Fuente Nueva
18002 Granada
Spain
juliagp@ugr.es

Shao Yong Jiang

Inorganic Geochemist

Department of Earth Sciences
Nanjing University
22 Hankou Road
Nanjiang 210093
People's Republic of China
shyjiang@public1.ptt.js.cn

Qianyu Li

Paleontologist (foraminifers)

School of Ocean and Earth Science
Tongji University
Shanghai 200092
People's Republic of China
qli01@mail.tongji.edu.cn

Hui Long

**Physical Properties Specialist/
Downhole Tools Specialist**

Energy and Geo-Environmental Engineering
Pennsylvania State University
305 Deike Building
University Park PA 16802
USA
hlong@geosc.psu.edu

J. Casey Moore

Sedimentologist/Structural Geologist

Earth Sciences Department
University of California, Santa Cruz
1156 High Street
Santa Cruz CA 95064
USA
cmoore@es.ucsc.edu

Takuro Nunoura

Microbiologist

Subground Animalcule Retrieval Program
(SUGAR PR)
Japan Agency for Marine-Earth Science and
Technology (JAMSTEC)
2-15 Natsushima-cho
Yokosuka 237-0061
Japan
takuron@jamstec.go.jp

Carlos Pirmez

Sedimentologist

Turbidites Research Team
Shell International Exploration and Production Inc.
3737 Bellaire Boulevard
Houston TX 77025
USA
carlos.pirmez@shell.com

Marc Reichow

Logging Trainee

Department of Geology
University of Leicester
University Road
Leicester LE1 7RH
United Kingdom
mkr6@le.ac.uk

Derek E. Sawyer

Sedimentologist

Department of Geosciences
Pennsylvania State University
313 Deike Building
University Park PA 16802
USA
dsawyer@geosc.psu.edu



Julia Schneider
Sedimentologist

Marine Engineering Geology/Marine Geotechnics
Universität Bremen
FB 05 Geowissenschaften
Leobenerstrasse, MARUM Gebäude
28359 Bremen
Germany
juliasch@uni-bremen.de

Anatoliy V. Shumnyk
Paleontologist (nannofossils)

Department of Geological Sciences
Carraway Building: Antarctic Circle
Florida State University
4100 FSU
Tallahassee FL 32306-4100
USA
anatoliy.shumnyk@bugware.com

Takahiro Suzuki
Sedimentologist

Earth Evolution Sciences
University of Tsukuba
1-1-1 Tennodai
c/o Professor Y. Ogawa
Tsukuba, Ibaraki 305-8572
Japan
Taka3242@arsia.geo.tsukuba.ac.jp

Yoshinori Takano
Organic Geochemist

Department of Earth and Planetary Sciences
Hokkaido University
N8W10, Kita-ku
Sapporo 060-0810
Japan
takano@nature.sci.hokudai.ac.jp

Roger Urgeles
Physical Properties Specialist

Department of Stratigraphy, Paleontology, and
Marine Geosciences
Facultat de Geologia
Universitat de Barcelona
c. Martí i Franqués s/n
08028 Barcelona, Catalonia
Spain
urgeles@ub.edu

Yuzuru Yamamoto
Sedimentologist/Structural Geologist

Institute of Geosciences
Shizuoka University
836 Oya
Shizuoka, Shizuoka 422-8529
Japan
syyamam@ipc.shizuoka.ac.jp

Valentina Zampetti
Sedimentologist

Faculty of Earth Sciences
Vrije Universiteit
1085 De Boelelaan
1081 HV Amsterdam
The Netherlands
valentina.zampetti@falw.vu.nl



Expedition 308 summary¹

Expedition 308 Scientists²

Chapter contents

Abstract	1
Introduction	1
Scientific objectives	3
Operational strategy	3
Site results	4
Discussion and conclusions	10
Overview of expedition achievements and preliminary scientific assessment	20
References	21
Figures	24
Tables	70

Abstract

Integrated Ocean Drilling Program (IODP) Expedition 308 is the first stage of a two-component program dedicated to the study of overpressure and fluid flow on the Gulf of Mexico continental slope. Drilling at six sites revealed an active hydrodynamic environment and provided insight into geological processes near the seafloor. We tested a multidimensional flow model by examining how physical properties, pressure, temperature, and pore fluid composition vary within low-permeability mudstones that overlie a permeable and overpressured aquifer. We drilled, logged, and made in situ pressure and temperature measurements in Brazos-Trinity Basin IV off the Texas Gulf Coast where low sedimentation rates and normal pressures were predicted. We contrasted these observations with experiments in the Ursa region off the Mississippi Delta where rapid Pleistocene sedimentation occurred. At Ursa, multiple pore pressure penetrometer measurements recorded values that lie halfway between the hydrostatic pressure and the lithostatic pressure. Porosity-depth profiles suggest that these overpressures are maintained by compaction disequilibrium. Log, core, and seismic data illustrate that this overpressured region was subject to multiple events of slope instability, which generated mass transport deposits. A surprising result is that mudstones beneath Brazos-Trinity Basin IV are undercompacted, and most likely overpressured, relative to mudstones at the basin margin. Interbedded sands and mudstones within Brazos-Trinity Basin IV record a fascinating stratigraphic history that relates turbidite formation to eustatic sea level change. Postcruise science on both areas investigated will combine theoretical modeling and laboratory analysis to further illuminate coupled processes of flow, sedimentation, and deformation on passive continental margins.

Introduction

Rapid sediment loading (>1 mm/y) drives overpressure (P^* ; pressure in excess of hydrostatic) in basins around the world (Rubey and Hubbert, 1959; Fertl, 1976). Sedimentation is so rapid that fluids cannot escape, the fluids bear some of the overlying sediment load, and pore pressures become greater than hydrostatic (Fig. F1).

¹Expedition 308 Scientists, 2006. Expedition 308 summary. In Fleming, P.B., Behrmann, J.H., John, C.M., and the Expedition 308 Scientists, *Proc. IODP, 308*: College Station TX (Integrated Ocean Drilling Program Management International, Inc.). doi:10.2204/iodp.proc.308.101.2006

²Expedition 308 Scientists' addresses.



13. DATA REPORT: $^{40}\text{Ar}/^{39}\text{Ar}$ CHRONOLOGY OF DISCRETE ASH LAYERS IN THE NORTHWESTERN PACIFIC: ODP SITES 1149 AND 1179¹

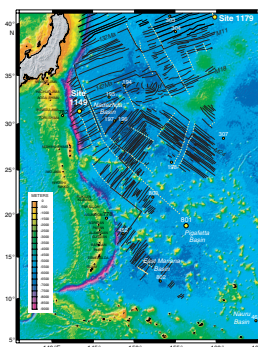
C. Escutia,² M. Canon,³ and J. Gutierrez-Pastor²

INTRODUCTION

Site 1149, drilled during Ocean Drilling Program (ODP) Leg 185, is located in the Nadezhda Basin southeast of Japan and ~100 km east of the Izu-Bonin Trench axis (Fig. F1). Site 1149 is located on magnetic Anomaly M11 (Nakanishi et al., 1992) with an assigned age of ~132 Ma (Gradstein et al., 1994, 1995; Plank, Ludden, Escutia, et al., 2000). The principal objective of Leg 185 was to determine the inputs into the Izu-Bonin Trench for “subduction factory” studies. Site 1179, on the abyssal seafloor ~1650 km east of Japan (Fig. F1), was drilled during ODP Leg 191. Site 1179 is located on magnetic Anomaly M8 (Nakanishi, et al., 1992) with an assigned age of 129 Ma (Gradstein et al., 1994, 1995). The main objectives of Leg 191 were to install a seismic monitoring station and to test the drilling and casing capabilities of the hard-rock re-entry system (“hammer drill”) (Kanazawa, Sager, Escutia, et al., 2001).

Despite the different scientific objectives of Legs 185 and 191, the sedimentary sections recovered from Sites 1149 and 1179 are the two most complete sections recovered from the northwestern Pacific Basin by either the Deep Sea Drilling Project (DSDP) (i.e., Legs 6, 20, 32, and 86) or ODP (i.e., Legs 185 and 191) (see Fig. F4 in Shipboard Scientific Party [2001]). During Leg 185, a complete sedimentary section (410 m) and an additional 133 m of highly altered volcanic basement were recovered. The Miocene to Pleistocene section (i.e., upper ~150 m) recovered from Site 1149 includes lithostratigraphic Unit I (0–118.2 meters below sea floor [mbsf]) and Subunit IIA (118.2–149.5 mbsf) of Plank,

F1. Site 1149 and 1179 locations, p. 9.



¹Escutia, C., Canon, M., and Gutierrez-Pastor, J., 2006. Data report: $^{40}\text{Ar}/^{39}\text{Ar}$ chronology of discrete ash layers in the northwestern Pacific: ODP Sites 1149 and 1179. In Ludden, J.N., Plank, T., and Escutia, C. (Eds.), *Proc. ODP, Sci. Results*, 185, 1–20 [Online]. Available from World Wide Web: <http://www-odp.tamu.edu/publications/185_SR/VOLUME/CHAPTERS/015.PDF>. [Cited YYYY-MM-DD]

²C.S.I.C.-Universidad de Granada. Instituto Andaluz de Ciencias de la Tierra, Campus de Fuentenueva, 18002 Granada, Spain. Correspondence author: cescutia@ugr.es

³Scandpower Petroleum Technology, 11490 Westheimer Road, Suite 500, Houston Texas 77082, USA.

Paleoenvironmental implications of tephra sedimentation in the northwestern Pacific since the Late Miocene

Implicaciones paleoambientales en la sedimentación de cenizas volcánicas del Pacífico noroeste desde el Mioceno superior

C. Escutia¹, J. Gutiérrez-Pastor¹ y M. Canon²

- 1 C.S.I.C.-UGR, Instituto Andalúz de Ciencias de la Tierra. Campus de Fuentenueva. 18002 Granada, cescutia@ugr.es, juliagp@ugr.es
2 Scandpower Petroleum Technology, 11490 Westheimer Road Suite 500, H, Houston, TX 77082, USA

Resumen: Niveles de cenizas volcánicas recuperadas durante los Legs 185 y 191 del ODP en el Pacífico noroeste indican que los cambios en las tasas de sedimentación a 3.6Ma y 0.780 Ma en el Pozo 1149 y a 2.5-3.0 Ma en el Pozo 1179, coinciden con picos en la frecuencia y en los espesores acumulativos de las cenizas. Se sugiere que el incremento de las tasas de sedimentación en ambos pozos está asociado con un aumento en el transporte de sedimento desde el continente asiático resultado de climas fríos y fuertes vientos del oeste que transportan polvo y cenizas desde una Asia en progresiva aridificación. Esto está apoyado por la posición de niveles de cenizas datados de ambos pozos durante los últimos 2.1 Ma, que se correlacionan con tendencias frías o estadios fríos de la curva isotópica.

Palabras clave: Pacífico noroeste, estratigrafía de cenizas volcánicas, paleoambientes

Abstract: Ash layers recovered from ODP Legs 185 and 191 in the northwestern Pacific Ocean at Sites 1149 and 1179 indicate that major changes in the sedimentation rates, at 3.6 Ma and 0.780 Ma at Site 1149, and at 2.5-3.0 Ma at Site 1179, coincide with peaks in ash frequency and cumulative ash thickness. We suggest that increased transport of sediment to these areas may be associated with cool climates and stronger trade winds carrying both dust and ash from an increasingly arid Asia. This is supported by the position of dated ash layers at both Site 1149 and Site 1179 for the last 2.1 Ma, which correlate with cooling trends or cold stages in the isotopic curve.

Key words: NW Pacific, ash stratigraphy, paleoenvironments

INTRODUCTION

Sites 1149 and 1179 were drilled during Ocean Drilling Program (ODP) Leg 185, about ~100 km east of the Izu-Bonin Trench axis, and Leg 191 on the abyssal seafloor about 1650 km east of Japan (Fig. 1). According to the paleomagnetic record obtained shipboard, Sites 1149 and 1179 have occupied their present positions since the end of the Miocene (Plank et al., 2000; Kanazawa et al., 2001). Sites 1149 and 1179 recovered a complete sedimentary sequence of 410 m and 375 m-thick, respectively, which are two of the most complete sections obtained from the northwestern Pacific basin. The Miocene to Pleistocene section (upper ~150 m) recovered from Site 1149 consists of ash- and biogenic silica-bearing clay, silty clay, ash-bearing siliceous ooze, and diatomaceous clay, with numerous discrete volcanic ash layers (Plank et al., 2000). At Site 1179, the upper 221.5 m of the sedimentary section consist of Late Miocene to Pleistocene clay- and radiolarian-bearing diatom ooze containing numerous discrete ash layers (Kanazawa et al., 2001). Escutia et al. (2006)

conducted $^{40}\text{Ar}/^{39}\text{Ar}$ dating of glass shards from the discrete ash layers to refine the

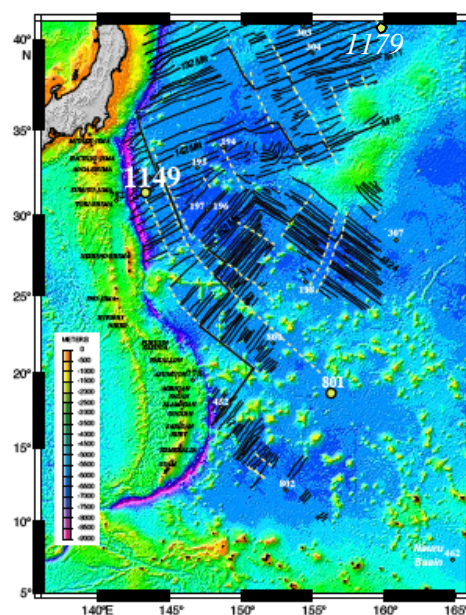


FIGURE 1. Map showing locations of Site 1149 and Site 1179 drilled during ODP Legs 185 and 191, respectively.



Instituto Andaluz de Ciencias de la Tierra

Las Fotografías de portada de los capítulos de este volumen de tesis han sido tomadas por la tripulación del Roger Revelle, 2002, en el Océano Pacífico